

**A COMPARATIVE STUDY OF THE ORIGIN OF CARBONATE-HOSTED
GEM CORUNDUM DEPOSITS IN CANADA**

by

Tashia Jayne Dzikowski

B.Sc., The University of Manitoba, 2004
M.Sc., The University of British Columbia, 2006

A THESIS SUBMITTED IN PARTIAL FULFILLMENT OF
THE REQUIREMENTS FOR THE DEGREE OF

DOCTOR OF PHILOSOPHY

in

THE FACULTY OF GRADUATE AND POSTDOCTORAL STUDIES

(Geological Sciences)

THE UNIVERSITY OF BRITISH COLUMBIA

(Vancouver)

August 2013

© Tashia Jayne Dzikowski, 2013

Abstract

This detailed scientific study of the carbonate-hosted gem corundum occurrences near Revelstoke, British Columbia and Kimmirut, Nunavut, Canada was completed in order to: (1) characterize the gem corundum mineralization; (2) develop genetic models for gem corundum mineralization; and (3) develop exploration strategies for gem corundum in carbonate-hosted deposits. These unique localities were chosen to help develop exploration strategies for gem corundum deposits in Canada since existing models of gem corundum genesis are unable to explain their origin.

The Revelstoke occurrence is located in the Monashee Complex of the Omineca belt of the Canadian Cordillera. Pink (locally red or purple) corundum crystals occur in thin, folded and stretched layers containing the assemblage of green muscovite + Ba-bearing K-feldspar + anorthite \pm phlogopite \pm Na-poor scapolite. Mineral assemblages and textures in these silicate layers and thermodynamic modeling suggest that corundum formed from muscovite dehydration at the peak of metamorphism (~650-700 °C at 8.5-9 kbar). Observed trends in whole rock geochemical data indicate that the corundum-bearing silicate (mica-feldspar) layers formed by mechanical mixing of carbonate with the host gneiss protolith; the bulk composition of the silicate layers was modified by Si and Fe depletion during prograde metamorphism. High element mobility is supported by homogenization of $\delta^{18}\text{O}$ and $\delta^{13}\text{C}$ values in carbonates and silicates for the marble and silicate layers.

The Kimmirut Sapphire Occurrence is located in the Lake Harbour Marble of the Baffin Island segment of the Trans Hudson Orogen. Blue and colourless zoned gem corundum crystals occur in coarse-grained calc-silicate pods with albite + calcite + muscovite \pm K-feldspar. Corundum-bearing zones are separated from a phlogopite + plagioclase symplectite around violet diopside crystals by scapolite which fluoresces in UV light. Corundum likely formed during retrograde metamorphism at P-T < 710°C and 6 kbar due to: 1) hydrous fluid alteration of the assemblages nepheline + scapolite and/or nepheline + anorthite or 2) Na-bearing hydrous fluid alteration of anorthite. Comparison of the prograde mineral assemblages, whole rock geochemistry, field relations, and one oxygen isotope measurement of corundum suggest that the most likely protolith is the metamorphism and metasomatism of evaporite-black shale layers within marble.

Preface

This dissertation is original, unpublished, independent work by the author, Tashia Dzikowski, with assistance in data interpretation in Chapter 3 from Jan Cempírek, Greg Dipple, Lee Groat, and Dan Marshall and Chapter 4 from Andrew Fagnan, David Turner, and Lee Groat.

Table of Contents

Abstract.....	ii
Preface.....	iii
Table of Contents	iv
List of Tables	ix
List of Figures.....	x
Acknowledgements	xvii
Dedication	xix
Chapter 1: Introduction.....	1
1.1 Why Study Ruby and Sapphire Deposits in Marble?.....	1
1.2 What are Rubies and Sapphires?.....	2
1.3 Why is Corundum Rare?.....	2
1.4 Overview of Gem Corundum Deposits in Marble	3
1.5 Relevance of Proposed Study Localities	6
1.6 Previous Studies on the Revelstoke Occurrence Area	6
1.7 Previous Studies on the Kimmirut Sapphire Occurrence (KSO) Area	6
1.8 Objectives of Thesis.....	7
1.9 Research Approach	7
Chapter 2: Methods.....	11
Chapter 3: Revelstoke Occurrence: High-pressure Origin of Gem Corundum in Micaceous Layers in Marble.....	15
3.1 Introduction.....	15
3.2 Geological Setting.....	15
3.3 Lithological Units of the Monashee Complex	16
3.4 Geology and Petrography of the Revelstoke Occurrence	17
3.4.1 Marble.....	17
3.4.2 Mica-Feldspar-Rich Layers	18
3.4.3 Diopside-Tremolite Laminations.....	20
3.4.4 Minor Assemblages in the Marble.....	20

3.4.5	Non-Siliceous Laminations	20
3.4.6	Brittle Deformation in Marble	21
3.4.7	Calc-Gneiss.....	21
3.4.8	SEDEX Mineralization.....	23
3.5	Mineralogy	23
3.5.1	Corundum	23
3.5.2	Calcite and Dolomite	24
3.5.3	Trioctahedral Mg,Fe-Micas	24
3.5.4	Muscovite and Margarite.....	25
3.5.5	Feldspars	26
3.5.6	Scapolite	26
3.5.7	Pyroxene	27
3.5.8	Garnet	27
3.5.9	Amphiboles.....	27
3.5.10	Other Accessory Minerals	28
3.6	Whole Rock Geochemistry	29
3.7	⁴⁰ Ar- ³⁹ Ar Dating of Micas.....	30
3.8	Stable Isotopes	31
3.9	Fluid Inclusions.....	31
3.10	Discussion	32
3.10.1	Protolith of Silicate Assemblages in the Marble	32
3.10.2	Chromium and Vanadium Enrichment.....	35
3.10.3	P-T Metamorphic Path in Frenchman Cap Dome	36
3.10.4	P-T-X Evolution of the Marble	37
3.10.5	Retrograde Fluids	39
3.10.6	Comparison to Other Deposits	41
3.11	Summary	42
	Chapter 4: Kimmirut Sapphire Occurrence	67
4.1	Introduction.....	67
4.2	Regional Geology	67
4.3	Local Geology:.....	69
4.4	Lake Harbour Marble.....	70
4.5	Geology and Petrography of the Sapphire Occurrence.....	70
4.5.1	Marble.....	70

4.5.2	Course-Grained Calc-Silicate Pods in Marble.....	71
4.5.2.1	Beluga	71
4.5.2.2	Bowhead	73
4.6	Mineralogy	73
4.6.1	Sapphire	73
4.6.2	Nepheline.....	74
4.6.3	Diopside.....	74
4.6.4	Phlogopite.....	74
4.6.5	Muscovite	75
4.6.6	Plagioclase	75
4.6.7	Scapolite	75
4.6.8	Other Accessory Minerals	77
4.7	Whole Rock Geochemistry	77
4.7.1	Major and Trace Elements.....	77
4.7.2	Rare Earth Elements	78
4.8	Oxygen Isotopes of Corundum	79
4.9	U-Pb Geochronology	79
4.10	^{40}Ar - ^{39}Ar dating.....	80
4.11	Discussion	80
4.11.1	Prograde and Retrograde Mineral Assemblages at both the Beluga and Bowhead Showings	80
4.11.2	Retrograde Corundum + Albite + Muscovite-Bearing Zones at the Beluga Showing	82
4.11.3	Isotopic Evidence	85
4.11.4	Protolith of the Beluga Showing	85
4.11.4.1	Contact Metamorphism of a Mafic Protolith	85
4.11.4.2	Alkaline Intrusions Formed by the Assimilation of Carbonate and Siliciclastic Rocks into a Mafic Magma	86
4.11.4.3	Alkaline Intrusions into Marble	87
4.11.4.4	Na-Metasomatism of Metasediments or Volcanic Rocks	88
4.11.4.5	Metamorphism of an Evaporite-Shale-Marble Protolith.....	89
4.11.5	Proposed Beluga Model of Formation	90
4.11.6	Late Fluid Infiltration	91
	Chapter 5: Comparison of the Revelstoke and Kimmirut corundum occurrences.....	117
5.1	Introduction.....	117

5.2	Age	117
5.3	Petrology	117
5.4	Whole Rock Composition.....	118
5.5	Mineral Chemistry	119
5.5.1	Corundum	119
5.5.2	Micas	119
5.5.3	Scapolite	120
5.6	Oxygen Isotopes of Corundum	120
5.7	Discussion	120
Chapter 6: Exploration Strategies	128	
6.1	Introduction to Exploration Strategies	128
6.2	Recommended Exploration Techniques and Strategies.....	128
6.2.1	Review of Known Geology and Mapping	129
6.2.2	Prospecting and Indicator Minerals	130
6.2.3	Detailed Sampling Grid	130
6.2.4	Whole Rock Analyses.....	131
6.2.5	Airborne Hyperspectral Imaging Surveys for Identification of Indicator Minerals	131
6.2.6	Identification of Chromophore Sources.....	132
6.2.7	Magnetic Geophysical Survey	132
6.2.8	Heavy Mineral Concentrates	133
6.2.9	Ultraviolet Light Surveys for Identification of Scapolite Associated with Corundum.	133
6.2.10	Ground Penetrating Radar (GPR) for 3-D imaging of Target Zones at Depth.....	133
6.3	Exploration for Revelstoke-type Occurrences in Other Parts of the World.....	134
6.4	Exploration for Beluga-type Occurrences in Other Parts of the World	134
6.5	Summary	134
Chapter 7: Conclusions and Future Work.....	140	
7.1	Conclusions - Revelstoke.....	140
7.2	Conclusions - Kimmirut Sapphire Occurrence	141
7.3	Conclusions from Comparison of the Revelstoke Occurrence with the Beluga Showing	142
7.4	Conclusions from Comparison of the Revelstoke Occurrence with the KSO and other Gem Corundum Deposits Around the World	143
7.5	Future Work	143
7.5.1	Revelstoke.....	143

7.5.2 Kimmirut Sapphire Occurrence.....	144
References	146
Appendices.....	160
Appendix A Compositional Data for the Revelstoke Occurrence	160
A.1 Corundum	161
A.2 Carbonates	166
A.3 Phlogopite	178
A.4 Muscovite and Margarite.....	192
A.5 Feldspars.....	200
A.6 Scapolite	211
A.7 Diopsid.....	215
A.8 Garnet	219
A.9 Amphibole	221
A.10 Other Accessory Minerals	222
A.11 Classification of allanite	223
A.12 Classification of tourmaline.....	224
A.13 Whole-Rock Geochemistry of Lithologies from the Revelstoke Occurrence.	225
A.14 Microthermometry Results of Fluid Inclusions within Corundum at the Revelstoke Occurrence.....	226
Appendix B Compositional Data for the Kimmirut Sapphire Occurrence	227
B.1 Corundum	228
B.2 Nepheline.....	230
B.3 Diopsid.....	232
B.4 Phlogopite	236
B.5 Muscovite	241
B.6 Plagioclase	242
B.7 Scapolite	248
B.8 Other Accessory Minerals	255
B.9 Whole Rock Major and Trace Elements.....	258

List of Tables

Table 3.1: Mineral Assemblages from Different Lithologies within the Revelstoke Occurrence	44
Table 5.1 Comparison between the Revelstoke and Kimmirut Sapphire Occurrences.....	122
Table 6.1: Factors to consider for exploration – a comparison between the Revelstoke and Beluga occurrences	139

List of Figures

Figure 1.1: Major and minor commercial world sources of gem corundum (Giuliani et al. 2007).....	9
Figure 1.2: Map of Canadian gem corundum localities. Blue stars indicate sapphire occurrences, and red stars indicate ruby and pink sapphire occurrences. The study localities are denoted by RO = Revelstoke Occurrence and KSO = Kimmirut Sapphire Occurrence, and other Canadian localities are denoted as: 1 = Slocan Valley, 2 = Bancroft-York River area, 3 = Nova Scotia, 4 Labrador.....	9
Figure 1.3: Calculated theoretical corundum-producing reactions at different X_{H_2O} [$X_{H_2O} = H_2O/(H_2O+CO_2)$]. Mineral equilibria were calculated with the program Theriaak-Domino (de Capitani and Petrakakis 2010) using end member compositions and the internally consistent thermodynamic database of Holland and Powell (1998). A) Breakdown of diaspore, margarite, and spinel. B) Breakdown of muscovite.....	10
Figure 2.1: Comparison of $\delta^{13}C$ and $\delta^{18}O$ values collected using an Isotope Ratio Mass Spectrometer (IRMS) and Mineral Isotope Analyzer (MIA).	13
Figure 3.1: Position and geology of the Revelstoke occurrence. (A) Map of Canadian carbonate-hosted gem-corundum localities; (B) Tectonic assemblage map of part of the Monashee complex (modified after Höy 2001). The studied area is marked by a star; (C) Regional geological map of the Revelstoke occurrence (modified after Höy 1987). The studied localities (from east to west: float, outcrop 1, outcrop 2) are marked by yellow stars. Map legend: (1) orthogneiss, (2) paragneiss, (3) quartzite, micaceous schist, (4a) Calc-silicate gneiss, kyanite-sillimanite schist, quartzite, amphibolite, (4b) Kyanite-sillimanite schist, gneiss, minor quartzite (q), (4c) Calc-silicate schist, gneiss, kyanite-sillimanite schist, marble (m), quartzite (q), (5) marble, (6a) Calc-silicate gneiss, kyanite-sillimanite schist, marble (m), (6b) Kyanite-sillimanite schist, minor amphibolite, marble (m), quartzite (q)...	45
Figure 3.2: Revelstoke corundum. (A) Zoned corundum grain in marble (picture width 3 cm); (B) Faceted Revelstoke sapphire and ruby (photo courtesy of B.S. Wilson).....	46
Figure 3.3: Photographs of the Revelstoke occurrence. (A) The corundum-bearing marble within diopside gneiss (unit 6a); (B) Pyroxene-gneiss with pelitic layers, containing garnet porphyroblasts (dark spots); (C) Corundum-bearing mica-feldspar layers, with secondary	

scapolite after anorthite; (D) Coarse-grained diopside-tremolite zone and fine-grained, graphite -enriched cataclasite layers; (E) Magnetite and graphite layers in marble; (F) Deformed, altered muscovite-feldspar nodules in phlogopite and graphite layers in marble.	47
Figure 3.4: Schematic drawing of mineralogical zoning of mica-feldspar layers. Hexagons represent corundum crystals; solid pink hexagons are not zoned, pink hexagons with blue rims are zoned crystals. The pink hexagons represent corundum, which sometimes are zoned.....	48
Figure 3.5: Optical microscope photographs and BSE images of mineral assemblages in mica-feldspar layers and garnet in marble. (5A) SEM photomicrograph of replacement of muscovite by anorthite and K-feldspar. Note relicts of muscovite in anorthite and phlogopite and muscovite in K-feldspar. (5B) SEM photomicrograph of replacement of muscovite by anorthite and K-feldspar. Note the intergrowth of anorthite and K-feldspar as well as relicts of muscovite in anorthite and phlogopite in K-feldspar. (5C) SEM photomicrograph of Ba-enrichment in K-feldspar replacing muscovite and anorthite. The light areas in the K-feldspar and muscovite are enriched in Ba. (5D) SEM photomicrograph of corundum alteration to muscovite then K-feldspar. The corundum has inclusions of apatite, zircon, muscovite, K-feldspar, and rutile. (5E) SEM photomicrograph of corundum with anorthite inclusions surrounded by anorthite, phlogopite, and calcite, altered to margarite. (5F) CPL optical microscope image of Type 2 skeletal euhedral corundum with calcite inclusions within marble. (5G) SEM photomicrograph of Type 3 fine-grained corundum with alteration to margarite and Ba-enriched muscovite within plagioclase. (5H) SEM photomicrograph of scapolite and amphibole coronas around garnet. Amphibole also replaces pyroxene.....	50
Figure 3.6: Optical microscope photographs and BSE images of the host rock thin sections	51
Figure 3.7: Trace elements in corundum of different color.....	52
Figure 3.8: Chemical composition of trioctahedral micas. A) Fe vs. V; B) Ti vs. $[^6]\text{Al}$ and Ba+Ca vs. $[^6]\text{Al}$; C) $[^4]\text{Al}$ vs. Mg/(Mg+Fe); D) $[^6]\text{Al}$ vs. $[^4]\text{Al}$	53
Figure 3.9: Chemical composition of muscovite. A) V vs. Ti; B) Cr vs. Ti; C) Ba vs. Ti; D) Fe+Mg vs. Ti.....	54
Figure 3.10: Variation of Ba and Na vs. K in K-feldspar.....	55
Figure 3.11: Compositional diagram for scapolite showing the meionite, marialite, mizzonite solid solution in terms of Cl/(Cl + CO ₃ + SO ₄) and equivalent anorthite EqAn = (Al-3)/3.	

The curves indicate NaCl content of fluids according to the experimental data of Ellis (1978) for 4 kbar and 750 °C.....	56
Figure 3.12: Composition of (A)clinopyroxene and (B) garnet from marble, SEDEX, host rocks and the garnet assemblage in the marble.....	57
Figure 3.13: Composition of amphiboles. A) Classification diagram for Ca-amphiboles with (Na+K) < 0.5 apfu; B) Classification diagram for Ca-amphiboles with (Na+K) > 0.5 apfu..	58
Figure 3.14: Contents of immobile trace elements (Cr, Ti, and V), selected mobile major elements (Si, Fe), and partially mobile elements K, Ca, Mg) in different lithologies.....	59
Figure 3.15: Geochemistry of selected trace elements in host rock and marble. Data for amphibolites in Unit 6B are from Höy (2001).....	60
Figure 3.16: Chondrite-normalized (Sun and McDonough 1989) REE-plots for (A) calc-gneiss and marble, (B) mica-feldspar layers in the marble.....	61
Figure 3.17: ^{40}Ar - ^{39}Ar plateau ages for Revelstoke corundum occurrence from A) phlogopite; B) muscovite.	62
Figure 3.18: Coupled $\delta^{13}\text{C}$ - $\delta^{18}\text{O}$ values for carbonate from different lithologies. (A) Published values for other marbles from the Mica Creek (MC), Esplanade Range (E), and Dogtooth Range (DT) ~ 50 km north of the Monashee Complex in the Selkirk Allochthon (Ghent and O'Neil 1985), Thor-Odin Dome (Holk and Taylor 2000) and Asian ruby deposits in marble (Garnier et al. 2008) compared to the studied Revelstoke lithologies. (B) Values for the studied lithologies from the Revelstoke (Rev) occurrence.	63
Figure 3.19: Range of $\delta^{18}\text{O}$ values for carbonate and silicate minerals compared to potential protoliths in the Monashee Complex near the Thor Odin dome (Holk and Taylor 2000) and to average values for pelites (Hoefs 2004), skarns (Bowman 1998), and marbles (Valley 1986).	64
Figure 3.20: Two-phase primary liquid-vapour CO_2 (with minor $\text{CH}_4\text{-N}_2$) fluid inclusions in corundum.	65
Figure 3.21: Major mineral forming reactions and PT evolution of the Revelstoke occurrence marble. Bolded mineral names indicate observed mineral assemblages. Arrows indicate position of curves with increasing $X_{\text{H}_2\text{O}}$. Corundum fluid inclusion isochores are also plotted.	66

Figure 4.1: Location and regional geology of the Kimmirut Sapphire Occurrence (KSO). A) Map of Canadian gem-corundum localities. RO = Revelstoke occurrence, 1 = Slocan Valley, 2 = Bancroft-York River area, 3 = Nova Scotia, 4 Labrador. B) Geological map of southern Baffin Island. The Level 1-2 terrane boundary fault is the Bergeron suture and the Level 2-3 terrane boundary fault is the Soper River suture (St-Onge et al. 2000). The yellow star indicates the location of the Kimmirut Sapphire Occurrence (KSO).	92
Figure 4.2: A) Distinctive texture of the coarse-grained Beluga lens in contact with finer-grained marble. Note the rectangular outline of violet diopside + symplectite (phlogopite + plagioclase). B) Muscovite-albite-calcite-sapphire zone.....	93
Figure 4.3: Sample B8-04b in A) incandescent and B) UV light. Note the bright yellow fluorescence of scapolite in UV light.....	93
Figure 4.4: Plagioclase-phlogopite symplectite rimmed by scapolite. Note random orientation of phlogopite and inclusions of calcite in plagioclase. FOV = 0.9 mm	94
Figure 4.5: Photomicrographs displaying the distinctive texture and mineralogical zones of calc-silicate rocks from the Beluga showing. A) Zoning of mineral phases; diopside (at the upper left corner) is rimmed by the plagioclase-phlogopite symplectite, followed by scapolite, then the corundum-albite zone. Note the presence of the area of extensive alteration which can occur as an inclusion within scapolite, but also as part of the corundum-bearing zone. B) Zoning of mineral phases; diopside is not visible in this photomicrograph possibly because it has all been consumed in the production of the plagioclase-phlogopite symplectite. Note the random orientation of phlogopite grains within the symplectite, the presence of scapolite within the corundum zone, and the presence of the area of extensive alteration along the boundary between scapolite and the corundum-bearing zone, possibly indicating fluid pathways.....	95
Figure 4.6: Albite and calcite surrounding corundum next to scapolite.	96
Figure 4.7: Symplectite with calcite and titanite on the edge of scapolite.	97
Figure 4.8: Calcite inclusions in phlogopite, on the edge of phlogopite, or in the intergranular space between plagioclase.....	97
Figure 4.9: Symplectite with scapolite and plagioclase inclusions in phlogopite.	98
Figure 4.10: Symplectite with calcite and titanite.	98
Figure 4.11: Plagioclase-phlogopite-calcite and phlogopite inclusions in scapolite.	99

Figure 4.12: Photomicrographs of the nepheline-bearing Bowhead showing. A) The plagioclase-phlogopite symplectite develops between diopside and nepheline grains. B) Scapolite rimming plagioclase-phlogopite symplectite and nepheline. FOV = 0.8 mm, C) Plagioclase-phlogopite symplectite in contact with calcite. FOV = 0.5 mm, D) Plagioclase-muscovite nodule within scapolite. FOV = 0.3 mm	100
Figure 4.13: A) Beluga blue and colourless cut sapphires from the Beluga showing. C) 1.17 ct. in pavilion view with tweezers for scale. All sapphires are natural and untreated. Photos are courtesy of True North Gems.....	101
Figure 4.14: A) Barrel-shaped corundum crystal from the Beluga showing. Image is from Wilson (2010). B) Scanning electron microscope image of a zoned sapphire crystal with calcite (cc) and rare apatite (ap) inclusions. Prismatic thomsonite (th) crystals penetrate corundum along fractures. Image is from LeCheminant et al. (2005).....	101
Figure 4.15: Compositional variation of sapphires from the Beluga occurrence.	102
Figure 4.16: Pyroxene classification and major elemental variation diagram.....	103
Figure 4.17: Compositional variation of pyroxene at the Beluga and Bowhead showings: A) Al vs Na apfu; B); Mg vs Fe ³⁺ apfu; C) Ti vs Fe ³⁺ apfu; and D) Ti vs Mg apfu.....	104
Figure 4.18: Compositional variation of phlogopite from the Beluga and Bowhead showings. A) ^[4] Al vs. Mg/(Mg+ Fe ²⁺); B) ^[6] Al vs. ^[4] Al; C) Ti vs. Fe ²⁺ ; D) Ti vs.Mg; E) F vs Fe ²⁺ + Mg + Mn.....	105
Figure 4.19: Chemical composition of muscovite from the Beluga and Bowhead showings: A) Al vs Ti and B) K vs Na.	106
Figure 4.20: Compositional variation of scapolite from the Beluga and Bowhead showings. Meionite, marialite, mizzonite solid solution end members are expressed in terms of X _{Cl} = Cl/(Cl + CO ₃ + SO ₄) and equivalent anorthite EqAn = (Al-3)/3. The curves indicate NaCl content of fluids according to the experimental data of Ellis (1978) for 4 kbar and 750 °C.	107
Figure 4.21: Compositional variation of scapolite. A) Zoning of EqAn across scapolite grains at the Beluga showing. B) Tie-lines of coexisting scapolite-plagioclase pairs at the Beluga and Bowhead showings.	107
Fig. 4.22: High resolution hyperspectral image of a rock from the Beluga showing collected by David Turner. The two generations of scapolite are identified by blue and purple.....	108

Figure 4.23: Major element variation for the Beluga rocks as well as other lithologies from the Lake Harbour Group, Blandford Bay assemblage, Narsajuaq Terrane, Ramsay River orthogneiss, and Cumberland batholith: A) Fe_2O_3 vs SiO_2 , B) SiO_2 vs Al_2O_3 , C) Fe_2O_3 vs MgO , D) Na_2O vs MgO , and E) CaO vs MgO	109
Figure 4.24: Major elements vs TiO_2 wt.% for the Beluga rocks as well as other lithologies from the Lake Harbour Group, Blandford Bay assemblage, Narsajuaq Terrane, Ramsay River orthogneiss, and Cumberland batholith.	110
Figure 4.25: Major elements vs V ppm for the Beluga rocks as well as other lithologies from the Lake Harbour Group, Blandford Bay assemblage, Narsajuaq Terrane, Ramsay River orthogneiss, and Cumberland batholith.	111
Figure 4.26: REE patterns of lithologies from the Lake Harbour Group compared to the Beluga showing.....	112
Figure 4.27: REE patterns of lithologies with elevated V (170-280 ppm) from the Beluga showing, Narsajuaq terrane (Nar), Lake Harbour Group (LHG), and Blandford Bay assemblage (BB).	113
Figure 4.28: The $\delta^{18}\text{O}$ values of gem corundum from different protoliths (Giuliani et al. 2005). The Beluga sapphire is denoted as a blue hexagon.	114
Figure 4.29: U-Pb ages of deformation, metamorphic and magmatic events in the Meta Incognita microcontinent and Narsajuaq arc (St-Onge et al. 2007). A U-Pb zircon date from the Beluga showing (LeCheminant et al. 2005) plots amongst other post-D ₂ thermal/fluid activity ages. (BS = Bergeron suture; SRS = Soper River suture.)	115
Figure 4.30: ^{40}Ar - ^{39}Ar age spectra of (A) phlogopite and (B) muscovite from the Beluga showing. Box heights are 2σ , plateau steps are filled, and rejected steps are open.....	116
Figure 5.1: Comparison of the whole rock compositions from the Kimmirut sapphire occurrence and the Revelstoke occurrence.	123
Figure 5.2: Comparison of corundum compositions from the Beluga showing and the Revelstoke occurrence.	124
Figure 5.3: Comparison of phlogopite compositions from the Kimmirut sapphire occurrence and the Revelstoke occurrence (excluding host rocks).....	125
Figure 5.4: Comparison of muscovite compositions from the Kimmirut sapphire occurrence and the Revelstoke occurrence.....	126

Figure 5.5: Comparison of scapolite compositions from the Kimmirut sapphire occurrence and the Revelstoke occurrence (including host rocks).	127
Figure 6.1: Corundum-bearing mica-feldspar layers, with secondary scapolite after anorthite exposed on a foliation plane.	136
Figure 6.2: Schematic drawing of the mineralogical zoning of mica-feldspar layers. The pink hexagons represent non-zoned corundum and the pink hexagon rimmed with blue represents zoned corundum with a pink core and blue rim.....	136
Figure 6.3: Scapolite- and corundum-bearing rocks under incandescent and ultraviolet light. Note the yellow fluorescence of scapolite in ultraviolet light.	137
Figure 6.4: Schematic of a geochemical sampling grid that could be applied to exploration for corundum deposits. Results are plotted on Fig. 6.5 to facilitate interpretation.....	137
Figure 6.5: Whole rock or Niton XRF geochemical diagrams highlighting target zones at the Revelstoke occurrence. The gray shaded areas highlight where values should lie if there was mechanical mixing between the two lithologies without any element loss or gain. The target area highlights samples that are depleted in SiO_2 and FeO_{TOT}	138

Acknowledgements

First and foremost, I would like to thank my PhD supervisors Lee Groat and Greg Dipple for all of their support and guidance. Thank you Lee for providing me with this project, all of your help in the field, and your unique perspective as a mineralogist. Thank you Greg for your help in Revelstoke, your unique perspective as a metamorphic petrologist, and for helping me see the big picture. I have learned so much from both of you and am very grateful for all of our discussions.

I would like to sincerely thank Jan Cempírek for being incredibly supportive over the past 2 years. I really appreciate all of your hands on help and for spending those long days in the lab with me hashing out details. Your guidance during the completion of my Revelstoke chapter will never be forgotten.

I would like to thank various organizations for providing me with funding during completion of this dissertation. The National Sciences and Engineering Research Council of Canada (NSERC) awarded me a 2-year Post Graduate Scholarship (PGSD) scholarship and the University of British Columbia awarded me a 2-year University Graduate Scholarship. In addition, the Society of Economic Geologists and Geoscience BC awarded me research grants which assisted with the costs of my field work and thin section preparation.

I would not have been able to complete this project without the support of Brad Wilson for the Revelstoke project and True North Gems for the Kimmirut project. They allowed me access to their claims, provided me with samples, and assisted me with my field work.

Data collection was assisted by many people: Dan Marshall helped me collect fluid inclusion data, Janet Gabites, Shaun Barker, and Gaston Giuliani helped me collect oxygen isotope data, Jenny Lai and Elisabetta Pani for being there when I needed help with the SEM, and Mati Raudsepp and Edith Czech helped me collect numerous electron microprobe data. I would especially like to thank Mati Raudsepp for all the wonderful conversations over the years. I always looked forward to spending time with you.

I would like to thank my lab members Leo Millonig, David Turner, and Andrew Fagan, Andrea Dixon, Jim Evans, and Mallory Dixon for your camaraderie and the bi-weekly tea parties. More specifically I would like to thank Leo for introducing me to Theriak

Domino and for helping me improve speaking German, Dave for our discussions about gemstones and exploration geology, and especially Andrew for reviewing many chapters of this thesis and helping me see the light at the end of the tunnel. I really appreciate all that you did during my final push to finish. I would also like to thank Mackenzie Parker for proof reading this thesis and for providing me with constructive feedback.

Last but not least I would like to thank my friends and family. Victoria, Janina, Julia, Laura were a great source of support for me and helped me have an amazing time while living in this great city of Vancouver. My partner Frank was always there when I needed him (thank you for being my 'tide' and an amazing source of encouragement) and I'm looking forward to our new adventure together. I would like to thank my parents and sister for encouraging me to achieve my dreams; I would not have made it this far without your support. This thesis was written in loving memory of my father who introduced me to the world of science and geology in both the classroom and the field. You are a source of inspiration to me and I know you would be very proud to see how far I've come.

Dedication

To my father, Raymond Dzikowski

Chapter 1: Introduction

1.1 Why Study Ruby and Sapphire Deposits in Marble?

The origin of gem corundum (Al_2O_3), which includes ruby (red variety) and sapphire (blue and other colors), has recently been the subject of significant interest due to the growing economic potential of the gem corundum market, the discovery of new deposits, and advances in understanding of their geological origin (e.g., see reviews in Giuliani et al. 2007, Simonet et al. 2008). Ruby and sapphire are arguably the world's most widely sold colored gemstones, accounting for approximately one-third of global colored stone sales by value (BUZ Consulting 2009, in Shor and Weldon 2009), and commanding some of the highest prices paid for any gem.

Gem corundum deposits can be very valuable and are rare; currently, one of the most valuable gem corundum specimens is a 6.04ct Burmese ruby that sold in 2011 for \$3.3 million (or \$551,000/ct) and there are fewer than 25 producing regions in the world (Fig. 1.1). Given that rubies are the world's most valuable gemstone, and that some of the best quality deposits are being exhausted and occur in politically volatile areas, it is even more important to explore for new deposits to meet the market demand.

Currently there are five known gem corundum deposits in Canada (Fig. 1.2): carbonate-hosted red, pink, and zoned pink-blue sapphires near Revelstoke, British Columbia (this study), carbonate-hosted blue, yellow, and colorless sapphire near Kimmirut on Baffin Island (discovered in 2002; LeCheminant et al. 2005, Gertzbein 2005); sapphire in southeastern Newfoundland (discovered in 1987; Wight 1999); carbonate-hosted “low-grade ruby” near Sydney, Nova Scotia (discovered in 2004; Durstling 2005); carbonate-associated blue sapphire near Bancroft, Ontario (Wight 2004); and star sapphire hosted in plumasite dikes, calcareous biotite syenite gneiss, and felsic augen gneiss from several localities near Passmore in south-central British Columbia (discovered in the early 1980s; Wilson 2010; Walker 2012). Four of the Canadian gem corundum occurrences are associated with carbonate rocks.

Despite much previous research, the origin of many gem corundum (Al_2O_3) deposits remains unclear and, as a result, only primitive exploration strategies exist for some deposit types. Five hypotheses have been proposed for the origin of carbonate-hosted gem corundum

deposits in Asia, the US, Europe, Africa, and the Middle East (Giuliani et al. 2007), but these hypotheses do not explain the genesis of the Canadian gem deposits in this study (see Chapters 3 and 4). An understanding of the origin and development of exploration strategies for carbonate-hosted deposits is important because some of the best rubies have historically originated from this type of deposit.

I chose to study two very different carbonate-hosted gem corundum occurrences in Canada: (1) the Revelstoke gem corundum occurrence in British Columbia, and (2) the Kimmirut sapphire occurrence (KSO) in Nunavut. The main goals of this project were to: (1) characterize the corundum/sapphire/ruby mineralization; (2) develop genetic models for mineralization at these occurrences; and (3) develop exploration strategies for these carbonate-hosted gem corundum deposits.

1.2 What are Rubies and Sapphires?

Rubies and sapphires are the gem form of corundum (Al_2O_3); ruby is red and sapphire is any other colour of gem corundum. Pure corundum is colourless (white), and coloured varieties form because of impurities that substitute for Al into the crystal structure. The red colour in ruby is caused by the substitution of Cr for Al, which can also impart red fluorescence (Muhlmeister et al. 1998). A blue colour in sapphires is caused by intervalence charge transfer between Fe and Ti when they substitute for Al (Fritsch and Rossman 1988). A very small amount of Fe and Ti (0.01 wt %) is needed to produce intense colour in sapphire, whereas a much larger amount of Cr (0.2-2.5 wt %) is needed to produce a similar intensity of colour in ruby.

1.3 Why is Corundum Rare?

Corundum only forms in Al-rich assemblages deficient in Si; in order to form ruby and sapphire, chromophores such as Cr, V, Ti, and Fe must also be present and available to substitute into the crystal structure (i.e., they must not be locked up in other minerals). The enrichment in both Al and Cr is problematic because both are considered to be immobile elements and require special conditions to reach the necessary concentrations. Gem corundum deposits are rare and in general poorly understood because they originate in a

variety of tectonic settings, under variable pressure and temperature (P-T) conditions, and are derived from diverse source materials. In addition, they are commonly involved in multi-stage metamorphic, metasomatic and retrograde processes that can obscure the primary textures of the host mineral assemblages. As a result, no general exploration strategies can currently be applied to prospecting for gem corundum (Groat and Laurs 2009, Simonet et al. 2008, Garnier et al. 2008).

1.4 Overview of Gem Corundum Deposits in Marble

Carbonate-hosted deposits are one of the most important sources of high-quality gem corundum. They are usually minor constituents of large metasedimentary sequences typically metamorphosed in amphibolite or lower granulite-facies (Kievlenko 2003, Simonet et al. 2008). The corundum mineralization is usually stratiform and occurs in veinlets, gash-veins, lenses, or disseminated in the carbonate gangue. Accessory minerals present in corundum-bearing marbles typically include spinel, diopside, phlogopite, Cr-muscovite, feldspar, garnet, chlorite, margarite, tremolite, pargasite, edenite, and forsterite; less common are scapolite, zoisite, epidote, uvite, and sulfides (Giuliani et al. 2007).

Kievlenko (2003), Giuliani et al. (2007), and Simonet et al. (2008) provide comprehensive reviews and classifications of gem corundum deposits. Deposits are classified as either primary (magmatic or metamorphic) or secondary (xenocrysts or placers). Metamorphic deposits can be subdivided into metamorphic *sensu stricto* (s.s.) (meta-limestones, mafic granulites, aluminous gneisses and granulites), metasomatic (desilicated rocks, skarns), or anatetic types (Simonet et al. 2008).

Carbonate-hosted corundum occurrences can be either metamorphic s.s. or metasomatic. The concentration mechanisms of Al and chromophore elements can be related to: (1) depositional and/or weathering processes prior to metamorphism, such as bauxite formation, or clay sedimentation within a sedimentary sequence; and (2) metasomatic processes such as skarn formation, desilification, or hydrothermal transport in vein systems (Giuliani et al. 2007 and references therein).

Corundum in carbonate rocks is most commonly produced by the following reactions:

- [1] $2 \text{ diaspore} \leftrightarrow \text{corundum} + \text{H}_2\text{O}$
- [2] $\text{margarite} \leftrightarrow \text{anorthite} + \text{corundum} + \text{H}_2\text{O} + \text{CO}_2$
- [3] $3 \text{ dolomite} + \text{muscovite} \leftrightarrow \text{phlogopite} + 3 \text{ calcite} + \text{corundum} + 3 \text{ CO}_2$
- [4] $\text{calcite} + \text{spinel} + \text{CO}_2 \leftrightarrow \text{dolomite} + \text{corundum}$
- [5] $\text{muscovite} \leftrightarrow \text{K-feldspar} + \text{corundum} + \text{H}_2\text{O}$

More than one of these reactions can take place in a deposit (Garnier et al. 2008; this work). The pressure-temperature conditions of these reactions are strongly dependent on $\text{CO}_2/\text{H}_2\text{O}$ activity of the system (Fig. 1.3). In some deposits, the stability of corundum also appears to be dependent on the activity of Mg in the system; Kissin (1994) argued that the activities of Mg and CO_2 are more critical factors in corundum formation during the retrograde breakdown of spinel than the actual Al_2O_3 content of the marble. The higher the activity of Mg, the higher likelihood that spinel will be stable over corundum.

Various interpretations of the origin and mechanism of Al-enrichment in gem-corundum deposits of metamorphic origin (s.s.) exist. At the well-known Hunza Valley locality in Pakistan, aluminum enrichment in carbonate sediments due to lateritic (Okrusch et al. 1976), weathered pelitic (“terrigenous”; Rossovskii et al. 1982), and non-marine evaporate sedimentation (Garnier et al. 2008) have all been suggested. Terrigenous or non-marine evaporate sedimentation has also been proposed for other ruby localities, e.g. Jegdalek, Afghanistan; Mogok, Myanmar (Rossovskii et al. 1982, Spiridonov 1998, Garnier et al. 2008); and south-western Pamirs (Rossovskii et al. 1982). At all localities, corundum preferentially formed by reaction [4], or less commonly by reaction [5], or by a combination of [1] and [2]. Aluminum-enrichment in carbonate sediments due to lateritic weathering of an impure limestone has been well documented in the Naxos metamorphic complex where corundum forms by reaction [1] during prograde metamorphism (Feenstra and Wunder 2002).

The role of an evaporite sedimentary precursor in the origin of carbonate-hosted gem corundum occurrences has been discussed by Spiridonov (1998) and Garnier et al. (2008). For ruby deposits in central and southeastern Asia, Garnier et al. (2008) suggested that corundum precipitated from $\text{CO}_2\text{-H}_2\text{S}\text{-COS-S}_8\text{-AlO(OH)}$ -bearing fluids during retrograde metamorphism as the result of “*molten salts [that] mobilized in situ Al and metal transition*

elements contained in marbles, leading to crystallization of ruby”. The corundum formed predominantly by retrograde reaction [4] at high CO₂ fugacity, and rarely by reaction [5] at these localities.

The metasomatic origin of gem corundum deposits typically includes the interaction of carbonate rocks with mineralogically contrasting intrusive rocks, e.g., pegmatite, granite or syenite intrusions (Silva and Siriwardena 1988, Harlow et al. 2006, Rakotondrazafy et al. 2008). At the Bakamuna deposit in Sri Lanka (Silva and Siriwardena 1988), skarn mineralization occurs around a coarse-grained orthoclase-quartz-bearing pegmatite within a calcite-dolomite marble. The deposit is characterized by zones with spinel + scapolite ± corundum ± phlogopite and scapolite + corundum + spinel assemblages. Corundum is commonly replaced by spinel. The skarn formed by the interaction of Al-rich fluid from the intrusion with an impure marble. Other examples of skarn-generated corundum deposits occur in the Tranomaro area of Madagascar (Rakotondrazafy et al. 2008), where corundum formed along with meionite, spinel, and thorianite in skarn zones (scapolite + clinopyroxene ± titanite) in calcitic marble at peak P-T conditions of T ~850 °C and P ~5 kbar. The sapphire formed in late veins (K-feldspar + Fapatite + calcite + phlogopite) at T ~500 °C and P ~2 kbar. Skarn-generated corundum deposits may also occur in the Mogok Stone Tract in Myanmar (Harlow et al. 2006), where rubies are locally found with cancrinite + scapolite + sodalite ± nepheline and phlogopite ± spinel ± pargasite ± tourmaline. The rubies are interpreted to have originated from skarn metasomatism because of the typical skarn silicate mineral assemblages and because the rubies are surrounded by or are connected to skarn-silicate veins.

Terekhov et al. (1999) suggested that corundum from the Kukurt gemstone field, eastern Pamirs, Tadzhikistan, formed as a result of Al-precipitation from fluids during alkaline metasomatism of marble. Further work by Dufour et al. (2007) on the same localities suggested that the corundum-bearing lenses originated from the alkaline metasomatism of terrigenous (pelitic?) layers in marble. In the Kukurt field the corundum occurs with biotite, spinel, pyrite, tourmaline, apatite, and rutile, and minor amounts of Mg-calcite, scapolite, and muscovite.

1.5 Relevance of Proposed Study Localities

As outlined above, the origin of gem corundum (Al_2O_3) deposits remains unclear and as a result, only primitive exploration strategies exist for some deposit types. These localities are unique in terms of their mode of occurrence, mineral assemblages, age, colour, and genesis. At the Revelstoke occurrence, pink sapphire and ruby occur with muscovite, phlogopite, K-feldspar, anorthite, and accessory minerals such as rutile in thin and laterally extensive layers throughout marble lenses within a calc-gneiss unit. At the KSO, blue, yellow, and colourless sapphire occurs with albite, muscovite, calcite, scapolite, phlogopite, oligoclase, and violet diopside in pod-shaped calc-silicate lenses within a regionally extensive marble unit. An understanding of how the Revelstoke occurrence formed will be used to help determine the origin of the more complex KSO.

1.6 Previous Studies on the Revelstoke Occurrence Area

The Revelstoke occurrence is located in the Shuswap Metamorphic Core Complex (MCC), in the southern part of the Omineca belt of the Canadian Cordillera in British Columbia (Fig. 1.2). It is hosted in a marble layer within the Monashee complex cover sequence northwest of the Frenchman Cap dome. The regional geology and PT conditions affecting the Frenchman Cap dome (Brown 1980, Brown et al. 1986, Journeay 1986, Höy 1987, Johnson 2006, Crowley 1999, Crowley and Parish 2001) and nearby Thor Odin Dome (Teyssier et al. 2005, Hinckley et al. 2006, Gervais et al. 2010, and Gervais and Brown 2011) have been extensively studied and thus provide a basis for my study.

1.7 Previous Studies on the Kimmirut Sapphire Occurrence (KSO) Area

The KSO occurs in a localized area of the Paleoproterozoic Lake Harbour marble of the metasedimentary Lake Harbour Group (LHG) on Baffin Island near the town of Kimmirut, Nunavut (Fig. 1.2; LeCheminant et al. 2005, Butler 2007, Fagan & Miller 2012), as part of the Meta Incognita microcontinent (MIM) within the Quebec-Baffin segment of the Trans Hudson orogen (St-Onge et al. 1996). Various studies on the tectonostratigraphy,

polymetamorphic events (St-Onge et al. 2007), and age dating have been completed here, providing a basis for my study (Davison 1959, Jackson and Taylor 1972, Scott and Gauthier 1996, St-Onge et al. 1996, Scott 1997, Wodicka and Scott 1997, Scott and Wodicka 1998, St-Onge et al. 1998, Scott et al. 2002, and St-Onge et al. 2007).

1.8 Objectives of Thesis

The primary questions that I intend to answer in my study are:

1. How does gem corundum form in carbonate rocks at the Revelstoke occurrence and at the Kimmirut sapphire occurrence?
2. How do these localities compare to each other and to other localities in terms of: (1) the type of gem corundum present, (2) *P-T* conditions, (3) nature of the protolith, and (4) nature of the fluid?
3. Can existing models of corundum genesis explain the genesis of corundum at the Revelstoke and Kimmirut occurrences? If these models are unable to do so, new models will be proposed.
4. What is unique about these localities relative to other corundum deposits that make them conducive to the formation of gem corundum?
5. What are the implications of mode of occurrence and formation for the exploration of other deposits?

1.9 Research Approach

- In order to address the objectives, I determined the following for each occurrence:
- (1) The nature of the protolith. The localities that I am studying have been metamorphosed to upper amphibolite-granulite facies; as a result, the nature of the protolith is not

obvious from field observations. Whole rock geochemistry, mineral associations, and oxygen isotopes were used to determine the protolith and source of aluminum and chromophores. I also compared my results to other gem-corundum localities to determine similarities and differences.

- (2) Conditions of formation. This study addresses how the protolith was affected during deformation and metamorphism and the conditions necessary for corundum formation. I determined the *P-T* conditions and fluid characteristics that affected the corundum-bearing zones.
- (3) The influence of local and regional geology on mineralization. This study examined the unique geological environment at each corundum-bearing locality, including stratigraphic, structural, and metasomatic controls on mineralization.
- (4) The role of marble in corundum formation. This study determined that the silica-depleted environment and production of CO₂ during decarbonation assisted in corundum formation.

The answers to these questions were used to evaluate existing models of gem corundum formation and were used to propose new models for the Revelstoke and Kimmirut occurrences. Similarities and differences between the different localities were outlined new exploration strategies were developed.

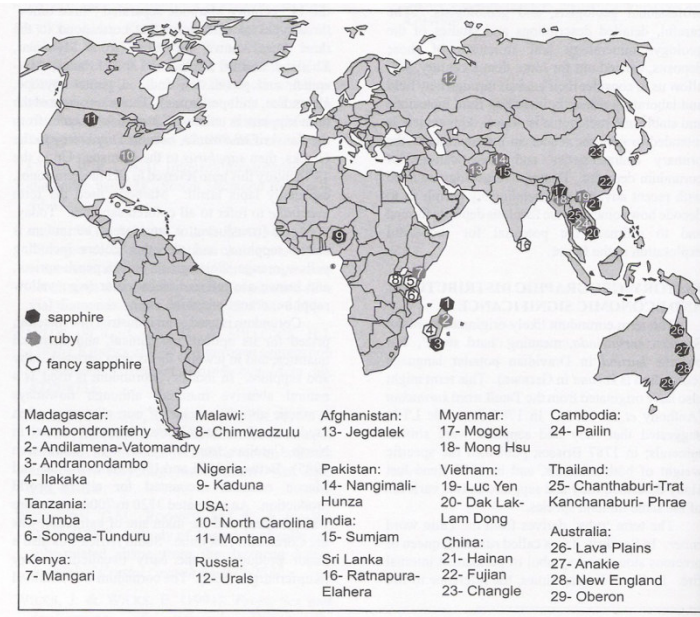


Figure 1.1: Major and minor commercial world sources of gem corundum (Giuliani et al. 2007).

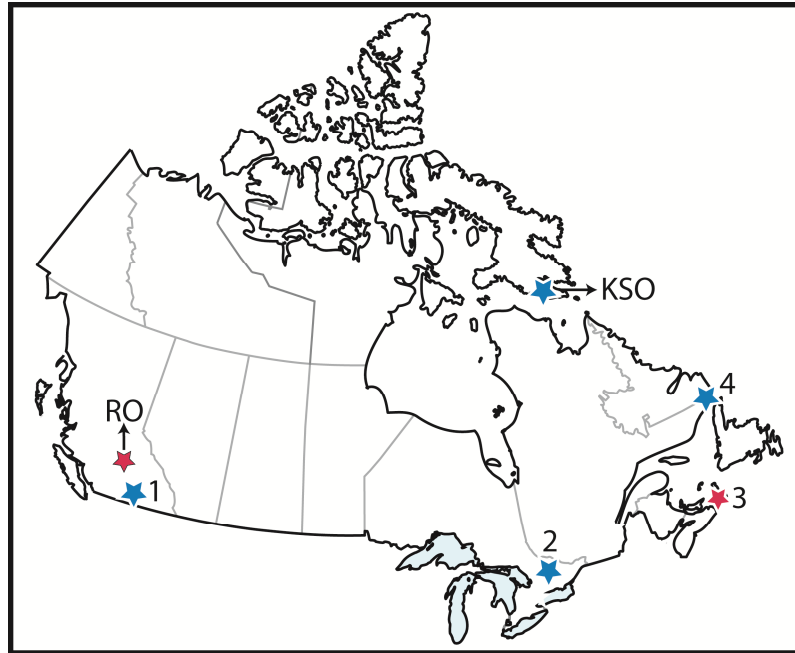


Figure 1.2: Map of Canadian gem corundum localities. Blue stars indicate sapphire occurrences, and red stars indicate ruby and pink sapphire occurrences. The study localities are denoted by RO = Revelstoke Occurrence and KSO = Kimmirut Sapphire Occurrence, and other Canadian localities are denoted as: 1 = Slocan Valley, 2 = Bancroft-York River area, 3 = Nova Scotia, 4 Labrador.

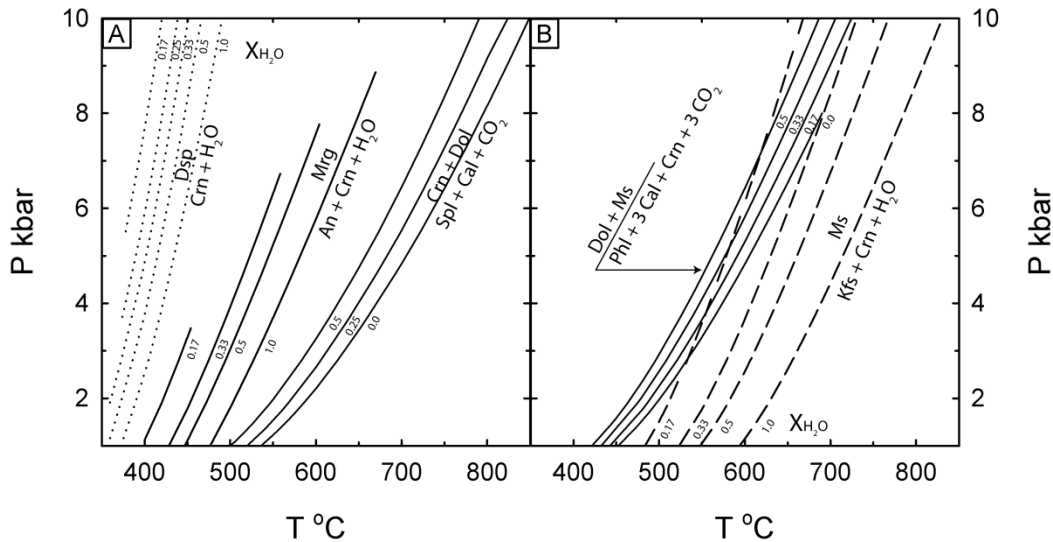


Figure 1.3: Calculated theoretical corundum-producing reactions at different $X_{\text{H}_2\text{O}}$ [$X_{\text{H}_2\text{O}} = \text{H}_2\text{O}/(\text{H}_2\text{O}+\text{CO}_2)$]. Mineral equilibria were calculated with the program Theriault-Domino (de Capitani and Petrakakis 2010) using end member compositions and the internally consistent thermodynamic database of Holland and Powell (1998). A) Breakdown of diaspore, margarite, and spinel. B) Breakdown of muscovite.

Chapter 2: Methods

At the Revelstoke occurrence, samples of the host gneiss, marble, and corundum-bearing mica-feldspar layers within marble were sampled from both float and outcrop. Outcrop samples were collected from two parallel north-south traverses across the marble unit including samples of the host gneiss at both the north and south contacts. Calc-silicate samples from the Kimmirut Sapphire Occurrence were collected by Lee Groat and True North Gems from the Beluga pit using a rock saw.

Representative polished thin sections of host gneiss, marble, and corundum-bearing calc-silicate layers within marble were studied using optical and scanning electron microscopy (SEM) and cathodoluminescence (CL) microscopy to characterize the minerals and determine the paragenetic sequence.

Whole rock major and trace element analyses of the major rock types were done at ALS Chemex in Vancouver using a combination of ICP-AES and ICP-MS (package CCP-PKG01). Chondrite normalization after Sun and McDonough (1989) is used for data presentation.

Chemical compositions of minerals were determined using a fully automated CAMECA SX-50 electron microprobe, operating in the wavelength-dispersion mode. The following operating conditions were used for feldspars, scapolite, rutile: excitation voltage, 15 kV; beam current, 20 nA; peak count time, 20 s; background count-time, 10 s; spot diameter, 5 µm. The following operating conditions were used for corundum: excitation voltage, 15 kV; beam current, 40 nA; peak count time, 20 s for Al, 180 s for others; background count-time, 10 s for Al, 90 s for others; spot diameter, 10 µm. The following operating conditions were used for calcite: excitation voltage, 15 kV; beam current, 10 nA; peak count time, 20 s; background count-time, 10 s; spot diameter, 5 µm. The following operating conditions were used for amphibole and pyroxene: excitation voltage, 15 kV; beam current, 20 nA; peak count time, 20 s (40 s for F, Cl); background count-time, 10 s (20 s for F, Cl); spot diameter, 5 µm. The following operating conditions were used for micas: excitation voltage, 15 kV; beam current, 10 nA; peak count time, 20 s (40 s for F, Cl); background count-time, 10 s (20 s for F, Cl); spot diameter, 10 µm. Data reduction was done using the 'PAP' $\phi(\rho Z)$ method (Pouchou and Pichoir 1985). The standards used are listed in tables containing the analytical data within Appendix A and B of this thesis.

The carbon and oxygen stable isotopic composition of carbonate from the Revelstoke occurrence was analyzed using different techniques at different labs. Whole rock carbonate and calcite mineral separates were analyzed at the Pacific Centre of Isotopic and Geochemical Research at UBC in Vancouver, Canada. Analyses were carried out using the gas bench and a Delta PlusXL stable isotope ratio mass spectrometer in continuous flow mode. Samples were acidified with 99% phosphoric acid in helium-flushed sealed vials, and the headspace gas was measured in a helium flow. The $\delta^{13}\text{C}$ (VPDB) and $\delta^{18}\text{O}$ (VSMOW) results are based on an average of multiple analyses of NBS-18 and -19 standards. The analyses were corrected for fractionation using repeated analyses of UBC internal carbonate standards BN 13, BN 83-2, and H6M, which were previously calibrated against NBS-18 and -19.

Carbonate drill powder analyses were also performed at UBC using the Mineral Deposit Research Unit Mineral Isotope Analyzer (MDRU-MIA; Barker et al. 2011). Samples were acidified with 85% phosphoric acid in sealed, non-flushed glass vials and the headspace gas was measured. The analyses were corrected for fractionation using repeated analyses of UBC internal carbonate standards BN 13, BN 83-2, and H6M, which were previously calibrated against NBS-18 and -19.

A majority of the carbonate $\delta^{13}\text{C}$ and $\delta^{18}\text{O}$ values collected by the Stable Isotope Ratio Mass Spectrometer (IRMS) and the Mineral Isotope Analyzer (MIA) correlate within error (Fig. 2.1). Interpretations of data collected by these two methods can be made with confidence.

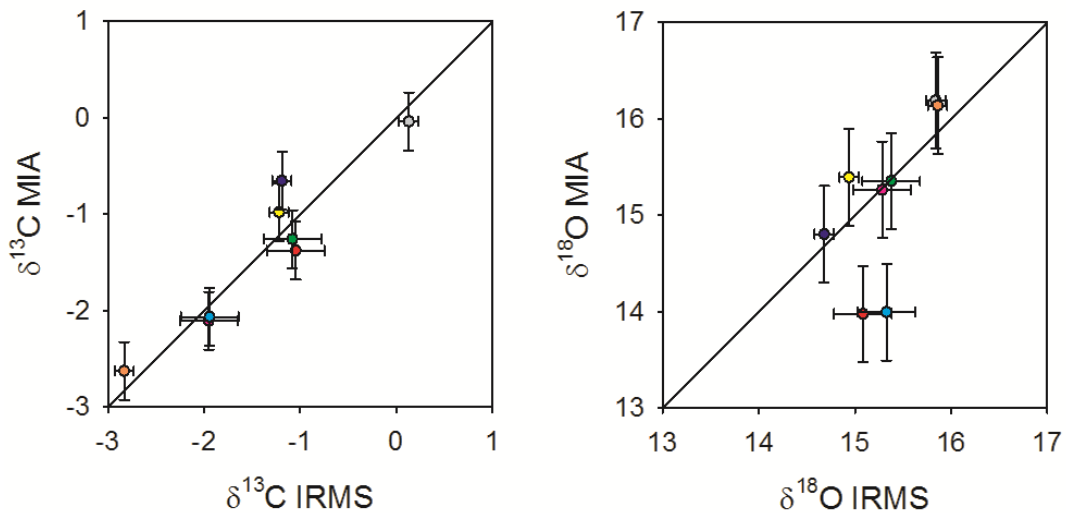


Figure 2.1: Comparison of $\delta^{13}\text{C}$ and $\delta^{18}\text{O}$ values collected using an Isotope Ratio Mass Spectrometer (IRMS) and Mineral Isotope Analyzer (MIA).

Whole rock carbonate and silicate analyses were performed at Queen's Facility for Isotope Research, Queen's University, Canada. Analyses were carried out using the Finnigan GasBench II and a Finnigan MAT 252 isotope-ratio mass spectrometer. The analytical procedure was analogous to that used by Uvarova et al. (2011).

Corundum $\delta^{18}\text{O}$ analyses were performed at the Isotope Geosciences Unit, Scottish Universities Environmental Research Centre, Glasgow Scotland, using the method described by Giuliani et al. (2005). Only unaltered corundum grains embedded in calcite were analyzed.

Ar-Ar dating of muscovite and phlogopite from corundum-bearing calc-silicate layers were analyzed at the Noble Gas Laboratory, Pacific Centre for Isotopic and Geochemical Research (PCIGR), University of British Columbia, Vancouver, BC, Canada. Mineral separates were hand-picked, washed in acetone, dried, wrapped in aluminum foil and stacked in an irradiation capsule with similar-aged samples and neutron flux monitors (Fish Canyon Tuff sanidine, 28.02 Ma; Renne et al., 1998). The samples were irradiated at the McMaster Nuclear Reactor in Hamilton, Ontario, for 90 MWH, with a neutron flux of approximately 6×10^{13} neutrons/cm²/s. Analyses ($n = 45$) of 15 neutron flux monitor positions produced errors of <0.5% in the J value. Subsequently, they were analyzed at PCIGR. The mineral

separates were step-heated at incrementally higher powers in the defocused beam of a 10W CO₂ laser (New Wave Research MIR10) until fused. The gas evolved from each step was analyzed by a VG5400 mass spectrometer equipped with an ion-counting electron multiplier. All measurements were corrected for total system blank, mass spectrometer sensitivity, mass discrimination, radioactive decay during and subsequent to irradiation, as well as interfering Ar from atmospheric contamination and the irradiation of Ca, Cl, and K. The plateau and correlation ages were calculated using Isoplot ver.3.09 (Ludwig, 2003). Errors are quoted at the 2-sigma (95% confidence) level and are propagated from all sources except mass spectrometer sensitivity and age of the flux monitor. The best statistically justified plateau and plateau age were picked based on the following criteria: (1) three or more contiguous steps comprising more than 50% of the ³⁹Ar; (2) probability of fit of the weighted mean age greater than 5%; (3) slope of the error-weighted line through the plateau ages equals zero at 5% confidence; (4) ages of the two outermost steps on a plateau are not significantly different from the weighted-mean plateau age (at 1.8 σ , six or more steps only); and (5) outermost two steps on either side of a plateau must not have nonzero slopes with the same sign (at 1.8 σ , nine or more steps only).

Mineral abbreviations used follow Whitney and Evans (2010).

Chapter 3: Revelstoke Occurrence: High-pressure Origin of Gem Corundum in Micaceous Layers in Marble

3.1 Introduction

A carbonate-hosted gem corundum locality northwest of Revelstoke in British Columbia (at 51° 31.3' N, 118° 46.7' W, 82M/10) was staked as the Goat claims by Bradley S. Wilson in 2002 (Fig. 3.1). Several gem-quality sapphires and rubies from this locality have been faceted with the largest being slightly less than 0.5 ct. (Fig. 3.2A,B).

The objectives of this work are to: 1) characterize the geology, geochemistry, mineralogy, and corundum fluid inclusions; 2) compare the mineralogy and geochemistry of different lithologies at the occurrence, and 3) identify a genetic model of mineralization at the Revelstoke occurrence in order to develop an exploration strategy for this type of deposit.

3.2 Geological Setting

The Revelstoke occurrence is located in the Shuswap Metamorphic Core Complex (MCC), in the southern part of the Omineca belt of the Canadian Cordillera in British Columbia. It is hosted in a marble layer within the Monashee complex cover sequence northwest of the Frenchman Cap dome (Fig. 3.1A,B).

The Omineca Belt is a northwest trending uplifted region of metamorphic and plutonic rocks separating accreted terranes from the ancestral North America continental margin in the Canadian Cordillera (Johnson 2006). Rocks within the Omineca Belt are typically highly deformed and variably metamorphosed.

The Shuswap MCC is the most deeply exhumed part of the southern Omineca Belt in the core of the Canadian Cordillera (Johnson 2006). The Monashee complex is the lowest exposed part of the Shuswap MCC and is the largest exposure of Precambrian crystalline rock in the Canadian Cordillera (Crowley 1999). The Monashee complex, which contains the Frenchman Cap dome to the north and the Thor-Odin dome to the south (Fig. 3.1B), is bounded by the Monashee décollement in the west and the Columbia River fault in the east (Brown 1980, Brown et al. 1986, Journeay 1986, Johnson 2006, Crowley 1999).

During the formation of the Frenchman Cap and Thor-Odin domes, initial compressional tectonism was succeeded by extension of the orogen along the Columbia River and Okanagan-Eagle River fault system following a path of isothermal decompression and isobaric cooling. The exact mechanism of decompression and uplift is discussed by Teyssier et al. (2005), Hinckley et al. (2006), Gervais et al. (2010), and Gervais and Brown (2011). All suggest similar P-T paths with peak metamorphic conditions of ca. 750-800 °C and 8-10 kbar followed by isothermal decompression to 300-150 °C and <5 kbar. The observed inverted metamorphic gradient in the northern part of the Frenchman Cap dome (Journeay 1986) was explained by Crowley and Parish (2001) as a juxtaposition of high-grade rocks over a lower-grade metapelitic rock sequence with regular metamorphic zonation. The Monashee décollement was active during both Mesozoic orogenesis (Read and Brown 1981) and early Tertiary (~58 Ma) extension and uplift (Lane 1984). Work by Crowley and Parrish (1999) shows that the pelitic schist which borders the marble hosting the Revelstoke occurrence has thermal peak U-Pb monazite and zircon ages that range from 57 to 51 Ma.

3.3 Lithological Units of the Monashee Complex

The Monashee complex contains Paleoproterozoic to Cambrian shallow marine metasedimentary cover rocks up to 2-3 km thick which unconformably overlay a core of Paleoproterozoic basement migmatitic paragneiss and granitoid orthogneiss rocks (Crowley 1999, Crowley et al. 2001). Höy (1987) suggested the marble-hosting metapelitic sedimentary sequence in the northern part of the Frenchman Cap dome was deposited on a shallow marine shelf to intertidal platform environment. He interpreted the scapolite-bearing metapelitic assemblages as former muds and silts with varying amounts of carbonate that were deposited under saline conditions, with halite as a possible constituent of the original sedimentary rock.

According to Höy (1987), the stratigraphic succession of autochthonous cover rocks above the basement gneiss is divided into three units (Fig. 3.1C): the lower assemblage (Unit 3, quartzite), the middle assemblage (Unit 4, calcareous and pelitic schists with the extrusive Mount Grace carbonatite, and Unit 5, marble), and the upper assemblage (Unit 6a,b,

calcareous and pelitic schist). The Revelstoke gem corundum occurrence occurs in a marble layer within the upper assemblage (Unit 6a).

The upper assemblage is divided into two parts. Unit 6a contains interlayered light grey to green scapolite-bearing calc-silicate gneiss and sillimanite schist, an impure marble (which hosts the corundum), and the Cottonbelt sulfide-magnetite layer, which is interpreted as a sedimentary-exhalative (SEDEX) deposit with some features of Broken Hill-type deposits (Höy 2001). Unit 6b contains interlayered sillimanite schist, quartz feldspar gneiss, thin chert, and impure quartzite layers (Höy 1987).

3.4 Geology and Petrography of the Revelstoke Occurrence

The corundum-bearing marble is exposed for several kilometers along strike within unit 6a (Fig 3.1C) and is bounded on both sides by a heterogeneous calc-gneiss with pelitic layers (Fig 3.3A,B). The boundaries between the marble and the host gneiss are sharp, but intercalations of the marble with gneiss layers at the boundaries are common. Minor sediment-hosted Pb-Zn ("SEDEX") mineralization is associated with the marble layer, especially west and north of the studied area (Höy 2001). The host rocks and the marble are extensively folded.

Rock samples were obtained from boulders of marble float with common corundum and green muscovite, as well as from a marble outcrop with common green muscovite and rare corundum (outcrop 1), and a marble outcrop with common scapolite and rare corundum and muscovite (outcrop 2; Fig. 3.1C). Samples of gneiss and various layers in marble (diopside, magnetite, graphite, and garnet) were collected from the outcrops. A sample of SEDEX mineralization in contact with marble was observed near outcrop 2. A tourmaline sample was collected between the float locality and outcrop 1. Mineral assemblages for all lithologies are in Table 3.1.

3.4.1 Marble

The marble is composed of fine- to medium-grained calcite; only very rare dolomite was observed at the contact with the host rock and as microscopic relicts in calcite within the magnetite-rich layers. The calcite matrix contains impure siliceous and non-siliceous

laminations and layers, generally parallel to the contact. The siliceous layers can be divided into 3 contrasting types: (1) mica-feldspar-bearing (with corundum; Fig. 3.3C); (2) diopside-tremolite-bearing (Fig. 3.3D); and very rare (3) diopside-garnet-amphibole-scapolite-bearing. The non-siliceous layers are graphite- and/or magnetite-bearing (Fig. 3.3E). The graphite layers are more common than the siliceous ones, and the magnetite layers are relatively rare. The marble is commonly folded, with boudins and broken grains of feldspars and scapolite enclosed in deformed mica-feldspar-bearing layers. The marble locally shows evidence of post-metamorphic pressure-induced calcite grain boundary migration recrystallization and cataclasis. Rare cross-cutting calcite veins with deformed coarse-grained carbonate crystals in a fine-grained matrix have been observed.

3.4.2 Mica-Feldspar-Rich Layers

Mica-feldspar-rich layers with minor corundum (Fig. 3.3C) are dispersed throughout the marble unit and individual layers can be traced for several tens of meters on the outcrop surface. They range in thickness from 1 to 20 cm and are thickest near the contact with the host gneiss. The grain size ranges from ~0.1-40 mm. The layers are foliated, and are commonly folded and boudinaged (Fig. 3.3F).

The layers are locally mineralogically zoned (Fig. 3.4); they contain green muscovite aggregates rimmed by anorthite, K-feldspar, phlogopite, and corundum (zone 1), which are enclosed by calcite + phlogopite ± plagioclase ± K-feldspar ± corundum (zone 2). Surrounding calcite layers (zone 3) rarely contain crystals of corundum or aggregates of anorthite + K-feldspar + muscovite, which are isolated from the adjacent silicate layer due to shearing of the marble. Zones 1 and 2 sometimes contain minor amounts of scapolite; zones 2 and 3 may also contain accessory quartz. Corundum can occur in all three zones, but it has never been observed in contact with quartz.

Zone 1 contains deformed lensoidal aggregates of green muscovite (V- and Cr-bearing) which are commonly rimmed by phlogopite, anorthite, K-feldspar and minor corundum (Figs. 3.3C, 4, 5A-D). Anorthite and K-feldspar usually contain common inclusions of coarse-grained phlogopite, muscovite and calcite, and minor rutile and apatite. Muscovite aggregates contain only minor fine-grained phlogopite, rutile, apatite and rare zircon and Th-rich uraninite (Fig. 3.5A,B). Anorthite and K-feldspar can occur as isolated grains in the

calcite matrix or they can occur as aggregates of intergrown crystals with K-feldspar typically concentrated around the rim of the aggregates as the latest phase. K-feldspar grains are commonly zoned and enriched in Ba on their rims (Fig. 3.5C). Phlogopite in the marble is rarely overgrown by muscovite. Pseudomorphs after titanite are locally present as an assemblage of rutile + K-feldspar + anorthite ± calcite ± titanite in the muscovite aggregates. Where large rutile inclusions are in contact with calcite or anorthite, newly formed titanite is rarely observed.

Zone 2 is characterized by calcite with dispersed phlogopite, anorthite, K-feldspar, and minor aggregates of anorthite and K-feldspar with relict muscovite. Accessory phases present in this zone are corundum, scapolite, and rutile, along with trace amounts of apatite, Fe-oxide, graphite ± quartz ± pyrite. Scapolite locally occurs as isolated anhedral grains replacing anorthite, or as euhedral crystals in sulfide-filled pockets in carbonate veinlets.

Zone 3 marble layers contain calcite ± trace quartz ± apatite ± euhedral corundum. The calcite in the marble layers is mostly coarse-grained (0.5-2 mm), although it is locally rimmed by fine-grained calcite (<0.1 mm) as a result of recrystallization. Apatite and quartz occur with the fine-grained calcite, but their crystals are rounded and not recrystallized.

Corundum occurs in three morphological types: (1) euhedral, sometimes zoned crystals or their fragments enclosed in Zone 1, in feldspars or in muscovite aggregates (Fig. 3.5D,E); (2) euhedral zoned corundum with calcite inclusions, enclosed in calcite or in feldspar on the border of muscovite aggregates (Zones 2 and 3; Fig. 3.5F); and (3) fine-grained aggregates of corundum with very common inclusion of rutile and apatite, enclosed in feldspar or calcite (Zones 2 and 3; Fig. 3.5G). The euhedral type (1) forms crystals ~3-10 mm in diameter, with minor euhedral inclusions of rutile, apatite and rare zircon; in mica-feldspar aggregates it locally encloses grains of muscovite and Ba-rich K-feldspar. Rare inclusions of anorthite were found in anorthite-rimmed corundum. In phlogopite-rich mica-feldspar layers, corundum may enclose phlogopite crystals. The euhedral corundum type (2) forms large crystals up to 3 cm long and 1 cm wide, with an average width of 5-10 mm, sometimes with typical hexagonal dipyramids. The corundum crystals usually contain rounded inclusions of calcite, and if the inclusions are abundant, they give the crystals a skeletal appearance. The fine-grained type (3) grain size is generally less than 1 mm. The aggregates are usually rather small (<1 cm), sometimes intergrown with Ba-rich K-feldspar

or anorthite, overgrown by phlogopite and can be strongly altered. All of the corundum types seem to have non-preferred orientations.

In some instances euhedral crystals of scapolite replace anorthite; they can enclose common muscovite. Corundum associated with anorthite, scapolite and K-feldspar was replaced by margarite or Ba-enriched muscovite where it was accessible to late fluids (Fig. 3.5G).

3.4.3 Diopside-Tremolite Laminations

Laminations with common fibrous tremolite replacing euhedral crystals of diopside occur sporadically throughout the marble unit (Fig. 3.3D). The laminations are occasionally folded and vary in grain size and thickness; euhedral diopside crystals can be up to 8 cm long (typically 2-4 cm), and the thickness ranges between 1 and 15 cm. The pseudomorphed diopside grains contain tremolite with very small quartz and calcite blebs. Graphite laminations sometimes intersect the diopside-bearing layers as veinlets along the intergranular spaces between calcite grains; graphite aggregates form around the tremolite pseudomorphs and around diopside relics within them. A rare prograde tremolite + calcite assemblage was found in the marble.

3.4.4 Minor Assemblages in the Marble

Very rare diopside-garnet-K-amphibole-scapolite assemblage was found close to a rare quartz lens in the marble. Garnet and diopside are primary minerals in the assemblage. The garnet is rimmed by coronas of scapolite and Na-K-amphibole (major ferropargasite and minor hastingsite). The Na-K amphibole appears to replace diopside when in contact with garnet and scapolite (Fig. 3.5H), otherwise the diopside is replaced by tremolite.

A single sample of a fine-grained aggregate of brown tourmaline was found in a coarse-grained calcite layer. The tourmaline rarely forms euhedral crystals up to 5 mm in a calcite pockets.

3.4.5 Non-Siliceous Laminations

Rare magnetite-rich layers occur in the marble. The magnetite is enclosed in calcite with relicts of dolomite. The graphite laminations are common throughout the marble and

they also occur as irregular veinlets in other zones. In most cases they appear to post-date the metamorphic assemblages.

3.4.6 Brittle Deformation in Marble

Cataclasite zones extend for many meters on the surface of the outcrop and vary in grain size and mineral abundance (Fig. 3.3D). Their thickness ranges from 1 mm to 20 cm. The amount of grain size-reduction varies depending on the abundance of mineral phases. Very fine-grained laminations are very dark and typically contain graphite, apatite, and pyrite, whereas coarser laminations are grey in color and contain more silicate minerals.

The matrix of the cataclasites is composed of fine-grained calcite. Its grain size is highly variable, ranging from below 0.2 mm (the prevailing fraction) to deformed grains up to 4 mm. The matrix contains abundant graphite and broken and deformed rounded grains (<0.5 mm) of apatite, anorthite, K-feldspar, pyrite, titanite, \pm scapolite \pm Fe-oxide \pm quartz \pm corundum. Some relict muscovite-K-feldspar and K-feldspar-anorthite aggregates remain in the fine-grained areas. Anorthite and minor K-feldspar grains are altered to muscovite, quartz, and albite. Pyrite and titanite occur both as euhedral grains and as broken to anhedral fragments. Graphite, pyrite, and fine-grained muscovite locally rim silicate and apatite grains. One corundum grain enclosed in anorthite was found in the fine-grained cataclasite.

Carbonate near the cataclasite zones shows extremely irregular and lobate grain borders due to extensive grain boundary migration recrystallization. This feature gradually disappears away from the cataclasite zones.

3.4.7 Calc-Gneiss

The calc-gneiss, which hosts the marble, is strongly foliated, with biotite and feldspathic leucosome layers defining the foliation of the rock (Fig. 3.3B). The gneiss is inhomogeneous and contains variable proportions of Ca-rich minerals; with increasing calcium in the rock, diopside, K-feldspar, calcite, and titanite increase in abundance, and biotite, quartz, plagioclase, and garnet decrease. The rock fabric is heterogeneous with: (1) K-feldspar and diopside-rich (Fig. 3.6A,B), (2) plagioclase-rich (Fig. 3.6C), and (3) biotite-rich/pelitic layers (Fig. 3.6D,E). Trace amounts of graphite are locally present. All minerals are anhedral with the exception of subhedral diopside and titanite.

The K-feldspar and diopside-rich layers contain the stable assemblage K-feldspar (Or_{90-95}) + diopside \pm titanite \pm phlogopite \pm plagioclase (~An₉₃). The diopside grains contain inclusions of titanite and allanite, and are enclosed in K-feldspar and minor plagioclase; sometimes they are overgrown by phlogopite ($X_{\text{Mg}} \sim 0.4-0.6$). Rare garnet (~Alm₅₂₋₅₃Grs₃₁₋₄₀) was observed in an assemblage with clinopyroxene (Wo₄₇₋₄₉En₂₅₋₃₅Fs₁₆₋₂₇), K-feldspar, and minor plagioclase (Fig. 3.6B). Myrmekites are frequent on the plagioclase contacts with K-feldspar. The assemblage of tremolite + calcite + quartz and later phlogopite commonly replace diopside; phlogopite is replaced by chlorite.

Plagioclase-rich layers with stable assemblage plagioclase feldspar (An₉₁₋₉₄) + calcite + clinopyroxene (Wo₄₈En₂₆Fs₂₅) \pm K-feldspar ($\text{Or}_{91-93}\text{Ab}_{7-9}$) \pm titanite \pm scapolite typically contain diopside and scapolite in the plagioclase matrix, together with common titanite, K-feldspar, calcite, and rare quartz. Scapolite may occur as inclusions in diopside (Fig. 3.6C). K-feldspar in the matrix has tartan twinning and contains inclusions of diopside and biotite; K-feldspar rimming diopside porphyroblasts does not show twinning. Replacement of diopside by tremolite or phlogopite is common.

The less-common biotite-rich pelitic layers (biotite + quartz + plagioclase feldspar \pm garnet) are up to 30 cm thick, fine-grained, heterogeneous, and foliated, with thin layers of feldspar-rich leucosome containing rare garnet porphyroblasts; biotite, kyanite, sillimanite, and late-stage hematite are major minerals defining the foliation in the rock (Fig. 3.6D,E,F). The typical mineral assemblage in the biotite-rich layers is K-feldspar (~Or₉₃Ab₇) + quartz + biotite ($X_{\text{Mg}} \sim 0.45-0.55$) + kyanite/sillimanite + garnet + plagioclase, where the quartz is always enclosed in K-feldspar. Garnet porphyroblasts are usually corroded, rimmed by plagioclase (An₃₃₋₅₀)-quartz-kyanite/sillimanite leucosome and together with K-feldspar replaced by biotite, or by chlorite and muscovite; relic grains of K-feldspar in biotite typically display myrmekitic textures. In some samples, the original biotite + kyanite + K-feldspar + quartz assemblage was replaced by the assemblage biotite + sillimanite + muscovite \pm K-feldspar \pm kyanite. Common zoned tourmaline crystals were observed replacing biotite, sillimanite and plagioclase (Fig. 3.6E). Accessory phases include allanite, graphite, fluorapatite, zircon, monazite and rutile. The andalusite and cordierite identified by Höy (1987) were not observed in this study.

Porphyroblasts of plagioclase ($\sim\text{An}_{47}$) and garnet ($\sim\text{Alm}_{66-69}\text{Grs}_{17-21}$) are common in sillimanite-free assemblages (Fig. 3.6F). The lens-shaped, twinned plagioclase grains ($\sim\text{An}_{47}$) up to 2 mm in diameter have abundant randomly oriented inclusions of quartz, minor biotite, and graphite \pm apatite. The garnet porphyroblasts (4-8 mm) contain abundant inclusions of quartz, minor plagioclase, biotite, chlorite, ilmenite, rutile, and rare kyanite; the inclusions form trails with curved ends indicating syn-metamorphic origin. Relics of an equilibrium assemblage of biotite + plagioclase feldspar + kyanite + quartz were observed in garnet, equivalent to the metamorphic peak reaction biotite + albite + sillimanite + quartz = garnet + K-feldspar + liquid observed by Hinckley et al. (2006) in the Thor-Odin dome. The rock displays evidence of syn-kinematic partial melting, e.g., poorly developed layers and ribbons of plagioclase + quartz leucosome, myrmekites, or concentration of accessory phases in pressure shadows of porphyroblasts and in the leucosome.

3.4.8 SEDEX Mineralization

One sample of olivine-hedenbergite rock in contact with marble was found near the contact of marble with calc-gneiss. Sulfide minerals form void fillings and veinlets within secondary assemblages together with coarse grained aggregates of graphite. Olivine ($\text{Fa}_{87}\text{Fo}_{10}\text{Tep}_3$ in the core to $\text{Fa}_{89}\text{Fo}_8\text{Tep}_4$ on the grain rim) and hedenbergite ($X_{\text{Mg}}\sim 0.4$) are partially replaced by secondary amphiboles. The sulfide minerals are sometimes altered to Fe-oxides. Associated calcite appears to be in equilibrium with olivine.

3.5 Mineralogy

3.5.1 Corundum

Most of the studied corundum is pink, but blue, violet and colorless varieties were found as well. The amount of gem-quality material is limited and a very small percentage can be called ruby.

Some crystals have a pink core and blue-violet rim alternating with colorless zones. Growth zoning is visible in the pink grains under cathodoluminescence. All except the small amount of colorless material fluoresce brilliantly in long wave ultraviolet light. The pink

corundum is characterized by elevated contents of Cr₂O₃ and low to moderate amounts of TiO₂ (Fig. 3.7, Appendix A.1). The blue corundum is enriched in TiO₂; the Fe₂O₃ content in such grains is generally similar to that in the pink variety, ranging from 0.01 to 0.07 wt.%. Contents of V₂O₃ are low in both varieties (usually <0.03 wt.%). The colorless variety exhibits extremely low contents of all trace elements (Fig. 3.7).

3.5.2 Calcite and Dolomite

Calcite is the dominant carbonate in the marble. It contains only trace amounts of MgO (<1.1 wt.%), FeO (<1.8 wt.%), and MnO (<0.63 wt.%; Appendix A.2). There is a slight enrichment in Mn and Fe near the contact with the gneiss. There is also a slight enrichment in FeO near the contact of mica-feldspar layers with marble. The trace MgO contents appear to vary randomly within the marble body. Dolomite was identified in a single sample by powder XRD, but was not analyzed by EPMA. Dolomite was also identified as small relict crystals within calcite in a magnetite-rich layer in the marble.

3.5.3 Trioctahedral Mg,Fe-Micas

Phlogopite from the float locality was observed in two textural and compositional varieties. Rare phlogopite that occurs as inclusions within calcite grains in the carbonate matrix shows elevated contents of V (0.05-0.08 apfu), Ti (0.1-0.12 apfu), and Cr (0.012-0.016 apfu). The most common phlogopite type occurs within mica-feldspar layers, either in the calcite matrix or rimming muscovite aggregates. It has higher contents of Al (~1.9 apfu), and lower contents of the trace elements (<0.025 apfu V; 0.06-0.10 apfu Ti; 0-0.011 apfu Cr). Both phlogopite varieties contain low contents of F (0.05-0.2 apfu), Na (<0.025 apfu) and Ba (<0.05 apfu). In rocks from both outcrop locations phlogopite was observed as inclusions in anorthite (aggregates with Ba-rich K-feldspar ± corundum); it shows significantly elevated contents of Fe (0.25-0.35 apfu) compared to the normal values for phlogopite in samples from the float (Fig. 3.8; Appendix A.3). Several trace elements in phlogopite (e.g., F, Ti, and Ca) are on average slightly higher in samples from outcrop locations.

The K,Mg-micas observed in the marble represent a solid solution between major phlogopite (42-77 %) and eastonite (42-0 %), minor muscovite and low amounts of oxy-phlogopite and kinoshitalite/ganterite components. Although Ba and Ti could substitute for

K and Mg in the phlogopite structure as a kinoshitalite component, their high ratio and negative correlation of Ti and Mg suggest that they enter the mica independently by substitutions $\text{BaAlK}_{-1}\text{Si}$ (phlogopite/muscovite – kinoshitalite/ganterite), and $(\text{Ti}\square)\text{Mg}_{-2}$ (phlogopite – oxy-phlogopite). Barium-rich phlogopite is a common accessory mineral in marbles or schists associated with metavolcanics (Bol et al. 1989) or with base metal and barite hydrothermal deposits (e.g., Pan and Fleet 1991, Doležalová et al. 2006).

Fe,Mg-micas from the host rocks show significantly higher Fe/Mg ratio, lower amounts of $^{[6]}\text{Al}$ and elevated contents of Ti (<0.29 apfu) compared to micas from marble. Micas from diopside-rich layers contain higher amounts of $^{[4]}\text{Al}$ than those in biotite-rich layers. Host rock micas are solid solution between major annite and phlogopite, and minor eastonite and siderophyllite. The major substitutions are $\text{Al}_2(\text{Mg},\text{Fe})_{-1}\text{Si}_{-1}$ (to eastonite/siderophyllite), $\text{Al}_2\square(\text{Mg},\text{Fe})_{-3}$ (muscovite) and FeMg_{-1} .

3.5.4 Muscovite and Margarite

Muscovite in marble contains elevated contents of Ti (≤ 0.094 apfu) and Mg (≤ 0.297 apfu); contents of Fe, Ba, and Na are low (Fig. 3.9; Appendix A.4). The main chromophores responsible for the green color in micas (Cr and V) are present in trace amounts only; the green muscovite contains 0-0.23 wt.% Cr_2O_3 (0.07 wt.% avg; < 0.013 apfu) and 0-0.29 wt.% V_2O_3 (0.09 wt.% avg; < 0.016 apfu). While contents of V^{3+} increase with Ti, Cr^{3+} does not show a similar trend in most samples, although its ionic radius is more similar to that of Ti^{4+} in octahedral coordination (Shannon 1976). The composition of some of the muscovite from outcrop is enriched in Ba and Fe + Mg compared to the majority of data from both float and outcrop localities (Fig. 3.9). The enrichment is related to patchy zoning in muscovite inclusions in K-feldspar replacing the muscovite aggregates.

Fine-grained margarite locally replaces corundum crystals along fractures and rims. Its composition is $(\text{Ca}_{0.82}\text{Na}_{0.11}\text{K}_{0.07})\text{Al}_{3.84}\text{Si}_{2.16}\text{O}_{10}(\text{OH})_2$, and it contains minor paragonite and muscovite components. The high Na content is similar to the composition of retrograde scapolite and rare albite.

3.5.5 Feldspars

The prevailing feldspar in the mica-feldspar layers is plagioclase. Its composition ranges from $An_{0.85}$ to $An_{1.00}$, but most of the data fall in the range $An_{0.90}$ to $An_{0.98}$ (Fig. 3.10; Appendix A.5). The outcrop samples are less variable (An_{89} - An_{97}). Contents of trace elements (K, Ba, Fe) are below their detection limits.

The compositional data for K-feldspar in the mica-feldspar zones show low amounts of Na (Ab_{3-10}) and elevated contents of Ba, ranging from ~0.02 to 0.16 apfu (Appendix A.5), falling in the field of hyalophane (Deer et al. 2001). The highest Ba and Na-contents were found in anhedral grains of fine-zoned K-feldspar around muscovite aggregates (especially from the outcrop) where it forms at the expense of Ba-bearing muscovite.

3.5.6 Scapolite

Scapolite from mica-feldspar layers exhibits narrow compositional variability in meionite-marialite components ranging in X_{Ca} [$Ca/(Ca + Na + K)$] from ~0.66-0.80, except for two isolated analytical spots from tips in a carbonate pocket showing only $X_{Ca} \sim 0.48$ (Fig. 3.11; Appendix A.6). The Cl contents between 0.05 and 0.27 apfu are lower than expected for ideal marialite-meionite solid solution due to a significant “mizzonite” component (Na-bearing, Cl-free meionite) introduced in the scapolite structure by the substitution $(NaSi)(Ca_1Al_1)$. Minor amounts of K (0.05-0.32 apfu) show positive correlation with Na and Cl contents. Rare scapolite in coronas around garnet in marble have high amounts of the marialite component (<0.5 apfu Cl, <2.17 apfu Na + K) comparable to the extreme values from mica-feldspar layers. Scapolite from the host rocks is compositionally distinct; it is Cl-free and contains significant “mizzonite” with $X_{Ca} = 0.81$ -0.84 only (Fig. 3.11). Any results containing lower Na and higher Cl than expected for ideal marialite-meionite solid solution are likely the result of Na mobility away from (and Cl mobility towards) the electron beam during electron microprobe analysis (Fig. 4.20; Vanko and Bishop 1982).

The anorthite associated with scapolite shows a wide compositional range of $An_{0.85}$ - $An_{1.00}$. The scapolite which originated by anorthite replacement has higher Na contents, which is expressed by lower equivalent anorthite values (0.47-0.74). This feature was also observed in secondary scapolite after anorthite at other localities (Pan et. al 1994, Markl and Piazolo 1998, Kullerud and Erambert 1999). The elevated albite component in plagioclase

associated with steeper tie-lines in Figure 3.11 indicates partial reequilibration of plagioclase with late Na,Cl-enriched fluids at the end of scapolite crystallization.

3.5.7 Pyroxene

The pyroxene in the marble is pure diopside with negligible amounts of Na, Fe, and Al. The pyroxene observed in SEDEX assemblage is hedenbergite with average composition Hdn₆₀Di₄₀ (Fig. 3.12A; Appendix A.7). The Fe content slightly increases from core to rim of the hedenbergite crystals. In the garnet-scapolite assemblage, the pyroxene is compositionally zoned with X_{Mg} ranging from 0.53 to 0.65.

Clinopyroxene in the host rock exhibits compositional zoning with X_{Mg} = 0.64-0.71 in the crystal cores and X_{Mg} = 0.47-0.58 on their rims. Elevated contents of Al₂O₃ up to 1.81 wt.% and Na₂O up to 0.25 wt.% were locally found in crystal cores, most likely representing non-equilibrated remnants of the peak metamorphic assemblage.

3.5.8 Garnet

Rare garnet found in marble (Alm₄₈₋₆₇Grs₂₁₋₃₅Sps₆₋₁₁Prp₅₋₁₀) is compositionally similar to the garnet that occurs in the host rocks (Fig. 3.12B; Appendix A.8). In the pelite, the garnet is Ca-poor and falls within the compositional range of Alm₆₆₋₆₉Grs₁₇₋₂₁Sps₁Prp₉₋₁₆ with slightly elevated Mg and Ca in the rims; in the diopside gneiss the garnet is enriched in Ca with composition Alm₃₁₋₄₀Grs₅₂₋₅₃Sps₂₋₄Prp₅₋₁₄.

3.5.9 Amphiboles

Amphibole that replaces diopside within the marble is tremolite containing minor ^TAl and Na (tschermakite and edenite components; Fig. 3.13; Appendix A.9). In the garnet assemblage in the marble, the amphibole has a lower Mg/Fe ratio, higher contents of Al and Fe³⁺, and the composition ranges from ferro-actionlite and actinolite to ferrohornblende, with very low amounts of Na + K (Fig. 3.13B). However, amphiboles replacing garnet in the same assemblage are major potassic-ferropargasite and minor hastingsite; they are rich in Na + K (>0.5 apfu) and Al + Fe³⁺ (>1.5 apfu), and have Mg>Fe²⁺. The major chemical changes in the amphiboles can be expressed by combination of edenite (Na^TAl_□.₁Si₁) and tschermakite (Al^TAlR²⁺.₁Si₁) substitutions (Fig. 3.13C). For most of the data they show

ideal trend with 1:1 ratio towards hastingsite/pargasite as a substitution $(\text{Na},\text{K})(\text{Al},\text{Fe}^{3+})_1^T \text{Al}_2\text{□}_{-1}(\text{Mg},\text{Fe}^{2+})_{-1}\text{Si}_{-2}$. However, data lying out of the ideal trend, and those with Si < 6 apfu indicate minor substitution $(\text{Na},\text{K})(\text{Al},\text{Fe}^{3+})_2^T \text{Al}_3\text{□}_{-1}(\text{Mg},\text{Fe}^{2+})_{-2}\text{Si}_{-3}$ (1:2 ratio of edenite:tschermakite substitutions) towards sadangaite occurs as well.

At the contact between the marble and calc-gneiss, ferro-actinolite occurs as a breakdown product of clinopyroxene, whereas associated olivine is replaced by grunerite or ferro-anthophyllite (Fig. 3.13A). Both substitution schemes observed in tremolite apply to a lesser extent in ferro-actinolite ($\text{Al} + \text{Fe}^{3+} \leq 0.18$ apfu) and grunerite ($\text{Al} + \text{Fe}^{3+} \leq 0.14$) as well; contents of Na are lower than 0.04 apfu in both amphiboles.

3.5.10 Other Accessory Minerals

Apatite is the most common accessory phase. It contains low concentrations of the usual minor cations like Mn, Fe, Mg, and Sr (<0.004 apfu). It is always F-dominant (0.63-0.79 apfu) with elevated Cl (0.07-0.17 apfu) and OH (0.08-0.23) contents. Rarely, compositions with 0.51 apfu F, 0.13 apfu Cl, and 0.36 apfu OH were observed (Appendix A.10). The elevated chlorine content is in contrast with pure fluorapatite reported from the nearby Mount Grace carbonatite (Höy 1987).

Rutile in mica-feldspar layers contains elevated contents of Nb_2O_5 (< 1.24 wt.%), V_2O_3 (< 0.64 wt.%), and trace amounts of Cr_2O_3 (< 0.18 wt.%), CaO (< 0.38 wt.%), and FeO (< 0.12. wt.%; Appendix A.10). Rutile from host rocks is V-free and contains trace amounts of Nb_2O_5 (<0.35 wt.%), Cr_2O_3 (< 0.22 wt.%), and FeO (<0.47 wt%). Elevated Nb_2O_5 (up to 0.9 wt.%) and V_2O_3 (up to 5.39 wt.%) are commonly reported from graphite-rich metasedimentary rocks worldwide (e.g., Canet et al. 2003, Houzar and Cempírek 2011).

Titanite in the marble and host rock have very similar chemical composition (Appendix A.10). They exhibit significant $(\text{Al},\text{Fe}^{3+})(\text{OH},\text{F})(\text{TiO})_{-1}$ substitution with up to 0.14 apfu F, 0.14 apfu Al, and 0.03 apfu Fe^{3+} , commonly with $(\text{Al}+\text{Fe}) \gg \text{F}$. Other substitutions (involving e.g. Nb, Zr, Sn, Cr, V; Cempírek et al. 2008) usually observed in titanite are below detection limits. The substitution of Al and OH in titanite is typical in high pressure metamorphic rocks (e.g. Tropper et al. 2002, Harlov et al. 2006) whereas Al,F-rich titanite is typical in low-pressure calcsilicate rocks (e.g. Markl and Piazolo 1999, Cempírek et al. 2008). Allanite was also observed in the calc-gneiss (Appendix A.11).

Rare tourmaline from marble is Ca,F,O-rich dravite ($\text{Ca} \leq 0.36$ apfu, $\text{F} \leq 0.31$ apfu, $^{\text{W}}\text{O} \leq 0.38$ apfu; Appendix A.12). A single spot representing fluor-dravite was observed. It differs from the tourmaline in the host rocks, which contain cores of Ca,F-rich dravite ($\text{Ca} \leq 0.34$ apfu, $\text{F} \leq 0.21$ apfu) and rims of Na-rich uvite and fluor-uvite (0.33-0.41 apfu Na, 0.53-0.20 apfu F). Members of dravite-uvite solid solution with variable contents of F are common in metacarbonates with an evaporite component (e.g. Garnier et al. 2008).

3.6 Whole Rock Geochemistry

Marble, calc-silicate within marble, and the gneiss were analyzed for major and trace elements in order to determine possible sources of elements in corundum (Al, V, Cr, Ti, Fe) and their relative mobility (Appendix A.13).

Figure 3.14 shows major and trace element of analyzed samples compared to Al_2O_3 which is considered one of the least mobile elements in skarn systems (Meinert et al. 2005) and represents the aluminosilicate components in each rock. Contents of the main immobile elements (Ti, Cr, and V) in marble and host rocks positively correlate within a narrow range with Al_2O_3 (Fig. 3.14) suggesting the same homogenous source of the calc-gneiss and mica-feldspar layers and their formation by mechanical mixing of the two lithologies.

Contents of SiO_2 are strongly depleted in mica-feldspar layers compared to the mechanical mixing line between marble and calc-gneiss (Fig. 3.14); the same feature is present in FeO contents whereas, K_2O and CaO in the mica-feldspar layers fit to the mechanical mixing range. Contents of MgO are variable in agreement with their higher mobility and original heterogeneity within marble. Diopside-rich calc-gneiss samples are depleted in major elements (except for V) compared to the biotite-rich calc-gneiss samples. In mica feldspar layers, contents of U and Th are elevated and slightly depleted, respectively (Fig. 3.14).

Besides the aluminosilicate component, the contents of V also correlate well with Ti, Cr, Ni, and Co (Fig. 3.15). The correlation of Ti and V can be also observed in the partial chemical data from metapelitic rocks and amphibolites in Units 6a and 6b published by Höy (2001).

The REE patterns in the gneiss show elevated REE-contents (~244 ppm), enrichment in LREE ($\text{La}_{\text{CN}}/\text{Lu}_{\text{CN}} \sim 15.5$), and distinct negative Eu-anomaly ($\text{Eu}/\text{Eu}^* \sim 0.55$; Fig. 3.16). The marble REE values are close to their detection limits (0.11-1.66 ppm); their patterns are enriched in LREE. The carbonate layers between mica-feldspar layers are enriched in REE (8.15-15.09 ppm) compared to the pure marble. They are enriched in LREE ($\text{La}_{\text{CN}}/\text{Lu}_{\text{CN}} \sim 8.3\text{-}18.2$) and exhibit a positive Eu anomaly ($\text{Eu}/\text{Eu}^* 1.53\text{-}2.86$). The mica-feldspar layers are compositionally heterogeneous and the REE contents vary between 5.48 and 165.15 ppm (Fig. 3.16). All samples are enriched in LREE ($\text{La}_{\text{CN}}/\text{Lu}_{\text{CN}} \sim 6.4\text{-}23.7$). The Eu anomaly is most pronounced and negative in REE- and silicate-rich samples ($\text{Eu}/\text{Eu}^* \sim 0.3$) and it gradually increases to positive values in more carbonate-rich samples ($\text{Eu}/\text{Eu}^* 0.5\text{-}1.27$). Contents of Y show positive correlation with Dy and Ho and with REE in general.

3.7 ^{40}Ar - ^{39}Ar Dating of Micas

Phlogopite and muscovite from samples of mica-feldspar layers within marble from the float locality were dated using the ^{40}Ar - ^{39}Ar method in order to help constrain the thermal history of the study area. Both micas provided similar ages of 47.32 (± 0.29) Ma and 47.10 (± 0.26) Ma, respectively. Data are provided in Fig. 3.17. Closure temperatures of phlogopite and muscovite are ~500 and 529 °C (for cooling gradient of 100 °C/Ma; Baxter 2010), so both ages are interpreted to represent late cooling stage of the marble.

Crowley and Parrish (1999) and Crowley et al. (2001) summarized and provided new age data for the Monashee Complex and reconstructed the uplift history of units below the Monashee décollement. Using zircon and monazite U-Pb data, they identified the thermal peak conditions of the Frenchman Cap dome rocks around 58 Ma. Subsequent isothermal decompression was followed by fast isobaric cooling starting from ~51 Ma in the Monashee cover sequence (Crowley and Parish 1999).

Our phlogopite and muscovite ages are ~ 1 Ma younger than those reported by Sanborn (1996) for biotite and confirm the fast exhumation in the Frenchman Cap dome.

3.8 Stable Isotopes

Carbonate $\delta^{18}\text{O}$ values for marble (13.4-17.5 ‰), mica-feldspar layers within marble (13.5-16.6 ‰), and host calc-gneiss (14.8-15.4 ‰) at the Revelstoke occurrence are variable (Fig. 3.18A). An anomalously low $\delta^{18}\text{O}$ was recorded in a magnetite-bearing marble sample (12.1 ‰).

Most of the values of $\delta^{13}\text{C}$ in the marble are between ~0 and -1.2 ‰ with several lower values down to -2.9 ‰ in samples with minor fluid alteration or close proximity to mica-feldspar layers; dolomite-marble has a low value of $\delta^{13}\text{C}$ of -2.8 ‰. Most $\delta^{13}\text{C}$ carbonate values from mica-feldspar layers range between -3.1 to -1.1 ‰ and are generally lower than carbonate from marble. The lowest $\delta^{13}\text{C}$ values were found in the garnet-scapolite rock (-3.2 ‰) and host calc-gneiss (-4.48 to -2.55 ‰). The $\delta^{13}\text{C}$ values generally decrease in the direction from the marble to mica-feldspar layers (Fig. 3.18A).

Whole rock $\delta^{18}\text{O}$ silicate values for mica-feldspar layers within marble (11.1-16.2 ‰) and calc-gneiss (14.4-15.8 ‰) at the Revelstoke occurrence are generally high compared to average pelite, but fall within the data range from metasediments in the Monashee Complex and Selkirk Allochthon (Fig. 3.18B, Fig. 3.19). Isolated grains of corundum in calcite have $\delta^{18}\text{O}$ values of 10.7 and 11.1 ‰.

3.9 Fluid Inclusions

Two-phase liquid CO₂-vapor (LCO₂-V) primary fluid inclusions occur within color zones of corundum at the Revelstoke occurrence. The inclusions are ~30 µm to 144 µm in size and include concave, rectangular, elongate and irregularly shapes (Fig. 3.20). The CO₂ vapor at room temperature occupies ~4% of the inclusion volume. The composition of fluid inclusions within corundum was determined by microthermometry (Appendix A.14). After rapid cooling of the sample to -190 °C, slow warming caused phase changes from solid to liquid to vapor; i.e., melting of CO₂ ice (-93.5 to -73 °C), CO₂ solid (-58.2 to -56.6 °C), and homogenization of CO₂-liquid-vapor (24.7-27.2 °C). Melting temperatures below the triple point for CO₂ (-56.6 °C) indicate the presence of minor CH₄ and/or N₂ (Vanden Kerkhof and Thiéry 2001). Isochores calculated for carbonic (CO₂-CH₄-N₂) fluid inclusions within corundum at the Revelstoke occurrence using the Flincor program (Brown 1989).

Fluid inclusions in corundum from a variety of different protoliths typically have irregular or negative shapes and commonly contain nearly pure CO₂ fluids (Giuliani et al. 2003). Other fluids in addition to CO₂ that can occur within corundum fluid inclusions are H₂O, H₂S, N₂, and COS (Limtrakun et al. 2001, Takayuki et al. 2001, Giuliani et al 2003). Solids are uncommon in corundum fluid inclusions, however, crush leach analysis of fluid inclusions in corundum within marble has revealed the presence of Na, Cl, K, NO₃, and SO₄ at the ppb level (Giuliani et al. 2003). Laser Raman analysis is commonly used to detect other liquid species in corundum fluid inclusions, but use of this technique was not possible for the Revelstoke corundum due to its high fluorescence under the laser beam. The pure CO₂ fluid inclusions in the Revelstoke samples indicate the prevalence of CO₂ over H₂O in the metamorphic fluids and low *a*H₂O during corundum crystallization.

3.10 Discussion

3.10.1 Protolith of Silicate Assemblages in the Marble

The whole-rock geochemical data show that the silicate-rich part of the marble has the same or similar protolith as the host gneisses. Ratios of immobile elements suggest that the two lithologies were mechanically mixed without change in the ratio of aluminosilicates and the main Ti-,V-, Cr-bearing minerals i.e. rutile and titanite (Fig. 3.14). The mixing could have occurred during primary sedimentation or during tectonic emplacement of the gneiss into the marble. Depletion in SiO₂ and FeO in mica-feldspar layers suggests that these elements were removed from the original silicate layers mixed within marble. Textural evidence for fluid flow and mass exchange typical for reaction zones (skarns) between rocks with contrasting compositions (e.g., Meinert et al. 2005) was not observed, which suggest the depletion process took place during the prograde path of metamorphism before the main mineral transformations. Prograde fluid-assisted removal of SiO₂ and FeO from the silicate layers, due to high chemical potential gradients between the silicate layers and the marble, is in agreement with the homogenization of oxygen isotopes in carbonates and silicates observed in the marble, mica-feldspar layers, and host calc-gneiss (Figs. 3.14 and 3.18) and with the general chemical mobility trends documented at other localities at the contacts of

two contrasting lithologies (e.g. Brady 1977 and Joesten 1977). The combination of the high chemical potential gradient of SiO_2 between the silicate layers and marble, along with the increasing solubility of SiO_2 with increasing temperatures and the formation of H_3SiO_4^- complexes in aqueous fluids (Walther and Woodland 1993, Seward 1974), could cause extensive SiO_2 mobilization and explain the depletion in mica-feldspar layers. Furthermore, the chemical potential (and diffusion) gradients could have been enhanced by the thinning of silicate layers within marble during tectonism because of stretching and folding. The reduced solubility and mobility of K and Na compare to Si could be due to the low salinity of reacting fluids (Fig. 1 in Pak et al. 2003).

The low Sr contents and their positive correlation with CaO (Appendix A.13) are consistent with a non-evaporitic origin for the original sediment (Moine et al. 1981), and the compositions of all the rock types correspond to those of shales or marls derived from platform sediments (Moine et al. 1981, Garnier et al. 2008). This is in agreement with the original interpretation of the Revelstoke metasedimentary sequence by Höy (1987). Contents of V, Ti Cr, Co, and Ni show positive correlation (Fig. 3.15), which could indicate a common source from a mafic protolith (e.g., Grapes and Palmer 1996). With regard to the local geology and presence of SEDEX mineralization in contact with the marble and common sulfide minerals within the marble, we also considered the influence of the sedimentary-exhalative protolith (e.g., Canet et al. 2003). The scarce data from the Monashee complex SEDEX mineralization show no correlation of V with Ti, Co, and Ni contents (Höy 2001), and there is no evidence of significant mixing of the two lithologies. Therefore, the preferred explanation for the elevated Cr and V contents in the marble is the dispersed mafic component (protolith of amphibolites) in the pelitic sediments in Units 6a and 6b and its mixing with the carbonate material before metamorphic overprint.

The variation in REE and Y contents is generally related to the amounts of silicate component in the individual samples. The LREE enrichment in all patterns is compatible with the presence of accessory apatite, allanite, zircon, and titanite in the gneiss and silicate-rich parts of the marble. The difference in LREE/HREE fractionation in the host gneiss and the most LREE-enriched mica-feldspar layers may be related to the partial melting and remobilization processes in the host gneiss which may have also caused the observed

depletion in U due to partial dissolution/alteration of accessory phases (e.g., Rubatto et al. 2008).

The $\delta^{18}\text{O}$ and $\delta^{13}\text{C}$ values from carbonate vary at the Revelstoke occurrence (Fig. 3.18A). $\delta^{18}\text{O}$ carbonate values for marble (13.5-17.5 ‰) are lower than expected for normal marble (20-28 ‰; Valley 1986; Fig 3.19), but the $\delta^{13}\text{C}$ values (-2.7-0.1 ‰) are within the normal range for marine carbonates (Hoefs 2004). The distribution of $\delta^{18}\text{O}$ and $\delta^{13}\text{C}$ carbonate values follow a generalized devolatilization trend (Valley 1986) where $\delta^{13}\text{C}$ is more greatly affected than $\delta^{18}\text{O}$. The decrease of $\delta^{13}\text{C}$ values in calcite towards silicate assemblages is likely the result of decarbonation reactions that produce silicates during metamorphism (Fig. 3.18A; Valley 1986).

The $\delta^{18}\text{O}$ and $\delta^{13}\text{C}$ results fall within the range of values observed in marbles from the Mica Creek area and the Thor-Odin dome (Fig. 3.18B; Ghent and O'Neil 1985, Holk and Taylor 2000). The $\delta^{13}\text{C}$ values also fall within the range of Asian ruby-bearing marbles, but the $\delta^{18}\text{O}$ values are much lower (19.9-28.9 ‰; Garnier et al. 2008).

The similarity of $\delta^{18}\text{O}$ and $\delta^{13}\text{C}$ values of carbonates and $\delta^{18}\text{O}$ values silicates at the Revelstoke occurrence, Mica Creek area, and Thor-Odin dome likely indicate that sediments at these localities had similar protoliths and/or underwent similar fluid-rock interactions during metamorphism (Valley 1986), unlike those of the Asian ruby deposits. Ghent and O'Neil (1985) attribute the range of $\delta^{18}\text{O}$ values at the Mica Creek area to varied protoliths and metamorphic formation conditions; whereas, the elevated $\delta^{13}\text{C}$ values could be attributed to depositional processes prior to metamorphism: 1) Precambrian carbonate-secreting algae, 2) organic material, or 3) travertines. Holk and Taylor (2000) suggest the homogenized $\delta^{18}\text{O}$ values in rocks above and less than 200 m below the Monashee décollement at the Thor-Odin dome were caused by the interaction of recycled H₂O -bearing fluids (derived from anatetic and metamorphic processes) and CO₂-fluids (derived from devolatilization of calc-silicate rocks) with the host rocks during the metamorphic evolution of the core complex. These fluids didn't penetrate >200 m into the Monashee Complex because they were channeled along the Monashee décollement. Thick marble units at the Thor-Odin dome are interpreted to be relatively impermeable and retained higher $\delta^{18}\text{O}$ values (18-22 ‰) in contrast to thinner units in leucogranite-rich sections (12.4-15.2 ‰).

Even though Holk and Taylor (2000) did not see any homogenization of $\delta^{18}\text{O}$ values in the Monashee complex between 200 to 400 m below the Monashee décollement, extensive fluid-rock interaction must have affected the Revelstoke rocks which are much deeper (~2 km) below the Monashee décollement because of: 1) the lack of preservation of any normal marine carbonate $\delta^{18}\text{O}$ values throughout the entire marble unit (Fig. 3.18A), 2) similar carbonate $\delta^{18}\text{O}$ values in the calc-gneiss and marble (Fig. 3.18A), and 3) similar silicate $\delta^{18}\text{O}$ values in the calc-gneiss and mica-feldspar layers (Fig. 3.19). The small variation and depletion of $\delta^{18}\text{O}$ values of carbonates across the entire marble unit is likely due to variability in the isotopic composition of the original sediments and fluid-rock interactions during metamorphism between carbonate sediments mixed with thin layers of pelitic sediments. Elevated $\delta^{18}\text{O}$ silicate values in the host gneiss were also likely influenced by mixing of carbonate and pelitic components or infiltration of late CO₂-rich fluids from the marble. Stretching of pelite layers within marble during deformation would have decreased their thickness increasing the rate at which exchange could take place between the two lithologies. Recrystallization of carbonate minerals during retrograde metamorphism could also have affected the $\delta^{18}\text{O}$ values.

The corundum $\delta^{18}\text{O}$ values are much lower than those from worldwide corundum occurrences in marbles, and plot in the skarn field according to Giuliani et al. (2005). However, this classification does not include corundum from mixed pelitic and marble protoliths. The low corundum $\delta^{18}\text{O}$ values reflect the $\delta^{18}\text{O}$ values of the host marble and mica-feldspar layers. Previous studies of Revelstoke occurrence host rocks (Unit 6ab) by Journeay (1986) and Höy (1987) characterize the unit as a metamorphic equivalent of marls and attributed the presence of scapolite to the salt content of original sediments. Our geochemical and isotopic data support this interpretation and show that mixing of pelitic and carbonate sedimentary material caused elevated Cr and V contents in the marble.

3.10.2 Chromium and Vanadium Enrichment

Occurrences of Cr- and V-bearing minerals in marbles, dolomites, and skarns are rather common; they typically occur as a part of metasedimentary sequence containing black shales, SEDEX mineralization, and/or mafic rocks (e.g., Treloar 1987, Pan and Fleet 1991, Canet et al. 2003, Uher et al. 2008). Genetically similar Cr- or V-rich assemblages are also

commonly found in graphite quartzites and graphite metacherts (e.g., Snetsinger 1966, Lee and Lee 2003, Houzar and Cempírek 2011, Bačík et al. 2011). The common association of high vanadium contents with reduced carbonate rocks is not coincidental. Breit and Wanty (1991) showed mechanisms of vanadium accumulation in carbonaceous rocks with high contents of organically bound sulfur. Vanadium is deposited in sediments under reduced conditions where it is adsorbed to clay minerals; further metamorphic overprint can cause vanadium incorporation in newly formed muscovite and silicates. Geochemical data show that the increased amounts of Cr and V most likely originate from the breakdown of mafic rocks. If the Cr and V were released from their original minerals, their retention in reducing conditions could be an important factor in the Revelstoke rocks, which typically contain minor amounts of sulfide minerals and graphite.

Enrichment in Cr and V in the corundum-bearing assemblages is also significantly related to their preferential binding in phlogopite and muscovite. Although minor rutile is enriched in V_2O_3 and Cr_2O_3 (≤ 0.64 and ≤ 0.18 wt.%), the majority of Cr, V, and Ti in the marble is stored in micas (≤ 0.09 wt.% V_2O_3 and ≤ 0.23 wt.% Cr_2O_3 in muscovite; ≤ 1.41 wt.% V_2O_3 and ≤ 0.27 wt.% Cr_2O_3 in phlogopite). At the Revelstoke occurrence Cr and V were likely originally bound in silicates and clay minerals, making them available to micas during diagenesis. If Cr and V were originally bound in detrital chromite or rutile, their release would be restricted to high metamorphic temperatures in a H_2O -poor and quartz-free marble system.

3.10.3 P-T Metamorphic Path in Frenchman Cap Dome

The observed mineral assemblages in metapelites at the Frenchman Cap dome are in agreement with similar rocks at the Thor-Odin dome as described by Hinckley et al. (2006). The P-T path defining assemblages include prograde reaction biotite + albite + sillimanite + quartz = garnet + K-feldspar + melt (Spear et al. 1999). Journeyay (1986) and Höy (1987) identified the clockwise P-T metamorphic path for the pelitic rocks of the Frenchman Cap dome, with the peak metamorphic assemblages followed by the medium-pressure overprint during unroofing and isobaric cooling.

Calculations of stable equilibrium assemblages from whole rock data were done using Theriak-Domino software package (De Capitani and Petrakakis 2010) using the

thermodynamic dataset HP98 (Holland and Powell 1998) and employing the activity-composition relationships outlined by White et al. (2001). The observed assemblage of garnet + biotite + plagioclase + K-feldspar + kyanite is stable in the range of 700-900 °C and 7.0-12 kbar. The minimum P-T conditions of 720 °C and 8.0 kbar are well constrained by the absence of phengite/muscovite and the presence of kyanite. Ilmenite is not stable in the phengite-free kyanite assemblages; hence, the observed inclusions of ilmenite in garnet are interpreted as relicts of pre-peak prograde metamorphism. During decompression, the retrograde assemblages observed in sillimanite-bearing metapelitic of biotite+ sillimanite + K-feldspar and biotite + muscovite + plagioclase feldspar became stable between 575-700 °C and 4-8 kbar. These values generally agree with the P-T path defined by Norlander et al. (2002) and Hinckley et al. (2006). However, the presence of andalusite and cordierite identified by Höy (1987) indicate that the retrograde part of the P-T path took place at lower pressure than suggested for Thor-Odin dome by Hinckley et al. (2006).

The assemblage of garnet + biotite on the border of garnet porphyroblasts in biotite-rich layers and the garnet + clinopyroxene assemblage (core compositions) rarely observed in the K-feldspar-rich layers were used for estimation of equilibrium temperatures (Bhattacharya et al. 1992, Krogh 1988). The calculated temperatures using garnet + biotite and garnet + clinopyroxene thermometers are 675-695 °C and 766-771 °C, respectively. The garnet + biotite temperatures are about 25 °C lower than the lowest values observed by Norlander et al. (2002) in the Thor-Odin dome. The values may be influenced by biotite re-equilibration during retrograde metamorphism and do not represent the peak of metamorphic conditions. On the other hand, the garnet + clinopyroxene temperatures should reflect the peak metamorphic conditions.

3.10.4 P-T-X Evolution of the Marble

Major equilibrium mineral assemblages in the marble are diopside + calcite, phlogopite + calcite, rare tremolite + calcite, and fibrous tremolite + calcite + quartz in the siliceous layers, and magnetite + calcite ± dolomite in the non-siliceous layers. The assemblages of garnet + diopside + scapolite + K,Na-amphiboles are rare.

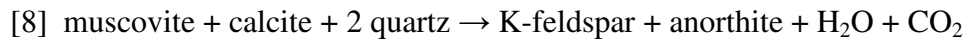
Dolomite and quartz remnants identified in thin section and the observed metamorphic products suggest that the original material was a hydrated dolomitic marble (Spear 1995).

The first likely prograde reactions that occurred were:



The occurrence of major diopside + calcite and rare prograde tremolite + calcite assemblages found in the marble agrees with the steep P-T path proposed by Hinckley et al. (2006) and high X_{CO_2} in the marble at the pressure peak of metamorphic conditions (Fig. 3.21A).

Textural relations in the mica-feldspar layers suggest that the mineral assemblage before formation of corundum was muscovite + K-feldspar + anorthite + calcite \pm dolomite. Most of the quartz was likely removed from the system by the following prograde reaction at $\sim 600^\circ\text{C}$ and ~ 9 kbar, which produced the K-feldspar and anorthite rims around muscovite aggregates:



Absence of relict kyanite and zoisite in products of the reaction [8] indicates that the maximum pressure should be ~ 9 kbars, which is \sim approx. 1 kbar lower than the prograde P-T-evolution at the Thor-Odin Dome (Hinckley et al. 2006).

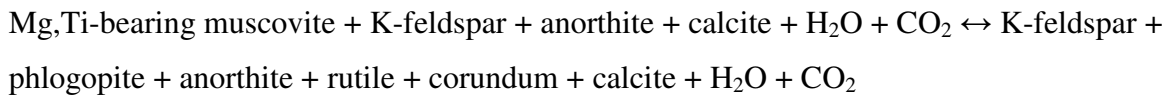
Decarbonation reactions forming phlogopite [7] and feldspars [8] during prograde metamorphism increased the activity of CO_2 in the system and decreased the reaction temperatures of subsequent reactions promoting the formation of the corundum from muscovite in the absence of quartz:



The corundum-forming reactions probably started during prograde metamorphism and high X_{CO_2} in the range ~650-700 °C at 8.5-9 kbar (Fig. 3.21B) and continued during marble decompression. The dry conditions are supported by the pure CO_2 fluid inclusions observed in corundum and by formation of new phlogopite overgrowing muscovite and corundum; the reaction started at the beginning of decompression at ~760 °C and 9 kbar (Fig. 3.21A).

The majority of corundum (types I and II) at the Revelstoke occurrence was produced by the dehydration of muscovite (reaction 5). This is inferred from the presence of corundum with muscovite and K-feldspar and the absence of diaspore, margarite, dolomite, and spinel. In some cases, breakdown of muscovite together with rare dolomite (reaction 3) probably took place, producing corundum (type III), phlogopite, calcite, and fluids. We assume that the system retained high X_{CO_2} during the prograde stage and part of decompression, until influx of scapolite-forming fluids.

The observed mineral assemblages resulted from non-ideal stoichiometry of the reacting phases. When the dehydration curve for muscovite + calcite is calculated using the electron microprobe analysis of the muscovite from the muscovite-anorthite-K-feldspar aggregates in association with corundum, the resulting stable mineral assemblage is consistent with those observed in thin sections:



The model results indicate minor formation of anorthite in the corundum stability field. It explains the presence of rare anorthite + corundum assemblage (Fig. 3.5E). This corundum-forming reaction takes place at the same PT conditions as when calculated using the theoretical muscovite formula.

3.10.5 Retrograde Fluids

The occurrence of scapolite, retrograde alteration of diopside, feldspars and corundum, and breakdown of titanite in mica-feldspar layers all indicate the presence of retrograde fluids. Although most of the alteration features can be attributed to hydration of the system during decompression and cooling, the presence of scapolite indicates high salinity of fluids

at relatively high temperature. For the observed scapolite composition, most authors estimate its origin in the range 600-750 °C and pressure ~2-5 kbar (Ellis 1978, Piazolo and Markl 1999). At the Revelstoke occurrence, these PT conditions match with the end of decompression and their validity is supported by the late origin of scapolite, after formation of feldspars, micas and corundum. Scapolite in the marble formed after crystallization of corundum, by the replacement of anorthite and calcite by saline fluids.

The NaCl content of the late fluids was estimated from the scapolite compositions using the experimental data of Ellis (1978) for 4 kbar and 750 °C (cf. Markl and Piazolo 1998). The experimental data assume only NaCl-H₂O fluid without CO₂; therefore, the results should be regarded as rough estimations of the maximum contents of NaCl in the fluids (for detailed discussion see Mora and Valley 1989, Markl and Piazolo 1998). The estimated ratio NaCl/(NaCl + H₂O) varies between 0.05 and 0.3 for most of the data, corresponding to ~15 to 58 wt.% NaCl present in the fluid; the highest marialite compositions in garnet assemblage in the marble indicate the presence of highly saline fluids with the ratio NaCl/(NaCl + H₂O) up to 0.5 (~76 wt.% NaCl). Although similar values are reported for evaporite brines, the source of high Na and Cl contents in Revelstoke marble is not clear. The only Cl- or Na-bearing phases are apatite, scapolite, amphiboles and late albite in alteration products; the origin of the amphiboles and albite can be related to the scapolite-forming saline fluids, but apatite appears to be one of the earliest primary minerals in the marble. The Cl- and S-absent composition of scapolite from the host rock indicates low salinity of fluids at peak metamorphic conditions; therefore, the fluids must have been derived from an isolated external source or by dissolution of speculative evaporite beds in the marble.

Scapolite in the marble and in the host rock is typically accompanied by crack-filling sulfide mineralization. The sulfide minerals in the host rock are commonly concentrated on fractures along foliation planes and in retrograde assemblages, especially those replacing garnet porphyroblasts. A sulfide veinlet cross-cutting the gneiss was observed on its contact with marble, depositing silicate and sulfide minerals in the marble. The scapolite is always free of (SO₄)²⁻ and it does not contain sulfide inclusions; hence, the sulfide mineralization likely represents a different stage of fluid flow.

Replacement of clinopyroxene by tremolite, calcite and quartz by the reaction:



took place below ~550 °C at 4 kbar (Fig. 3.21A); its low Na-contents suggest significant removal of NaCl, either due to fractionation or mixing of the fluids with an external low-saline source. At approximately the same temperature, low-saline fluids altered primary minerals in the marble assemblages; replacement of corundum and anorthite, scapolite and K-feldspar by margarite and muscovite took place at ~520-550 °C (Fig. 3.21B). Further late fluid-driven reactions also include chloritization of biotite, sericitization of feldspars, and veinlets of Fe-oxides.

Graphite in the marble mineral assemblages usually occurs as fissure filling and coats and rims both prograde and retrograde minerals. We assume that it precipitated from late retrograde fluids during cooling and during cataclasis of the rock at low temperature during brittle deformation in the marble. The physical and chemical breakdown (decarbonation) of calcite during cataclasis was the likely source of carbon which precipitated graphite.

3.10.6 Comparison to Other Deposits

Different models have been used to explain corundum formation in carbonate rocks (e.g. Giuliani et al. 2007). The Revelstoke deposit shares some common features with other ruby deposits from central and southeast Asia (Garnier et al. 2008) including: “(1) they are hosted by metamorphosed marine carbonates (within gneisses); (2) they formed during amphibolite to lower granulite facies metamorphism; (3) ruby has no relationship with dikes or pegmatites; and (4) the ruby-bearing marbles contain scattered ruby mineralization which is concordant with the surrounding stratigraphic units.” Moreover, the corundum assemblages were affected by highly saline retrograde fluids producing scapolite, which is a typical feature of south-Asian gem corundum deposits (Garnier et al. 2008).

However, numerous differences exist between the Revelstoke occurrence and other localities including corundum-bearing mineral assemblages, mineral and fluid inclusions in corundum, oxygen isotopes of corundum and marble, and the quality and intensity of color of corundum crystals. Most importantly, the Revelstoke corundum formed by prograde

muscovite breakdown at high pressure whereas the Asian rubies are the product of retrograde low pressure breakdown of spinel.

At the south-Asian ruby deposits, Garnier et al. (2008) observed the following which are not present at Revelstoke: (1) corundum formation by the breakdown of spinel during retrograde metamorphism, (2) Na,S,B mineralization (tourmaline, aspidolite, pargasite, edenite, anhydrite) and Mg mineralization (chlorite and saphirine) associated with corundum; (3) fluid inclusions in corundum with the composition of COS-S₈-AlO(OH); and (4) inclusions of anhydrite and salts in corundum. In contrast at the Revelstoke occurrence, corundum formed prior to spinel by prograde muscovite dehydration and the Na,S,B minerals are either not directly associated with ruby (pargasite, hastingsite, edenite, tourmaline) or clearly post-date its formation (scapolite, sulfide minerals). The scapolite associated with corundum is also sulfur-free and poor in Na (~0.75-1.5 apfu in scapolite) and Cl (usually <0.3 apfu Cl in scapolite). Even though we did not see evidence for anhydrite or COS-S₈-AlO(OH) fluid inclusions in corundum, we cannot discount that they exist. Although the brines responsible for formation of scapolite could have originated from evaporite pods in the rock, it was volumetrically insignificant compared to the siliciclastic component. This is expressed by the lower values of oxygen isotopes for corundum and marble minerals and the scarcity of Na,S,B-mineralization, which differ significantly from those observed by Garnier et al. (2008).

3.11 Summary

This study has contributed to both the petrology of metasediments in the Frenchman Cap dome as well as the formation of gem corundum in carbonate rocks during prograde metamorphism and metasomatism of pelitic layers within marble. Whole rock geochemistry data indicate that the corundum-bearing silicate (mica-feldspar) layers formed by the mechanical mixing of carbonate with the protolith of the host gneiss. The silicate layers and the gneiss contain elevated contents of Cr and V due to the presence of a volcanoclastic component in their protolith. The bulk composition of the silicate layers was depleted in Si and Fe during prograde metamorphism. Si and Fe depletion was also enhanced by extensive

fluid-rock interaction, which is also evident in the homogenization of $\delta^{18}\text{O}$ and $\delta^{13}\text{C}$ values in carbonates and silicates in the marble and silicate layers as well as low $\delta^{18}\text{O}$ in corundum.

Corundum occurs in thin, folded and stretched layers with the predominant assemblage of green muscovite + Ba-bearing K-feldspar + anorthite ($\text{An}_{0.85-1}$) \pm phlogopite \pm Na-poor scapolite. Gem corundum was produced in the mica-feldspar layers by mica dehydration at the peak of metamorphism (~650-700 °C at 8.5-9 kbar) following a clockwise PT path. Fluid inclusions in corundum are pure CO_2 indicating the presence of a CO_2 - rich fluid during corundum formation. The micas associated with corundum in the mica-feldspar layers have elevated Cr, V, Ti, indicating that they were the source of Cr, V and Ti in the corundum crystals. The mica-feldspar layers were an ideal environment for corundum formation because of the lack of Si and Fe, and enrichment of Cr, V and Ti.

Table 3.1: Mineral Assemblages from Different Lithologies within the Revelstoke Occurrence.

Rock Type	Mineral Assemblages
Mica-Feldspar Layers	Ms+Phl+Kfs+An+Cal±Rt±Fe-oxide±Crn Phl+An+Scp+Cal+Crn±Ms Phl+Cal±Scp±Crn Mrg+An+Crn
Diopside Layers	Di+Tr+Cal±Qtz
Minor Assemblage	Di+K-amp+Grt+Scp+Cal
Non-siliceous layers	Mag+Cal±Dol
Host-Rock	
Calc-Gneiss (Bt)	Bt+Grt+Kfs+Plg+Ky+Sil+Qtz±Hem±Tur
Calc-Gneiss (Di+Kfs)	Di+Phl+Kfs+Ttn±Tr±Grt
Calc-Gneiss (Di+Plg)	Di+Scp+Cal+Kfs+Plg+Ttn±Qtz
SEDEX	Hd+Ol+Cal+Sulphides±Fe-oxides

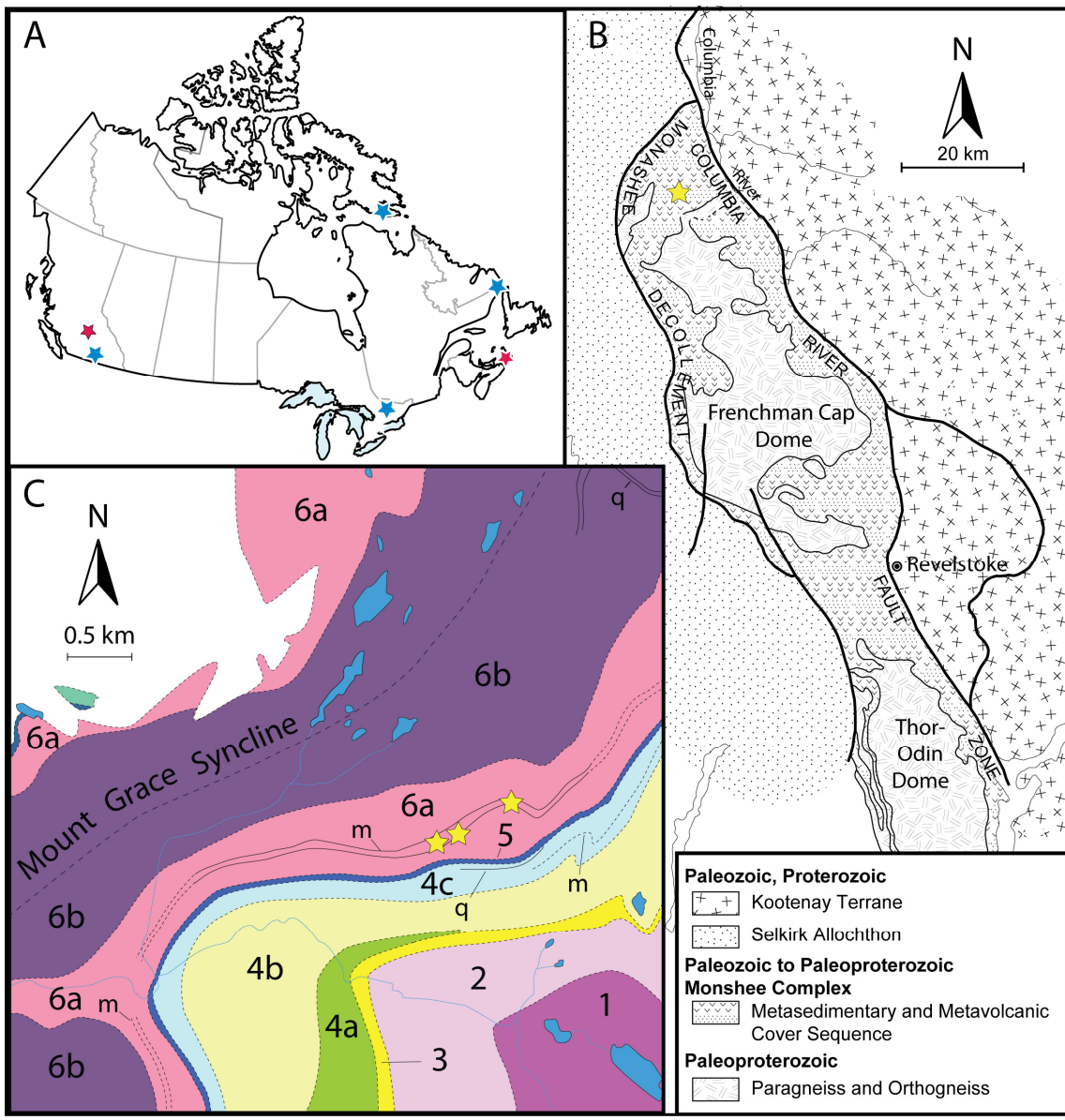


Figure 3.1: Position and geology of the Revelstoke occurrence. (A) Map of Canadian carbonate-hosted gem-corundum localities; (B) Tectonic assemblage map of part of the Monashee complex (modified after Höy 2001). The studied area is marked by a star; (C) Regional geological map of the Revelstoke occurrence (modified after Höy 1987). The studied localities (from east to west: float, outcrop 1, outcrop 2) are marked by yellow stars. Map legend: (1) orthogneiss, (2) paragneiss, (3) quartzite, micaceous schist, (4a) Calc-silicate gneiss, kyanite-sillimanite schist, quartzite, amphibolite, (4b) Kyanite-sillimanite schist, gneiss, minor quartzite (q), (4c) Calc-silicate schist, gneiss, kyanite-sillimanite schist, marble (m), quartzite (q), (5) marble, (6a) Calc-silicate gneiss, kyanite-sillimanite schist, marble (m), (6b) Kyanite-sillimanite schist, minor amphibolite, marble (m), quartzite (q).



Figure 3.2: Revelstoke corundum. (A) Zoned corundum grain in marble (picture width 3 cm); (B) Faceted Revelstoke sapphire and ruby (photo courtesy of B.S. Wilson).

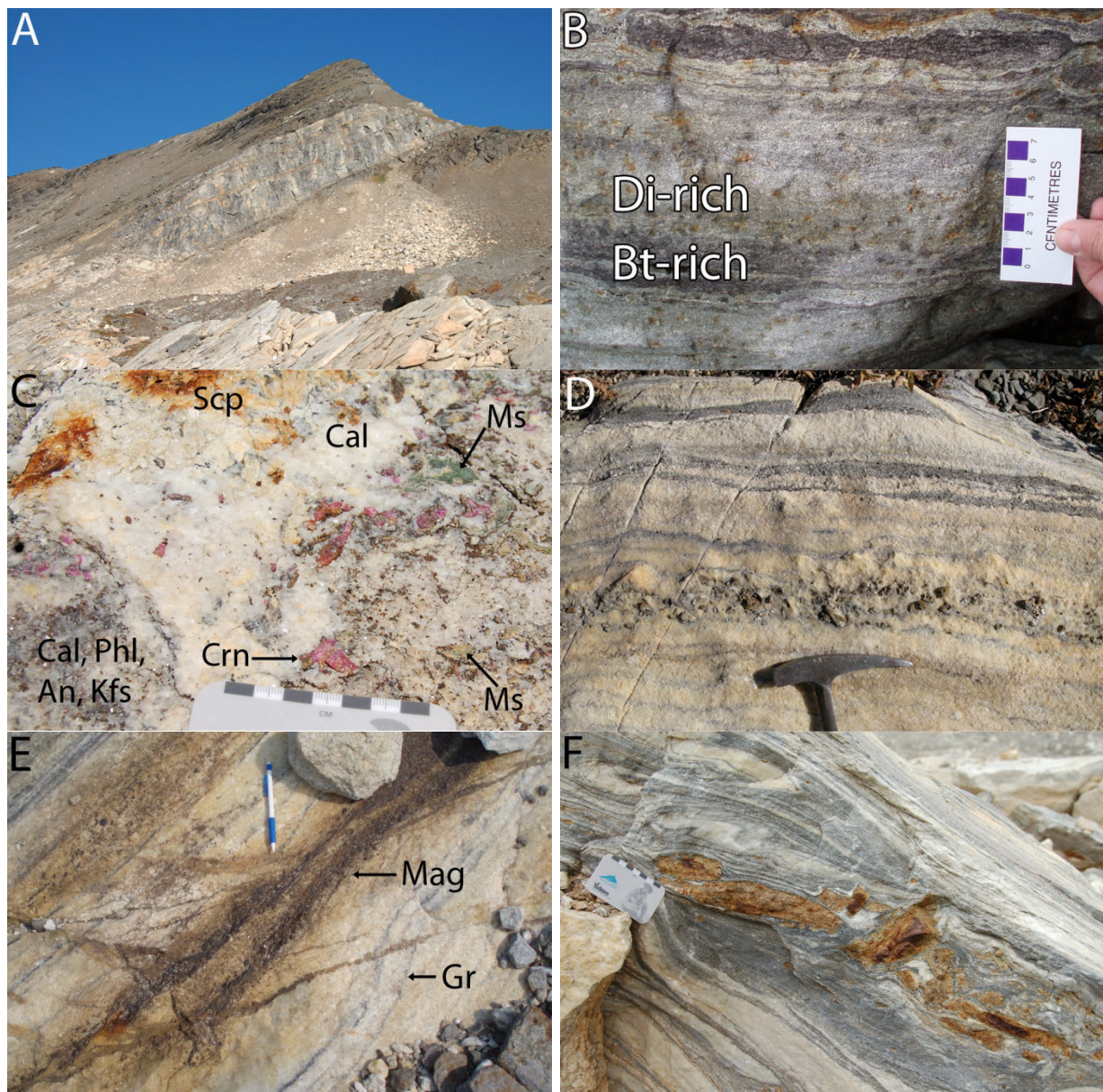


Figure 3.3: Photographs of the Revelstoke occurrence. (A) The corundum-bearing marble within diopside gneiss (unit 6a); (B) Pyroxene-gneiss with pelitic layers, containing garnet porphyroblasts (dark spots); (C) Corundum-bearing mica-feldspar layers, with secondary scapolite after anorthite; (D) Coarse-grained diopside-tremolite zone and fine-grained, graphite -enriched cataclasite layers; (E) Magnetite and graphite layers in marble; (F) Deformed, altered muscovite-feldspar nodules in phlogopite and graphite layers in marble.

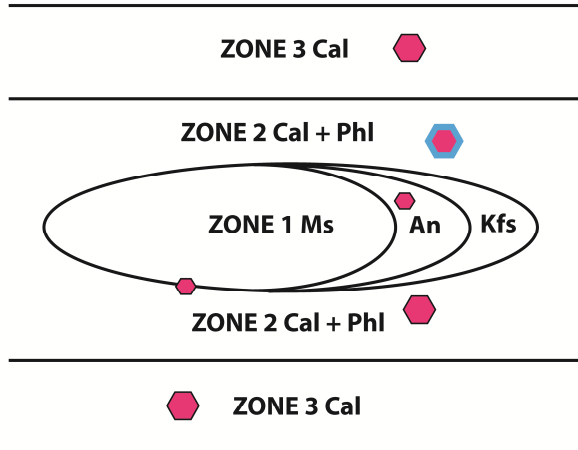
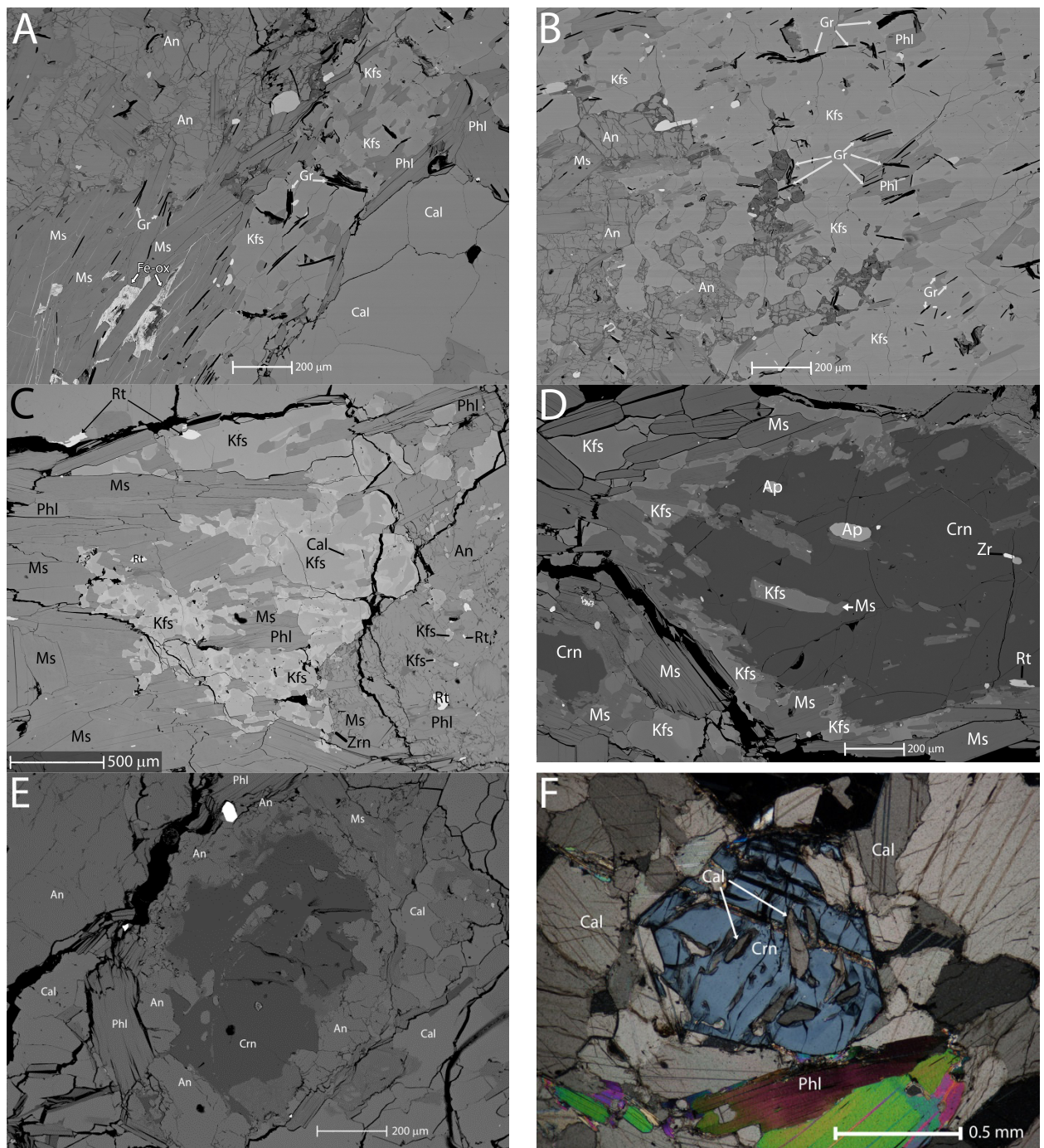


Figure 3.4: Schematic drawing of mineralogical zoning of mica-feldspar layers. Hexagons represent corundum crystals; solid pink hexagons are not zoned, pink hexagons with blue rims are zoned crystals. The pink hexagons represent corundum, which sometimes are zoned.



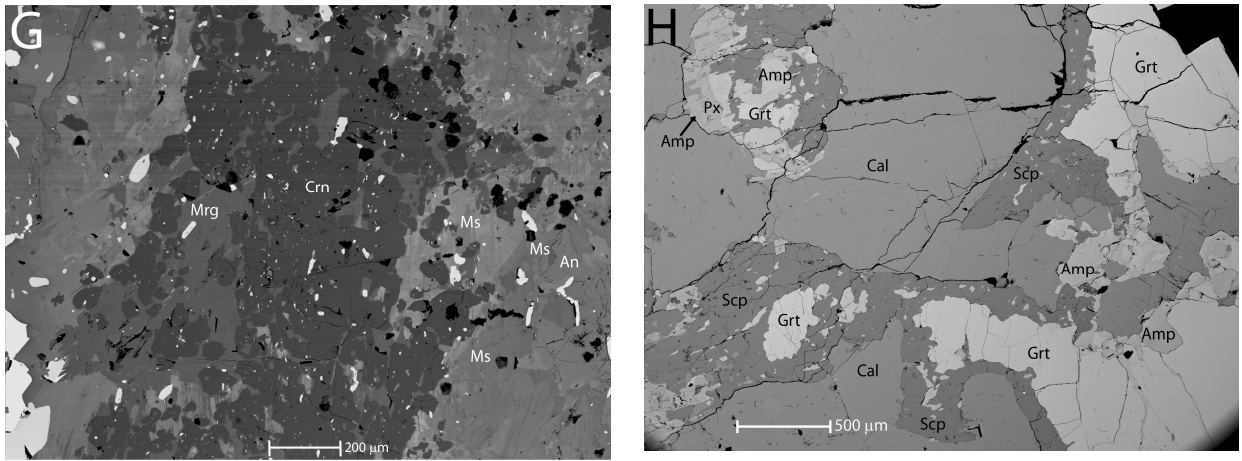


Figure 3.5: Optical microscope photographs and BSE images of mineral assemblages in mica-feldspar layers and garnet in marble. (5A) SEM photomicrograph of replacement of muscovite by anorthite and K-feldspar. Note relicts of muscovite in anorthite and phlogopite and muscovite in K-feldspar. (5B) SEM photomicrograph of replacement of muscovite by anorthite and K-feldspar. Note the intergrowth of anorthite and K-feldspar as well as relicts of muscovite in anorthite and phlogopite in K-feldspar. (5C) SEM photomicrograph of Ba-enrichment in K-feldspar replacing muscovite and anorthite. The light areas in the K-feldspar and muscovite are enriched in Ba. (5D) SEM photomicrograph of corundum alteration to muscovite then K-feldspar. The corundum has inclusions of apatite, zircon, muscovite, K-feldspar, and rutile. (5E) SEM photomicrograph of corundum with anorthite inclusions surrounded by anorthite, phlogopite, and calcite, altered to margarite. (5F) CPL optical microscope image of Type 2 skeletal euhedral corundum with calcite inclusions within marble. (5G) SEM photomicrograph of Type 3 fine-grained corundum with alteration to margarite and Ba-enriched muscovite within plagioclase. (5H) SEM photomicrograph of scapolite and amphibole coronas around garnet. Amphibole also replaces pyroxene.

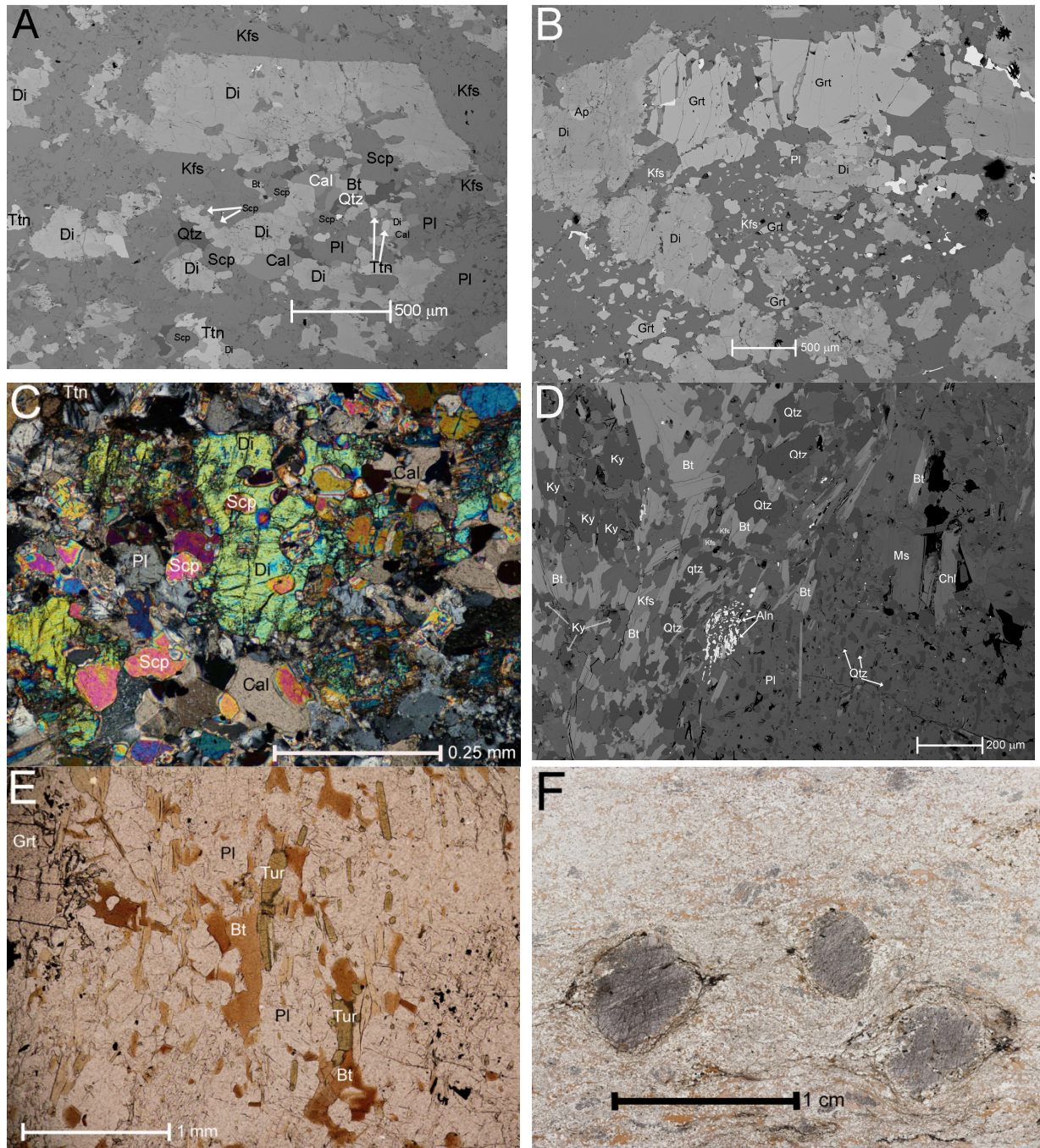


Figure 3.6: Optical microscope photographs and BSE images of the host rock thin sections
 A) K-feldspar-diopside rich layer with scapolite, plagioclase titanite, and biotite; B) K-feldspar-rich layer with an assemblage of diopside, garnet, K-feldspar and plagioclase; C) Plagioclase-rich layer, diopside with inclusions of scapolite; D) Biotite-rich layer with poikiloblastic plagioclase in quartz, biotite, K-feldspar groundmass with muscovite in its pressure shadow; E) Biotite-rich layer with tourmaline, biotite, plagioclase, and garnet porphyroblasts; F) Garnet porphyroblasts in biotite-rich pelitic layers.

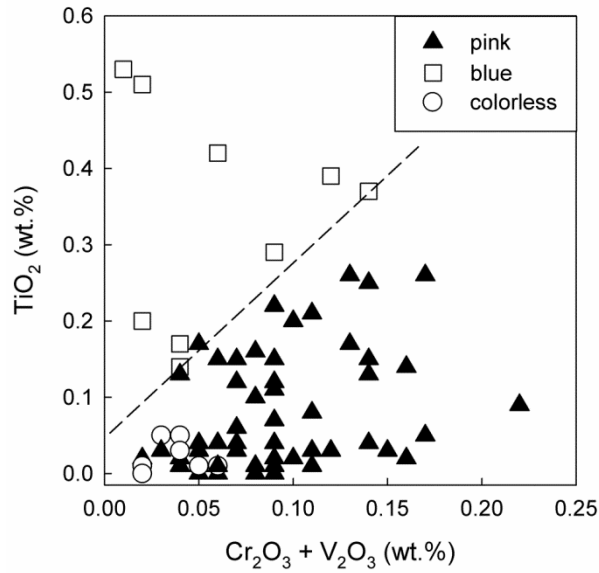


Figure 3.7: Trace elements in corundum of different color.

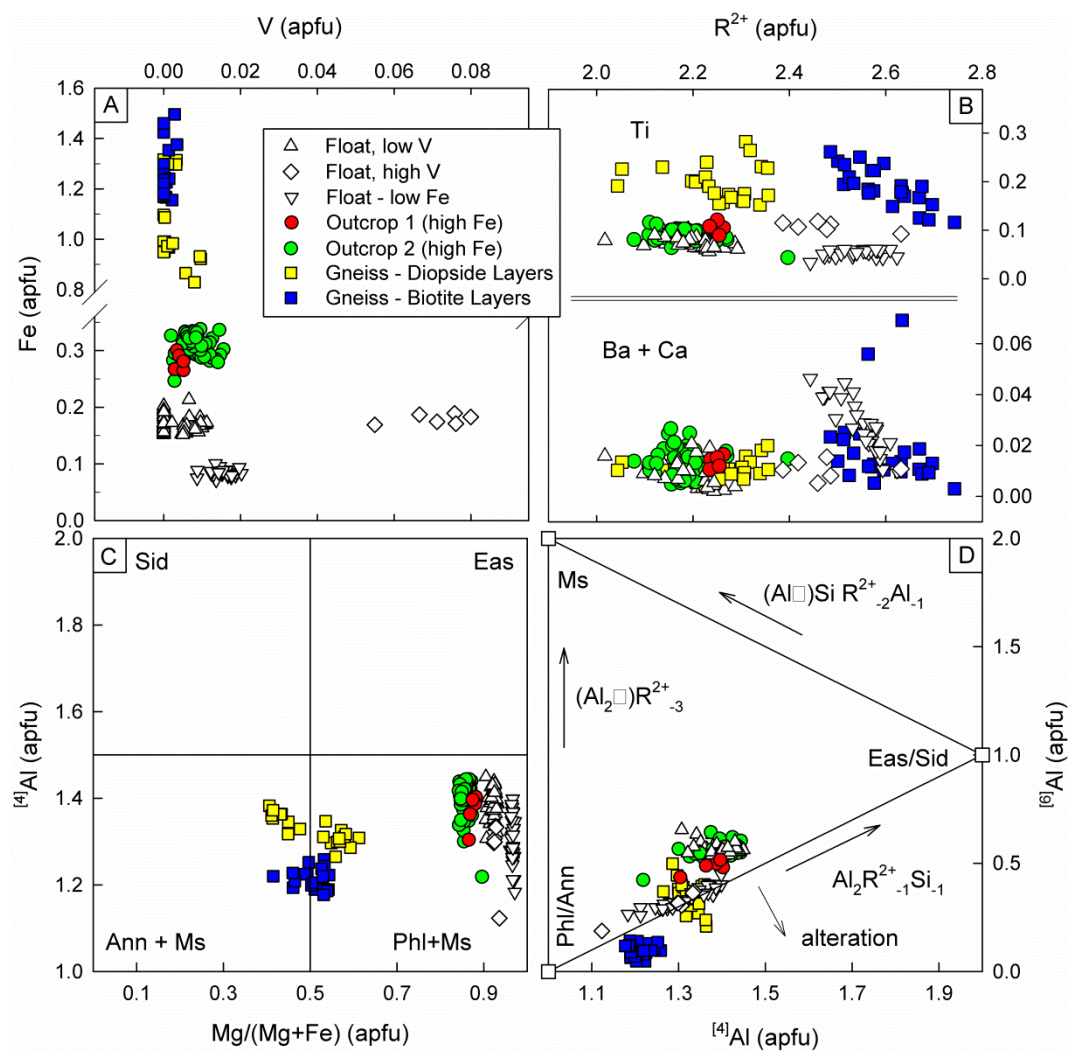


Figure 3.8: Chemical composition of trioctahedral micas. A) Fe vs. V; B) Ti vs. $[6]\text{Al}$ and Ba+Ca vs. $[6]\text{Al}$; C) $[4]\text{Al}$ vs. $\text{Mg}/(\text{Mg}+\text{Fe})$; D) $[6]\text{Al}$ vs. $[4]\text{Al}$.

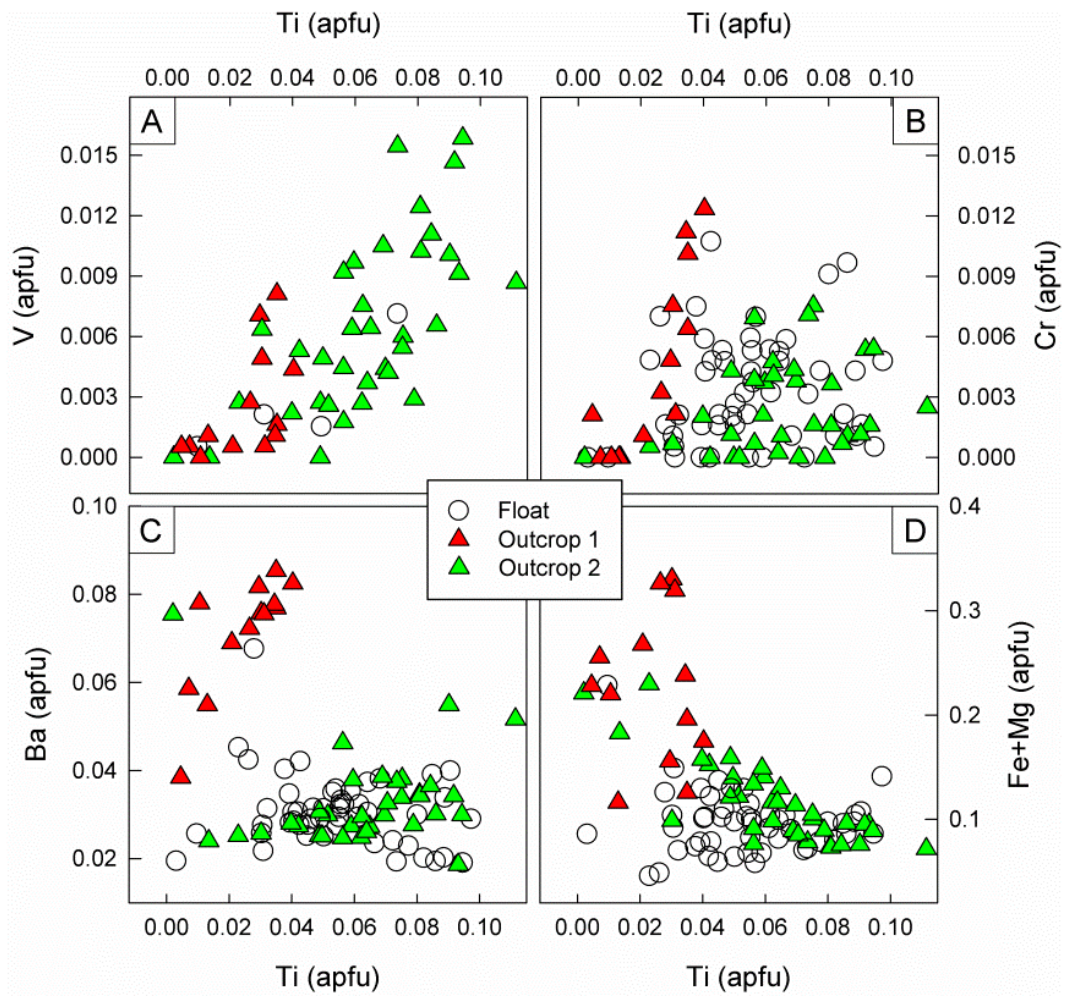


Figure 3.9: Chemical composition of muscovite. A) V vs. Ti; B) Cr vs. Ti; C) Ba vs. Ti; D) Fe+Mg vs. Ti.

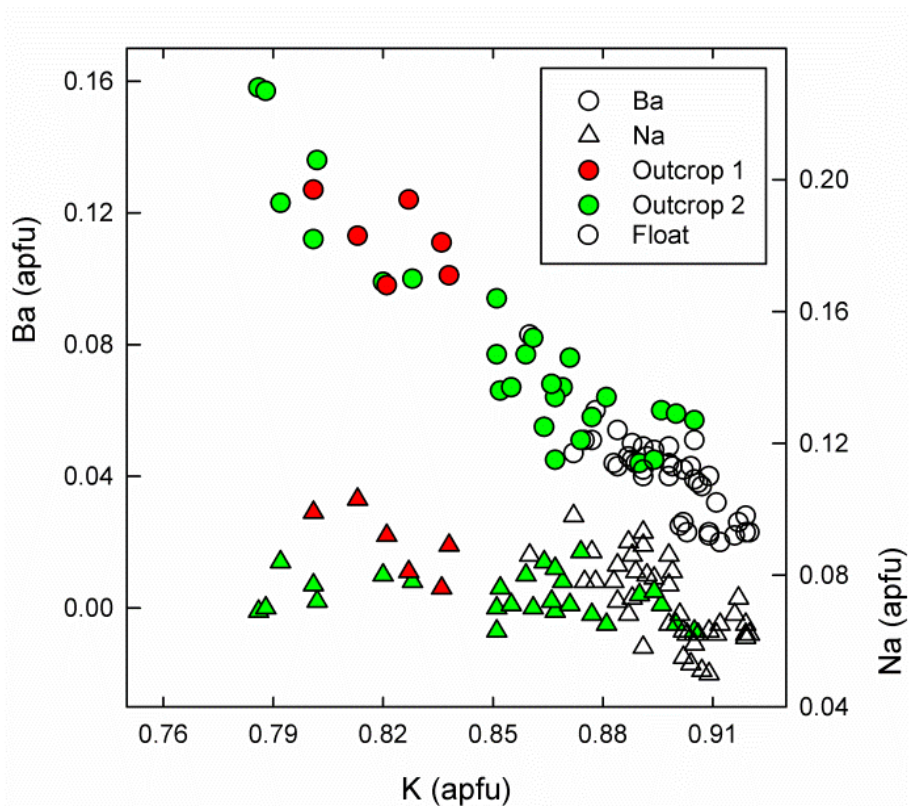


Figure 3.10: Variation of Ba and Na vs. K in K-feldspar.

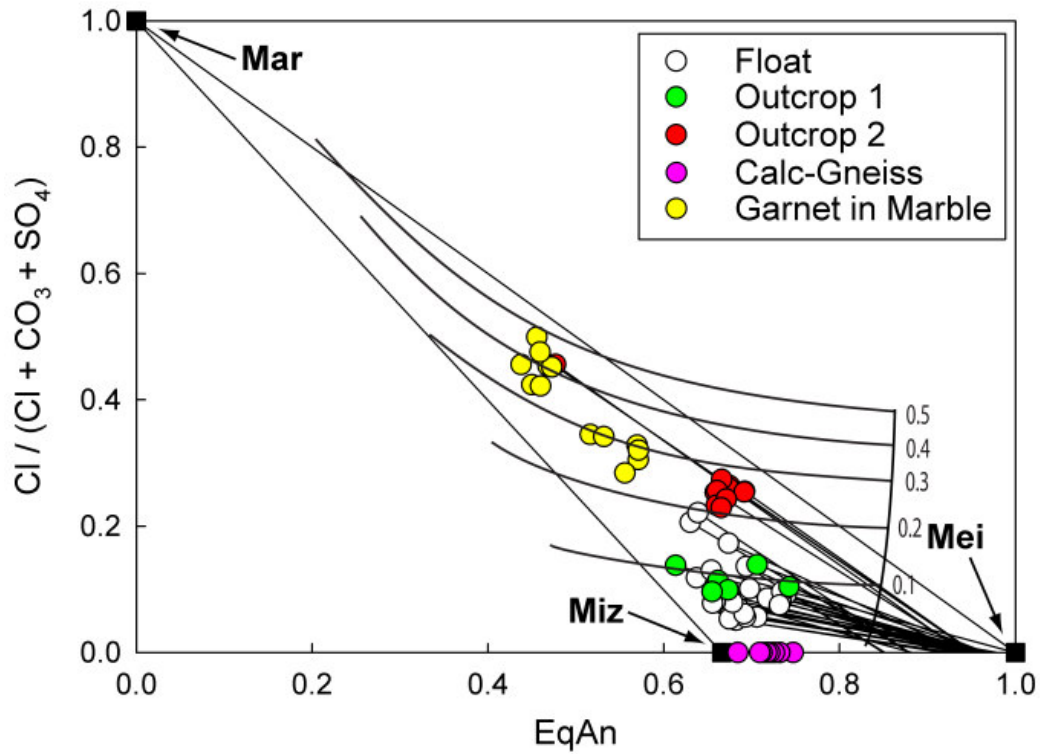


Figure 3.11: Compositional diagram for scapolite showing the meionite, marialite, mizzonite solid solution in terms of $\text{Cl}/(\text{Cl} + \text{CO}_3 + \text{SO}_4)$ and equivalent anorthite $\text{EqAn} = (\text{Al}-3)/3$. The curves indicate NaCl content of fluids according to the experimental data of Ellis (1978) for 4 kbar and 750 °C.

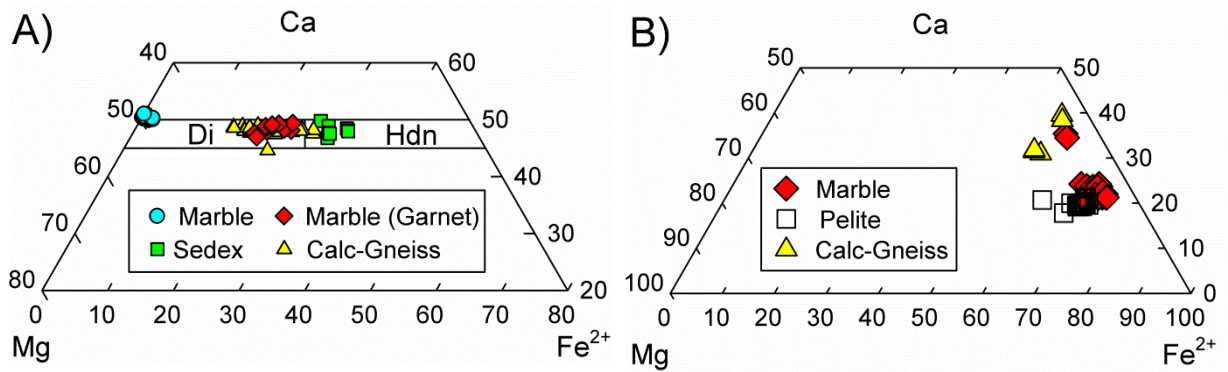


Figure 3.12: Composition of (A)clinopyroxene and (B) garnet from marble, SEDEX, host rocks and the garnet assemblage in the marble.

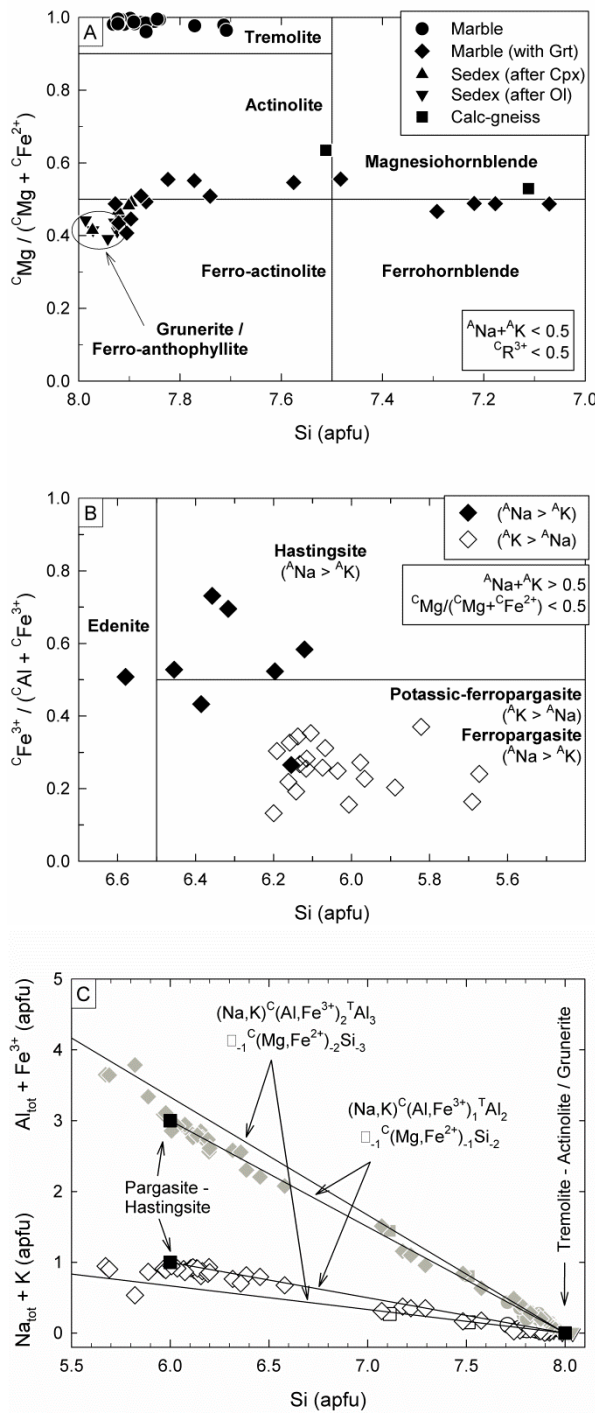


Figure 3.13: Composition of amphiboles. A) Classification diagram for Ca-amphiboles with $(\text{Na} + \text{K}) < 0.5$ apfu; B) Classification diagram for Ca-amphiboles with $(\text{Na} + \text{K}) > 0.5$ apfu.

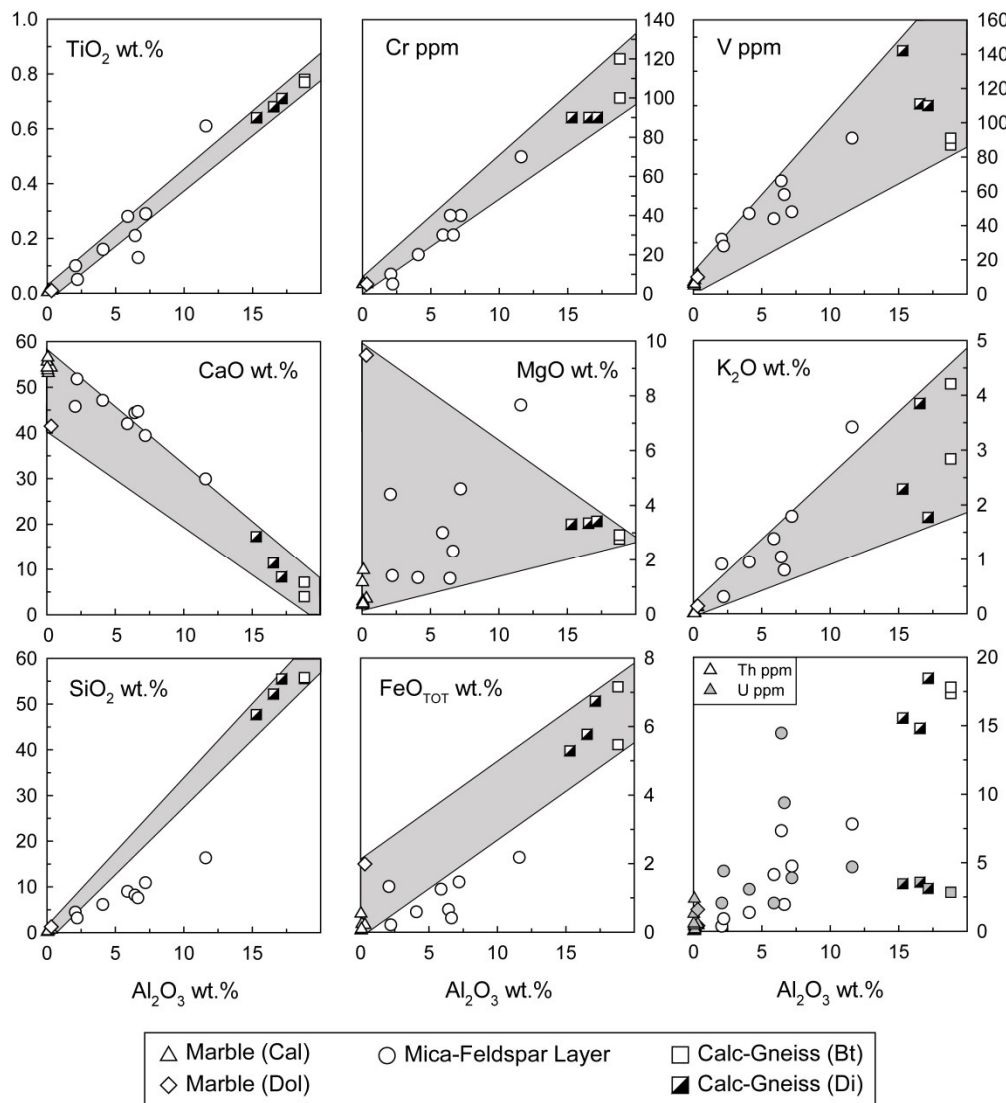


Figure 3.14: Contents of immobile trace elements (Cr, Ti, and V), selected mobile major elements (Si, Fe), and partially mobile elements K, Ca, Mg in different lithologies.

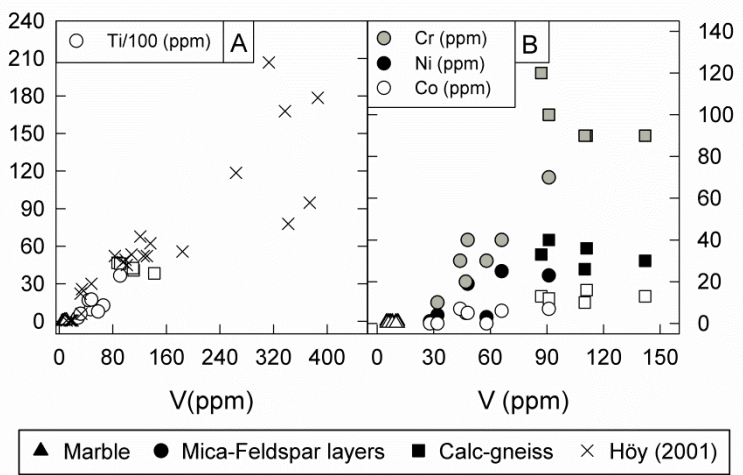


Figure 3.15: Geochemistry of selected trace elements in host rock and marble. Data for amphibolites in Unit 6B are from Höy (2001).

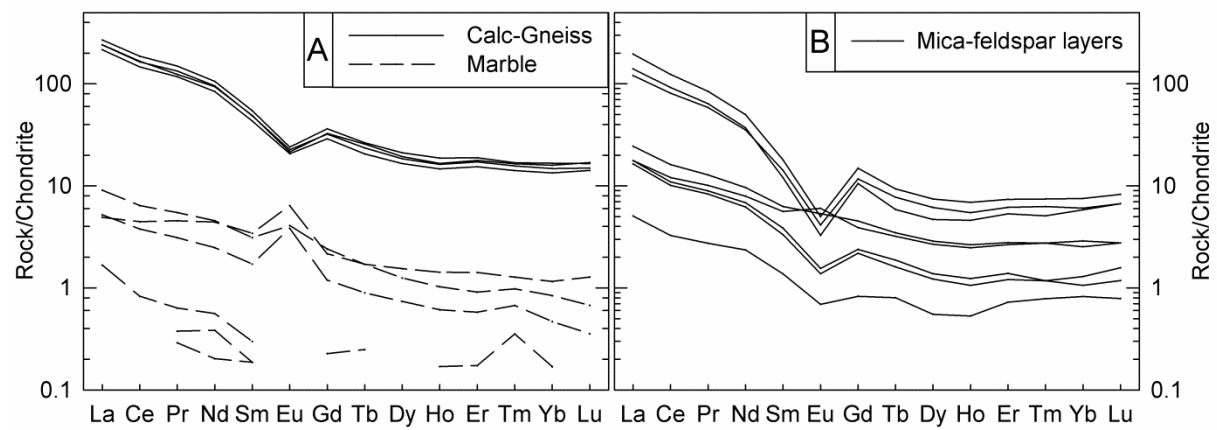


Figure 3.16: Chondrite-normalized (Sun and McDonough 1989) REE-plots for (A) calc-gneiss and marble, (B) mica-feldspar layers in the marble.

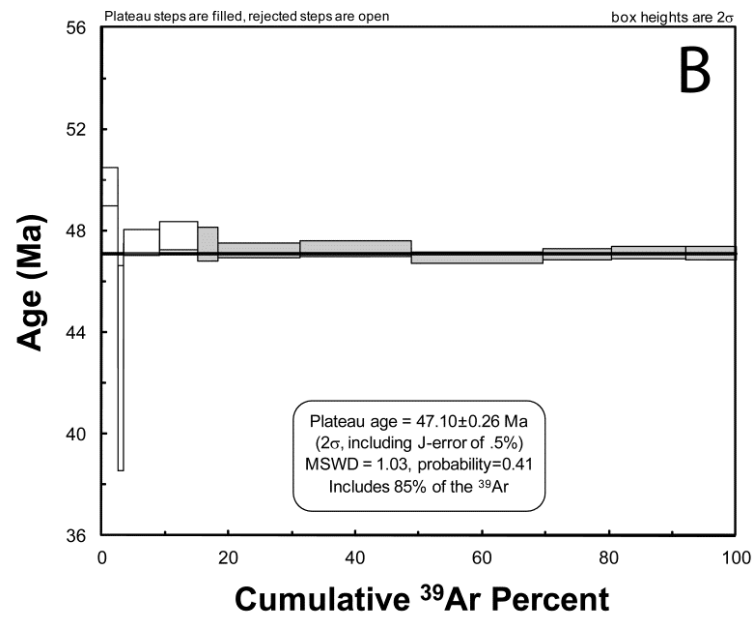
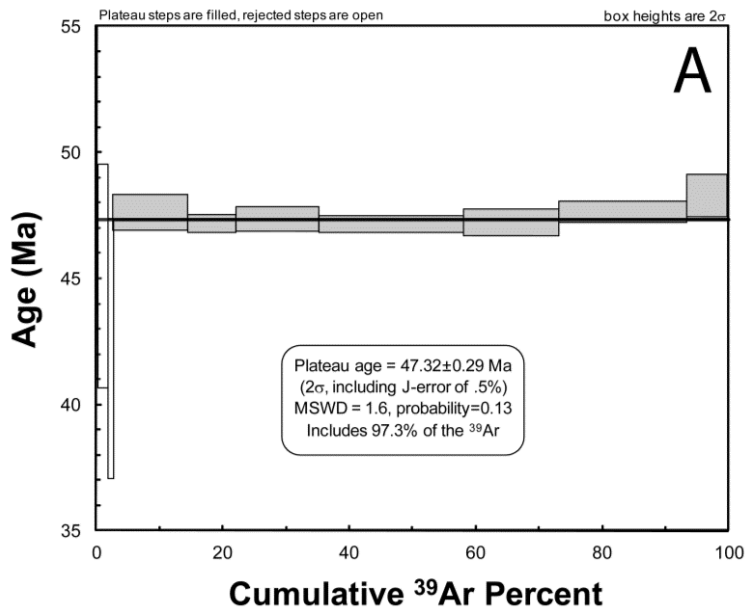


Figure 3.17: ^{40}Ar - ^{39}Ar plateau ages for Revelstoke corundum occurrence from A) phlogopite; B) muscovite.

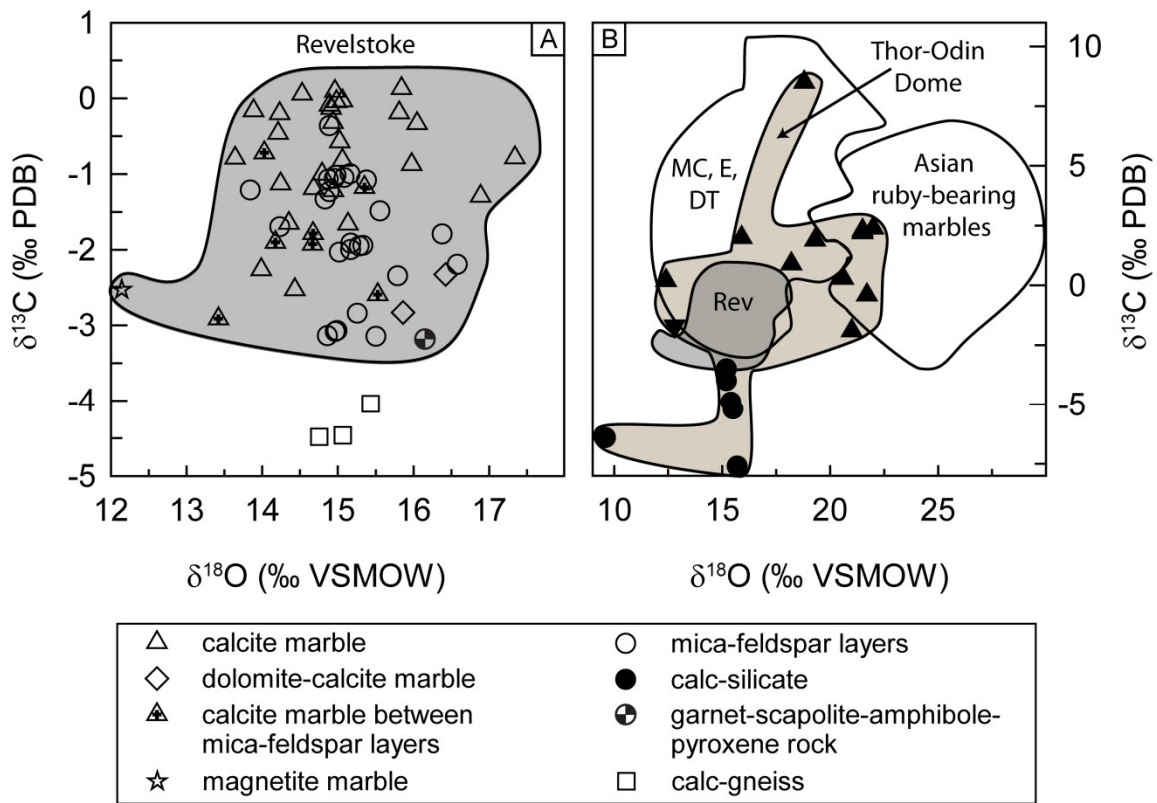


Figure 3.18: Coupled $\delta^{13}\text{C}$ - $\delta^{18}\text{O}$ values for carbonate from different lithologies. (A) Published values for other marbles from the Mica Creek (MC), Esplanade Range (E), and Dogtooth Range (DT) ~ 50 km north of the Monashee Complex in the Selkirk Allochthon (Ghent and O'Neil 1985), Thor-Odin Dome (Holk and Taylor 2000) and Asian ruby deposits in marble (Garnier et al. 2008) compared to the studied Revelstoke lithologies. (B) Values for the studied lithologies from the Revelstoke (Rev) occurrence.

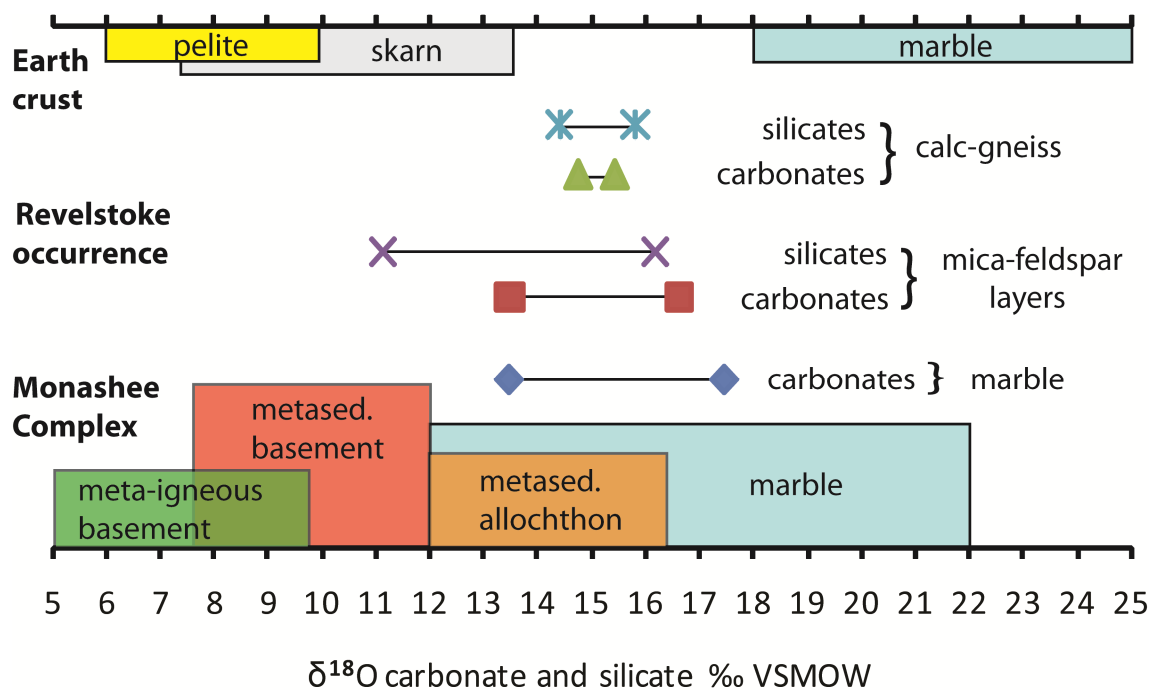


Figure 3.19: Range of $\delta^{18}\text{O}$ values for carbonate and silicate minerals compared to potential protoliths in the Monashee Complex near the Thor Odin dome (Holk and Taylor 2000) and to average values for pelites (Hoefs 2004), skarns (Bowman 1998), and marbles (Valley 1986).

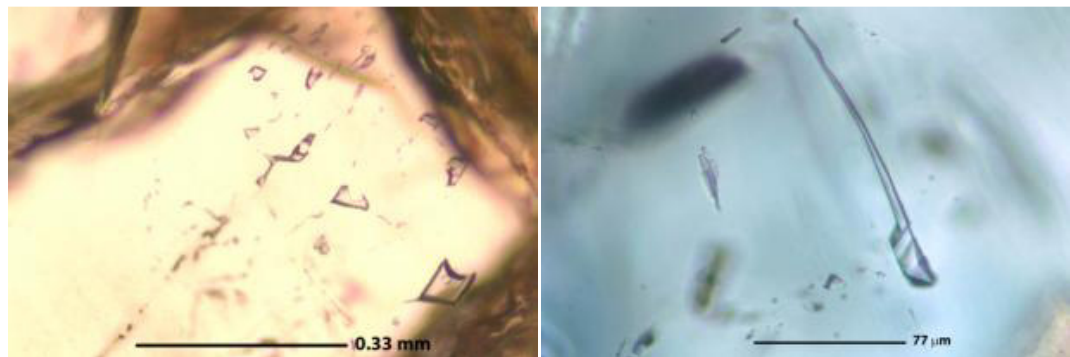


Figure 3.20: Two-phase primary liquid-vapour CO_2 (with minor $\text{CH}_4\text{-N}_2$) fluid inclusions in corundum.

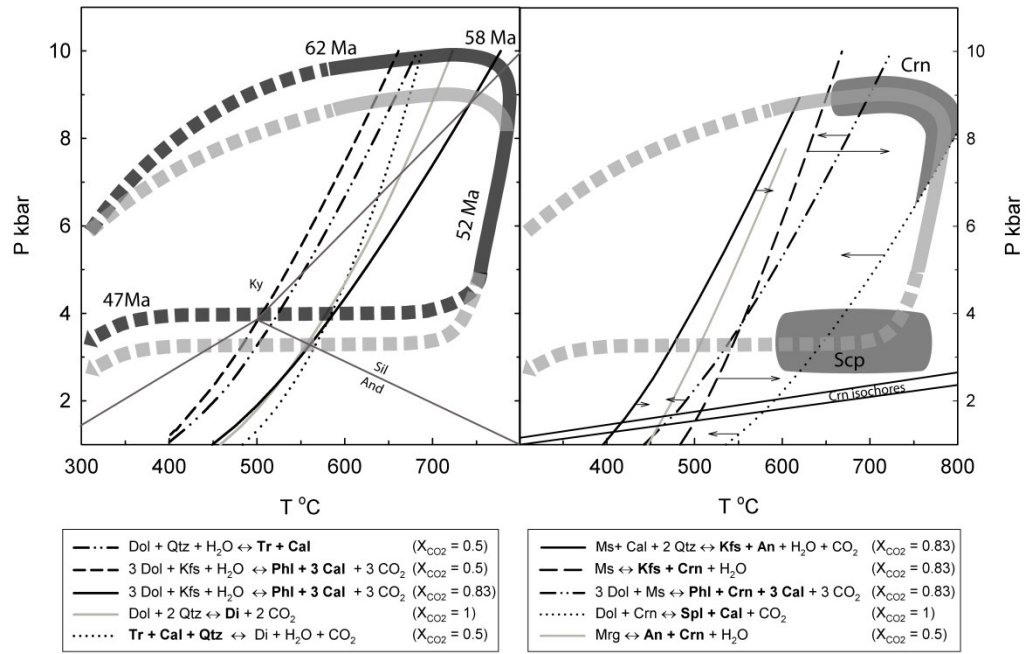


Figure 3.21: Major mineral forming reactions and PT evolution of the Revelstoke occurrence marble. Bolded mineral names indicate observed mineral assemblages. Arrows indicate position of curves with increasing $X_{\text{H}_2\text{O}}$. Corundum fluid inclusion isochores are also plotted.

Chapter 4: Kimmirut Sapphire Occurrence

4.1 Introduction

The Kimmirut sapphire occurrence (KSO) is hosted in calc-silicate lenses within a localized area of the Paleoproterozoic Lake Harbour marble of the metasedimentary Lake Harbour Group (LHG) approximately 1.5 km southwest of Kimmirut (formerly Lake Harbour), near the south coast of Baffin Island, Nunavut ($62^{\circ}49.7'N$, $69^{\circ}53'W$, 25K/13, 1:50,000, Fig. 4.1; Rohtert and Pemberton 2004, Rohtert 2005, Gertzbein 2004 and 2005, Lecheminant *et al.* 2004 and 2005, Wilson 2009, Fagan and Miller 2012). The KSO was discovered by local Kimmirut prospectors Seemeega and Nowdla Aqpid in 2002. Subsequently, True North Gems Inc. bought the project from the brothers and went on to discover 35 additional sapphire showings.

Southern Baffin Island is exceptional because it contains complexly deformed, high-grade metamorphic rocks (St-Onge *et al.* 2007) that host many gem minerals in addition to sapphire, including garnet (almandine), spinel, tourmaline, cordierite (Walker 1915; Wilson 2009), scapolite (Walker 1915), pargasite (Wight 1986; Tait *et al.* 2001), lapis lazuli (Hogarth and Griffin 1978), and zircon (Wilson 2007). For the most part, these gem localities were discovered serendipitously and have not been studied in detail.

The objectives of this work are to characterize the sapphire mineralization in the KSO and to develop a genetic model of mineralization in order to develop an exploration strategy for this type of deposit. The mineralogy and geochemistry of two coarse-grained calc-silicate pods called the Beluga (sapphire-bearing) and Bowhead (nepheline-bearing without sapphire) showings are compared because of their close proximity (170 m between showings) and similar mineralogy and texture. The results from these two deposits are also compared to the whole rock geochemistry of different lithologies in the region (Thériault *et al.* 2001, Butler 2007) in an attempt to find potential protoliths for the deposit.

4.2 Regional Geology

The Kimmirut sapphire occurrence is hosted within calc-silicate lenses within a marble unit (Fagan 2010) of the metasedimentary Lake Harbour Group (LHG), which is part

of the Meta Incognita microcontinent (MIM) within the Quebec-Baffin segment of the Trans Hudson orogen (St-Onge et al. 1996). The Trans-Hudson orogen is a Himalayan-scale collisional orogenic belt extending over 4600 km in strike length from the central part to the northeastern edge of North America (St-Onge et al. 2007). The Meta Incognita micro-continent is separated from the Narsajuaq magmatic arc by the Soper River suture (Fig. 4.1). The MIM is composed of (1) a clastic-carbonate shelf succession (Lake Harbour Group; Davison 1959, Jackson and Taylor 1972, Scott 1997) and its crystalline basement (Ramsay River orthogneiss; St-Onge et al. 1998); (2) an overlying foreland basin succession (Blandford Bay assemblage; Scott et al. 1997); and (3) an extensive suite of quartz diorite to monzonogranitic plutons (Cumberland batholith; Jackson and Taylor 1972) that intrude the platformal and foreland basin rocks and underlying crystalline basement (St-Onge et al. 1999).

Two metamorphic and three deformation events are recorded in the area over a *ca.* 80 Ma period (St-Onge et al. 2007). The first deformation event, D₀, post-dates deposition of the Lake Harbour Group and pre-dates emplacement of the Cumberland Batholith (St-Onge et al. 1999, St-Onge et al. 2007). This event involved the accretion of the MIM to the Rae craton and closing of the Baffin suture. The second event, D_{1a}, involved continued convergence of the southern margin of the MIM to the Narsajuaq arc and formation of the Soper River suture. The Soper River suture is the structural base of the MIM.

The first metamorphic event (M₁) corresponds with the waning stages of the Cumberland batholith magmatism and crustal thickening (D_{1a}) related to collision and accretion of the Narsajuaq arc (St-Onge et al. 2007). It can be further subdivided into: 1) M_{1a}, a granulite-facies metamorphic event characterized by a compressional P-T path with peak P-T conditions of up to 810 °C and 8.3 kbar, and 2) M_{1b}, a high-temperature thermal perturbation event that occurred, possibly related to either a prolonged M₁, or to the intrusion of felsic dikes and plugs.

The third deformation event (D₂) involved collision of the northern Churchill plate, consisting of the Rae craton plus the MIM, Narsajuaq arc, and ophiolite units, with the Superior craton. This resulted in (1) closure of the Bergeron suture and (2) reactivation and further shortening of the Soper River suture.

The second metamorphic event (M_2) is characterized by retrograde upper-amphibolite facies metamorphism of granulites related to a clockwise decompression P-T path with P-T conditions of up to 710 °C and 6.0 kbar, and crustal deformation corresponding to D_2 (St-Onge et al. 2007).

The final event recorded in the area is characterized by greenschist facies retrograde assemblages, which may be related to post- D_2 thermal and fluid activity associated with crustal magmatism (St-Onge et al. 2007). This event corresponds to the emplacement of syenogranite pegmatite dykes in the Churchill plate (St-Onge et al. 2007).

The continental collision setting, as well as the type, duration and extent of polymetamorphic evolution in southern Baffin Island, is believed to be analogous to gem-producing areas within the India-Asia collision zone (*i.e.*, from Afghanistan to Vietnam) (LeCheminant et al. 2005; St-Onge et al. 2007 and references therein). Both orogens, "underwent early thermal metamorphism related to the emplacement of pre-collisional, Andean-type plutonic suites, followed by subsequent metamorphic events that were related to continental collision or to post-collisional crustal fluid flow" (St-Onge et al. 2007).

4.3 Local Geology:

The LHG is exposed as a continuous belt extending up to 500 km northwestward along the southern shore of Baffin Island, Nunavut. It dominantly contains: (1) semi-pelite and garnetiferous psammite, (2) garnetiferous psammite and quartzite, and (3) marble and calc-silicate schist (which hosts the Kimmirut sapphire occurrence) (Fagan 2010; St-Onge et al. 2007). These lithological layers are interpreted to be due to primary deposition in a shallow marine environment. Minor amounts of mafic schist are also present; granitoid plutons and gneisses surround the LHG (Scott and Godin 1995). The marble and calc-silicate schist are the characteristic features of the LHG.

Ultramafic (peridotite to pyroxenite) to mafic (diorite) sills intrude the LHG and predate the emplacement of the Cumberland batholith (St-Onge et al. 2000). Following the emplacement of the Cumberland batholith, other magmatic events include granitoid intrusions, partial melting derived monzogranites, and late undeformed syenite and syenogranite pegmatites (Scott 1997, Scott and Godin 1995, St-Onge et al. 2007).

4.4 Lake Harbour Marble

The composition of the Lake Harbour Marble and associated calc-silicate and micaceous siliciclastic layers vary considerably across the unit. The compositional layering ranges in thickness from centimeters to meters and extends up to tens of metres along strike. This layering is interpreted as relict primary compositional variation due to varying degrees of carbonate and siliciclastic input from an unknown source onto an unknown basement at <1.93 Ga (Scott 1997; St-Onge *et al.* 1998). The marble dominantly contains coarsely recrystallized calcite and diopside, along with minor amounts of forsterite, phlogopite, spinel, graphite, wollastonite, tremolite, pargasite, nepheline, and /or K-feldspar (Scott 1997, Herd et al. 2000, Butler 2007, Davison, 2005, 2006). Calc-silicate layers within the marble commonly contain diopside, pargasite, scapolite, phlogopite, calcite, titanite, quartz, and plagioclase (Herd et al. 2000, Butler 2007). Near the town of Kimmirut, calc-silicate lenses within the marble host sapphires (Cade *et al.* 2005, LeCheminant *et al.* 2005, True North Gems Inc. 2003). Throughout the marble there are also individual isolated bodies of micaceous siliciclastic rocks that commonly occur near contacts with adjacent siliciclastic rocks. These contact zones typically contain phlogopite, hornblende, diopside, hematite, and graphite with secondary goethite (Scott and Godwin 1995). These siliciclastic rocks may be associated with tabular bodies, concordant layers, or irregular pods of monzogranite likely derived from partial melting of host siliciclastic rocks during regional metamorphism (St-Onge *et al.* 2007; Scott and Gauthier 1996).

4.5 Geology and Petrography of the Sapphire Occurrence

4.5.1 Marble

The marble immediately surrounding the Beluga occurrence contains medium to very coarse grained (3 to 5 mm) calcite with fine to medium grained silicate layering composed of varying proportions of phlogopite + diopside (violet or green) + graphite + plagioclase + apatite ± scapolite (Gertzbein 2005). It rarely contains rafts or veins of extensively altered

mafic rocks and very rarely contains late tourmaline- (dravite) and Mg-chlorite-bearing veins. Graphite can also occur in late veins.

4.5.2 Course-Grained Calc-Silicate Pods in Marble

The pods (or boudins) range in diameter from 20 cm to 4 m and appear to occur randomly throughout the marble (Gertzbein 2005, Fagan pers. comm. 2013). In contrast to the surrounding marble, they are typically composed of the following coarse to very coarse-grained minerals: diopside (green or purple) + phlogopite + plagioclase + apatite (blue or green) ± graphite. Rare sapphire- or nepheline-bearing calc-silicate pods are always associated with scapolite. Very rare coarse-grained plagioclase (1-2 cm) or calcite (up to 20 cm) can also occur in the pods along with the typical assemblage.

The Beluga and Bowhead showings are very coarse-grained calc-silicate pods with their own unique mineralogy (described below). They have sharp contacts with the surrounding marble (Fig. 4.2). The Bowhead showing is 170 m SSW of the Beluga showing and has a surface exposure of 2 meters by 1.5 meters, whereas the Beluga has a surface exposure of 4.2 meters by 3.7 meters. There is speculation that the Beluga showing and the nearby Narwhale showing merge at depth; this could have potentially important economic implications (Fagan, pers. comm. 2013).

4.5.2.1 Beluga

The Beluga showing is characterized by randomly oriented, rectangular blocks of prograde (violet) diopside enclosed and eroded by a rim of retrograde phlogopite-plagioclase symplectite (Fig. 4.2, 4.3). The symplectite is commonly surrounded by scapolite (Fig. 4.3, 4.4, 4.5). This scapolite separates the symplectite from a very fine-grained and altered zone containing muscovite, albite, euhedral corundum (sapphire), minor calcite and scapolite, and rare graphite (Fig. 4.3, 4.4, 4.5). K-feldspar perthite was also observed in other sapphire-bearing calc-silicate pods, but not at the Beluga showing (Hansen 2008). Scapolite also surrounds zones of extensive alteration (Fig. 4.5).

The diopside grains range in size from 3 by 1 cm to <1 by <1 mm and have irregular edges (Fig. 4.5A). Large grains occasionally contain inclusions of phlogopite.

The phlogopite + plagioclase symplectite contains minor calcite, and accessory titanite, zircon, and relict diopside (Fig. 4.4, 4.7, 4.8, 4.9). Phlogopite within the symplectite can occur as randomly oriented groups of fine-grained subhedral grains (Fig. 4.5B), and/or preferentially oriented fine- to medium-grained subhedral grains aligned parallel to the length of the diopside grains (Fig. 4.5A). In both cases, subhedral plagioclase grains separate phlogopite grains (Fig. 4.7, 4.8, 4.9, 4.10). The preferentially oriented phlogopite grains give the diopside rimmed by phlogopite + plagioclase symplectite a rectangular appearance (Fig. 4.2, 4.3). Occasionally, medium-grained phlogopite surrounded by calcite occurs on the edge of diopside grains (Fig. 4.5A). Anhedral calcite grains with rounded edges typically occur in contact with or as inclusions within phlogopite, but can also occur in contact with both phlogopite and calcite, or as isolated grains between subhedral plagioclase (Fig. 4.7, 4.8, 4.10). Phlogopite adjacent to scapolite on the edge of the symplectite contains inclusions of scapolite and plagioclase (Fig. 4.11). Rare titanite rims calcite in contact with phlogopite and plagioclase (Fig. 4.7) or rims phlogopite in contact with plagioclase (Fig. 4.10). Extremely rare very fine-grained zircon occurs along the grain boundary between calcite and plagioclase grains.

Scapolite separates the phlogopite-plagioclase symplectite from the muscovite-albite-calcite-corundum zone. It contains minor inclusions of the symplectite and forms a distinct boundary next to the muscovite-albite-calcite-corundum zone. The scapolite crystals range in width from 0.6 mm to 2 cm (Fig. 4.3, 4.5, 4.11). They are typically monomineralic and rarely contain inclusions of phlogopite, plagioclase, and calcite. They are altered along fractures to calcite and plagioclase. It appears that fluids entered the crystals from the muscovite-albite-calcite-corundum side of the grain towards the symplectite side.

Zones of extensive alteration typically occur on the boundary between scapolite and the muscovite-albite-calcite-corundum zone. They are comprised of many very fine-grained intergrown minerals that cannot be distinguished or identified by SEM or petrography. These zones are commonly surrounded by scapolite and appear to be light brown in plane polarized light (Fig. 4.5A). X-ray diffraction analysis of these zones identified possible thomsonite, faujasite, muscovite, nepheline, prehnite, and sodian meionite.

Euhedral corundum (sapphire) occurs in a light-coloured, highly altered matrix of fine- to medium-grained muscovite and albite, minor calcite and scapolite, and rare graphite

(Fig. 4.2, 4.3, 4.5, 4.6). Albite commonly armors corundum. Corundum crystals may be fractured and have corroded grain boundaries. They may also contain ovoid calcite and apatite inclusions, and a coating of prismatic thomsonite, which can penetrate deeply into the crystals.

4.5.2.2 Bowhead

The Bowhead showing has similar mineralogy and textures to the Beluga occurrence, but is distinct because of the presence of nepheline and lack of both the mineralized albite-muscovite-corundum zone and the areas of extensive alteration. The Bowhead showing is characterized by randomly oriented, rectangular blocks of violet diopside grains that are enclosed and eroded by a rim of phlogopite-plagioclase symplectite when in close proximity to nepheline (Fig. 4.12). The symplectite only forms on the side of the nepheline nearest to the diopside, and will not form when nepheline is surrounded by coarse-grained calcite. Nepheline is altered along cleavage planes to an unidentified grainy isotropic mineral. The symplectite and nepheline are commonly rimmed by scapolite (Fig. 4.12). As at the Beluga showing, the scapolite also contains inclusions of possible relict phlogopite-plagioclase symplectite. Visually the pods appear to be quite similar.

4.6 Mineralogy

4.6.1 Sapphire

The following is summarized from LeCheminant et al. (2004). The Beluga showing dominantly contains deep blue sapphires with violet overtones, but colourless varieties are common as well (Fig. 4.13A). Throughout the KSO, corundum crystals are commonly euhedral barrel-shaped crystals with tapering ends (Fig. 4.14A). The average size of sapphire crystals at the Beluga showing is 15 x 4 mm, but large crystals up to 7.7 x 2.1 cm also occur. Most of the sapphires are characterized by colour and compositional zoning (Fig. 4.13B, 4.14A, B). Rarely, needles of thomsonite coat sapphire grain boundaries and may penetrate into the core of crystals. Smaller crystals are generally free of inclusions, whereas the larger

ones are more fractured and, in most cases, are included with calcite and/or apatite. There is no apparent link between the size of sapphire crystals and their clarity or colour; furthermore, the quality of sapphire crystals appears to be randomly distributed throughout the KSO (Fagan pers. comm. 2013).

Blue and colourless sapphires from the Beluga showing contain elevated FeO and TiO₂; FeO contents range from 0.01-0.13 wt%, with a majority of samples also having <0.15 wt% TiO₂ (Appendix B.1; Fig 4.15). A maximum of 0.30 wt% TiO₂ was recorded. V₂O₃ was below the detection limit.

4.6.2 Nepheline

Nepheline only occurs at the Bowhead showing; none was identified at the Beluga showing. Analyses from several grains of nepheline at the Bowhead showing are fairly homogeneous, with an average composition of Na_{2.89}K_{0.50}□_{0.39}Ca_{0.26}Al_{3.89}Si_{4.18}O₁₆ (Appendix B.2); the Na/(Na+Ca+K) ratio ranges from 0.79 to 0.81.

4.6.3 Diopside

Violet coloured diopside is very rare around the world, but is common within the LHM and KSO (Herd et al. 2000). The composition of diopside from the Beluga and Bowhead showings is distinct. Diopside from the Beluga showing has an average composition of Di₉₀Jd₇Ae₃, whereas diopside from the Bowhead showing has an average composition of Di₉₃Jd₆Ae₂ (Fig 4.16; Appendix B.3). Diopside at the Beluga showing is enriched in Al (0.23 to 0.33 apfu), Fe³⁺ (0.04 to 0.05 apfu), and Ti (0.03 to 0.04 apfu) and depleted in Mg compared to the Bowhead showing (Al: 0.15 to 0.29 apfu, Fe³⁺: 0.03 to 0.04 apfu, and Ti: 0.01 to 0.03 apfu; Fig. 4.17).

4.6.4 Phlogopite

Phlogopite within the symplectite from the Beluga and Bowhead showings can be distinguished. Phlogopite from both showings has a minor muscovite component (Fig. 4.18A, B; Appendix B.4) and the amount of ^[4]Al overlaps in the lower range (1.22 to 1.26 apfu); however the highest amounts of ^[4]Al (up to 1.37 apfu) and ^[6]Al (up to 0.11 apfu) are from the Beluga showing. The major distinction between the two localities can be observed

in terms of Ti, Fe²⁺, Mg, and F contents (Fig. 4.18 C, D, E). In general, Beluga phlogopites have elevated Ti (0.11 to 0.16 apfu), lower Mg (2.36 to 2.60 apfu), and lower F (0.25-0.41) than Bowhead phlogopites (Ti: 0.09 to 0.11 apfu; Mg: 2.57 to 2.65 apfu; F: 0.41 to 0.46 apfu).

4.6.5 Muscovite

Muscovite predominantly occurs in the muscovite-albite-calcite-corundum mineralized zone at the Beluga showing, but extremely fine-grained muscovite was also found at the Bowhead showing within a nodule enclosed by plagioclase and scapolite. Muscovite from the Beluga showing has contents of Al (2.94 to 2.97 apfu), Ti (0 to 0.009 apfu), K (0.87 to 0.94 apfu), and Na (0.085 to 0.135 apfu) (Fig. 4.19; Appendix B.5). Muscovite from the Bowhead showing has a significant paragonite component (Na: 0.21 to 0.25 apfu), elevated Al (3.01 apfu), and lower K (0.73 to 0.79 apfu) when compared to the Beluga showing.

4.6.6 Plagioclase

Plagioclase from within the symplectite at both showings is different from plagioclase in the muscovite + plagioclase + calcite + corundum-bearing mineralized zone at the Beluga showing. The composition of plagioclase in the symplectite is similar at both the Beluga (Ab₇₁ up to maximum of Ab₉₀) and Bowhead showings (Ab₇₄ to Ab₇₉) (Appendix B.6). At the Beluga showing, the anorthite content of plagioclase in the symplectite decreases (from ~An₂₅ to An₁₄) with increasing distance from the scapolite crystals. The composition of plagioclase in the muscovite + plagioclase + calcite + corundum-bearing zone at the Beluga showing is almost pure end-member albite (Ab₉₃ to Ab₁₀₀) as is the plagioclase (Ab₉₇ to Ab₉₉) in the plagioclase-muscovite nodule at the Bowhead showing; however, this does not mean that the Bowhead nodule and the corundum bearing zones at Beluga are similar.

4.6.7 Scapolite

Scapolite from the Beluga showing has a wide range of EqAn (0.36-0.69), whereas the scapolite from the Bowhead showing has a much narrower compositional range (EqAn = 0.50 to 0.67; Fig. 4.20; Appendix B.7). At both localities, X_{Cl} varies significantly (Beluga:

$X_{Cl} = 0.15$ to 1.0 ; Bowhead: $X_{Cl} = 0.43$ to 0.83). Analyses that contain lower Na and higher Cl than expected for ideal marialite-meionite solid solution are likely the result of Na mobility away from (and Cl mobility towards) the electron beam during electron microprobe analysis (Fig. 4.20; Vanko and Bishop 1982). The compositional range for scapolite grains varies depending on the sample analyzed. At both localities there is a cluster of analyses around X_{Cl} 0.7 to 0.9. Minor compositional zoning exists in grains at each locality, but the magnitude and direction of zoning appears to be random and is not related to proximity to other phases (Fig. 4.21A).

Preliminary high resolution hyperspectral images show two different reflectance spectra which may represent minor compositional differences in scapolite (Fig. 4.22; David Turner pers. comm. 2013). This suggests that two different generations of scapolite may exist at the Beluga occurrence, but they were not noticeable using traditional optical microscopy or back scatter electron images from scanning electron microscopy. If detailed high resolution hyperspectral images are collected from the thin sections, they could be used to target areas for future microprobe analysis.

One important characteristic of the scapolite from both the Beluga and Bowhead showings is that it fluoresces under UV light due to the presence of S^{2-} . This has successfully been used as an exploration tool to find corundum (and scapolite)-bearing calc-silicate pods (Fagan, 2010).

The composition of plagioclase ($\sim An_{0.23}$) associated with the symplectite and the plagioclase + muscovite + calcite + corundum on either side ($An_{0.01}$) of scapolite was compared at both localities (Fig. 4.21B). It is typical for scapolite to be Ca- and Al-rich (have greater anorthite content) relative to coexisting plagioclase (Rebbert and Rice 1997). Positively sloped tie lines between associated plagioclase and scapolite at both localities indicate possible equilibration of the plagioclase with a late Na-Cl enriched fluid phase (Rebbert and Rice 1997; Kullerud and Erambert 1999), possibly with a NaCl content of 0.3 to 0.5 (Fig. 4.21B; Ellis 1978). The slope of most natural scapolite-plagioclase pairs in equilibrium is $\sim 74\text{--}78^\circ$ (Rebbert and Rice 1997; Kullerud and Erambert 1999), suggesting that the plagioclase that is most likely in equilibrium with scapolite at both showings is the plagioclase from the symplectite (Fig. 4.21B).

4.6.8 Other Accessory Minerals

Accessory minerals from the Beluga showing were analyzed by a previous researcher (Andrea Cade), but maps containing the location of analyzed points cannot be found. See Appendix B.8 for the compositions of tourmaline (dravite) and sanbornite. See Appendix B.9 for the compositions of thorianite, monazite, and zircon. Other than titanite, most of these analyses were from metamict grains.

4.7 Whole Rock Geochemistry

4.7.1 Major and Trace Elements

Major and trace elements values from whole rock samples were only determined for the Beluga showing (Appendix B.10). The whole rock geochemical signature of the Beluga showing was compared to igneous, gneissic and siliciclastic metasedimentary lithologies from different packages of rocks within the Meta Incognita micro-continent (MIM; Thériault et al. 2001, Butler 2007) in an attempt to identify a potential protolith for the Beluga calc-silicates. The geochemistry of the Beluga showing is correlated with most of these packages in terms of CaO/MgO (Fig. 4.23E), SiO₂/V, MgO/V, and TiO₂/V (Fig. 4.25A,D,E) and it has average amounts of Al₂O₃ (11.47-15.32 wt.%) and Na₂O (2.43-2.96 wt.%; Figs. 4.23-4.25); however, it has the following distinct whole rock geochemical signature: (1) depletion in Fe₂O₃ (1.43-1.83 wt.%), SiO₂ (45.19-46.54 wt%), and Cr (100-130 ppm); and (2) enrichment in MgO (9.28-11.46 wt.%), CaO (15.82-18.86 wt.%), TiO₂ (0.92-1.07 wt.%), and V (218-263 ppm).

The Beluga showing was compared to a calc-silicate, marble, and quartz-feldspar metasediment from Aliquq Island (AI), which is within the LHG northwest of the Beluga showing (Fig. 4.23A; Butler 2007). The Beluga showing and calcsilicate rock are both depleted in Fe₂O₃ and SiO₂, but the Beluga showing has higher Al₂O₃, Na₂O, and TiO₂, (Fig. 4.23B,D, 4.24) and lower MgO. The Beluga showing and marble have very similar Fe₂O₃/MgO (Fig. 4.23C). The Fe₂O₃/MgO, Na₂O/MgO and CaO/MgO ratios of the Beluga

showing are roughly correlated with the quartz-feldspar metasediment and calc-silicate (Fig. 4.23 C,D,E). Vanadium and Cr were not analyzed in samples from Aliuguq Island, so they could not be compared to Figure 4.25. The Aliuguq Island quartz-feldspar metasediment sample has similar contents of Fe_2O_3 , SiO_2 , Al_2O_3 , and TiO_2 and elevated contents of Na_2O and MgO when compared to other regional metasediments (Fig. 4.23, 4.24).

The Beluga showing and the lapis lazuli rocks within the LHM both have very low Fe_2O_3 and SiO_2 , average Al_2O_3 , and high CaO and MgO (Fig. 4.23). The lapis lazuli rocks, however, have much higher Na_2O and much lower TiO_2 than the Beluga rocks (Fig. 4.23D, 4.24). Vanadium, Cr, and REEs were not analyzed in samples from the lapis lazuli rocks, so they could not be compared to Figures 4.24 and 4.25.

The Beluga showing and two diorite samples from the Narsajuaq terrane have similar contents of SiO_2 , Al_2O_3 , Na_2O , MgO , CaO , TiO_2 , and V (Fig. 4.23 B,D,E, 4.24A,B, 4.25A,C,D,E), but the Beluga showing has much less Fe_2O_3 and Cr (Fig. 4.23A,C, 4.24C, 4.25B,F).

The Beluga showing has similar V contents to two semipelites (210 ppm) from the Blandford Bay assemblage, and a pelite (210 ppm), semipelite (170 ppm) and psammite (213 ppm) from the LHG. These pelites and semipelites are also slightly depleted in SiO_2 and strongly enriched in TiO_2 (Fig. 4.25A,E).

4.7.2 Rare Earth Elements

The Rare Earth element (REE) patterns of the Beluga showing are characterized by low total REE-contents (~18 ppm), slightly enriched LREE ($\text{La}_{\text{CN}}/\text{Lu}_{\text{CN}} \sim 2.88$), and a negative Eu-anomaly ($\text{Eu}/\text{Eu}^* \sim 0.13$; Fig. 4.26). The HREE pattern from Gd-Lu is highly variable.

The REE patterns of the Beluga showing were compared to the other lithologies within the Lake Harbour Group. Calc-silicate, metasedimentary, and monzogranite samples are all enriched in LREE ($\text{La}_{\text{CN}}/\text{Lu}_{\text{CN}} = 5.8$ to 28.6) and total REE (71.6 to 375.3 ppm) compared to the Beluga showing. Most lithologies have a distinct negative Eu anomaly, but two pelites have a positive Eu anomaly, and three pelites have no Eu anomaly.

The REE patterns of the Beluga showing were compared to other regional rocks with high V (Fig. 4.27). The LHG pelite, semipelite, and psammite are enriched in total REE (98,

375.3, 285.8 ppm) compared to the Beluga showing. They all have distinct Eu anomalies ($\text{Eu/Eu}^* = 0.1$), enrichment in LREE ($\text{La}_{\text{CN}}/\text{Lu}_{\text{CN}} = 16.1, 7.0, 17.9$) and smooth, fairly flat HREE ($\text{Gd}_{\text{CN}}/\text{Yb}_{\text{CN}} = 1.9, 0.79, 1.74$). Heavy REE in the LHG pelite are only slightly elevated compare to Beluga. The Blandford Bay assemblage pelites are also enriched in total REE-contents (165-359 ppm) compared to Beluga. Their LREE slopes are similar the LHG patterns, but the HREE patterns are significantly depleted compared to LHG and they also do not have a Eu anomaly. The Narsajuaq arc diorites have low total REE-contents (24.9 and 41.1 ppm) and a very shallow slope (almost flat). One sample is enriched in LREE and one is depleted, but both are enriched in HREE compared to Beluga. Granodiorite from the Narsajuaq arc has high total REE-contents (152.3 ppm), strong enrichment in LREE ($\text{La}_{\text{CN}}/\text{Lu}_{\text{CN}} = 476.9$), depleted and steep HREE ($\text{Gd}_{\text{CN}}/\text{Yb}_{\text{CN}} = 7.03$), and no Eu anomaly. The HREE from Tb to Er are similar to Beluga.

4.8 Oxygen Isotopes of Corundum

Blue sapphire from the Beluga showing has a $\delta^{18}\text{O}$ value of $16.4\text{\textperthousand}$ (Fig. 4.28). This is consistent with the lower range of $\delta^{18}\text{O}$ from pink sapphire and ruby in marble from southeast Asia (Mogok, Myanamar, Afghanistan, Pakistan, Nepal, Tadjikistan, and Vietnam) as well as Tanzania, Ural Mountains in Russia, Switzerland, and Macedonia, which range from $16.3\text{\textperthousand}$ to $23\text{\textperthousand}$, but is slightly higher than blue sapphires from desilicated pegmatites in marble ($15.5\text{\textperthousand}$ and $15.9\text{\textperthousand}$, Mogok and Myanmar), as well as sapphires in marble skarn ($10.7\text{\textperthousand}$ to $15.6\text{\textperthousand}$, Andranondambo, Madagascar; Giuliani et al. 2005, 2007). This means the isotopic values correlate well with the expected deposit-type model.

4.9 U-Pb Geochronology

LeCheminant et al. (2005) analyzed the U-Pb geochronology of zircons from the Beluga showing in order to constrain the timing of sapphire crystallization. Zircon was chosen as a proxy for sapphire crystallization because both minerals have similar growth zones as well as calcite inclusions. The zircon fractions have high U contents (608-1258 ppm) and there is no evidence of an inherited component. The U-Pb age of $1782.5 +3.7/-0.8$

Ma, defined using five zircon fractions from the Beluga showing, is consistent with the timing of post-D₂ thermal/fluid activity (1797 ± 2 to $1784 +7/-9$ Ma; Scott and Gauthier 1996, Wodicka and Scott 1997, Scott 1997, Scott and Wodicka 1998, Scott et al. 2002, St-Onge et al. 2007) in the Meta Incognita microcontinent (Fig. 4.29).

4.10 ^{40}Ar - ^{39}Ar dating

Phlogopite and muscovite from the Beluga showing were dated during Andrea Cade's research using the ^{40}Ar - ^{39}Ar method in order to help constrain the thermal history of the study area. Phlogopite has a non-ideal saddle-shaped spectrum with a flat minimum yielding a plateau age of 1646.8 ± 8.6 Ma (Fig. 4.30A). Muscovite has a flat spectrum yielding a plateau age of 1510.4 ± 8.3 Ma (Fig. 4.30B). Closure temperatures of phlogopite and muscovite are ~ 500 and 529 °C (for a cooling gradient of 100 °C/Ma; Baxter 2010), so both ages are interpreted to represent late cooling stage of the marble, and thus the mineralization must pre-date this closure temperature date.

4.11 Discussion

This discussion will focus on the petrogenetic history of the Beluga showing and possible models of corundum formation using petrographic, geochemical, and isotopic evidence. Further research needs to be completed in order to identify thermodynamically possible corundum-forming reactions and to provide stronger arguments for the model of formation of the Beluga showing. All reactions identified in the following sections are based on mineral textures; their stability under different P-T conditions was not determined.

4.11.1 Prograde and Retrograde Mineral Assemblages at both the Beluga and Bowhead Showings

At both the Beluga and Bowhead showings, nepheline and diopside were identified as primary minerals based on mineral textures. Assuming that they formed from a carbonate + feldspar precursor, the assemblage could have been produced during M₁ at P-T conditions \leq

810 °C and 8.3 kbar (St-Onge et al. 2007) in either dolomite- or calcite-rich areas by the reactions:

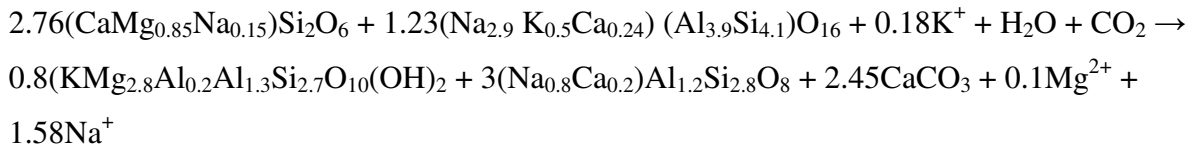
- [1] 3albite + dolomite + K-feldspar → diopside + nepheline + CO₂
- [2] phlogopite + 3calcite + 4quartz + 3albite → 3diopside + nepheline + H₂O + CO₂ + F

The presence of Al and Na in the diopside can be used as a barometer, and this indicates high pressures of formation (Deer et al. 2001).

The retrograde plagioclase-phlogopite symplectite and scapolite crystals at these showings formed at the expense of nepheline and diopside, likely during M₂ retrograde metamorphism at PT conditions ≤ 710 °C and 6 kbar due to the influx of fluids. Based on textural relationships, the following reactions occurred during the addition of (H₂O + CO₂ + Cl)-bearing fluids:

- [3] diopside + nepheline + (H₂O + CO₂ fluid) → phlogopite + albite + calcite + Na⁺
- [4] 3anorthite + calcite + Na,Cl-fluid → scapolite

The reaction [3] stoichiometry using actual mineral compositions is:



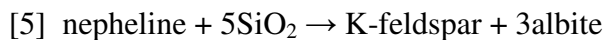
The absence of nepheline and the presence of alteration minerals at the Beluga showing could suggest that all the nepheline was consumed by this reaction. Similar enrichment of Fe, Ti and Mg in both diopside and phlogopite from the Bowhead and Beluga showings provides evidence that diopside was the source of these elements in the phlogopite product. The symplectite texture indicates that the breakdown of diopside + nepheline may have proceeded very quickly (Passchier and Trouw 2005) and the elevated Ti in phlogopite indicates temperatures were between 600-700 °C (Henry et al 2005). Increased Ti in both diopside and phlogopite at the Bowhead showing may indicate higher temperatures of formation (Henry et al. 2005) or that the original protolith was more enriched in Ti. As Mg,

Fe, and Ti were depleted in areas distal to the diopside grains, scapolite was able to form around the symplectite and nepheline. Inclusions of plagioclase and phlogopite in some scapolite grains and the fact that scapolite coats the symplectite areas indicate that the scapolite formed after the symplectite. The scapolite is enriched in Ca compared to the plagioclase because it forms by the addition of Ca and CO₃ into the structure.

4.11.2 Retrograde Corundum + Albite + Muscovite-Bearing Zones at the Beluga Showing

The retrograde formation of the corundum + albite + muscovite-bearing zones at the Beluga showing is difficult to explain. It is likely that these zones were subjected to intense fluid infiltration after the formation of the symplectite. This is evident by the alteration of most minerals in this zone, as well as the alteration of scapolite, which separates this zone from the symplectite. These zones are entirely absent at the Bowhead showing, hence why there is no corundum mineralization at that locality. Throughout the KSO, sapphires are only associated with extensively altered rocks that contain scapolite, indicating that the formation of sapphires is probably closely linked to the formation of scapolite.

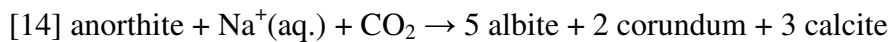
One suggestion for the absence of nepheline at the Beluga showing is that it is much more altered than the Bowhead showing. This means that nepheline was destabilized during retrograde metamorphism during the addition of fluids which may or may not have contained SiO₂(aq). If nepheline broke down due to the addition of siliceous fluids without reacting with any other phases, it could produce K-feldspar and albite by the following reaction:



Reaction [5] however, does not explain the presence of muscovite and corundum.

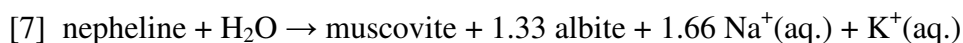
Seven possible reactions exist to explain the minerals present within the corundum + albite + muscovite-bearing zones at the Beluga Showing. These reactions only take mineral associations into account, and not thermodynamic stability. The first possible reaction could occur if the Beluga showing was not as enriched in nepheline as the Bowhead showing and

the majority of corundum formed by the breakdown of anorthite due to the infiltration of Na-CO₂-fluids by the reaction:



The source of Na⁺(aq.) in this reaction may have been produced during the destabilization of nepheline or it may be from another regional source.

The second possibility is if nepheline broke down due to the addition of H₂O-bearing fluids without reacting with any other phases, it could produce similar assemblages and excess alkalis by the following reactions:



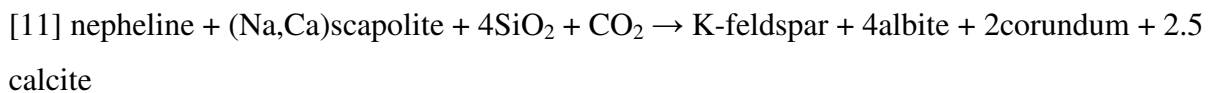
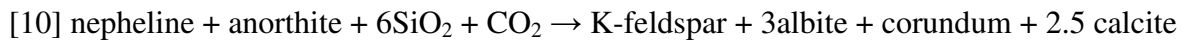
Reactions [6] and [7] are plausible; the dominance of K-feldspar + corundum over muscovite can be dependent on the activity of CO₂ in the system (see Chapter 1 Introduction).

Alternatively, if muscovite formed first in reaction [7], it could have dehydrated to form K-feldspar and corundum during the post-D₂ thermal/fluid activity because of increased temperatures, or increased CO₂ or a combination of the two (see the Revelstoke chapter).

Reactions [6] and [7] are unlikely to have formed all of the corundum, however, because albite is the predominant feldspar (sometimes the only feldspar) in the corundum-bearing zones. If corundum was produced by muscovite breakdown, there would be an approximate ratio of K-feldspar to corundum of 1:1, but this was not observed. Albite commonly armors the corundum, indicating that albite either formed at the same time or shortly after corundum.

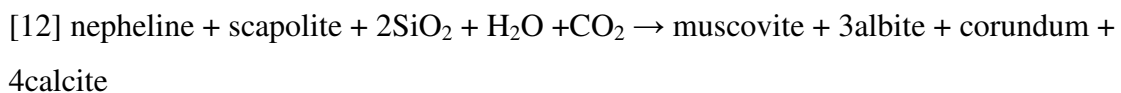
Although I did not see K-feldspar in the thin sections I studied from the Beluga showing, I cannot assume that it is not present in other parts of the showing, because it was documented in other corundum-bearing calc-silicate rocks within the KSO by Hansen (2008). The third possible way of producing mineral assemblages within the corundum + albite + muscovite-bearing zones at the Beluga Showing is if nepheline and plagioclase (or nepheline

and scapolite) are destabilized by the addition of CO₂-SiO₂-bearing fluids; K-feldspar, albite, corundum, and calcite could form by the following reactions:

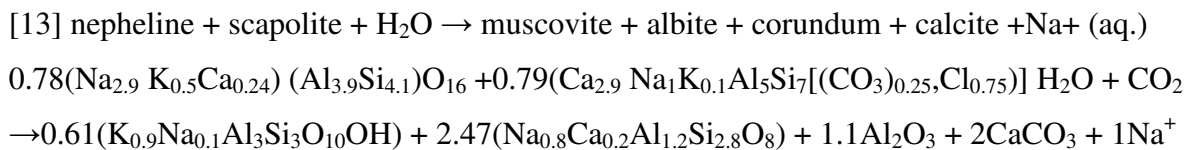


This reaction is unlikely because of the low probability of producing purely anhydrous fluids in this environment. This reaction could possibly occur in a hydrous environment if the products formed above the muscovite stability field.

The fourth possible way of producing mineral assemblages within the corundum + albite + muscovite-bearing zones at the Beluga Showing is if nepheline and scapolite react with the addition of SiO₂-H₂O-CO₂-bearing fluids. In this case, the fluids could produce muscovite, albite, corundum and calcite by the reaction:



The last and most probable way of producing mineral assemblages within the corundum + albite + muscovite-bearing zones at the Beluga Showing is if nepheline and scapolite react with the addition of non-siliceous, H₂O-CO₂-bearing fluids. In this case, the fluids could produce muscovite, albite, corundum and calcite by the reaction:



This reaction can explain the presence of the major minerals within the corundum-bearing zone and the relative proportion of all minerals in this zone, while not requiring a highly siliceous fluid.

4.11.3 Isotopic Evidence

Analysis of zircon grains within the sapphire-bearing lens at the Kimmirut sapphire occurrence by LeCheminant et al. (2005) yielded an age of 1782.5 Ma. This date is consistent with post D₂ thermal/fluid activity and probably indicates that the sapphires formed during retrograde metamorphism when P-T conditions were < 710 °C and 6 kbar. The >100 Ma difference between the Ar-Ar cooling age of the phlogopite and muscovite may be the result of muscovite cooling much later (or slower) than the phlogopite. The data obtained from the phlogopite used in this study was non-ideal; additional analysis of muscovite and phlogopite grains is needed before proceeding with any further interpretations or conclusions.

4.11.4 Protolith of the Beluga Showing

The mineralogy, major, trace, and REE chemistry, and oxygen isotopes of the Beluga showing were compared to potential igneous (alkaline and mafic), metasomatic (metasediments altered by Na-metasomatism), and metasedimentary (evaporite, black shale, and other siliciclastic metasedimentary rocks) protoliths. Only protoliths with low Fe and Si and/or high V, which contain the assemblage nepheline + CPX + plagioclase ± scapolite were considered.

4.11.4.1 Contact Metamorphism of a Mafic Protolith

Hellingwerf (1985) suggested that nepheline, scapolite and diopsidite were produced by contact metamorphism of fragments of a metabasic flow breccia cemented by calcite near Bergslagen, Sweden. Depending on the proximity to a granitic intrusion, different mineral assemblages were identified within the metabasic breccia; the distal mineral assemblage is hornblende + andesine + biotite + calcite + quartz + titanite, whereas the proximal assemblage is nepheline + scapolite + diopsidite + andesine + biotite + calcite with minor pyrrhotite + ilmenite + chalcopyrite + hematite + cubanite. The reaction that likely produced the nepheline-bearing assemblage was: andesine + calcite + hornblende + SO₂ = nepheline + meionite + diopsidite + CO₂ + 2H₂O + FeS.

Corundum-bearing rocks are also found nearby within the contact metamorphosed metatuffites containing the assemblage corundum + microcline + sericite + scapolite +

andalusite + biotite + titanite. Unaltered assemblages nearby are hornblende + biotite + quartz + plagioclase and microcline + diopside + scapolite + biotite + titanite.

Based on the major mineral assemblage alone, a mafic protolith within a calcite matrix could explain the Beluga assemblage. However, the presence of Fe-bearing major and minor mineral phases suggests that this source may have contained too much Fe to be the same source at the Beluga showing. The nepheline crystals at this locality are zoned with lower Ca in the core than the rim contrary to homogeneous nepheline at Beluga. Diopside has Fe represented as 30% hedenbergite component and scapolite has ~70% Me component, which is much more calcic than scapolite from Beluga. No comparisons of whole rock geochemical or oxygen isotope data are able to be made between the Beluga showing and the Bergslagen locality because this data was not collected at the Bergslagen locality. Serpentinized or chloritized intrusive amphibolites have been mapped across the wider Beluga Property, but none are proximal to the Beluga or Bowhead showings and none of the intrusions appear to have reacted with the surrounding marble (Fagan, pers. comm. 2013). Based on the Fe-bearing mineral compositions, the presence of Fe-bearing minerals at the Bergslagen locality, and the absence of any late intrusions causing contact metamorphism of the Beluga showing, it is highly unlikely that this model is valid for the Beluga showing.

4.11.4.2 Alkaline Intrusions Formed by the Assimilation of Carbonate and Siliciclastic Rocks into a Mafic Magma

A nepheline, pyroxene, and scapolite assemblage can also be produced by the assimilation of carbonate and siliciclastic metasediments in mafic magmas (Barnes et al 2005). At the Hortavær complex in Norway, this process can produce a nepheline-bearing monzodiorite with the typical mineral assemblage of plagioclase + K-feldspar + nepheline + amphibole + pyroxene + accessory scapolite + calcite + apatite + titanite + biotite + pyrrhotite + pyrite, and a nepheline-bearing monzonite with the typical mineral assemblage of clinopyroxene + ferropargasite + biotite + andesine or oligoclase ± nepheline and accessory apatite + pyrite + zircon.

Geochemically, these granitoid rocks have some similarities and differences to the Beluga showing. Clinopyroxene in these rocks has a Mg# = 0.25-0.77, which is much lower

than diopside from the KSO, but plagioclase and scapolite fall within the compositional range for the KSO (Barnes et al. 2005). These granitoid rocks also have higher Fe₂O₃, similar SiO₂, Al₂O₃, K₂O, CaO, lower Na₂O, MgO, V and Cr than the Beluga showing. Furthermore, they are enriched in LREE (Σ REE 32-173 ppm) relative to the Beluga showing.

Stable oxygen and carbon isotopes of igneous carbonate within nepheline-bearing diorites with ~7.6% carbonate and <0.5% carbonate is $\delta^{18}\text{O} = 14.12\text{\textperthousand}$ and $11.87\text{\textperthousand}$ and $\delta^{13}\text{C} = 2.53\text{\textperthousand}$ and $0.29\text{\textperthousand}$. The $\delta^{18}\text{O}$ is higher than expected for a typical monzonite intrusion. In addition, the variation of $\delta^{13}\text{C}$ in the complex can be modelled using Rayleigh fractionation, which supports the theory of metasedimentary carbon contamination in a mafic magma.

Even though the mineral assemblages of this protolith are similar to those at the Beluga showing, the presence of Fe-bearing minerals and elevated Fe₂O₃ whole rock geochemistry suggest that this is an unlikely protolith of the Beluga showing. Furthermore, the low values of Cr and V and elevated LREE also suggest that this protolith is not a good fit for the Beluga showing. Also, the $\delta^{18}\text{O}$ values of carbonate are likely somewhat lower than the carbonate from the Beluga showing. The $\delta^{18}\text{O}$ of corundum from the Beluga showing of $16.4\text{\textperthousand}$ indicates that the host carbonate was likely higher in $\delta^{18}\text{O}$ because the $\delta^{18}\text{O}$ of corundum within marble is usually lower than that of the host carbonate (see Revelstoke chapter).

4.11.4.3 Alkaline Intrusions into Marble

Nepheline-syenite pegmatite boudins within marble at the Cabonga Nepheline syenite complex in southwestern Quebec contain nepheline, plagioclase, orthoclase, perthite, microcline, blue to yellow euhedral corundum and biotite with locally abundant scapolite and calcite (Hudon et al. 2006). The host coarse-grained marble also occurs as enclaves in the nepheline syenite gneiss. The host marble contains calcite with minor phlogopite, blue scapolite, diopside, plagioclase, and hornblende with accessory titanite and apatite.

Regionally, this corundum-bearing syenite is poor in Ti, Fe, and Mn and is enriched in calcite compared to other nepheline-bearing rocks in the area. Low Fe and Mn are also

similar at the Beluga showing, but the Beluga showing is enriched in V and Ti, making this protolith unlikely.

4.11.4.4 Na-Metasomatism of Metasediments or Volcanic Rocks

In the York River area of southern Ontario, poly-metamorphosed and -deformed alkaline rocks are associated with metasediments (marbles, amphibolites, and paragneisses) and intrusive rocks (gabbros and granites; Anderson and Cermignani 1991). The mineral assemblage of corundum-bearing rocks is: nepheline + alkali feldspars + corundum + amphibole (hornblende?) + biotite + magnetite + scapolite + calcite + apatite with locally abundant zircon, tourmaline, and garnet (Moyd 1949). At some locations, the nepheline-rich gneisses were partially altered to rocks rich in alkali feldspars and corundum (Moyd 1949), similar to the association of corundum with alkali feldspars in the Beluga rocks.

There are three main theories that can be applied to the alkaline nature and presence of nepheline in these rocks: (1) Na-metasomatism of metasedimentary or volcanic rocks by granitic fluids (Gummer and Burr 1946) or alkaline fluids (Gittins 1961); (2) metasomatism of metasediments with Cl-rich brines from evaporitic layers (Appleyard and Stott 1975; Appleyard and Williams 1981); or (3) the protolith was an alkaline igneous rock that underwent very little metasomatism (Miller 1985). Anderson and Cermignani (1991) modeled the stability of different phases in calcite-saturated solutions containing carbonate and chloride ions of Na, Ca, and K with varying activities of NaCl and identified that nepheline could form from plagioclase while in equilibrium with K-feldspar and calcite in solutions with 0.3 to 1 molar NaCl. They also identified 3-phase liquid-vapour-NaCl solid fluid inclusions in diopside and nepheline, which could represent relict primary igneous inclusions or metasomatic inclusions.

Corundum in these rocks may have formed by: (1) the destabilization of muscovite (Carlson 1957) [muscovite \rightarrow K-feldspar + corundum], or (2) the destabilization of nepheline by the addition of CO₂-rich siliceous fluids to form perthite + corundum + sodium carbonate (Moyd 1949), or (3) the destabilization of Na,Ca plagioclase to corundum + albite + calcite by the addition of CO₂-rich fluids and Na₂CO₃ (Moyd 1949).

No whole rock geochemistry, mineral chemistry, or isotopic data exists for this locality, making it difficult to make a comparison with the Beluga showing. Furthermore, the model of formation for this locality has been debated by many authors. There are similarities between this locality and the Beluga showing in terms of the primary mineral assemblages and the alteration of nepheline zones to alkali-feldspar with corundum, but the presence of magnetite indicates that these rocks were more iron rich. Model 1 may be a valid protolith, but the enrichment of V and depletion of LREE cannot be explained by this model. Model 2 may be a valid protolith for the Beluga showing, if the primary metasediments were enriched in V. Model 3 is an unlikely protolith because the Beluga showing would be expected to have higher LREE and lower $\delta^{18}\text{O}$ of corundum.

4.11.4.5 Metamorphism of an Evaporite-Shale-Marble Protolith

Silica-undersaturated and Fe-depleted rocks can also be produced in metamorphosed evaporite-shale-marble sequences, such as has been proposed for the lapis lazuli locality within the LHM (Hogarth 1971, Hogarth and Griffin 1978). This locality commonly contains calcite + lazurite + diopside + phlogopite + amphibole (pargasite) + plagioclase (oligoclase) \pm nepheline \pm scapolite \pm titanite \pm sodalite \pm pyrite (Hogarth and Griffin 1978). Select minerals from the Lapis deposit have the following composition: diopside = $\text{Di}_{90}\text{Jd}_{10}$, scapolite = $\text{EqAn} = 0.44\text{-}0.48$, plagioclase = $\text{Ab}_{75\text{-}84}\text{An}_{14\text{-}24}\text{Or}_{0\text{-}1.6}$, and nepheline = $\text{Ne}_{80\text{-}87}$, end member phlogopite = (XMg_{100}) . Diopside from the Beluga showing has more Fe, Ti and Al than the diopside from the nearby lapis deposit, and the phlogopite from the lapis deposit contains more Mg and less Fe and Ti than the Beluga showing. Plagioclase and nepheline have similar compositions at both localities.

As described earlier, the Beluga showing and the lapis lazuli rocks within the LHM both have very low Fe_2O_3 and SiO_2 , typically average Al_2O_3 , and high CaO and MgO (Fig. 4.23). The lapis lazuli rocks, however, contain higher Na_2O and much lower TiO_2 than the Beluga rocks (Fig. 4.23D, 4.24). V, Cr, and REEs were not analyzed in samples from the lapis lazuli rocks, so they could not be compared to figures 4.25 and 4.26.

Even though there are some geochemical similarities, the lapis rocks have slightly different mineral assemblage, grain size, and much lower TiO_2 compared to the Beluga

deposit. If the primary shale had a different composition, this could explain the geochemical differences, but not the difference in grain size. The absence of oxygen isotopes, REE, V and Cr values make it difficult to compare the Lapis locality in its entirety to the Beluga showing. However the proximity of this showing to the sapphire deposits regionally throughout the LHM could indicate that the reactions responsible for the formation of the lapis showing could also have affected the development of the Beluga showing.

4.11.5 Proposed Beluga Model of Formation

The proposed model of formation for the Beluga Showing is the metamorphism of an evaporite-black shale-marble protolith, which was altered by late fluid infiltration. The destabilization of nepheline + (scapolite or anorthite), or the destabilization of anorthite formed the corundum-albite-muscovite assemblage. The interaction of evaporites and interbedded shales was proposed as a model for the formation of alkaline corundum-bearing rocks near York River, Ontario (Appleyard and Williams 1981) and the lapis lazuli deposit within the LHM on Baffin Island (Hogarth 1978). These rocks have similar primary mineral assemblages as well as elevated whole rock Mg and Ca and low Fe and Si, similar to the Beluga showing. If the primary sedimentary carbonate was dominantly dolomitic, it could explain the elevated Mg in the rocks. There are distinct dolomitic marble areas within the LHG marble near to the Beluga showing; these are clearly different from the majority of the marble host-rocks (Fagan, 2010). Elevated V (especially in comparison to Cr) at the Beluga Showing could be the result of primary accumulation in anoxic black shale deposits with greater than 10% total organic carbon (TOC; Brumsack 2006, Algeo and Maynard 2004). Vanadium can be enriched relative to Cr in nepheline syenites, but low total REE values and very low Fe relative to Si are not consistent with this protolith (Hudon et al 2006). Elevated Ti may be explained by large amounts of rutile accumulated in the primary sediment or by Ti-mobilization during prograde metamorphism.

Black shales are typically enriched in LREE, but low LREE values in the Beluga rocks may be explained by the dissolution of REE-bearing minerals, such as apatite or monazite, during diagenesis or as a result of dilution with carbonate minerals (Lev et al. 1999).

The relatively high $\delta^{18}\text{O}$ of corundum overlaps with the low end of corundum from marble-shale-evaporite protoliths (Giuliani et al. 2005). This result is consistent with a metasedimentary-metasomatic origin of corundum from the Beluga Showing.

4.11.6 Late Fluid Infiltration

LeCheminant et al. (2005) observed that the zoning and mineral inclusions within zircons from the Beluga showing are similar to corundum. They determined the date of zircon formation to be (1782.5 Ma) and presumed that this age is similar to the date of corundum crystallization. This date also corresponds to the age of post D₂ thermal/fluid activity of 1784 +7/-9 Ma determined by Scott (1997), which is related to syenite intrusions within the LHG. Butler (2007) also proposed fluids from syenogranites may have produced late scapolite in marble nearby within the LHM. These late intrusions could be the source of corundum producing fluids, but further research is needed to confirm or deny this.

The presence of corundum at the Beluga showing, and not at the Bowhead showing, suggests that the Bowhead showing was not infiltrated by the secondary fluids to the same extent (or at all) as the Beluga showing. This can possibly be explained the presence of a fault separating the two showings, but this needs to be confirmed with structural field work and laboratory oxygen isotope evidence. If the fault formed prior to or during late stage fluid infiltration, it may have acted as an impermeable barrier preventing the altering fluid from reaching the Bowhead showing. Alternatively, if the fault formed post-corundum formation it may have juxtaposed the showings which formed at different structural positions in the LHM with different geochemical characteristics.

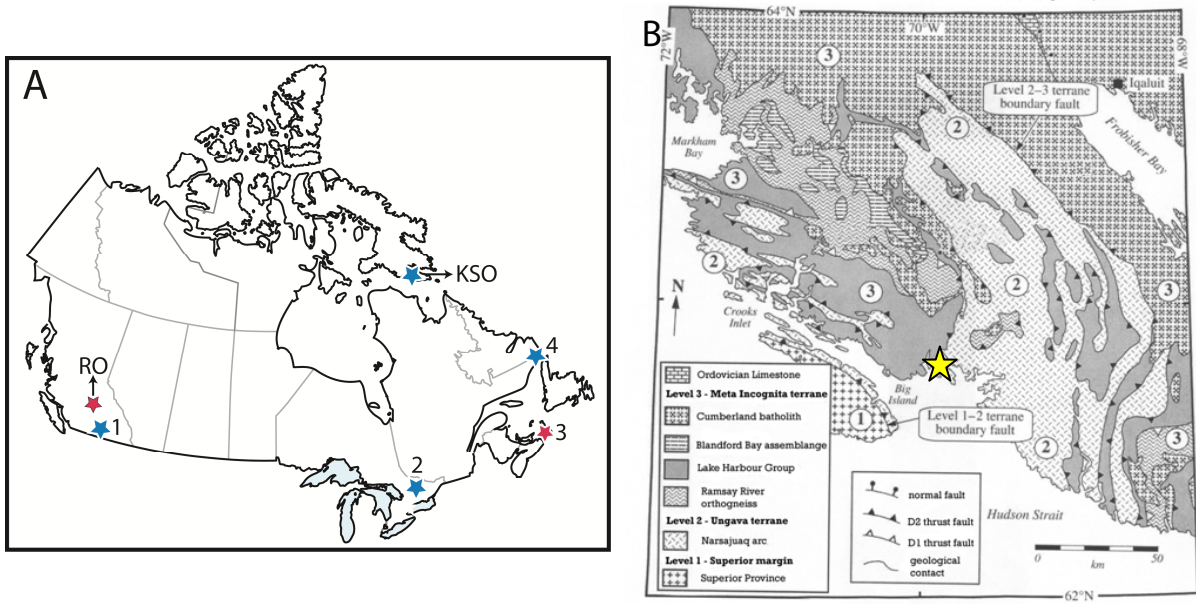


Figure 4.1: Location and regional geology of the Kimmirut Sapphire Occurrence (KSO). A) Map of Canadian gem-corundum localities. RO = Revelstoke occurrence, 1 = Slocan Valley, 2 = Bancroft-York River area, 3 = Nova Scotia, 4 Labrador. B) Geological map of southern Baffin Island. The Level 1-2 terrane boundary fault is the Bergeron suture and the Level 2-3 terrane boundary fault is the Soper River suture (St-Onge et al. 2000). The yellow star indicates the location of the Kimmirut Sapphire Occurrence (KSO).



Figure 4.2: A) Distinctive texture of the coarse-grained Beluga lens in contact with finer-grained marble. Note the rectangular outline of violet diopside + symplectite (phlogopite + plagioclase). B) Muscovite-albite-calcite-sapphire zone.

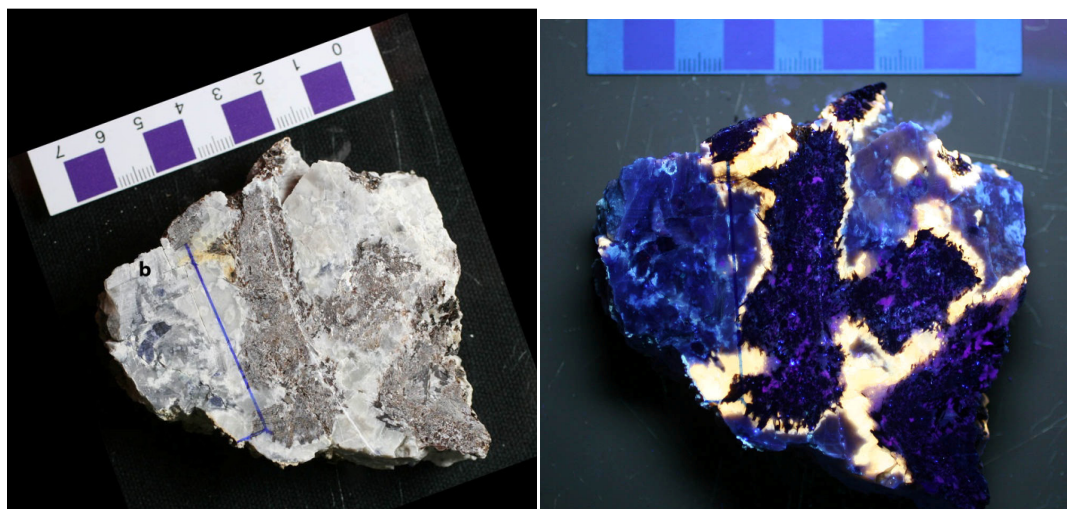


Figure 4.3: Sample B8-04b in A) incandescent and B) UV light. Note the bright yellow fluorescence of scapolite in UV light.

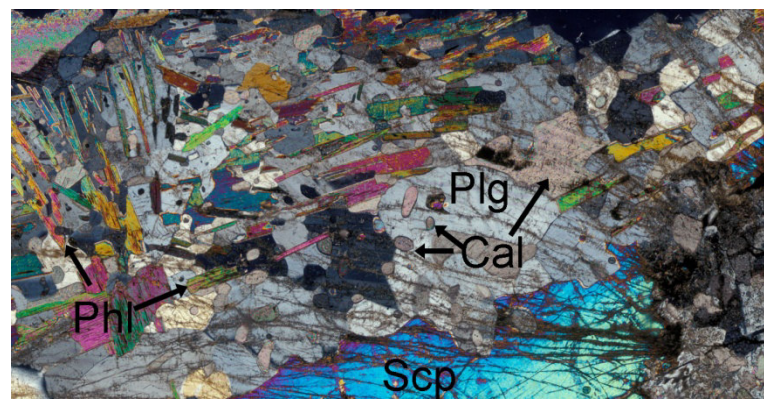
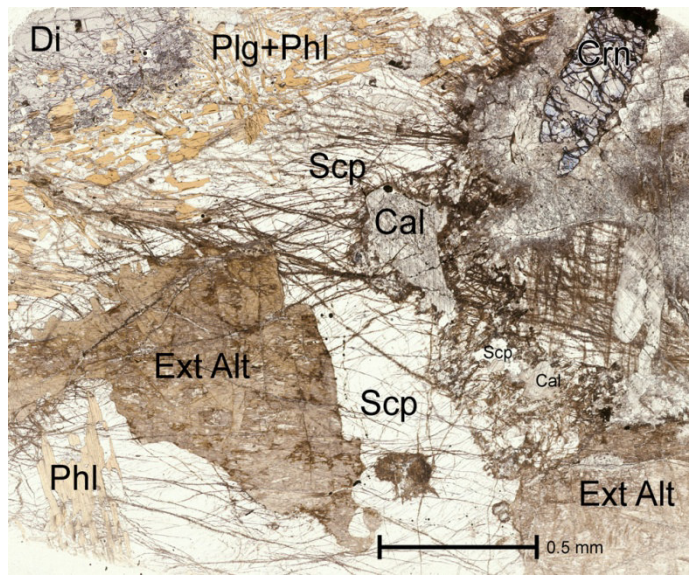


Figure 4.4: Plagioclase-phlogopite symplectite rimmed by scapolite. Note random orientation of phlogopite and inclusions of calcite in plagioclase. FOV = 0.9 mm

A)



B)

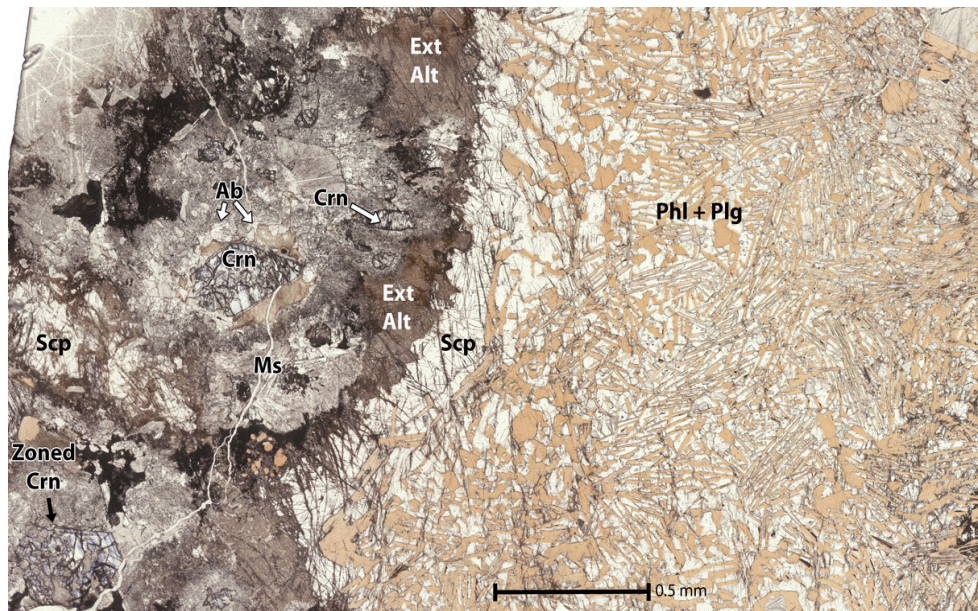


Figure 4.5: Photomicrographs displaying the distinctive texture and mineralogical zones of calc-silicate rocks from the Beluga showing. A) Zoning of mineral phases; diopside (at the upper left corner) is rimmed by the plagioclase-phlogopite symplectite, followed by scapolite, then the corundum-albite zone. Note the presence of the area of extensive alteration which can occur as an inclusion within scapolite, but also as part of the corundum-bearing zone. B) Zoning of mineral phases; diopside is not visible in this photomicrograph possibly because it has all been consumed in the production of the plagioclase-phlogopite symplectite. Note the random orientation of phlogopite grains within the symplectite, the presence of scapolite within the corundum zone, and the presence of the area of extensive alteration along the boundary between scapolite and the corundum-bearing zone, possibly indicating fluid pathways.

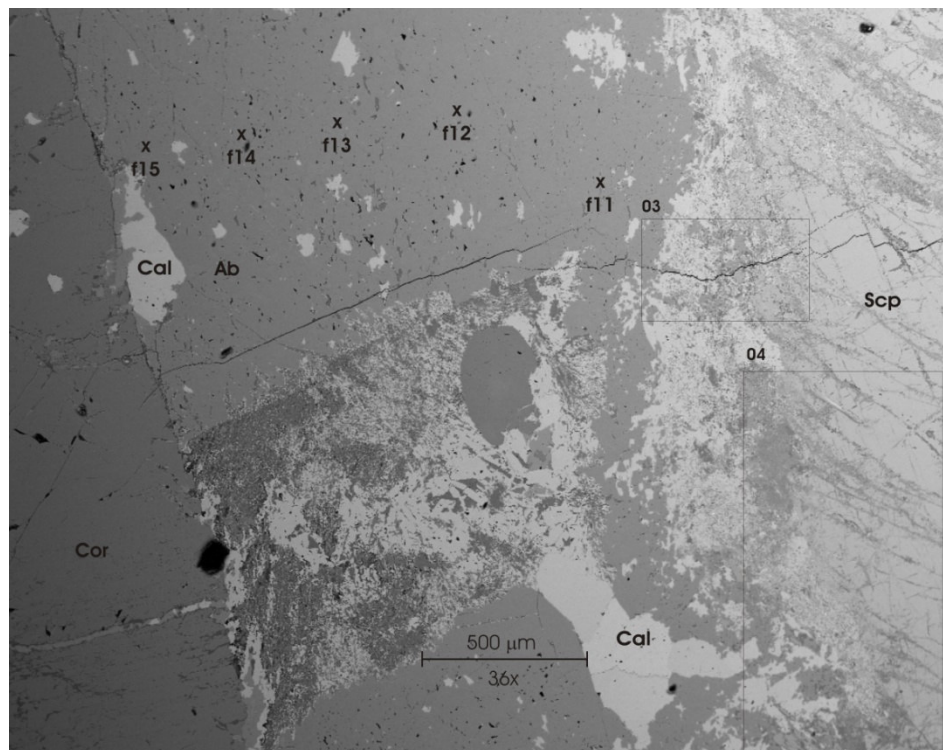


Figure 4.6: Albite and calcite surrounding corundum next to scapolite.

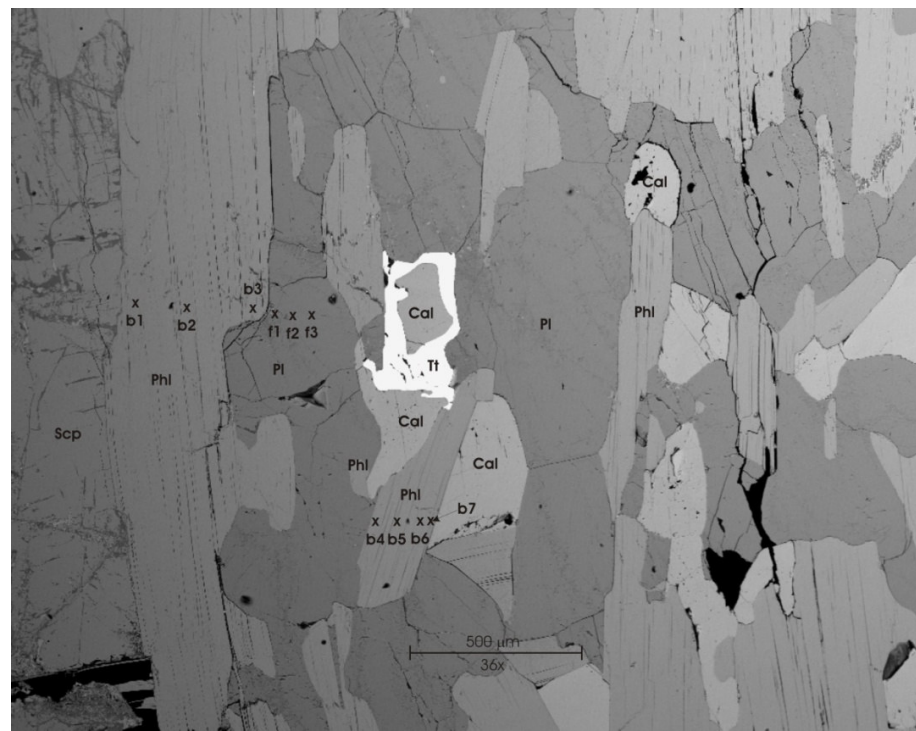


Figure 4.7: Symplectite with calcite and titanite on the edge of scapolite.

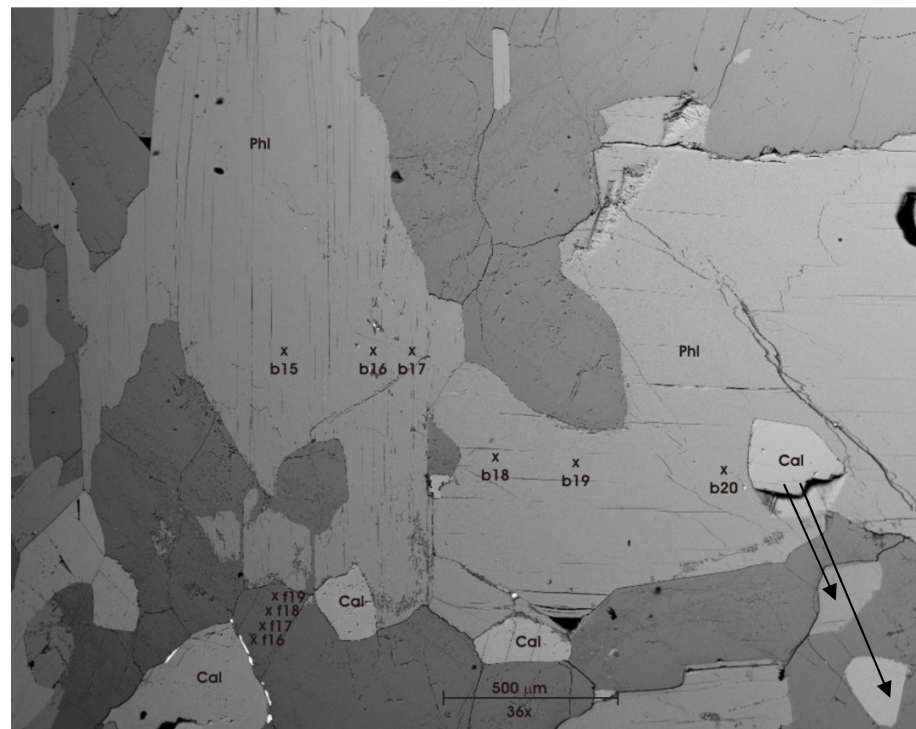


Figure 4.8: Calcite inclusions in phlogopite, on the edge of phlogopite, or in the intergranular space between plagioclase.

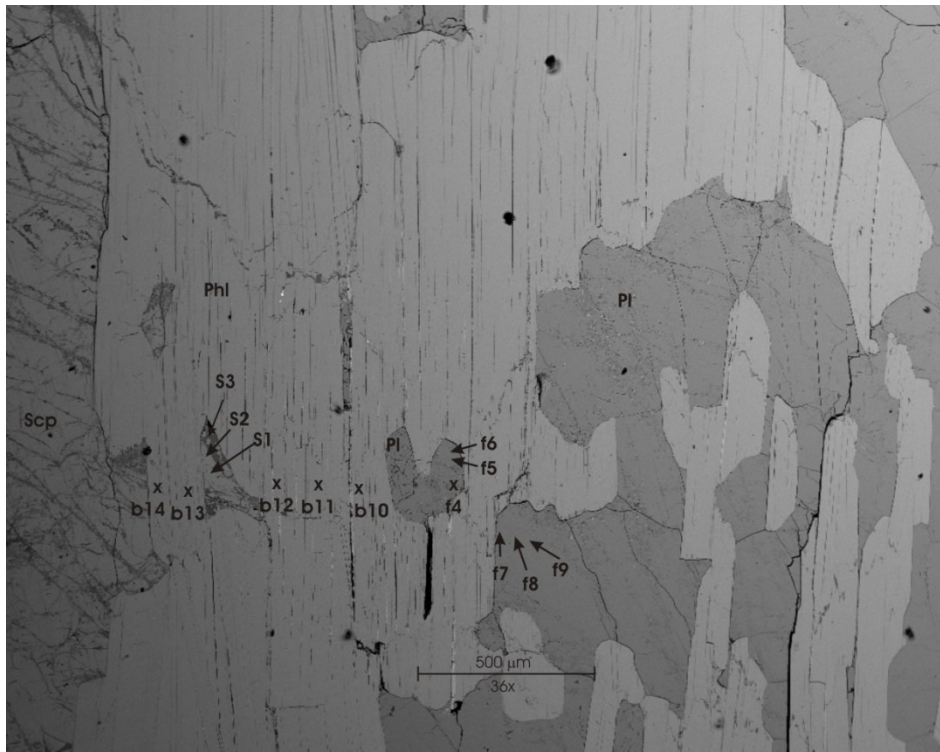


Figure 4.9: Symplectite with scapolite and plagioclase inclusions in phlogopite.

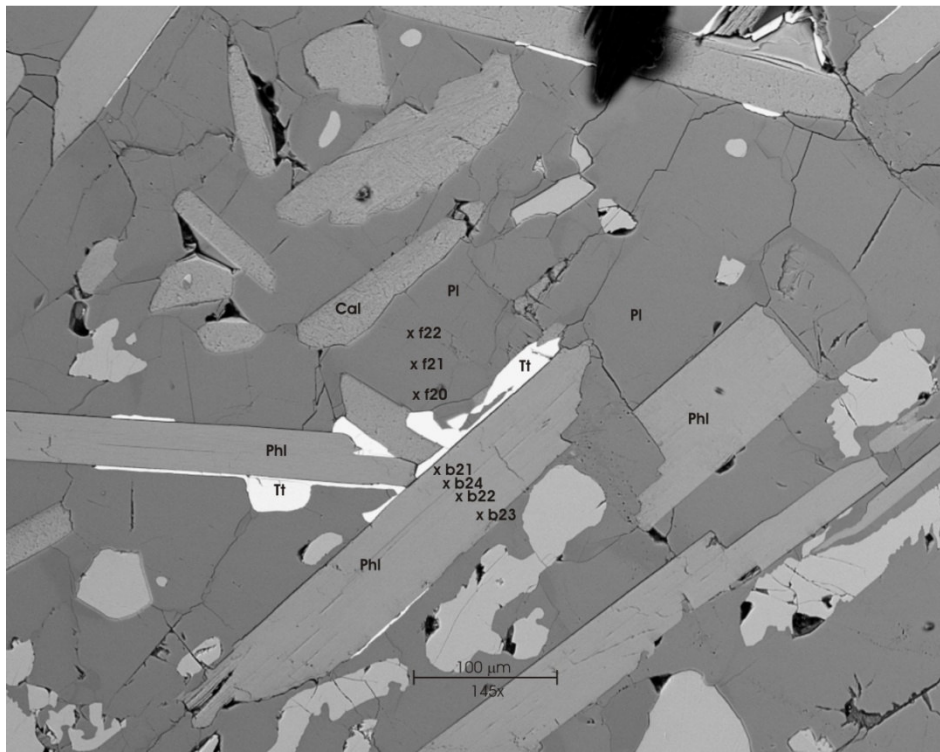


Figure 4.10: Symplectite with calcite and titanite.

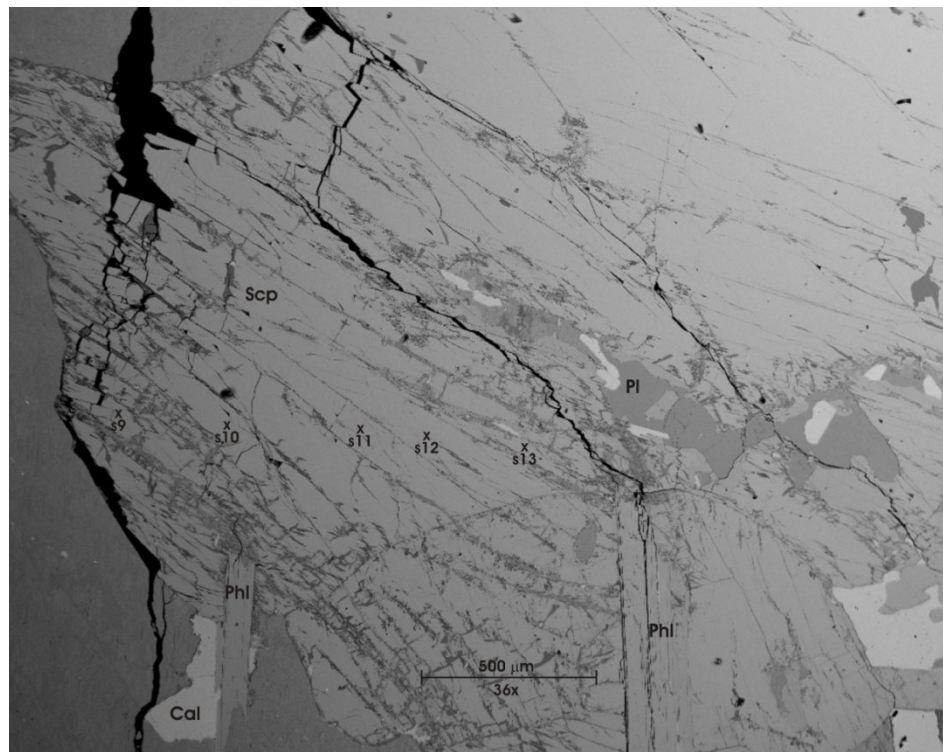


Figure 4.11: Plagioclase-phlogopite-calcite and phlogopite inclusions in scapolite.

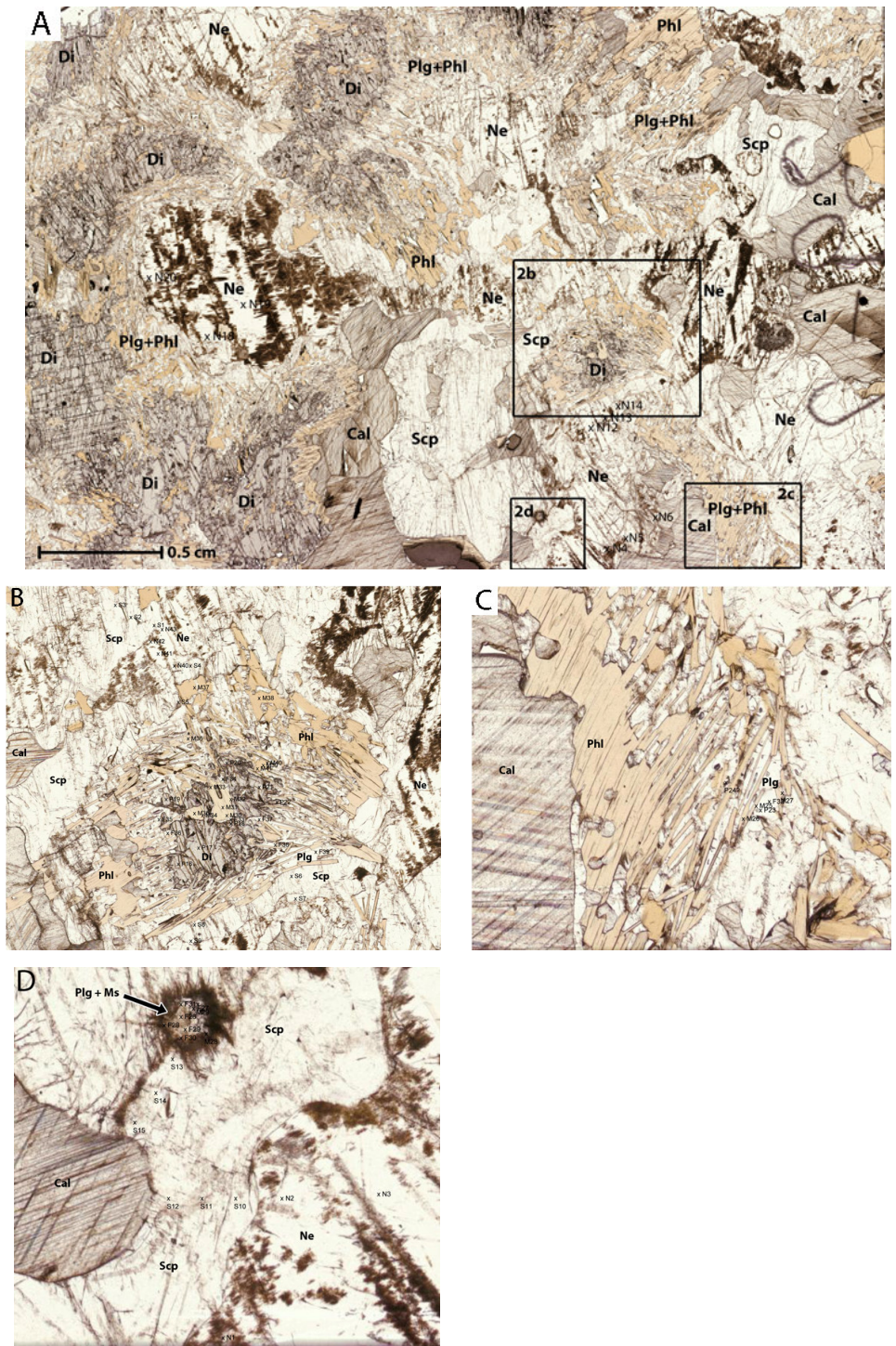


Figure 4.12: Photomicrographs of the nepheline-bearing Bowhead showing. A) The plagioclase-phlogopite symplectite develops between diopside and nepheline grains. B) Scapolite rimming plagioclase-phlogopite symplectite and nepheline. FOV = 0.8 mm, C) Plagioclase-phlogopite symplectite in contact with calcite. FOV = 0.5 mm, D) Plagioclase-muscovite nodule within scapolite. FOV = 0.3 mm



Figure 4.13: A) Beluga blue and colourless cut sapphires from the Beluga showing. C) 1.17 ct. in pavilion view with tweezers for scale. All sapphires are natural and untreated. Photos are courtesy of True North Gems.

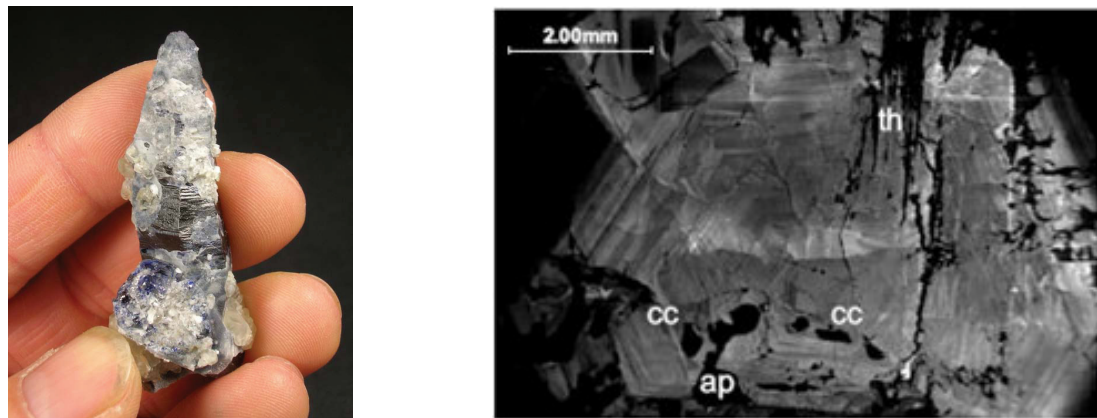


Figure 4.14: A) Barrel-shaped corundum crystal from the Beluga showing. Image is from Wilson (2010). B) Scanning electron microscope image of a zoned sapphire crystal with calcite (cc) and rare apatite (ap) inclusions. Prismatic thomsonite (th) crystals penetrate corundum along fractures. Image is from LeCheminant et al. (2005).

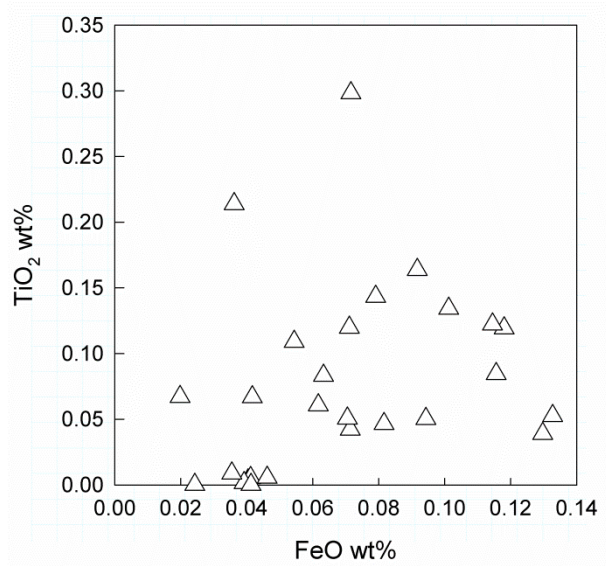


Figure 4.15: Compositional variation of sapphires from the Beluga occurrence.

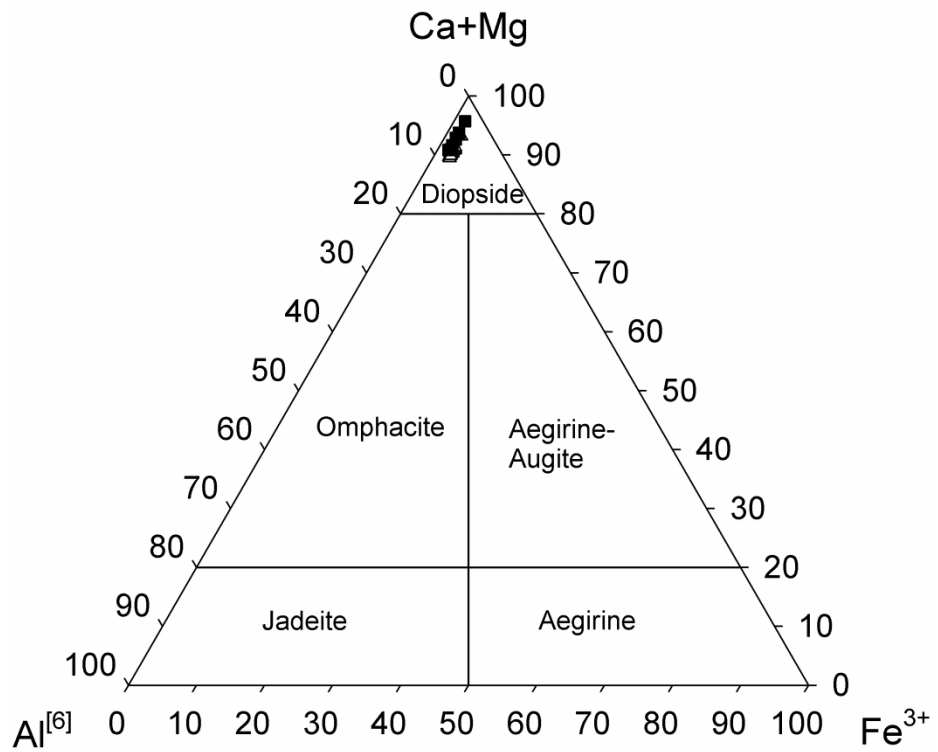


Figure 4.16: Pyroxene classification and major elemental variation diagram.

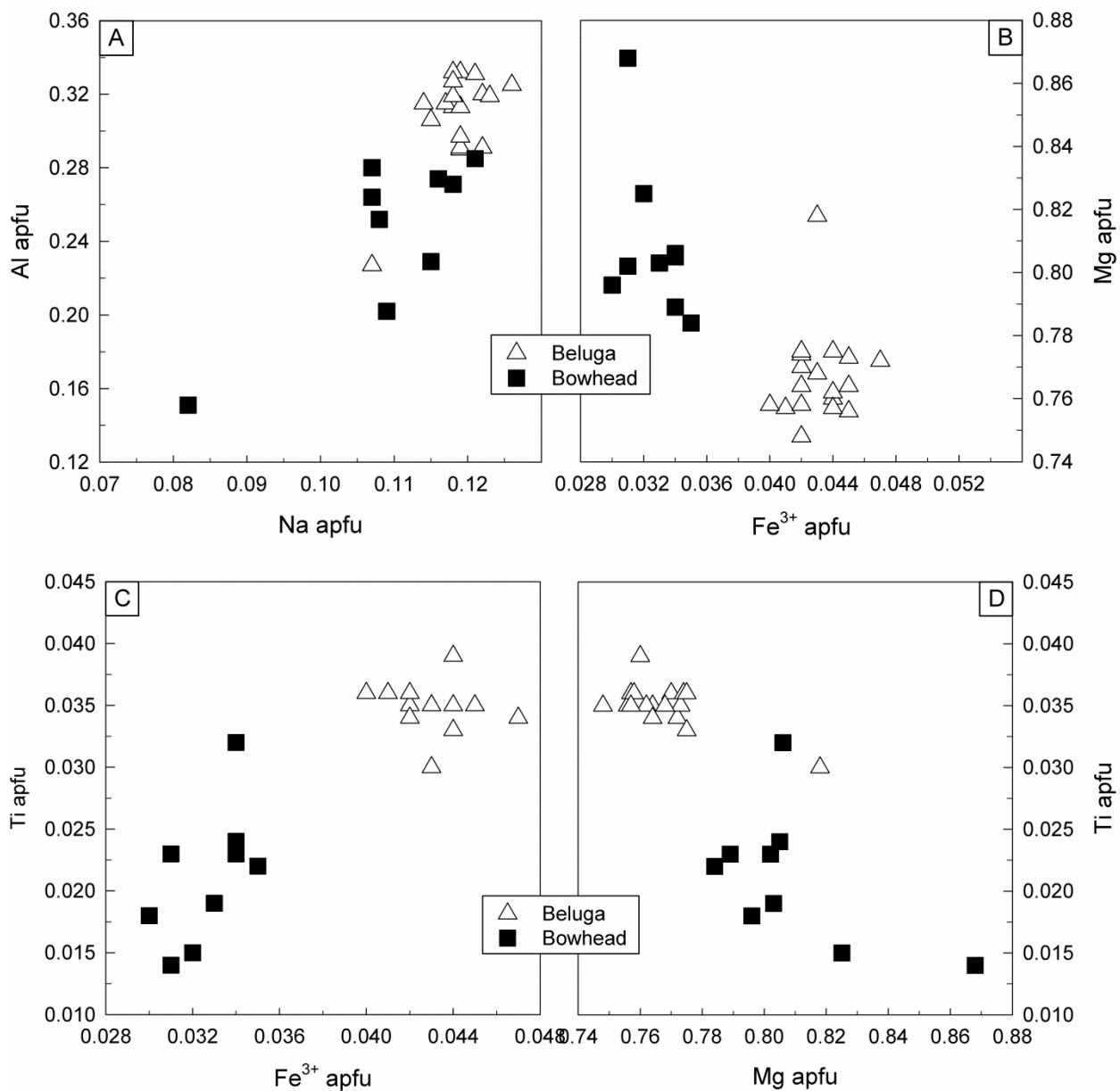


Figure 4.17: Compositional variation of pyroxene at the Beluga and Bowhead showings: A) Al vs Na apfu; B); Mg vs Fe³⁺ apfu; C) Ti vs Fe³⁺ apfu; and D) Ti vs Mg apfu.

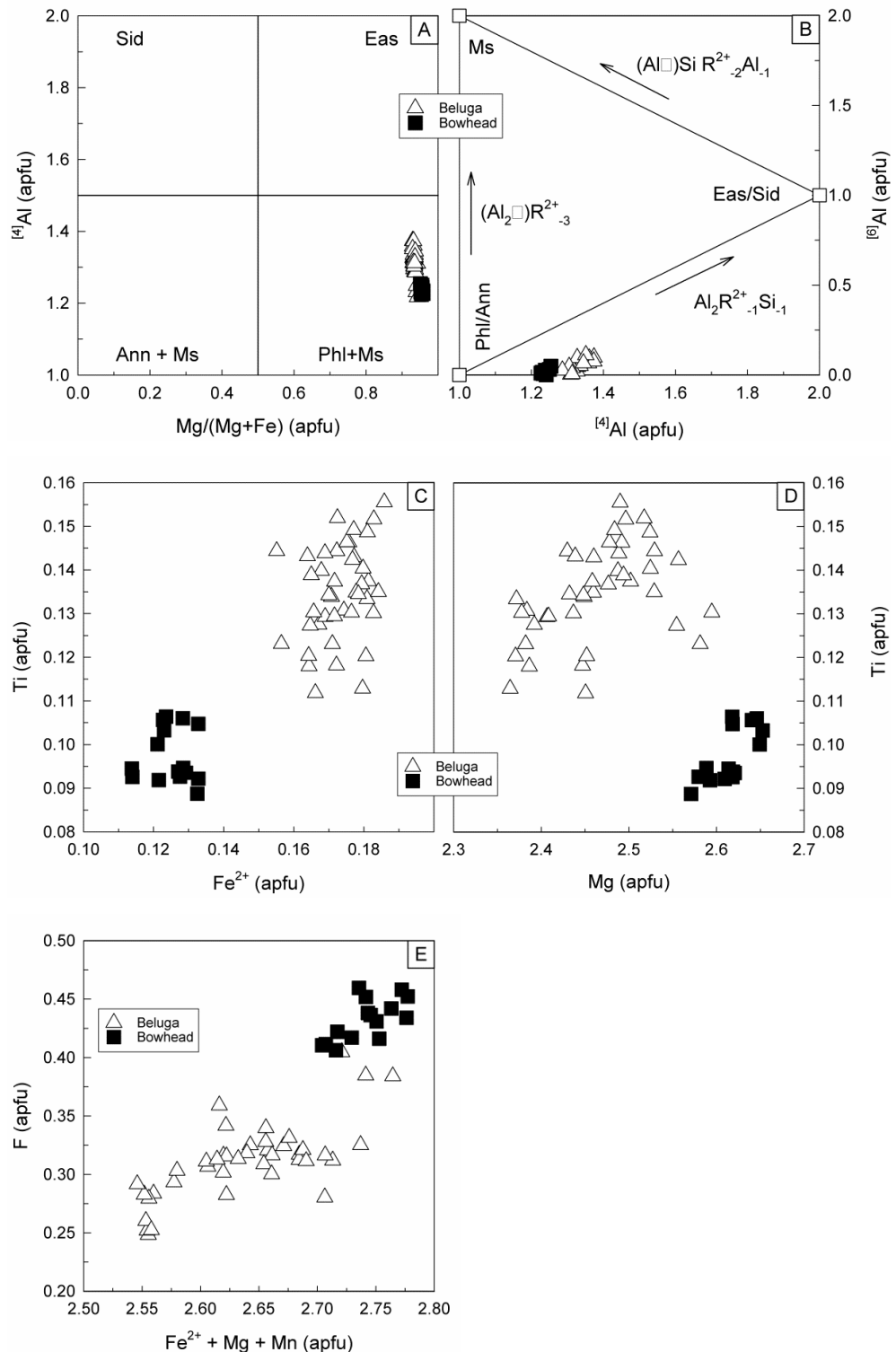


Figure 4.18: Compositional variation of phlogopite from the Beluga and Bowhead showings. A) $[{}^4\text{Al}]$ vs. $\text{Mg}/(\text{Mg}+\text{Fe}^{2+})$; B) $[{}^6\text{Al}]$ vs. $[{}^4\text{Al}]$; C) Ti vs. Fe^{2+} ; D) Ti vs. Mg ; E) F vs. $\text{Fe}^{2+} + \text{Mg} + \text{Mn}$.

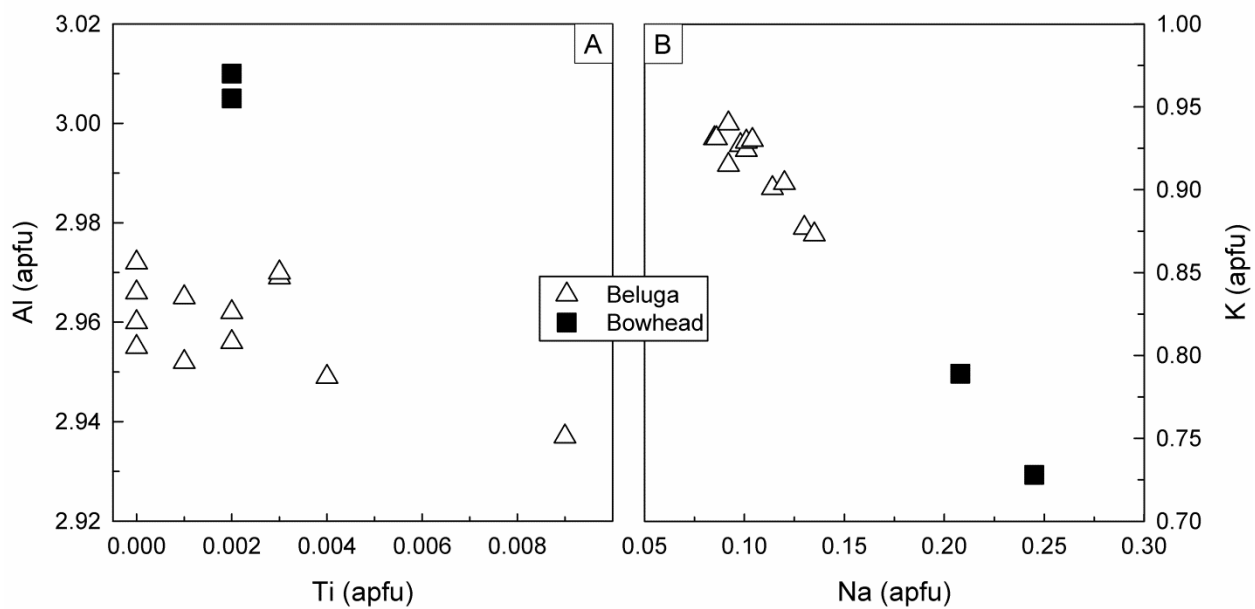


Figure 4.19: Chemical composition of muscovite from the Beluga and Bowhead showings:
A) Al vs Ti and B) K vs Na.

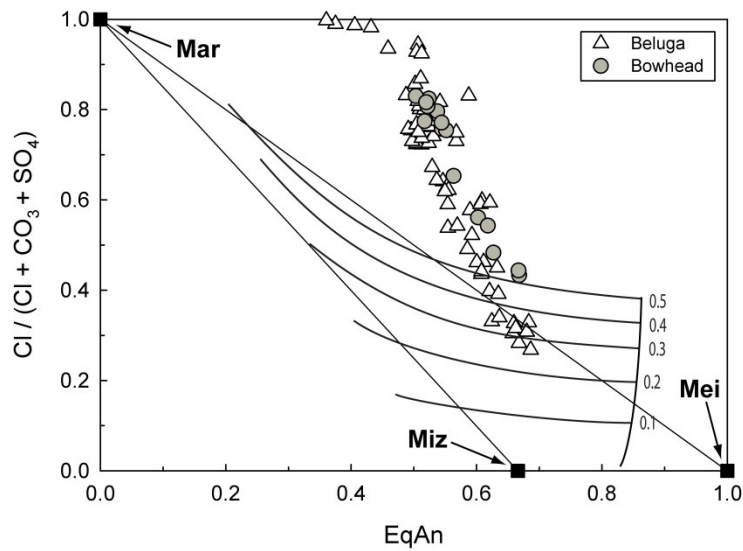


Figure 4.20: Compositional variation of scapolite from the Beluga and Bowhead showings. Meionite, marialite, mizzonite solid solution end members are expressed in terms of $X_{\text{Cl}} = \text{Cl}/(\text{Cl} + \text{CO}_3 + \text{SO}_4)$ and equivalent anorthite EqAn = $(\text{Al}-3)/3$. The curves indicate NaCl content of fluids according to the experimental data of Ellis (1978) for 4 kbar and 750 °C.

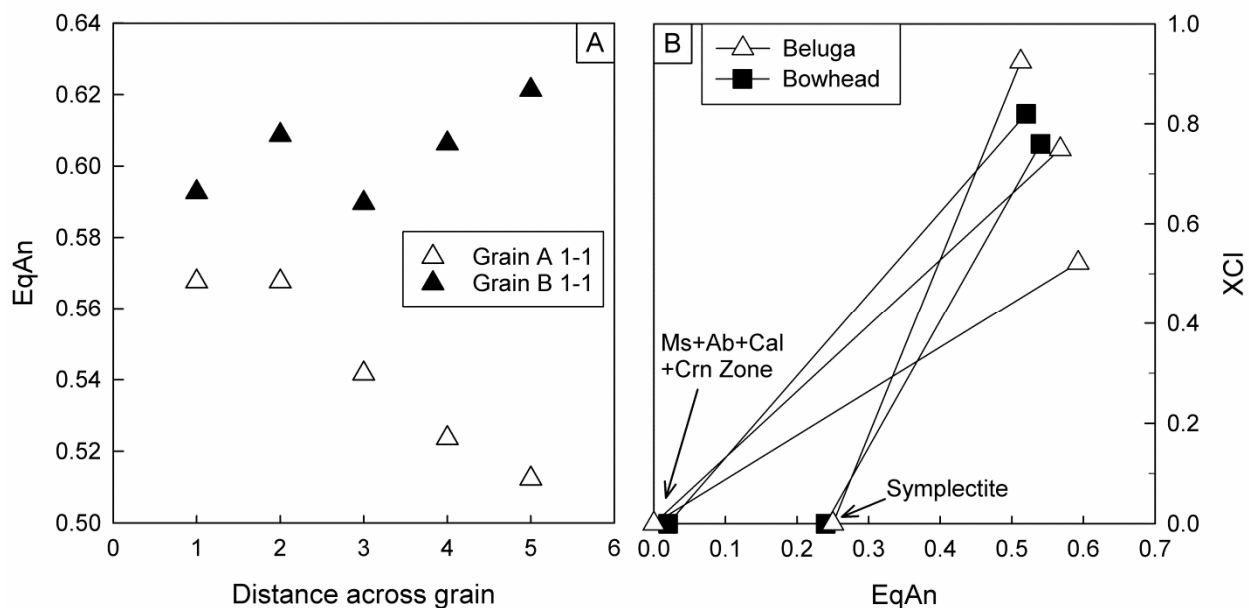


Figure 4.21: Compositional variation of scapolite. A) Zoning of EqAn across scapolite grains at the Beluga showing. B) Tie-lines of coexisting scapolite-plagioclase pairs at the Beluga and Bowhead showings.

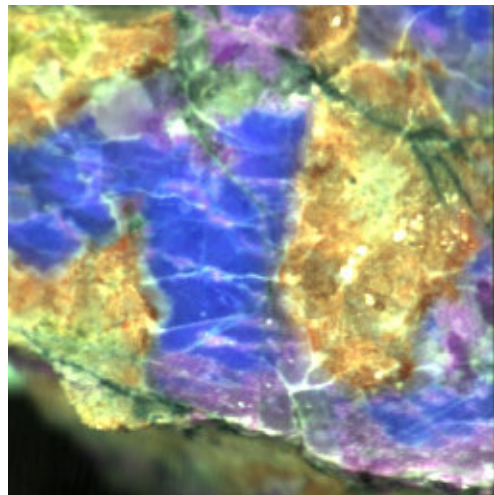


Fig. 4.22: High resolution hyperspectral image of a rock from the Beluga showing collected by David Turner. The two generations of scapolite are identified by blue and purple.

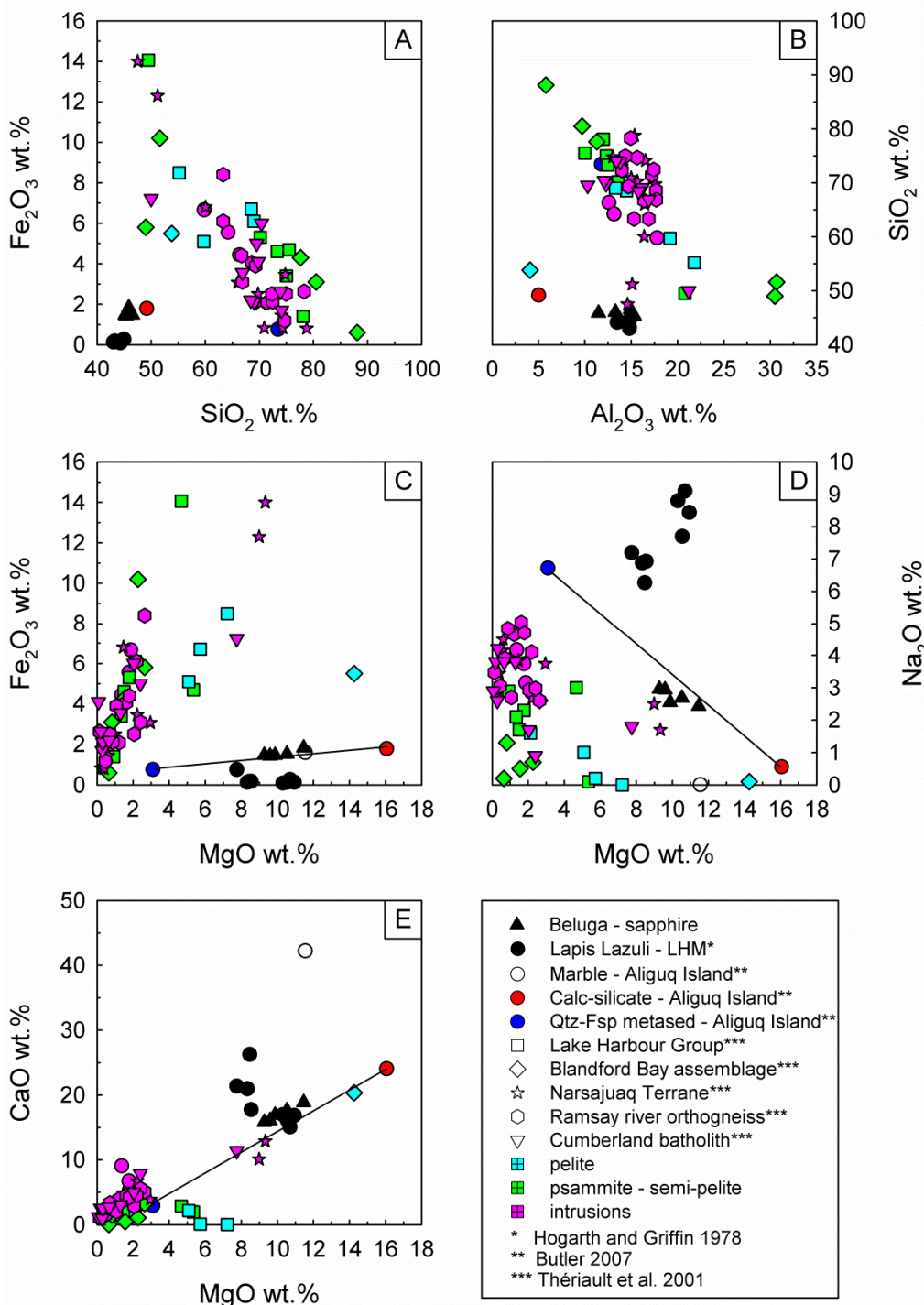


Figure 4.23: Major element variation for the Beluga rocks as well as other lithologies from the Lake Harbour Group, Blandford Bay assemblage, Narsajuaq Terrane, Ramsay River orthogneiss, and Cumberland batholith: A) Fe_2O_3 vs SiO_2 , B) SiO_2 vs Al_2O_3 , C) Fe_2O_3 vs MgO , D) Na_2O vs MgO , and E) CaO vs MgO .

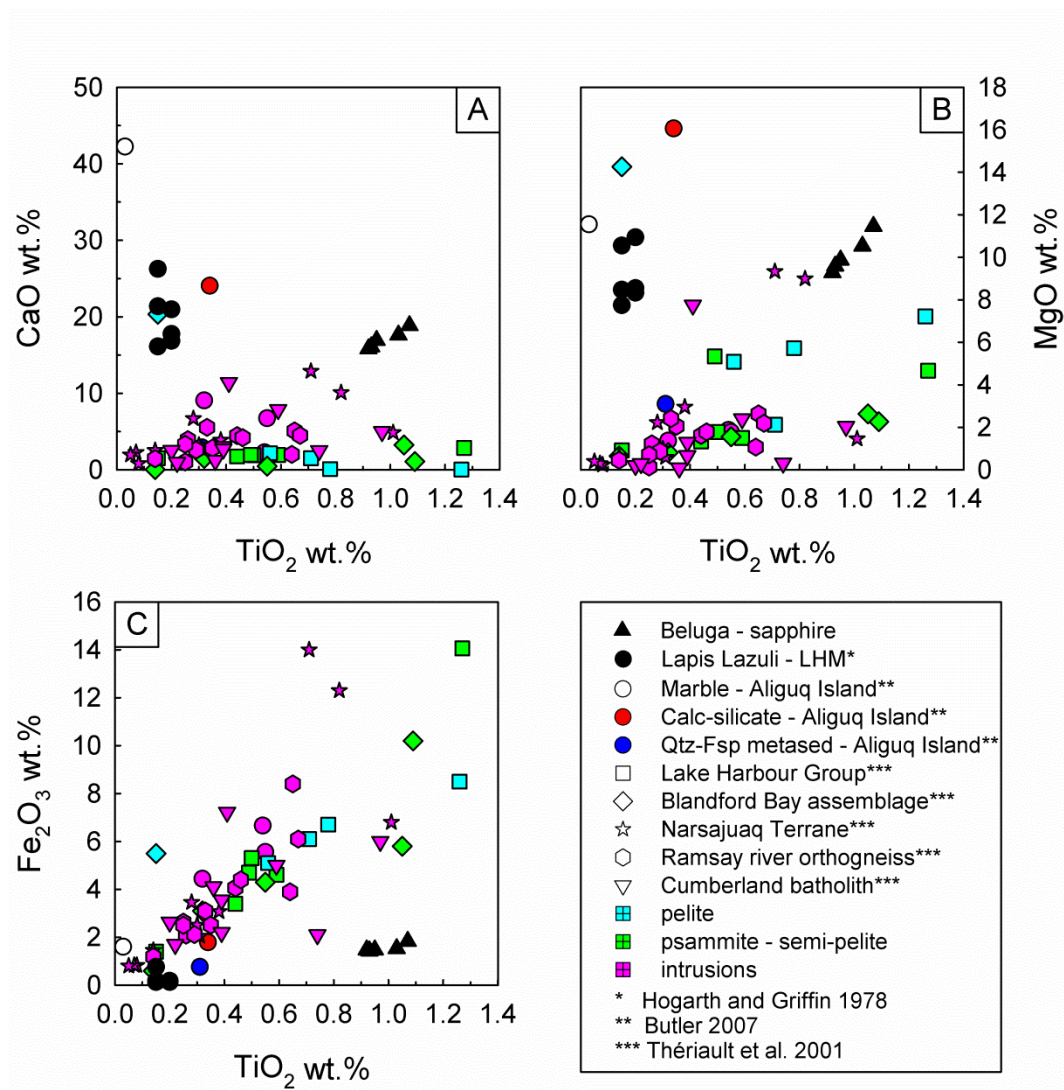


Figure 4.24: Major elements vs TiO_2 wt.% for the Beluga rocks as well as other lithologies from the Lake Harbour Group, Blandford Bay assemblage, Narsajuaq Terrane, Ramsay River orthogneiss, and Cumberland batholith.

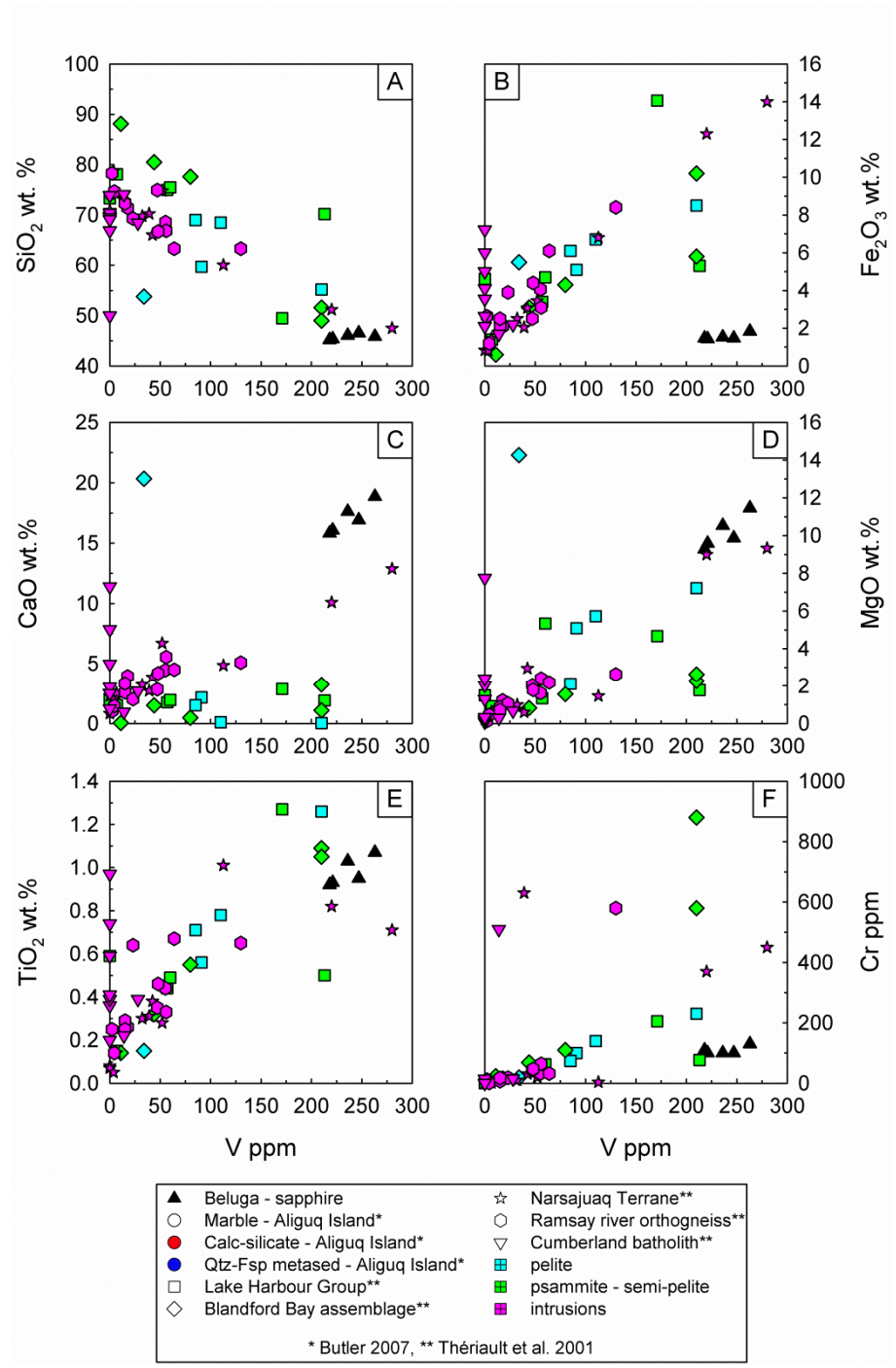


Figure 4.25: Major elements vs V ppm for the Beluga rocks as well as other lithologies from the Lake Harbour Group, Blandford Bay assemblage, Narsajuaq Terrane, Ramsay River orthogneiss, and Cumberland batholith.

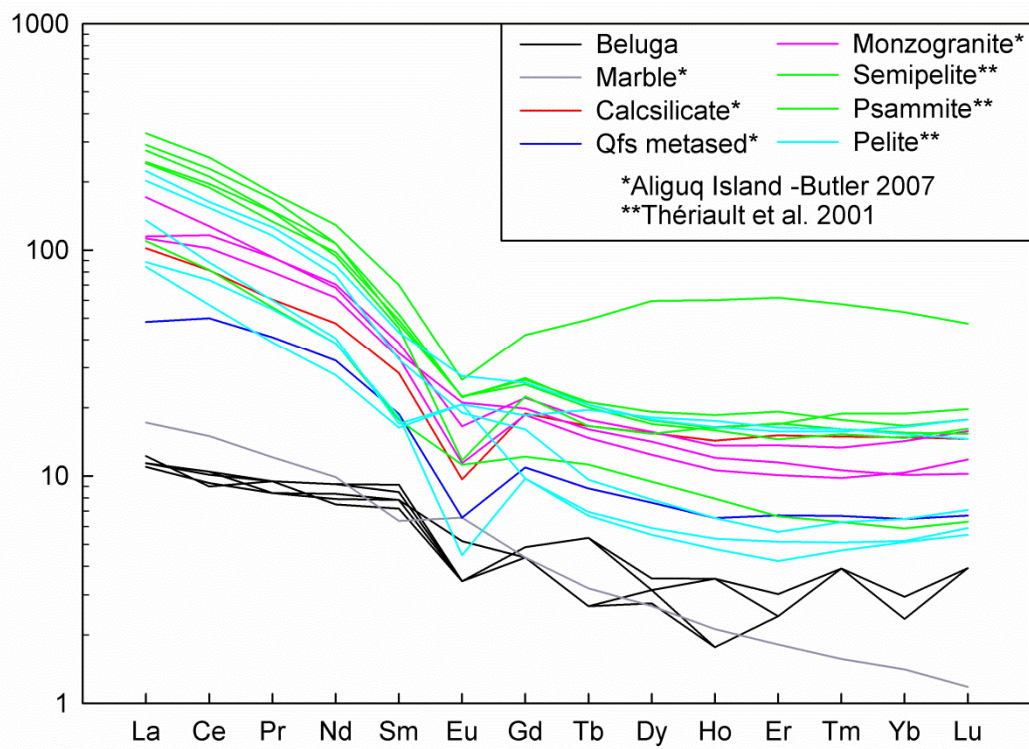


Figure 4.26: REE patterns of lithologies from the Lake Harbour Group compared to the Beluga showing.

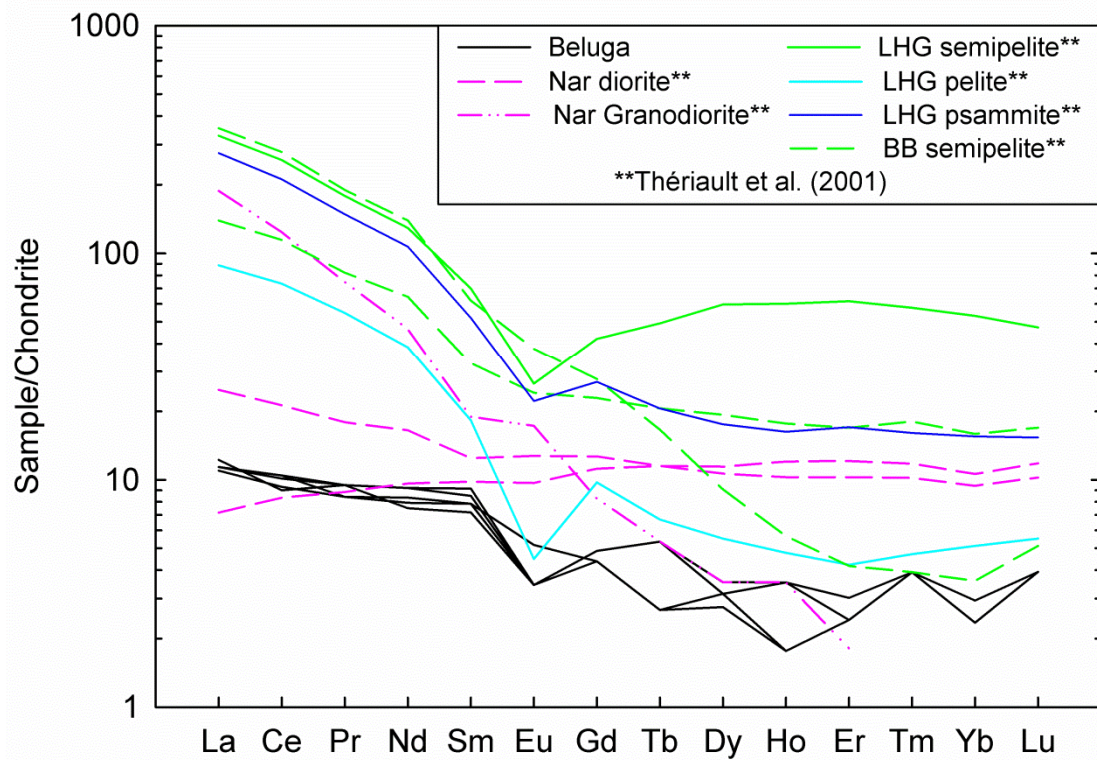


Figure 4.27: REE patterns of lithologies with elevated V (170-280 ppm) from the Beluga showing, Narsajuaq terrane (Nar), Lake Harbour Group (LHG), and Blandford Bay assemblage (BB).

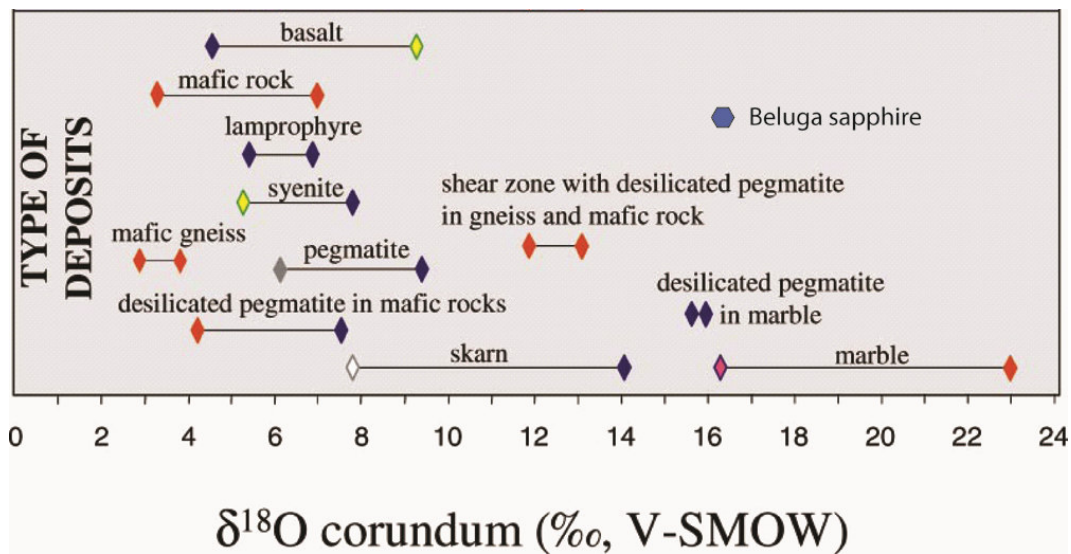


Figure 4.28: The $\delta^{18}\text{O}$ values of gem corundum from different protoliths (Giuliani et al. 2005). The Beluga sapphire is denoted as a blue hexagon.

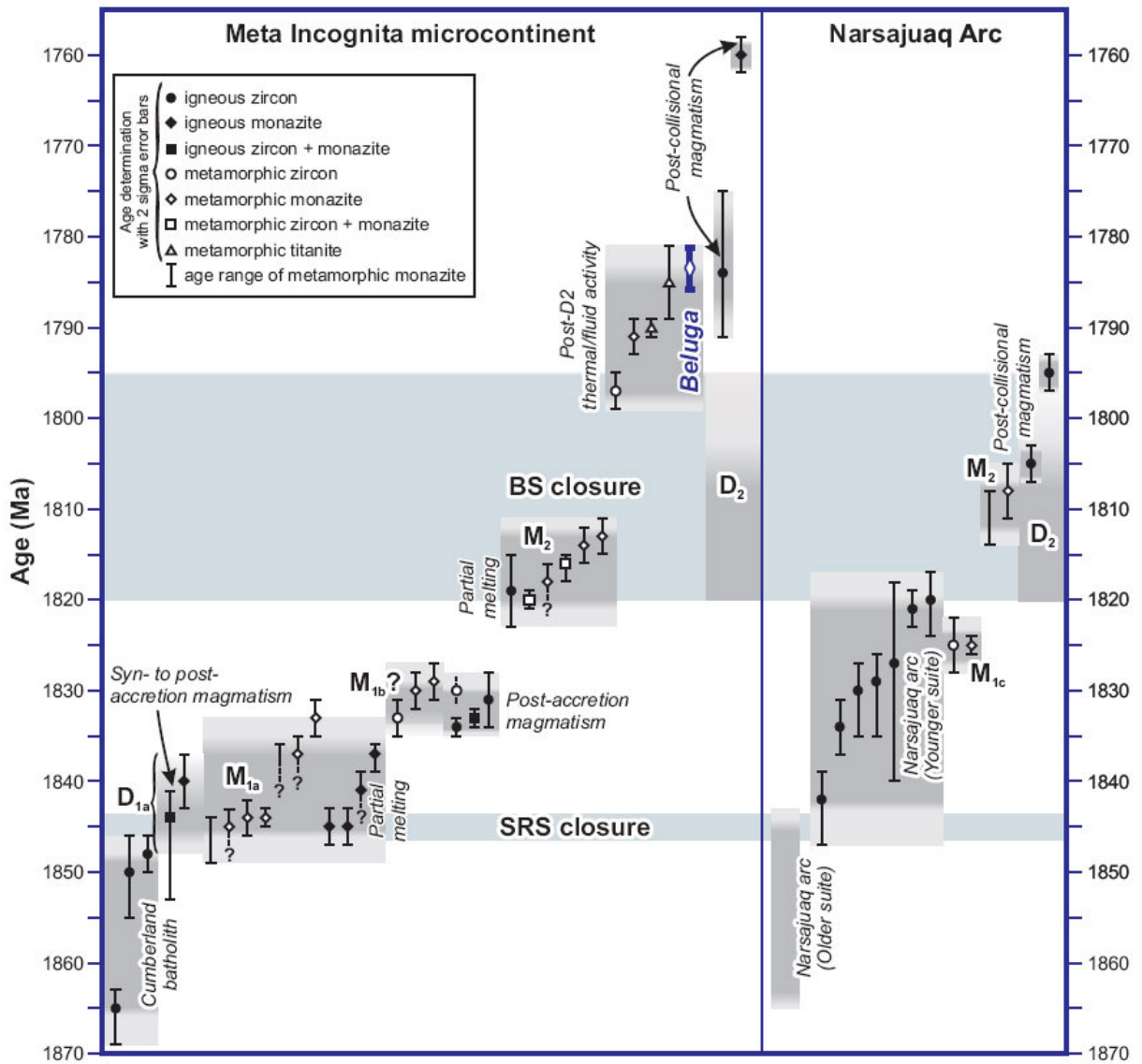


Figure 4.29: U-Pb ages of deformation, metamorphic and magmatic events in the Meta Incognita microcontinent and Narsajuaq arc (St-Onge et al. 2007). A U-Pb zircon date from the Beluga showing (LeCheminant et al. 2005) plots amongst other post-D₂ thermal/fluid activity ages. (BS = Bergeron suture; SRS = Soper River suture.)

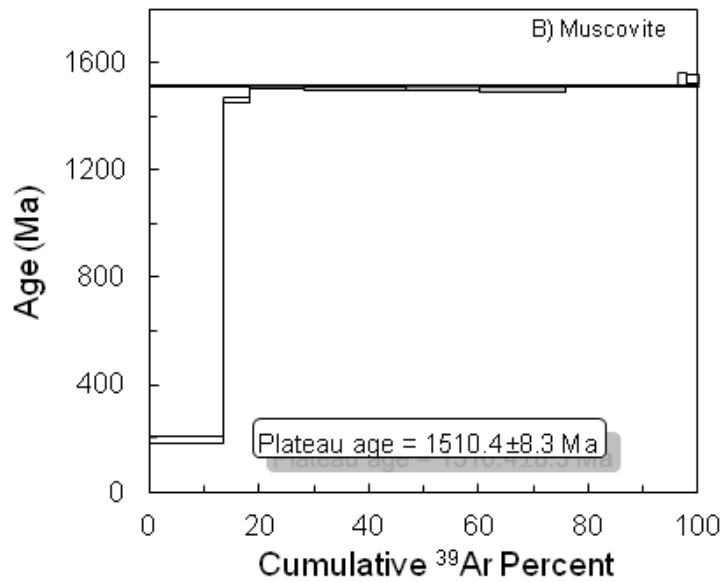
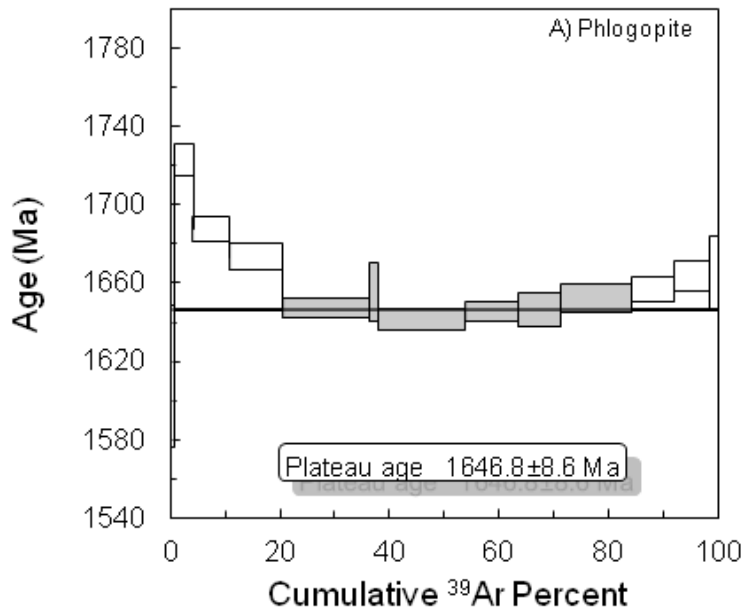


Figure 4.30: $^{40}\text{Ar}-^{39}\text{Ar}$ age spectra of (A) phlogopite and (B) muscovite from the Beluga showing. Box heights are 2σ , plateau steps are filled, and rejected steps are open.

Chapter 5: Comparison of the Revelstoke and Kimmirut corundum occurrences

5.1 Introduction

Even though there are some similarities between the Revelstoke occurrence and the Kimmirut sapphire occurrence (KSO), there are more differences (Table 5.1). Both of the carbonate-hosted gem corundum occurrences are found in poly-stage metamorphosed (peak metamorphism up to granulite facies) and highly deformed metasedimentary sequences that were subjected to extensive fluid infiltration (Chapters 3 and 4). At both localities, barrel shaped-corundum crystals with tapered ends (Chapter 3, LeCheminant et al. 2004) occur in lithologies that are depleted in Si and Fe compared to other local lithologies. The protolith of corundum-bearing rocks at each occurrence is composed of siliciclastic and evaporite components hosted in marble.

The differences between the two localities are discussed in detail in the following text and are summarized in Table 5.1.

5.2 Age

The Revelstoke occurrence is hosted in much younger rocks than the Kimmirut sapphire occurrence. It is hosted within the Monashee cover sequence of British Columbia which contains Paleoproterozoic to Cambrian sediments that were metamorphosed from 62 Ma to older than 47 Ma. The Kimmirut Sapphire occurrence is hosted within the Trans-Hudson Orogen on Baffin Island, Nunavut in < 1.93 Ga sediments that were metamorphosed from 1844 Ma to 1784 Ma (Scott 1997; St-Onge et al. 2007 and references within).

5.3 Petrology

At the Beluga showing of the KSO, blue sapphire occurs in medium- to coarse-grained calc-silicate pods with the assemblage diopside + phlogopite + plagioclase + scapolite + albite + muscovite + calcite, whereas at the Revelstoke occurrence, pink sapphire occurs in fine- to medium-grained foliated layers with green muscovite + anorthite + K-

feldspar + calcite \pm scapolite \pm rutile. Scapolite is always present in corundum-bearing rocks at the Kimmirut occurrence, but is only sometimes present at the Revelstoke occurrence.

Gem corundum formed by two very different mechanisms at the Beluga showing and the Revelstoke occurrence. At the Beluga showing, blue sapphire formed during late fluid infiltration from the destabilization of anorthite or nepheline + scapolite or nepheline + anorthite, whereas pink sapphire at the Revelstoke occurrence formed during the peak of metamorphism from the dehydration of muscovite. Indicator minerals at the Revelstoke occurrence are green muscovite aggregates, whereas scapolite and violet diopside are the indicator minerals at the Beluga showing.

5.4 Whole Rock Composition

The whole rock composition of corundum-bearing rocks at each locality is unique (Fig. 5.1). When comparing the mica-feldspar rocks from the Revelstoke occurrence with the calc-silicate rocks from the Beluga showing, the Beluga showing rocks are highly enriched in V (~220 to 275 ppm), SiO₂ (~45 wt. %), MgO (~9 to 12 wt. %), TiO₂ (~0.9 to 1.1 wt.%), Cr (~100 to 130 ppm), Al₂O₃ (12 to 15 wt.%) and Na₂O (2.3 to 3.1 wt.%). Both localities have similar contents of Fe₂O₃ (0 to 2 wt. %), but the mica-feldspar layers from the Revelstoke occurrence have elevated CaO (~30 to 50 wt. %).

When comparing the host rocks from the Revelstoke occurrence with the calc-silicate rocks of the Beluga showing, the Revelstoke host rocks have significantly lower Na₂O (< 1.5 wt.%) and MgO (<4 wt.%) and higher Fe₂O_{3TOT} contents (5 to 7.5 wt.%; Figure 5.1). Revelstoke host rocks also have slightly elevated SiO₂ (~46 to 58 wt.%), and Al₂O₃ (15 to 18 wt.%), and slightly lower CaO (~1 to 20 wt.%), TiO₂ (~0.6 to 0.6 wt.%) and Cr (~90 to 120 ppm).

5.5 Mineral Chemistry

5.5.1 Corundum

The colour, composition, and quality of gem corundum is unique at each locality. Pink sapphire from the Revelstoke occurrence contains elevated Cr_2O_3 (≤ 0.21 wt.%), TiO_2 (≤ 0.25 wt.%), and minor FeO (≤ 0.05 wt.%), whereas blue rims contain moderate Cr_2O_3 (≤ 0.11 wt.%), elevated TiO_2 (≤ 0.53 wt.%), and minor FeO (≤ 0.06 wt.%). In comparison, blue sapphire from the Beluga showing contains elevated TiO_2 (≤ 0.30 wt.%) and FeO (≤ 0.13 wt.%), with Cr_2O_3 near detection limits (≤ 0.01 wt.%). The main difference between the two localities is that the Revelstoke corundum contains elevated Cr, whereas the Beluga corundum is Cr-poor (Fig. 5.2); the total contents of Fe and Ti and the Fe/Ti ratio in corundum are similar at both localities. The difference in corundum composition from each locality is not related to whole rock composition, but rather to the composition of minerals and fluid involved in corundum-producing reactions.

The quality, quantity, and intensity of colour of gem corundum at the Kimmirut sapphire occurrence is much greater than at the Revelstoke occurrence.

5.5.2 Micas

Phlogopite composition at each locality is unique (Fig. 5.3). Revelstoke phlogopite is enriched in Al (~1.4 to 2.1 apfu) and depleted in Mg (~1.7 to 2.3 apfu) compared to Beluga and Bowhead phlogopite, which is depleted in Al (~1.1 to 1.2 apfu) and enriched in Mg (~2.3 to 2.7 apfu). Beluga and Bowhead phlogopite is enriched in Ti (≤ 0.16 apfu), but the lowest values overlap with some phlogopite from the Revelstoke occurrence with elevated Ti (~0.09 to 0.12 apfu). The Fe content of Revelstoke phlogopite is dependent on the outcrop analyzed. One population of Revelstoke phlogopite contains elevated (0.27 to 0.34 apfu) and depleted (~0.06 to 0.10 apfu) Fe compared to the Beluga and Bowhead showings. Moderate Fe values from the Revelstoke occurrence overlap with the Beluga and Bowhead showings (~0.15 to 0.2 apfu).

Muscovite composition and colour at each locality is unique as well (Fig. 5.4). Revelstoke muscovite is green and contains elevated Fe+Mg (~0.05 to 0.34 apfu) and Cr (~0 to 0.013 apfu), and depleted Al (~2.65 to 2.92 apfu) and Na (0.015 to 0.06 apfu) compared to

the Beluga and Bowhead muscovite, which is colourless and contains very little Fe+Mg (~0 to 0.015 apfu), Cr (~0 to 0.004 apfu), and Ti (~0 to 0.01 apfu), and elevated Na (0.07 to 0.25 apfu). The Revelstoke and Beluga muscovite contain similar amounts of K (~0.85 to 0.98 apfu).

5.5.3 Scapolite

The composition of scapolite is unique at each locality (Fig. 5.5). The Beluga and Bowhead scapolite is enriched in Na and Cl compared to the scapolite from mica-feldspar layers at the Revelstoke occurrence. The Beluga and Bowhead analyses are outside of the normal range of analyses forming the solid solution between marialite and meionite because of Na and Cl mobility during electron microprobe analysis (See Chapter 4). Scapolite from non-corundum-bearing lithologies at the Revelstoke occurrence are either near pure end-member meionite containing no Cl, or enriched in Cl and Na compared to corundum-bearing lithologies.

5.6 Oxygen Isotopes of Corundum

Despite both the Revelstoke occurrence and the Kimmirut sapphire occurrence being carbonate-hosted, the $\delta^{18}\text{O}$ values of corundum from each locality are very different; pink corundum from the Revelstoke occurrence has $\delta^{18}\text{O}$ values of 10.7 and 11.1‰, whereas blue corundum from the Beluga showing has a $\delta^{18}\text{O}$ value of 16.4 ‰. The difference in these values reflects the $\delta^{18}\text{O}$ values of the different protoliths for each locality, as well as the composition of fluids during corundum crystallization.

5.7 Discussion

There are many more differences between the Revelstoke occurrence and the Kimmirut sapphire occurrence than there are similarities. The most striking differences between localities are: the geological position, age of deposition and metamorphism, mineral assemblages and mineral compositions, mineral textures, occurrence morphology, corundum forming reactions, timing of corundum crystallization, composition, colour and quality of

gem corundum, whole rock composition, protolith composition, and the $\delta^{18}\text{O}$ of corundum. All of these differences indicate that the two localities had different protolith compositions and conditions of formation. Additional evidence to support this is that, even though the whole rock composition of the Beluga calc-silicate rocks contain elevated Cr and V similar to the host rocks at the Revelstoke occurrence, the corundum at the Beluga showing contains almost no Cr and V, indicating that either the Cr and V were not mobile during corundum crystallization, or Cr and V were trapped in minerals that were not involved in the corundum producing reactions. The whole rock composition of corundum-bearing lithologies therefore may not be a good indication of the variety of corundum that can be found in the deposit.

The amount of gem quality corundum at the Kimmirut sapphire occurrence is far greater than at the Revelstoke occurrence. Asian ruby deposits which formed during retrograde metamorphism from a siliciclastic-evaporite protolith, also contain a large amount of gem quality material similar to the Kimmirut sapphire occurrence; however the colour (pink-red at the Asian deposits; blue to colourless at the KSO), morphology of the deposit (layers at the Asian deposits; pods at the KSO), whole rock composition, and mineral assemblages are very different compared to the KSO. Some possible reasons why retrograde gem corundum is better quality than prograde is that there is typically a lack of deformation after corundum crystallization, retrograde fluids may enhance crystallization, and P-T conditions may be more appropriate for better quality crystals. At the Revelstoke deposit, there is clear evidence that the sapphire-bearing layers are the products of mechanical mixing between the host sediments and the marble, whereas at the Kimmirut sapphire occurrence and the Asian deposits, there is no indicator of the source of siliciclastic material.

Table 5.1 Comparison between the Revelstoke and Kimmirut Sapphire Occurrences.

	Mineral Assemblage	Corundum Colour and Chromophores	PT of Corundum Formation
RO	Ms + An + Kfs + Cal ± Phl ± Scp ± Rt ± Crn	Pink-red (Cr), blue rims (Fe+Ti)	~650-700 °C at 8.5-9 kbar
KSO	Di + Phl + Plg + Scp + Ab + Ms + Cal ± Crn	Blue (Fe + Ti), colourless	Most likely < 710°C and 6 kbar*
Timing of Corundum Formation		Deposit morphology	
RO	~58 Ma		Layers, fine-med-grained
KSO	~1782.5 Ma		Pods, med-coarse-grained
Protolith			
RO	Mechanical mixing of host sediments into marble followed by Fe and Si depletion before prograde corundum crystallization		
KSO	Black shale-evaporite protolith that was infiltrated by late (Si)-H ₂ O-fluids during retrograde corundum crystallization		

RO = Revelstoke Occurrence, KSO = Kimmirut Sapphire Occurrence

*(St-Onge et al. 2007)

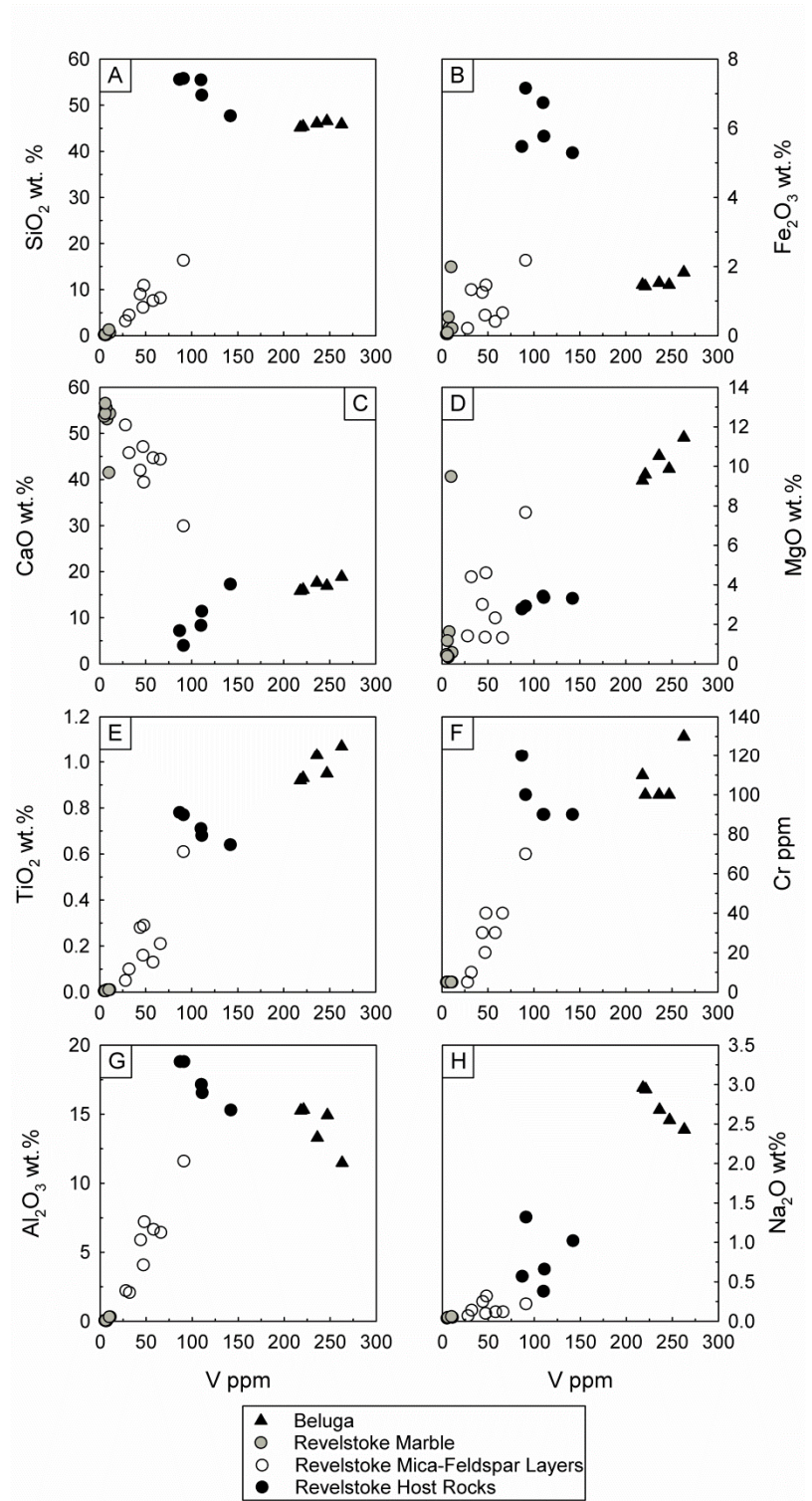


Figure 5.1: Comparison of the whole rock compositions from the Kimmirut sapphire occurrence and the Revelstoke occurrence.

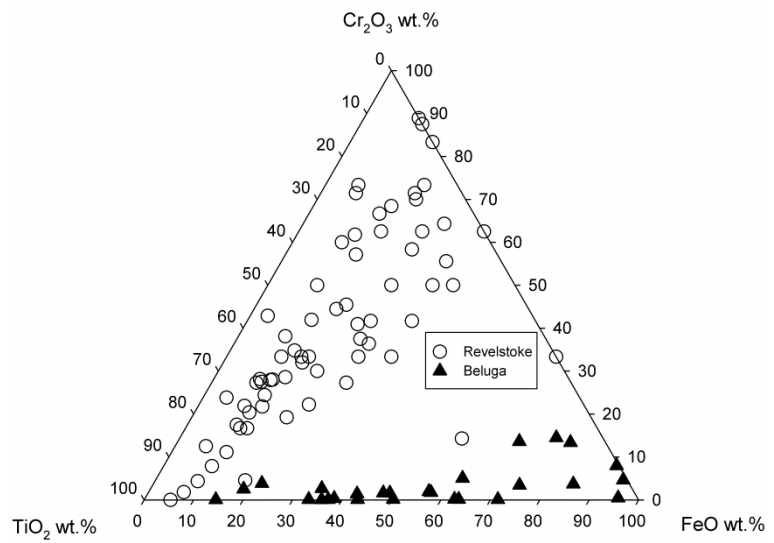


Figure 5.2: Comparison of corundum compositions from the Beluga showing and the Revelstoke occurrence.

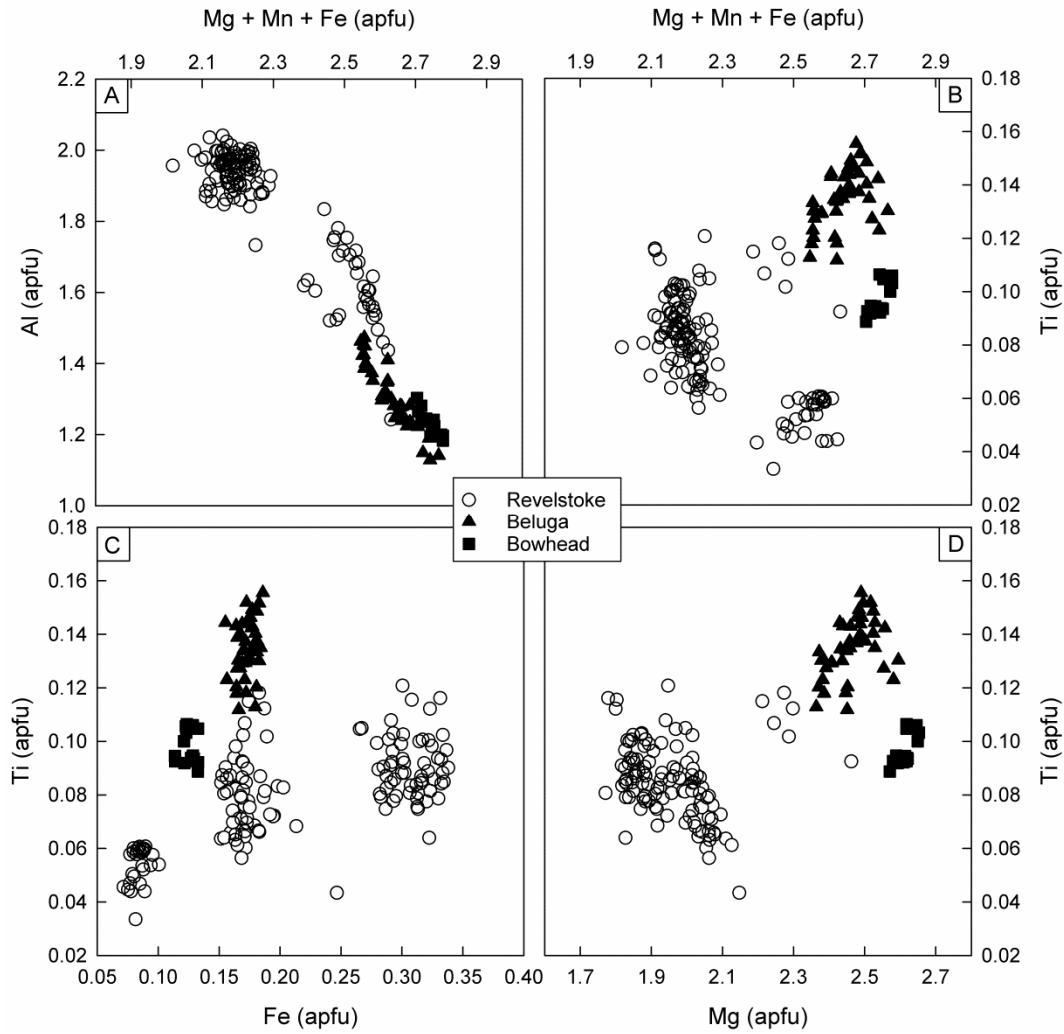


Figure 5.3: Comparison of phlogopite compositions from the Kimmirut sapphire occurrence and the Revelstoke occurrence (excluding host rocks).

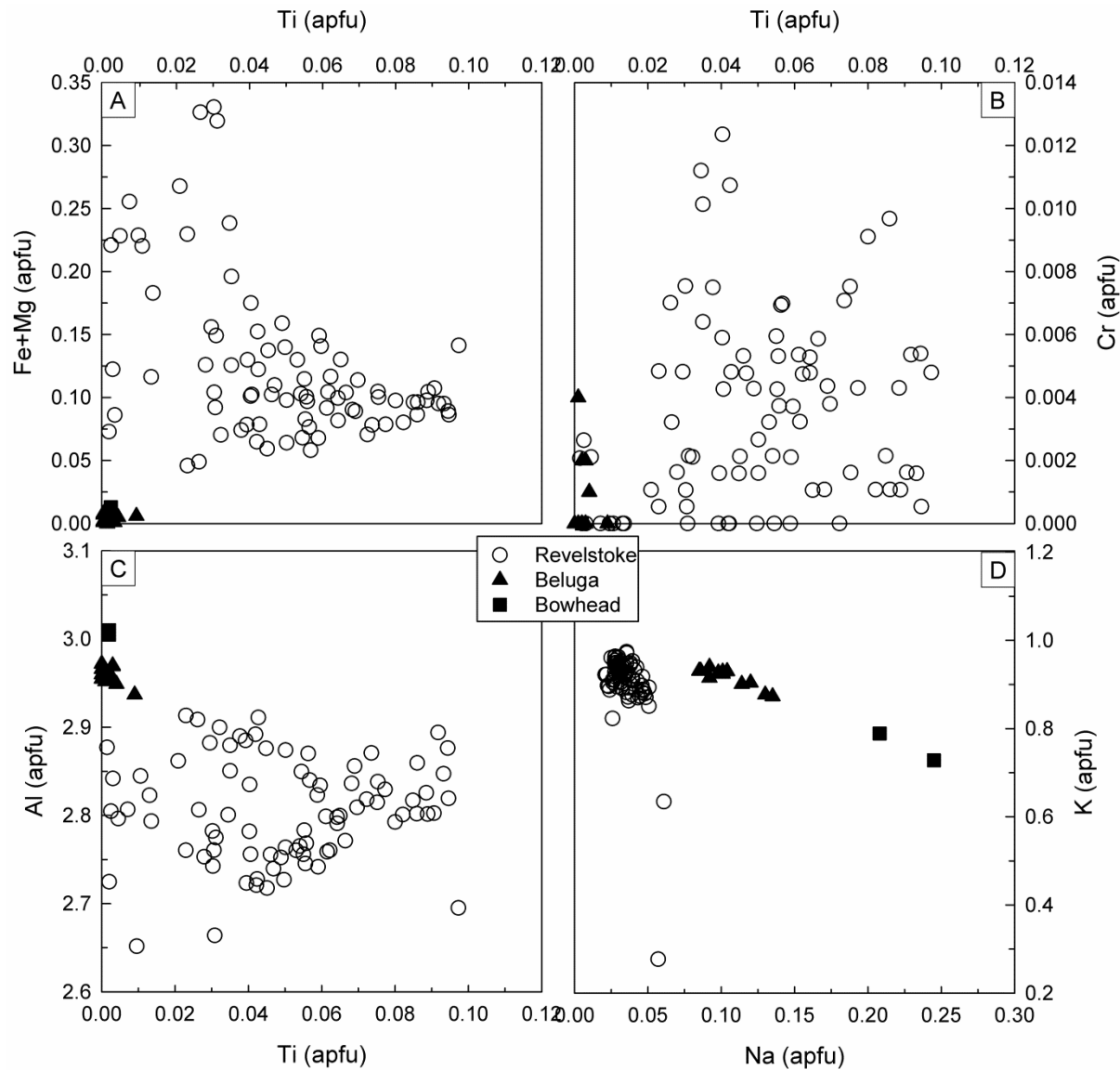


Figure 5.4: Comparison of muscovite compositions from the Kimmirut sapphire occurrence and the Revelstoke occurrence.

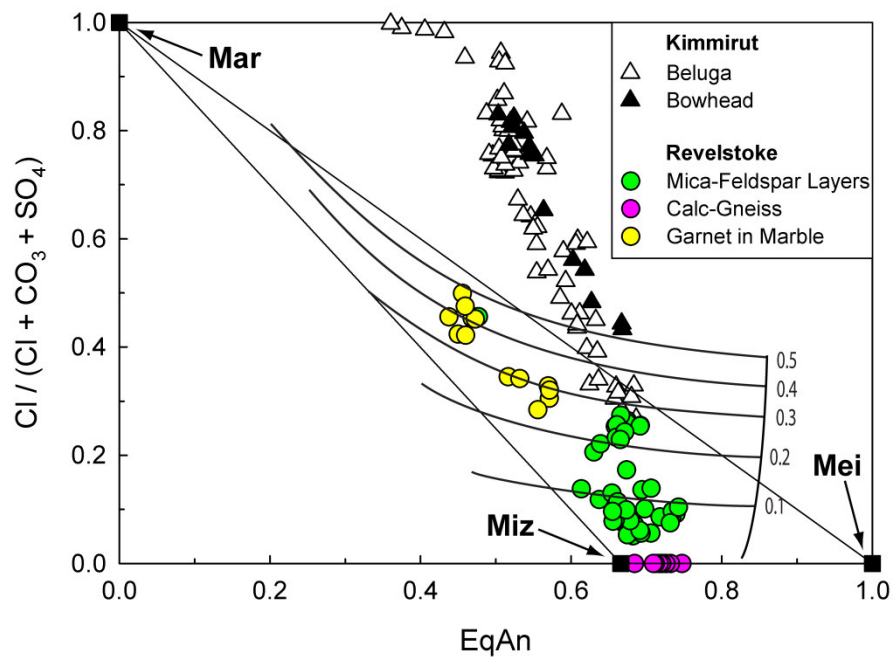


Figure 5.5: Comparison of scapolite compositions from the Kimmirut sapphire occurrence and the Revelstoke occurrence (including host rocks).

Chapter 6: Exploration Strategies

6.1 Introduction to Exploration Strategies

When considering exploration strategies for carbonate-hosted gem corundum deposits, it is important to recognize that each deposit is unique; therefore, the application of one exploration strategy to all deposit types will not be effective. Currently no formal or published exploration strategies exist for marble-hosted gem corundum deposits, but some standard exploration techniques have been proposed to locate magmatic gem corundum deposits or metamorphic deposits associated with magmatic bodies. Examples of these techniques include geological mapping, soil and stream geochemistry, detailed sample grids, satellite imagery, and airborne or land geophysical methods (Key and Ochieng 1991, Simonet and Okundi 2003). These techniques could also be useful for locating marble-hosted deposits, but the specific methods and application of each technique must be tailored to a specific type of carbonate-hosted deposit before any exploration project can begin.

Many factors about each target area must be considered during development of an exploration strategy to ensure feasibility and success. Just because something can be done, does not mean it should be done. It is important to take both geological and geographical features into consideration when choosing the best exploration methods to incorporate into an exploration strategy. The following should all be evaluated: (1) amount of exposed outcrop , (2) the topography (steep ridges vs. low rolling hills), (3) weathering rates (low rates may make placer accumulation and drainage zone tracing difficult), (4) the 3-dimensional shape and size of mineralized zones (laminar or podiform) and whether the deposit is lithologically controlled or not, (5) grain size of mineralized and non-mineralized areas, (6) indicator minerals and mineralogical contrasts, and (7) regional and local deformation.

6.2 Recommended Exploration Techniques and Strategies

Different approaches can be applied to extending the known size of a deposit or locating a new deposit during green-fields exploration (exploration far away from a known deposit). Both long established and newly proposed exploration techniques that can readily be applied to gem corundum exploration are outlined below. Some exploration techniques can be applied at both

the Revelstoke and Kimmirut gem corundum occurrences, but others will only be effective at one. Unless otherwise stated, all techniques mentioned are applicable at both Revelstoke and Kimmirut.

The goal of each technique is to identify target zones which may contain corundum. Once target zones are identified, the presence of gem corundum should be confirmed in person.

6.2.1 Review of Known Geology and Mapping

Prior to mapping, analysis of the regional and local scale structural geology is needed to identify where metamorphic isograds indicating upper amphibolite to granulite facies are located; this will ensure the geological mapping is completed in areas with the right P-T conditions for corundum formation. An understanding of the regional and local scale structural geology will be of assistance in extending the size of known mineralized areas, especially if the structural data can identify areas of high fluid flow or help predict the morphology of the deposit (folded, elongated, or boudinaged). Fold hinges are commonly found to concentrate fluids and will also contain the thickest units of corundum mineralization.

Geological mapping can be used to determine the extent of surface mineralization at both occurrences. Detailed mapping at a scale of 1:500 should be used to document the location of mineralized pods and/or layers. These mineralized zones are typically small and can be easily overlooked; only highly detailed mapping can document such mineralization. Corundum-bearing laminations at the Revelstoke occurrence are very thin (<20 cm thickness) and corundum-bearing calc-silicate pods at the Beluga occurrence are typically only a few metres in diameter.

Mapping at the Revelstoke occurrence should continue along strike of the marble in Unit 6A of the Monashee cover sequence (see chapter 3 for a full description of this unit) because the corundum mineralization is lithologically controlled and will likely extend out along strike from the known occurrence. Corundum-bearing mica-feldspar layers, which represent former pelite layers, will be thickest in fold hinges and thinnest along fold limbs – these are the highest priority targets for geological mapping and surface prospecting. Highly tectonized areas containing extensive stretching and folding prior to or during peak metamorphism are important at the Revelstoke occurrence because thinning of former pelite layers in marble enhanced

reactions between the pelitic material and the surrounding carbonate. These structures can also act as fluid pathways, which greatly enhance Si removal, and therefore corundum stability.

Mapping at the Kimmirut occurrence should continue within the Lake Harbour Group marble. The corundum mineralization within the calc-silicate pods is not predictable; in the absence of additional data, mapping must continue along the entire extent of the marble.

6.2.2 Prospecting and Indicator Minerals

At the Revelstoke occurrence, the primary indicator mineral is green muscovite which occurs as aggregates of crystals (Fig. 6.1, 6.2). The fastest way of determining the potential location of corundum is to locate a green muscovite-bearing mica-feldspar layer within the marble of Unit 6A of the Monashee cover sequence and trace its extent along strike. Whenever mica-feldspar layers are discovered they should be mapped in detail. It is fairly common to find phlogopite throughout the marble, but it is not as common to find the green muscovite aggregates. Locations of this key mineral should be recorded on the map.

At the Beluga occurrence, one should look for coarse-grained calc-silicate pods with scapolite and violet diopside within the Lake Harbour marble (LHM; Fig. 6.3). The location of corundum-bearing calc-silicate pods is not predictable within the very large LHM. Any information about scapolite-bearing zones that can be collected beforehand would be advantageous.

6.2.3 Detailed Sampling Grid

Completing a detailed geochemical sampling grid perpendicular to the strike of the marble and host rocks will provide rock-chip samples for geochemical assay. By following a sampling grid (Fig. 6.4), a representative amount of marble, mica-feldspar layers or calc-silicate pods, and host rocks can be obtained. Caution must be used when sampling to make sure that potential corundum-bearing layers are not overlooked because of their size, especially at the Revelstoke occurrence. The best exposure of corundum-bearing layers is on exposed foliation planes that are common in areas of talus. Collected samples can be analyzed by the whole rock analysis method below in order to define target areas on a map.

6.2.4 Whole Rock Analyses

Whole rock analyses can be determined in a lab or in the field. A handheld XRF can be utilized in the field to quickly determine the major element geochemistry of a particular rock sample and discriminate between corundum mineralized and non-mineralized layers within marble at the Revelstoke occurrence. By plotting the whole rock geochemical data (FeO and SiO_2 vs Al_2O_3) for each sample it should be possible to identify samples with lower $\text{SiO}_2/\text{Al}_2\text{O}_3$ and $\text{FeO}/\text{Al}_2\text{O}_3$ ratios; these are primary target areas for corundum mineralization (Fig. 6.5). This tool is new and to the author's knowledge has not been used for gem corundum exploration. This method can readily, cheaply and easily aid in the identification of corundum prospective zones in marble in the field.

6.2.5 Airborne Hyperspectral Imaging Surveys for Identification of Indicator Minerals

Hyperspectral surveys can quickly collect imagery and mineral abundance data from a large area by detecting reflected light from the surface of rocks. Currently, satellite hyperspectral surveys have a resolution of only ~30 m pixels and airborne hyperspectral surveys have a resolution of ~4 m pixels, depending on flight altitude (e.g., Bedini 2009). For this technique to be applied, the reflectance spectra of the known deposit host-rocks and minerals must first be characterized. Once this reference has been established, the ability to identify key corundum indicator minerals, such as phlogopite and muscovite at Revelstoke and scapolite at Kimmirut, can be applied on a regional scale using airborne data to identify potential targets. Ideally, this type of survey would be completed during the early stages of exploration and used to place ground exploration teams, saving both time and money. Currently, the cost of conducting fine-resolution airborne hyperspectral surveys is quite high, but ground based “pan and tilt” hyperspectral cameras could be used locally at a lower cost than airborne surveys. In addition to the cost, the primary drawbacks to this technique is that cloud cover, extreme weathering, and lichens can prevent reliable data from being collected.

Because there is good surface exposure at the Revelstoke occurrence, an airborne hyperspectral survey could potentially be used to identify indicator grains of phlogopite and muscovite in the marble (Clark 1999). However, the fine to medium-grain size of the minerals, very thin corundum-bearing mica layers (< 20 cm), and steep topography could make distinction between target and non-target rocks very difficult. Improvements will be required in the

resolution of hyperspectral surveys before they can be easily applied to the Revelstoke occurrence. Examples of such improvements are the implementation of more accurate detectors, low flying unmanned aircraft systems, and faster and more accurate data processing techniques.

An airborne hyperspectral dataset was collected over an area in southwestern Baffin Island in 2004 (Rogge et al 2009, Harris et al. 2010) with a ground sampling pixel size of ~7 m. This area is well suited to hyperspectral surveys because the rock exposure is excellent, the grain size of calc-silicate pods is medium to coarse, and the surface is relatively flat. Different lithological units were delineated from the data and correspond with traditional geological maps. Calcite, dolomite, and calc-silicate-(diopside)-bearing marbles, quartzites, iron-bearing metasediments, and gossans were successfully mapped (Harris et al. 2010) at this scale, but scapolite was neither sought nor identified in this survey. Preliminary high resolution laboratory-based hyperspectral imagery of corundum and scapolite-bearing rocks from the Kimmirut occurrence shows that scapolite-bearing pods on the surface associated with sapphire would be an excellent target in the future because scapolite has a distinct reflectance spectrum.

6.2.6 Identification of Chromophore Sources

Pure corundum is colourless; therefore, common chromophore elements such as V, Ti, Cr and Fe are required to produce desirable colours. Locating a Cr-source near rocks with low $\text{SiO}_2/\text{Al}_2\text{O}_3$ and $\text{FeO}/\text{Al}_2\text{O}_3$ values would be helpful when searching for ruby and pink sapphire showings.

Rocks with high concentrations of mafic elements are usually intrusive mafic rocks or pelitic layers in marble. Chromium is essential to producing the red colour in corundum; low Cr produces pink, moderate Cr produces red, and high Cr produces intense red corundum (ruby). The more intense the colour, the more valuable the gemstone will be. Iron will suppress the red colour in ruby, so it is important to avoid prospecting in areas with Fe-rich sediments when searching for rubies.

6.2.7 Magnetic Geophysical Survey

Mafic rocks commonly occur in association with magnetic minerals. Geophysically determining where the magnetic rocks occur in contact with or near the marble complex could indicate where the chromophore elements are concentrated, thus where economic corundum may

be located. This can be done on the ground or using airborne platforms and is a common exploration technique.

6.2.8 Heavy Mineral Concentrates

Heavy-mineral concentrates can be collected from stream sediments in areas of high weathering. Corundum has a specific gravity of 4, and will concentrate in stream sediments, like black sand and gold do. A simple panning or jigging system can be used to assess streams for corundum. After corundum is identified in a stream, individual drainage basins can be identified to trace the source of the corundum.

6.2.9 Ultraviolet Light Surveys for Identification of Scapolite Associated with Corundum

Ultraviolet light surveys done on foot during twilight with hand-held UV lamps have been successfully used to identify scapolite-bearing calc-silicate zones at the Beluga sapphire occurrence (Lepage, 2007). Special filters were used in the lamps to enhance the optimum wavelength needed to easily detect scapolite at the occurrence. The benefit of this technique is that the hand-held UV lamps have a beam diameter of ~5 meters allowing for rapid coverage of outcrop with little expense. Unfortunately, the surveys must be done at night or twilight, and human error may account for missed targets if a scapolite-bearing zone is overlooked.

6.2.10 Ground Penetrating Radar (GPR) for 3-D imaging of Target Zones at Depth

Once targets are identified, 3-D imaging of these zones at depth can be completed to assess the shape and size of the layers or pods. Ground penetrating radar surveys have been successfully used to determine the shape and depth of gem corundum-bearing pods within marble at the Beluga occurrence (Andrew Fagan, pers. comm. 2013). This technique uses radar pulses to image the subsurface. The effective depth of penetration is dependent on the complexity of geological features at depth, dielectric constants between adjacent rock types, degree of signal attenuation with each horizon, and the transmitting frequency (Francke and Utsi 2009).

6.3 Exploration for Revelstoke-type Occurrences in Other Parts of the World

Ideal targets are metasedimentary sequences of alternating carbonate and pelite sediments, metamorphosed to upper amphibolite to granulite facies and extensively deformed (folded and stretched) and flushed with fluids. Mica-feldspar layers in fold hinges and limbs are ideal targets. These layers may be identified remotely by hyperspectral surveys, or by mapping on foot. Once a location is identified, follow the procedure outlined above for mapping and sampling at the Revelstoke occurrence by prospecting or using a detailed sampling grid followed by whole rock analysis for the identification of SiO₂ and FeO depleted layers. The presence of Cr-bearing rocks, such as pelites or ultramafics, in the vicinity can also be useful. In areas of high weathering, heavy-mineral concentrates from corundum-bearing stream sediments may also help in tracing drainage basins back to their source.

6.4 Exploration for Beluga-type Occurrences in Other Parts of the World

As with Revelstoke-type occurrences, ideal targets for exploration are well exposed metasedimentary sequences containing calcic carbonate and pelitic sediments, which were metamorphosed from upper amphibolite to granulite facies. There is greater exposure of potential mineralized rocks in well exposed areas such as those above tree line. Each exploration strategy should involve the search for scapolite-bearing calc-silicate pods in marble units with odd mineralogy. The random nature of these pods requires that large-scale exploration such as hyperspectral surveys be completed first to constrain target areas. As with exploration for Revelstoke-type deposits, heavy-mineral concentrates from corundum-bearing stream sediments found in areas of high weathering may help to trace drainage basins back to the source of corundum.

6.5 Summary

Regardless of which type of carbonate-hosted gem corundum deposit is being sought, the search should focus on areas or rocks within the amphibolite to medium pressure granulite metamorphic facies (Simonet et al. 2008). Although corundum occurs in many rock-types, this study focused on mixed sedimentary packages within calcic marbles. Classical exploration

techniques – mapping, prospecting, and geochemical sampling – can be readily utilized, as can newer more advanced exploration techniques, such as hyperspectral analysis.

Important factors to consider for marble-hosted gem corundum exploration are: (1) the grade of metamorphism in the host-rocks; (2) availability of Cr and other chromophores from mixing of units; (3) lithologic control of mineralization (Garnier et al. 2008); (4) deformation; and (5) the presence of indicator minerals (dependent on deposit type; Table 6.1).

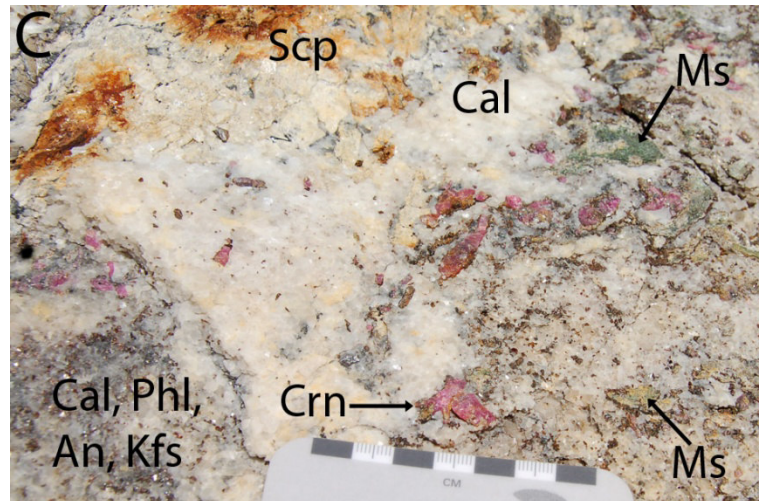


Figure 6.1: Corundum-bearing mica-feldspar layers, with secondary scapolite after anorthite exposed on a foliation plane.

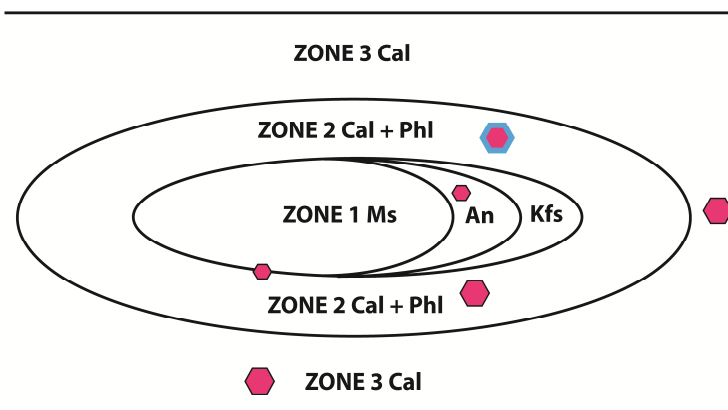


Figure 6.2: Schematic drawing of the mineralogical zoning of mica-feldspar layers. The pink hexagons represent non-zoned corundum and the pink hexagon rimmed with blue represents zoned corundum with a pink core and blue rim.

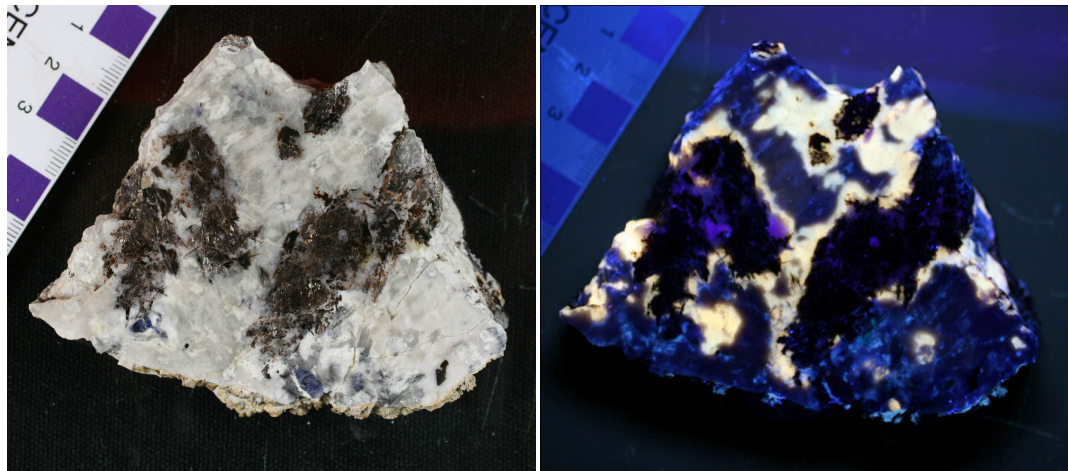


Figure 6.3: Scapolite- and corundum-bearing rocks under incandescent and ultraviolet light. Note the yellow fluorescence of scapolite in ultraviolet light.

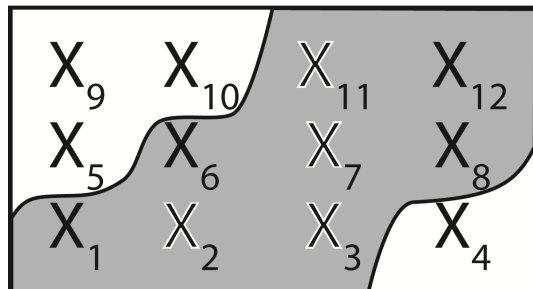


Figure 6.4: Schematic of a geochemical sampling grid that could be applied to exploration for corundum deposits. Results are plotted on Fig. 6.5 to facilitate interpretation.

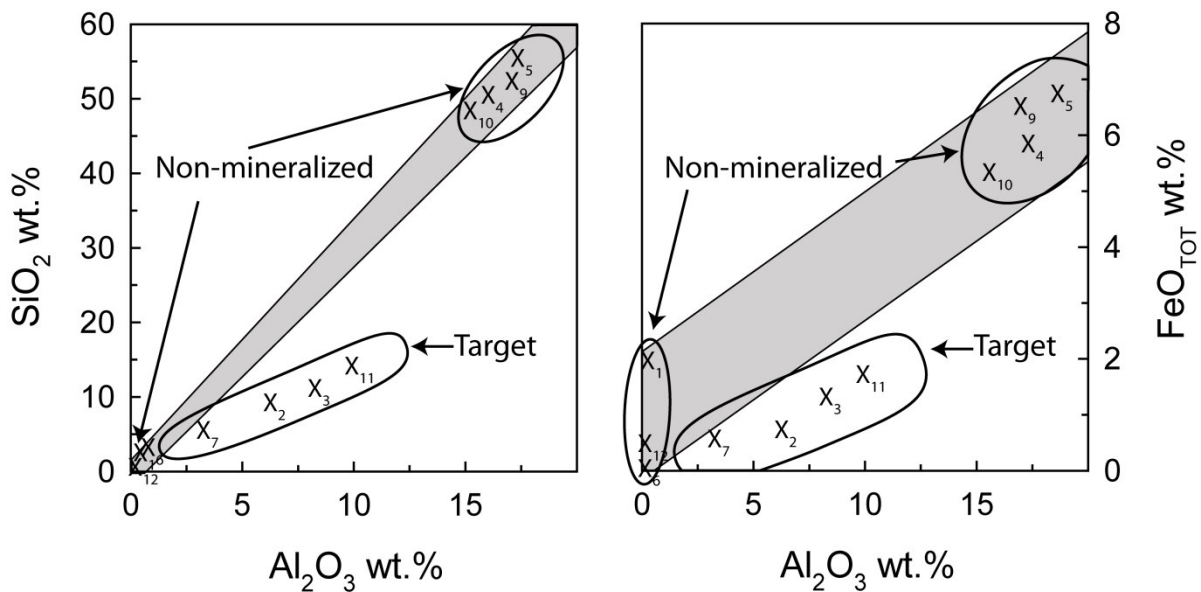


Figure 6.5: Whole rock or Niton XRF geochemical diagrams highlighting target zones at the Revelstoke occurrence. The gray shaded areas highlight where values should lie if there was mechanical mixing between the two lithologies without any element loss or gain. The target area highlights samples that are depleted in SiO_2 and FeO_{TOT} .

Table 6.1: Factors to consider for exploration – a comparison between the Revelstoke and Beluga occurrences

Deposit Type	Indicator Minerals	Depositional Environment	Lithologic control of mineralization	Peak Metamorphic Grade	Prograde or Retrograde fm of gem crn	Regional deformation
Revelstoke	Green muscovite + K-feldspar + anorthite, or muscovite + phlogopite	¹ Sediments deposited on a shallow marine shelf to intertidal platform. Muds and silts with varying amounts of carbonate deposited under saline conditions	yes	Upper Amphibolite/ Granulite	Prograde 650-700 °C 8.5-9 kbar	extensive
Baffin	scapolite, violet diopside	² Carbonate platform	no	² Upper Amphibolite/ Granulite	Retrograde	² extensive

¹(Höy 1987)

²(St-Onge)

Chapter 7: Conclusions and Future Work

7.1 Conclusions - Revelstoke

This study has contributed to both the understanding of the formation of gem corundum in carbonate rocks during prograde metamorphism and metasomatism of pelitic layers within marble as well as the petrology of metasediments in the Frenchman Cap dome. Whole rock geochemistry data indicate that the corundum-bearing silicate (mica-feldspar) layers formed by the mechanical mixing of carbonate with the protolith of the host gneiss. The silicate layers and the gneiss contain elevated contents of Cr and V due to the presence of a volcanoclastic component in their protolith. The bulk composition of the silicate layers was depleted in Si and Fe during prograde metamorphism. Silica and Fe depletion was also enhanced by extensive fluid-rock interaction, which is evident in the homogenization of $\delta^{18}\text{O}$ and $\delta^{13}\text{C}$ values in carbonates and silicates in the marble and silicate layers as well as low $\delta^{18}\text{O}$ in the corundum.

Corundum occurs in thin, folded and stretched layers with the predominant assemblage of green muscovite + Ba-bearing K-feldspar + anorthite ($\text{An}_{0.85-1}$) \pm phlogopite \pm Na-poor scapolite. Gem corundum was produced in the mica-feldspar layers by mica dehydration at the peak of metamorphism (~650-700 °C at 8.5-9 kbar) following a clockwise P-T path. Fluid inclusions in the corundum are pure CO₂, indicating the presence of a CO₂-rich fluid during corundum formation. The micas associated with corundum in the mica-feldspar layers have elevated Cr, V, and Ti, indicating that they were the source of these elements in the corundum crystals. The mica-feldspar layers were an ideal environment for corundum formation because of the depletion of Si and Fe, and enrichment of Cr, V and Ti.

Existing models of gem corundum genesis (Giuliani et al 2007) cannot explain the formation of sapphire at the Revelstoke occurrence. The Asian ruby deposits described by Garnier et al. (2008) share some common features with the Revelstoke occurrence, but there are also numerous differences that exist between the two localities, the most important of which is the prograde formation of corundum by muscovite dehydration at high pressure, compared to the retrograde alteration of spinel at low pressure.

The unique features of the Revelstoke occurrence that make it conducive to corundum formation are the presence of Si- and Fe-depleted Cr-mica-feldspar layers within marble that were subjected to granulite facies metamorphism.

Exploration strategies that have the greatest potential to be effective for expanding the extent of the Revelstoke occurrence are:

- 1) field based or lab based major element comparison between host rocks and micaceous laminations within marble.
- 2) detailed mapping and prospecting for micaceous laminations that contain green muscovite pods and phlogopite with feldspars.

7.2 Conclusions - Kimmirut Sapphire Occurrence

Two very similar coarse-grained calc-silicate rocks forming part of the Kimmirut Sapphire Occurrence within the Lake Harbour Marble (the less altered Bowhead nepheline-bearing corundum absent calc-silicate and the more altered Beluga corundum-bearing nepheline absent calc-silicate) were compared in order to identify possible sapphire producing reaction(s) and identify potential protoliths. The prograde assemblage of diopside + nepheline in these calc-silicate rocks likely formed at a P-T of ≤ 810 °C and 8.3 kbar and was likely altered by hydrous-NaCl-bearing fluids at a P-T of ≤ 710 °C and 6 kbar, forming a phlogopite-plagioclase symplectite rimmed by scapolite. Subsequently, either additional hydrous-fluids altered the assemblage of nepheline + scapolite (or anorthite) to form albite + muscovite + corundum, or Na-bearing hydrous fluids altered anorthite to form corundum during post D₂ thermal/fluid activity.

The Beluga and Bowhead showings are geochemically and texturally unique compared to other lithologies within the Lake Harbour Group. Comparison of the prograde mineral assemblages, whole rock geochemistry, field relations, and one oxygen isotope measurement of corundum suggest that the most likely protolith is the metamorphism and metasomatism of evaporite-black shale layers within marble that produced blue and colourless sapphire during late fluid infiltration around 1782.5 Ma.

Existing models of gem corundum genesis (Giuliani et al 2007) cannot explain the formation of sapphire at the Bowhead showing.

The unique features of the Beluga showing that make it conducive to corundum formation are the presence of Si- and Fe-depleted calc-silicate layers within marble that were subjected to late fluid infiltration which catalyzed corundum producing reactions.

Exploration strategies that have the greatest potential to be effective for expanding the extent of the Kimmirut Sapphire Occurrence are:

- 1) Identification of scapolite in coarse-grained, violet diopside-bearing calc-silicates by handheld UV lights or airborne hyperspectral surveys.
- 2) Identification of V-rich, coarse-grained, violet diopside-bearing calc-silicates
- 3) Use of ground penetration radar to determined the size and depth of sapphire-bearing calc-silicate pods.

7.3 Conclusions from Comparison of the Revelstoke Occurrence with the Beluga Showing

There are more differences than similarities between the carbonate-hosted Revelstoke (pink to red sapphire hosted in mica-feldspar layers) and Kimmirut (blue to colourless sapphire hosted in calc-silicate pods) sapphire occurrences. Both localities contain barrel shaped-corundum crystals with tapered ends (Chapter 3, LeCheminant et al. 2004) hosted in Si- and Fe-depleted siliciclastic- and evaporite-bearing lithologies which were subjected to poly-stage metamorphism (peak metamorphism up to granulite facies), intense deformation, and extensive fluid infiltration (Chapters 3 and 4).

The most striking differences between localities are: geographic location, age of deposition and metamorphism, mineral assemblages and mineral compositions, mineral textures, occurrence morphology, corundum forming reactions, prograde vs retrograde corundum crystallization, composition, colour and quality of gem corundum, whole rock composition, protolith composition, and the $\delta^{18}\text{O}$ of corundum. All of these differences indicate that the two localities had different protolith compositions and conditions of formation. Additional evidence to support this is that, even though the whole rock composition of the Beluga calc-silicate rocks contain elevated Cr and V similar to the host rocks at the Revelstoke occurrence, the corundum at the Beluga showing contains almost no Cr and V, indicating that either the Cr and V were not mobile during corundum

crystallization, or Cr and V were trapped in minerals that were not involved in the corundum producing reactions. The whole rock composition of corundum-bearing lithologies therefore may not be a good indication of the variety of corundum that can be found in the deposit.

7.4 Conclusions from Comparison of the Revelstoke Occurrence with the KSO and other Gem Corundum Deposits Around the World

The Revelstoke and Kimmirut gem corundum deposits in marble are unique compared to other world localities and as a result, existing models of formation are unable to explain these deposits. Comparison of the two study localities with other deposits indicates that the best quality rubies and sapphires from marble-hosted deposits are retrograde. The very low $\delta^{18}\text{O}$ carbonate and corundum values from the Revelstoke occurrence suggest that this method is not a reliable tool for identifying corundum from marble hosted deposits. More complete studies of ruby and sapphire occurrences in marble are needed in order to be able to accurately compare localities and define applicable exploration strategies.

7.5 Future Work

7.5.1 Revelstoke

Whole rock geochemistry (using the same element package as previous analyses) needs to be determined for pristine, non-carbonate contaminated host gneiss at varying distances from the corundum-bearing marble in order to determine a more realistic protolith composition.

Oxygen isotopes need to be determined for pristine, non-carbonate contaminated host gneiss at varying distances from the corundum-bearing marble in order to determine a more realistic protolith composition, and identify the extent of fluid infiltration. The oxygen isotopes of the marker marble in Unit 5 should also be collected to help constrain the extent fluid infiltration and provide a 'normal' value for marble in the area.

Additional P-T modeling should be completed using whole rock data for pristine, non-carbonate contaminated host gneiss in order to further constrain peak metamorphic conditions at the Frenchman Cap dome and corundum formation.

7.5.2 Kimmirut Sapphire Occurrence

Additional petrographic analysis of different rock types and mineralogic zones within the KSO is needed. Within the corundum-bearing zones, the following mineral phases will need to be identified: perthite, potassium feldspar, nepheline, and/or anorthite. Some reports have identified these phases in other corundum-bearing zones within the LHM, but they have not been observed by the author. If they are present in the Beluga rocks and are associated with corundum in some way, this information can be used to help constrain the corundum-producing reaction(s). It is also important to locate and identify any minor oxides, sulfides, titanite, zircon, and/or monazite phases in order to determine where Ti and REEs are hosted. Furthermore, mineral phases and textures within the host marble and other calc-silicate lenses, including other 'Beluga-type' calc-silicates, Bowhead-type calc-silicates, and regular calc-silicate layers within the LHM, will need to be determined in order to identify which mineralogy/geochemistry is considered 'normal' for the LHG calc-silicates, identify other areas of potential sapphire mineralization, constrain possible protoliths, and identify the type of fluid infiltration.

Additional geochemical analysis will also need to be completed on some existing and newly identified mineral phases as well as other rock types within the LHM. The V and Cr content of diopside, phlogopite, titanite, and rutile will need to be identified by EMPA in order to determine which phases contain V (V was not analyzed in previous experiments). Any newly identified phases will also need to be analyzed by EMPA in order to assist with reaction stoichiometries and P-T modeling. The whole rock geochemistry of the following rock types (using the same element program used in previous analyses for the Beluga showing) will need to be determined on the following rocks in order to help constrain the model of formation for the KSO: the Bowhead showing, the host marble of the Beluga calc-silicate units, any other calc-silicate layers/lenses within the LHM whether they are Beluga-type or not, and any igneous rocks near to the KSO.

Only one $\delta^{18}\text{O}$ analysis of corundum from the Beluga showing was determined. Additional $\delta^{18}\text{O}$ values of carbonates, silicates, and corundum within the rock types mentioned previously are needed to compile a complete dataset of values from different mineral phases and rock types in order to constrain potential protoliths and identify fluid composition and potential pathways.

No fluid inclusions were identified in corundum from the Beluga showing. It will be necessary to identify if there are any fluid inclusions in corundum from other showings, in order to determine fluid composition and P-T conditions during fluid entrapment. It will also be necessary to identify if fluid inclusions are present in diopside, scapolite, and/or nepheline in order to help constrain the prograde and retrograde fluid compositions and help identify potential protoliths.

P-T modeling using a program such as Theriak-Domino, PerpleX, or Thermocalc will need to be completed in order to identify which proposed corundum forming reactions are thermodynamically possible and to constrain the PT conditions of corundum formation. Modeling of T-X_{CO2} and P-X_{CO2} reactions will be useful to help constrain the fluid composition during corundum crystallization.

References

- Algeo, T.J. and Maynard, J.B. (2004) Trace-element behavior and redox facies in core shales of Upper Pennsylvanian Kansas-type cyclothsems. *Chemical Geology*, 206: 289–318
- Anderson, G.M. and Cermignani, C. (1991) Mineralogical and thermodynamic constraints on the metasomatic origin of the York River nepheline gneisses, Bancroft, Ontario. *Canadian Mineralogist*, 29: 965–980
- Appleyard , E.C. and Stott, G. M. (1975) Grenville gneisses in the Madawaska highlands, eastern Ontario. Geological Association of Canada, Mineralogical Association of Canada, Geological Society of America Field Trips Guidebook, Part A, 26-62
- Appleyard, E.C. and Williams, S.E. (1981) Metasomatic effects in the Faraday metagabbro, Bancroft, Ontario, Canada. *Tschermaks mineralogische und petrographische Mitteilungen*, 28: 81–97
- Bačík, P., Méres, S., Uher, P. (2011) Vanadium-bearing tourmaline in metacherts from Chvojnice, Slovak Republic: crystal chemistry and multistage evolution. *Canadian Mineralogist*, 49: 195-206
- Barker, S.L.L., Dipple, G.M., Dong, F., Baer, D.S. (2011) Use of laser spectroscopy to measure the $^{13}\text{C}/^{12}\text{C}$ and $^{18}\text{O}/^{16}\text{O}$ compositions of carbonate minerals. *Analytical Chemistry*, 83: 2220-2226
- Barnes, C.G., Prestvik, T., Sundvoll, B., and Surratt, D. (2005) Pervasive assimilation of carbonate and silicate rocks in the Hortavær igneous complex, north-central Norway. *Lithos*, 80: 179–199
- Baxter, E.F. (2010) Diffusion of Noble Gases in Minerals. *Reviews in Mineralogy and Geochemistry*, 72: 509-557
- Bedini, E. (2009): Mapping lithology of the Sarfartoq carbonatite complex, southern West Greenland, using HyMap imaging spectrometer data. *Remote Sens. Environ.* 113, 1208–1219.
- Bhattacharya, A., Mohanty, L., Maji, A., Sen, S.K., and Raith, M. (1992) Non-ideal mixing in the phlogopite-annite binary: constraints from experimental data on Mg-Fe partitioning and a reformulation of the biotite-garnet thermometer. *Contributions to Mineralogy and Petrology*, 111: 87-93

- Bol, L.C.G.M., Bos, A., Sauter, C.C., and Jansen, J.B.H. (1989) Barium-titanium-rich phlogopites in marbles from Rogaland, southwest Norway. *American Mineralogist*, 74: 439-447
- Bowman, J.R. (1998) Stable-isotope systematics of skarns. *Mineralogical Association of Canada Short Course*: 26, 99-146
- Brady, J.B. (1977) Metasomatic zones in metamorphic rocks. *Geochimica et Cosmochimica Acta*, 41: 113-125
- Breit, G.N. and Wanty, R.B. (1991) Vanadium accumulation in carbonaceous rocks: A review of geochemical controls during deposition and diagenesis. *Chemical Geology*, 91: 83-97
- Brown, P. (1989) FLINCOR: A microcomputer program for the reduction and investigation of fluid inclusion data. *American Mineralogist*, v. 74, p. 1390-1393.
- Brown, R.L. (1980) Frenchman Cap Dome, Shuswap Complex, British Columbia, *in Current Research, Part A, Geological Survey of Canada, Paper 80-1A*, 47-51
- Brown, R.L., Journeyay, J.M., Lane, L.S., Murphy, D.C., and Rees, C.J. (1986) Obduction, backfolding and piggyback thrusting in the metamorphic hinterland of the southeastern Canadian Cordillera. *Journal of Structural Geology*, 8: 225-268
- Brumsack, H.-J. (2006) The trace metal content of recent organic carbon-rich sediments: Implications for Cretaceous black shale formation. *Palaeogeography, Palaeoclimatology, Palaeoecology*, 232: 344-361
- Butler, J.P. (2007) Petrogenesis of nepheline- and scapolite-bearing metacarbonates from southwestern Baffin Island, Nunavut, Canada. B.Sc. thesis, Dalhousie University, Halifax, Nova Scotia.
- Cade, A.M., Dipple, G.M., and Groat, L.A. (2005) Geochemical study of the Kimmirut sapphire occurrence, Baffin Island, Canada. *Geochimica et Cosmochimica Acta*, 69: pp.279
- Canet, C., Alfonso, P., Melgarejo, J-C., and Jorge, S. (2003) V-rich minerals in contact-metamorphosed silurian SEDEX deposits in the Poblet area, southwestern Catalonia, Spain. *Canadian Mineralogist*, 41: 561-579
- Carlson, H.D. (1957) Origin of the corundum deposits of Renfrew County, Ontario, Canada. *Bulletin of the Geological Society of America*, 68: 1605-1636

- Cempírek, J., Houzar, S., and Novák, M. (2008) Complexly zoned niobian titanite from hedenbergite skarn at Písek, Czech Republic, constrained by substitutions Al(Nb, Ta)Ti₂, Al(F, OH)(TiO)₁ and SnTi₁. *Mineralogical Magazine*, 76, 1293-1305.
- Clark, R. N. (1999): Chapter 1: Spectroscopy of Rocks and Minerals, and Principles of Spectroscopy, *in* Manual of Remote Sensing, Volume 3, Remote Sensing for the Earth Sciences, (A.N. Rencz, ed.) John Wiley and Sons, New York, 3-58.
- Crowley, J.L. (1999) U-Pb geochronologic constraints on Paleoproterozoic tectonism in the Monashee complex, Canadian Cordillera: Elucidating an overprint geologic history. *GSA Bulletin*, 111: 560-577
- Crowley, J.L. and Parrish, R.R. (1999) U-Pb isotopic constraints on diachronous metamorphism in the northern Monashee complex, southern Canadian Cordillera. *Journal of Metamorphic Petrology*, 17: 483-502
- Crowley, J.L. Brown, R.L., and Parrish, R.R. (2001) Diachronous deformation and a strain gradient beneath the Selkirk allochthon, northern Monashee complex, southeaster Canadian Cordillera. *Journal of Structural Geology*, 23: 1103-1121
- Davison, W .L. (1959) Geology, Lake Harbour, Baffin Island, District of Franklin, Northwest Territories. Geological Survey of Canada, Map 29- 1958, scale 1:63 360
- Davison, W .L. (2005) Assessment Report for True North Gems Inc.
- Davison, W .L. (2006) Assessment Report for True North Gems Inc.
- De Capitani, C., and Petrakakis, K. (2010) The computation of equilibrium assemblage diagrams with Theriak/Domino software. *American Mineralogist*, 95, 1006–1016.
- Deer, W.A., Howie, R.A., and Zussman, J. (2001) Framework silicates: Feldspars. Volume 4A Second Edition. The Geological Society of London, p.972
- Doležalová, H., Houzar, S., Losos, Z, and Škoda, R. (2006) Kinoshitalite with a high magnesium content in sulphide-rich marbles from the Rožná uranium deposit, Western Moravia, Czech Republic. *Neues Jahrbuch für Mineralogie Abhandlungen*. 182: 165-171
- Dufour, M.S., Kol'tsov, A.B., Zolotarev, A.A., Kuznetsov, A.B. (2007) Corundum-bearing metasomatic rocks in the central Pamirs. *Petrology*, 15: 151-167
- Durstling, H. (2005) New Discovery: Rubies in Nova Scotia. *Canadian Gemmologist*, 26: 93-94

- Ellis, D.E. (1978) Stability and phase equilibria of chloride and carbonate bearing scapolites at 750°C and 4000 bar. *Geochimica et Cosmochimica Acta*, 42: 1271-1281
- Fagan, A.F. 2010 Assessment Report for True North Gems Inc.
- Fagan, A.F and Miller, E. (2012) Assessment Report describing prospecting, mapping, geochemical and water sampling at the beluga Sapphire Project, Nunavut; Confidential Report for True North Gems Inc.
- Feenstra, A. and Wunder, B (2002) Dehydration of diasporite to corundite in nature and experiment. *Geology*, 30: 119-122
- Francke, J. and Utsi, V. (2009) Advances in long-range GPR systems and their applications to mineral exploration, geotechnical and static correction problems. *Mining Geoscience*, 27: 85-93
- Fritsch, E. and Rossman, G.R. (1988) An update on color in gems. Part II. Colors caused by charge transfers and color centers. *Gems and Gemology*, 24: 3-15
- Garnier, V., Giuliani, G., Ohnenstetter, D., Fallick, A.E., Dubessy, J., Banks, D., Vinh, H.Q., Lhomme, T., Maluski, H., Pêcher, A., Bakhsh, KA, Van Long, P., Trong Trinh, P., Schwarz, D. (2008) Marble-hosted ruby deposits from Central and Southeast Asia: Towards a new genetic model. *Ore Geology Reviews*, 34: 169-191
- Gertzbein, P.J. (2004) The Coloured Gem Potential of Baffin Island and Nunavut. *Canadian Gemmologist*, 25: 10-17
- Gertzbein, P.J. (2005) Geology surrounding the Beluga sapphire occurrence, Kimmirut, Nunavut: A preliminary examination. *Canadian Gemmologist*, 26: 50–57
- Gervais, F. and Brown, R.L. (2011) Testing modes of exhumation in collisional orogens: synconvergent channel flow in the southeastern Canadian Cordillera. *Lithosphere*, 3: 55-75
- Gervais, F., Brown, R.L., Crowley, J.L. (2010) Tectonic implications for a Cordilleran orogenic base in the Frenchman Cap dome, southeastern Canadian Cordillera. *Journal of Structural Geology*, 32: 941-959
- Ghent, E.D., and O'Neil, J.R. (1985) Late Precambrian marbles of unusual carbon-isotope composition, southeastern British Columbia. *Canadian Journal of Earth Sciences*, 22: 324-329

- Gittins, J. (1961) Nephelinization in the Haliburton-Bancroft, Ontario, Canada. *Journal of Geology*, 69: 291-308
- Giuliani, G., Dubessy, J., Banks, D., Hoang Quang, V., Lhomme, T., Pironon, J., Garnier, V., Phan Trong, T., Pham Van, L. Ohnenstetter, D., Schwarz, D. (2003) $\text{CO}_2\text{-H}_2\text{S-COS-S}_8$ AlO-(OH)-bearing fluid inclusions in ruby from marble-hosted deposits in Luc Yen area, North Vietnam. *Chemical Geology*, 194: 167-185
- Giuliani, G., Fallick, A.E., Garnier, V., France-Lanord, C., Ohnenstetter, D., and Schwarz, D. (2005) Oxygen isotope composition as a tracer for the origins of rubies and sapphires. *Geology*, 33: 249–252
- Giuliani, G., Ohnenstetter, D., Garnier, V., Fallick, A.E., Rakotondrazafy, M., and Schwarz, D. (2007) Chapter 2: The geology and genesis of gem corundum deposits. *Mineralogical Association of Canada Short Course* 37, 23–78
- Grapes, R. and Palmer, K. (1996) (Ruby-sapphire)-chromian mica-tourmaline rocks from Westland, New Zealand. *Journal of Petrology*, 37: 293-315
- Groat, L.A. and Laurs, B.M. (2009) Gem formation, production, and exploration: why gem deposits are rare and what is being done to find them. *Elements*, 5: 153-158
- Gummer, W.K. and Burr, S.V. (1946) Nephelinized paragneisses in the Bancroft area, Ontario. *Journal of Geology*, 54: 137-168
- Hansen, M. (2008) A comparison of sapphire-bearing and non-sapphire bearing lenses from the Lake Harbour Group, southeastern Baffin Island. B.Sc. thesis, Carleton University
- Harlov, D., Tropper, P., Seifert, W., Nijland, T., and Förster, H-J. (2006) Formation of Al-rich titanite ($\text{CaTiSiO}_4\text{O-CaAlSiO}_4\text{OH}$) reaction rims on ilmenite in metamorphic rocks as a function of $f\text{H}_2\text{O}$ and $f\text{O}_2$. *Lithos*, 898: 72-84
- Harlow, G.E. and Pamukcu, A., Naung, U., Thu, U.K. (2006) Mineral Assemblages and the Origin of Ruby in the Mogok Stone Tract, Myanmar. *Gems and Gemology*, 42: 147
- Harris, J.R., McGregor, R., Budkevitsch, P. (2010) Geological analysis of hyperspectral data over southwest Baffin Island: methods for producing spectral maps that relate to variations in surface lithologies. *Canadian Journal of Remote Sensing*, 36: 412-435
- Hellingwer, R.H. (1985) A contact-metamorphic occurrence of the assemblage nepheline-scapolite-diopside in a metabasic flow breccia from Bergslagen, Sweden. *Mineralogical Magazine*, 49: 606-610

- Henry, D.J., Guidotti, C.V., and Thomson, J.A. (2005) The Ti-saturation surface for low-to-medium pressure metapelitic biotites: Implications for geothermometry and Ti-substitution mechanisms. *American Mineralogist*, 90: 316–328
- Herd, C.D., Peterson, R.C., and Rossman, G.R. (2000) Violet-colored diopside from southern Baffin Island, Nunavut, Canada. *Canadian Mineralogist*, 38: 1193–1199
- Hinchey, A.M., Carr, S.D., McNeill, P.D., Rayner, N. (2006) Paleocene-Eocene high-grade metamorphism, anatexis, and deformation in the Thor-Odin dome, Monashee complex, southeastern British Columbia. *Canadian Journal of Earth Science*, 43: 1341-1365
- Hoefs, J. (2004) Stable isotope geochemistry. 5th edition Springer p. 244
- Hogarth, D.D., (1971) Lapis Lazuli near Lake Harbour, Southern Baffin Island, Canada. *Canadian Journal of Earth Sciences*, 8: 1210–1217
- Hogarth, D.D., and Griffin, W.L. (1978) Lapis lazuli from Baffin Island — a Precambrian meta-evaporite. *Lithos*, 11: 37–60
- Holland, T.J.B., Powell, R., 1998. An internally consistent thermodynamic data set of petrological interest. *Journal of Metamorphic Geology* 16, 309–343
- Holk, G.J. and Taylor, H.P. (2000) Water as a Petrologic Catalyst Driving $^{18}\text{O}/^{16}\text{O}$ Homogenization and Anatexis of the Middle Crust in the Metamorphic Core Complexes of British Columbia. *International Geology Review*, 42: 97-130
- Houzar, S., and Cempírek, J. (2011): Akcesorický schreyerit ve vanadem bohatém grafitickém kvarcitu z Bílovánek (moldanubikum, západní Morava). – *Acta Mus. Moraviae, Sci. geol.*, 96, 2, 35–43. (in Czech)
- Höy, T. (1987) Geology of the Cottonbelt lead-zinc-magnetite layer, carbonatites and alkalic rocks in the Mount Grace area, Frenchman Cap Dome, southeastern British Columbia. *Bulletin - Ministry of Energy, Mines and Petroleum Resources*, vol.80, 99 pp.
- Höy, T. (2001) Sedex and Broken Hill-type deposits, northern Monashee mountains, southern British Columbia. *British Columbia Geological Survey, Geological Fieldwork 2000, Paper 2001-1*: 85-114
- Hudon, P., Friedman, R.M., Gauthier, G., and Martignole, J. (2006) Age of the Cabonga nepheline syenite, Grenville Province, western Quebec. *Canadian Journal of Earth Sciences*, 43: 1237–1249

- Jackson, G.D. and Taylor, F.C. (1972) Correlation of major Aphebian rock units in the northeastern Canadian Shield. *Canadian Journal of Earth Sciences*, 9: 1650 - 1669
- Joesten, R. (1977) Evolution of mineral assemblage zoning in diffusion metasomatism. *Geochimica et Cosmochimica Acta*, 41: 649-670
- Johnson, B.J. (2006) Extensional shear zones, granitic melts, and linkage of overstepping normal faults bounding the Shuswap metamorphic core complex, British Columbia. *Geological Society of America Bulletin*, 118: 366-382
- Journeay, J.M. (1986) Stratigraphy, internal strain and thermo-tectonic evolution of northern Frenchman Cap Dome; an exhumed duplex structure, Omineca Hinterland, S. E. Canadian Cordillera. Ph.D. thesis, Queen's University, Kingston, Ontario
- Key, R.M. and Ochieng, J.O. (1991). Ruby and garnet gemstone deposits in southeast Kenya: their genesis and recommendations for exploration. In: *African Mining* 91, Harare, June 10-12, 1991, Elsevier Science Publishers, Barking, Essex, p. 121-127.
- Kievlenko, E.Y. (2003) Geology of Gems. Ocean Pictures Ltd, Littleton, CO, USA
- Kissin, A.J. (1994) Ruby and sapphire from the southern Ural Mountains, Russia. *Gems and Gemology*, 30: 243-252
- Krogh, E.J. (1988) The garnet-clinopyroxene Fe-Mg geothermometer – a reinterpretation of existing experimental data. *Contributions to Mineralogy and Petrology*, 99, 44–48.
- Kullerud, K. and Erambert, M. (1999) Cl-scapolite, Cl-amphibole, and plagioclase equilibria in ductile shear zones at Nusfjord, Lofoten, Norway: Implications for fluid compositional evolution during fluid-mineral interaction in the deep crust. *Geochimica et Cosmochimica Acta*, 63: 3829-3844
- Lane, L.S. (1984) Brittle deformation in the Columbia River fault zone near Revelstoke, southeastern British Columbia. *Canadian Journal of Earth Sciences*, 21: 584-598
- LeCheminant, A.N., Groat, L.A., Dipple, G.M., Mortensen, J.K., Gertzbein, P.J., Rohtert, W., and Quinn, E.P. (2004) Sapphire from Baffin Island, Canada. *Gems and Gemology*, 40: 344-345
- LeCheminant, A.N., Groat, L.A., Mortensen, J.K., Gertzbein, P., Rohtert, W. (2005) Sapphires from Kimmirut, Baffin Island, Nunavut, Canada. *Geochimica et Cosmochimica Acta*, 69: A280

- Lee, C.H. and Lee, H.K. (2003) Vanadium- and barium-bearing green mica within coaly metapelite from the Ogcheon Supergroup, Republic of Korea. *Journal of Asian Earth Sciences*, 21: 343-351
- Lepage, L. (2007) Exploration advances with ultraviolet LED technology - Beluga sapphire, Nunavut. abstract, Geological Association of Canada-Mineralogical Association Canada Annual Meeting 2007.
- Lev, S.M., McLennan, S.M., and Hanson, G.N. (1999) Mineralogic controls on REE mobility during black-shale diagenesis. *Journal of Sedimentary Research*, 69: 1071-1082
- Limtrakun, P., Zaw, K., Ryan, C.G., Mernagh, T.P. (2001) Formation of the Denchai gem sapphires, northern Thailand: evidence from mineral chemistry and fluid/melt inclusion characteristics. *Mineralogical Magazine*, 65: 725-735
- Ludwig, K.R. (2003) Isoplot 3.09: A Geochronological Toolkit for Microsoft Excel. Berkeley Geochronology Center, Special Publication No. 4
- Markl, G. and Piazolo, S. (1998) Halogen-bearing minerals in syenites and high-grade marbles of Dronning Maud Land, Antarctica: monitors of fluid compositional changes during late-magmatic fluid-rock interaction processes. *Contributions to Mineralogy and Petrology*, 132: 246-268
- Markl, G. and Piazolo, S. (1999) Stability of high-Al titanite from low-pressure calcsilicates in light of fluid and host-rock composition. *American Mineralogist*, 84, 37-47.
- Meinert L.D. (1992): Skarns and skarn deposits. *Geoscience Canada* 19, 145-162.
- Miller, R. (1985) Age and Petrological Relationships of Some Igneous-Textured and Gneissic Alkaline Rocks in the Haliburton - Bancroft Area. Ph.D. thesis, Univ. Toronto, Toronto, Ontario
- Moine, B., Sauvan,P., Jarousse, J. (1981) Geochemistry of evaporite-bearing series: a tentative guide for the identification of metaevaporites. *Contributions to Mineralogy and Petrology*, 76: 401-412
- Mora, C.I. and Valley, J.W. (1989) Halogen-rich scapolite and biotite: implication for metamorphic fluid rock interaction. *American Mineralogist*, 74: 721-737
- Moyd, L., (1949) Petrology of the nepheline and corundum rocks of southeastern Ontario. *American Mineralogist*, 34: 736-751

- Muhlmeister, S., Fritsch, E., Devouard, B., Laurs, B.M. (1998) Separating natural and synthetic rubies on the basis of trace - element chemistry. *Gems & Gemology*, 34: 80-101
- Norlander, B.H., Whitney, D.L., Teyssier, C., Vanderhaeghe, O. (2002) Partial melting and decompression of the Thor-Odin dome, Shuswap metamorphic complex, Canadian Cordillera. *Lithos*, 61: 103-125
- Okrush, M., Bunch, T.E., Bank, H. (1976) Paragenesis and petrogenesis of a corundum-bearing marble at Hunza (Kashmir). *Mineralium Deposita* (Berlin), 11: 278-297
- Pan, Y. and Fleet, M.E. (1991) Barian feldspar and barian-chromian muscovite from the Hemlo area, ON. *Canadian Mineralogist*, 29: 481-498
- Pan, Y., Fleet, M.E., and Ray, G.E. (1994) Scapolite in two Canadian gold deposits: Nickel Plate, British Columbia and Hemlo, Ontario. *Canadian Mineralogist*, 32: 825-837
- Passchier, C.C.W., and Trouw, R.A.R.A.J. (2005) *Microtectonics*. Springer-Verlag Berlin Heidelberg.
- Pouchou, J.L. and Pichoir, F. (1985) PAP $\phi(pZ)$ procedure for improved quantitative microanalysis. *Microbeam Analysis*, 1985, 104–106
- Piazolo, S. and Markl, G. (1999) Humite- and scapolite-bearing assemblages in marbles and calcsilicates of Dronning Maud Land, Antarctica: new data for Gondwana reconstructions. *Journal of Metamorphic Petrology*, 17: 91-107
- Rakotondrazafy, A.F.M., Giuliani, G., Ohnenstetter, D., Fallick, A.E., Rakotosamizanany, S., Andriamamonjy, A., Ralantsoarison, T., Razanatseheno, M., Offant, Y., Garnier, V., Maluski, H., Dunaigre, C., Schwarz, D. and Ratrimo, V. (2008) Gem corundum deposits of Madagascar: A Review. *Ore Geology Reviews*: 34: 134-154
- Read, P.B. and Brown, R.L. (1981) Columbia River Fault Zone: Southeastern Margin of the Shuswap and Monashee Complexes, Southeastern British Columbia. *Canadian Journal of Earth Sciences*, 18: 1127-1145
- Rebbert, C.R. and Rice, J.M. (1997) Scapolite-plagioclase exchange: $\text{Cl}-\text{CO}_3$ scapolite solution chemistry and implications for peristerite plagioclase. *Geochimica et Cosmochimica Acta*, 61: 555-567

- Renne, P.R., C.Swisher, C.C., III, Deino, A.L., Karner, D.B., Owens, T. and DePaolo, D.J. (1998) Intercalibration of standards, absolute ages and uncertainties in $^{40}\text{Ar}/^{39}\text{Ar}$ dating. *Chemical Geology*, 145(1-2): 117-152.
- Rogge, D.M., Rivard, B., Harris, J., and Zhang, J. 2009, Application of hyperspectral data for remote predictive mapping, Baffin Island, Canada, In *Remote Sensing and Spectral Geology*, Eds. R. Bedell, A.P. Crosta, and E. Grunsky, *Reviews In Economic Geology*, Vol. 16, pp. 209-222.
- Rohtert, (2005) Assessment Report for True North Gems Inc.
- Rohtert and Pemberton (2004) Assessment Report for True North Gems Inc.
- Rossovskii, L.N., Konovalenko, S.I., and Ananjev, S.A. (1982) Conditions of ruby formation in marbles. *Geologiya Rudnyh Mestorozhdeniy* 24: 57-66 (in Russian)
- Rubatto D., Müntener O., Barnhoorn A., Gregory C. (2008): Dissolution-reprecipitation of zircon at low-temperature, high-pressure conditions (Lanzo Massif, Italy). *American Mineralogist*, 93: 1519-1529.
- Sanborn, N.M. (1996) Constraints on the timing and conditions of Cordilleran tectonism in Frenchman Cap dome, Monashee complex, southeast British Columbia, from $^{40}\text{Ar}/^{39}\text{Ar}$ geochronology. Unpublished BSc Thesis, Queens University, Kingston, Ontario, Canada
- Scott, D.J., and Gauthier, G. (1996) Comparison of TIMS (U-Pb) and laser ablation microprobe ICP-MS (Pb) techniques for age determination of detrital zircons from Paleoproterozoic metasedimentary rocks from northeastern Laurentia, Canada, with tectonic implications. *Chemical Geology*, 131: 127–142
- Scott, D.J., and Godin, L. (1995) Preliminary geological investigation of the Lake Harbour Group and surrounding gneissic rocks near Lake Harbour and Markham Bay, southern Baffin Island, NWT. Geological Survey of Canada, Paper 1995-1C, 67-76
- Scott, D.J. (1997) Geology, U-Pb, and Pb-Pb geochronology of the Lake Harbour area, southern Baffin Island: Implications for the Paleoproterozoic tectonic evolution of northeastern Laurentia. *Canadian Journal of Earth Sciences*, 34: 140–155
- Scott, D.J., Stern, R.A., St-Onge, M.R., and McMullen, S.M. (2002) U-Pb geochronology of detrital zircons in metasedimentary rocks from southern Baffin Island: implications for

- the Paleoproterozoic tectonic evolution of Northeastern Laurentia. Canadian Journal of Earth Sciences, 39: 611–623
- Scott, D. J., and Wodicka, N. (1998) A second report on the U-Pb geochronology of southern Baffin Island. Geological Survey of Canada, Paper 1998-F: 47-57
- Seward, T.M. (1974) Determination of the first ionization constant of silicic acid from quartz solubility in borate buffer solutions to 350°C. Geochimica et Cosmochimica Acta, 38: 1651-1664
- Shannon, R.D. (1976) Revised effective ionic radii and systematic studies of interatomic distances in halides and chalcogenides. Acta Crystallographica, A32: 751-767
- Silva, K.K.M. and Siriwardena, C.H.E.R. (1988) Geology and the origin of corundum-bearing skarn at Bakamuna, Sri Lanka. Mineralium Deposita, 23: 186-190
- Simonet, C., Fritsch, E., and Lasnier, B. (2008) A classification of gem corundum deposits aimed towards gem exploration. Ore Geology Reviews, 34: 127-133
- Simonet, C. and Okundi, S. (2003). Prospecting methods for coloured gemstone deposits in Kenya. African Journal of Science and Technology 4, 44-55.
- Shor, R. and Weldon, R. (2009) Ruby and Sapphire Production and Distribution: A Quarter Century of Change. Gems and Gemology, 45: 236-259
- Spear, F.S. (1995) Metamorphic phase equilibria and pressure-temperature-time paths. Mineralogical Society of America, p.799
- Spear, F.S. and Cheney, J.T. (1989) A petrogenetic grid for pelitic schists in the system SiO₂-Al₂O₃-FeO-MgO-K₂O-H₂O. Contributions to Mineralogy and Petrology, 101: 149-164
- Spiridonov, E.M. (1998) Gemstone deposits of the former Soviet Union. Journal of Gemmology, 26: 111-124
- Snetsinger, K.G. (1966) Barium-vanadium muscovite and vanadium tourmaline from Mariposa County, California. American Mineralogist, 51: 1623-1639
- St-Onge, M.R., Scott, D.J., Wodicka, N., and Lucas, S.B. (1998) Geology of the McKellar Bay-Wight Inlet-Frobisher bay area, southern Baffin Island, Northwest Territories, Geological Survey of Canada, Paper 1998-C: 43-53
- St-Onge, M. R., Lucas, S. B., Scott, D. J. and Wodicka, N. (1999) Upper and lower plate juxtaposition, deformation and metamorphism during crustal convergence, Trans-Hudson Orogen (Quebec-Baffin segment), Canada. Precambrian Research, 93: 27-49

- St-Onge, M.R., Hanmer, S., and Scott, D.J. (1996): Geology of the Meta Incognita Peninsula, south Baffin Island, Northwest Territories: tectonostratigraphic units and regional correlations. Geological Survey of Canada, Paper 1996-C, 63-72.
- St-Onge, M. R., Wodicka, N. & Lucas, S. B. (2000). Granulite- and amphibolite-facies metamorphism in a convergent-plate margin setting: synthesis of the Quebec-Baffin segment of the Trans-Hudson Orogen. Canadian Mineralogist 38, 379-398.
- St-Onge, M.R., Wodicka, N., and Ijewliw, O. (2007) Polymetamorphic Evolution of the Trans-Hudson Orogen, Baffin Island, Canada: Integration of Petrological, Structural and Geochronological Data. Journal of Petrology, 48: 271–302
- Sun, S.-s. and McDonough, W.F. (1989) Chemical and isotopic systematics of oceanic basalts: implications for mantle composition and processes. Geological Society, London, Special Publications, 42: 313-345
- Tait, K.T., Hawthorne, F.C., and Ventura, G.D. (2001) Al–Mg disorder in a gem-quality pargasite from Baffin Island, Nunavut, Canada. Canadian Mineralogist, 39: 1725–1732
- Takayuki, S., Sasaki, M., Fujimoto, K., Takeno, N., Tsukamoto, H., Sanada, K., and Maeda, S. (2001) Corundum and zincian spinel from the Kakkonda geothermal system, Iwate Prefecture, northeastern Japan. Journal of Mineralogical and Petrological Sciences, 96: 137-147
- Terekhov, E.N., Kruglov, V.A., and Levitski, V.I. (1999) Rare earth elements in corundum-bearing metasomatic and related rocks of the Eastern Pamirs. Geochimica International, 37: 202-212
- Teyssier, C., Ferré, E., Whitney, D.L., Norlander, B., Vanderhaeghe, O., and Parkinson, D. (2005) Flow of partially molten crust and origin of detachments during collapse of the Cordilleran orogen. In High-strain zones: structure and physical properties. Edited by D. Bruhn and L. Burlini. Geological Society Special Publication (London), No. 245, pp. 39-64
- Thériault, R., St-Onge, M., and Scott, D. (2001) Nd isotopic and geochemical signature of the Paleoproterozoic Trans-Hudson Orogen, southern Baffin Island, Canada: implications for the evolution of eastern Laurentia. Precambrian Research, 108: 113–138

- Treloar, P.J. (1987) The Cr-minerals of Outokumpu - their chemistry and significance. *Journal of Petrology*, 28: 867-886
- Tropper, P., Manning, C.E., Essene, E.J. (2002) The substitution of Al and F in titanite at high pressure and temperature: experimental constraints on phase relations and solid solution properties. *Journal of Petrology*, 43: 1787-1814
- True North Gems (2003) True North Gems acquires Baffin Island sapphire discovery. Press Release
- Uher, P., Kováčik, M., Kubiš, M., Shtukenberg, A., Ozdín, D. (2008) Metamorphic vanadian-chromian silicate mineralization in carbon-rich amphibole schists from the Malé Karpaty Mountains, Western Carpathians, Slovakia. *American Mineralogist*, 93: 63-73
- Uvarova, Y.A., Kyser, T.K., Sokolova, E., Kazansky, V.I., Lobanov, K.V. (2011) Significance of stable isotope variations in crustal rocks from the Kola Superdeep Borehole and their surface analogues. *Precambrian Research*, 189: 104-113
- Valley, J.W. (1986) Stable isotope geochemistry of metamorphic rocks. *Reviews in Mineralogy and Geochemistry*. 16: 445-489
- Vanden Kerkhof, A., and Thiéry, R. (2001) Carbonic inclusions. *Lithos*, 55: 49-68
- Vanko, D.A., and Bishop, F.C. (1982) Occurrence and origin of marialitic scapolite in the Humboldt Lopolith, N.W. Nevada. *Contributions to Mineralogy and Petrology*, 81: 277-289
- Walker, T. L. (1915) Minerals from Baffin Land. *Ottawa Naturalist*, 29:63–66
- Walker, R.T. (2012) Project report: Blu Starr Property, British Columbia, Canada. p.105
- Walther, J.V. and Woodland, A.B. (1993) Experimental determination and interpretation of the solubility of the assemblage microcline, muscovite, and quartz in supercritical H₂O. *Geochimica et Cosmochimica Acta*, 57: 2431-2437
- White, R.W., Powell, R., Holland, T.J.B., (2001) Calculation of partial melting equilibria in the system Na₂O–CaO–K₂O–FeO–MgO–Al₂O₃–SiO₂–H₂O (NCKFMASH). *Journal of Metamorphic Geology* 19, 139–153
- Whitney, D.L., and Evans, B.W. (2010) Abbreviations for names of rock-forming minerals. *American Mineralogist*, 95: 185-187

- Wight, W. (1986) Canadian gems in the national museum of Canada. *Canadian Gemmologist*, 7: 34–45, 50–55.
- Wight, W. (1999) Explosion of new interest in Canadian gemstones. *Canadian Gemmologist*, 20: 45-53
- Wight, W. (2004) Sapphire from Ontario. *Canadian Gemmologist*, 25: 30-32
- Wilson, B. (2010) Colored gemstones from Canada. *Rocks and Minerals*, 85: 24-43
- Wilson, B.S. (2007) Chapter 10: Colored gemstones from Canada. *Mineralogical Association of Canada Short Course*. 37, 255-270.
- Wilson, B.S. (2009) Colored Gemstones from Canada. *Rocks & Minerals*, 85, 24–43
- Wodicka, N. and Scott, D. J. (1997) A preliminary report on the U-Pb geochronology of the Meta Incognita Peninsula, southern Baffin Island, Northwest Territories. *Geological Survey of Canada Paper* 1997-C: 167-178

Appendices

Appendix A Compositional Data for the Revelstoke Occurrence

Appendix A.1: Representative compositions of corundum from the Revelstoke Occurrence

pos. and min. assoc.	cor sur by muscovite			altered cor to mica			altered cor within phl			altered cor by ms							
	c	m	r ms	c	m	c	c	c	c	m	r ms	c	m	r	r	c	r
EPMA point	G10-01-02-1	G10-01-02-2	G10-01-02-3	G10-01-10-1	G10-01-10-2	G11-02-09-1	G11-02-09-3	G11-02-09-4	G11-02-01-1	G11-02-01-2	G11-02-01-3	TD-G007-07-7-1	TD-G007-07-7-2	TD-G007-07-7-3	TD-G007-07-4-4	TD-G007-07-4-5	TD-G007-07-4-6
TiO ₂ wt.%	0.09	0.03	0.05	0.13	0.15	0.02	0.08	0.10	0.04	0.04	0.12	0.02	0.00	0.06	0.01	0.00	0.04
Al ₂ O ₃	99.68	99.83	99.82	99.77	99.70	99.47	99.73	99.92	99.74	99.83	99.77	100.50	100.80	97.81	100.50	100.30	100.20
Cr ₂ O ₃	0.21	0.13	0.15	0.02	0.05	0.15	0.09	0.06	0.05	0.05	0.06	0.04	0.08	0.06	0.03	0.05	0.05
V ₂ O ₃	0.01	0.02	0.02	0.02	0.01	0.01	0.02	0.02	0.02	0.01	0.01	0.00	0.00	0.01	0.01	0.00	0.00
MgO	0.00	0.00	0.00	0.01	0.01	0.01	0.01	0.01	0.01	0.01	0.01	0.00	0.00	0.01	0.00	0.00	0.00
MnO	0.00	0.00	0.01	0.00	0.00	0.00	0.00	0.00	0.00	0.00	0.00	0.00	0.01	0.00	0.00	0.00	0.01
FeO	0.04	0.03	0.04	0.01	0.01	0.04	0.05	0.04	0.02	0.03	0.03	0.02	0.01	0.04	0.02	0.01	0.01
TOTAL	100.03	100.04	100.09	99.96	99.93	99.70	99.98	100.15	99.88	99.97	100.00	100.58	100.90	97.99	100.57	100.36	100.31
Ti ⁴⁺ apfu	0.001	0.000	0.001	0.002	0.002	0.000	0.001	0.001	0.001	0.001	0.002	0.000	0.000	0.001	0.000	0.000	0.001
Al ³⁺	1.995	1.997	1.996	1.997	1.996	1.997	1.997	1.997	1.998	1.998	1.997	1.999	1.999	1.997	1.999	1.999	1.998
Cr ³⁺	0.003	0.002	0.002	0.000	0.001	0.002	0.001	0.001	0.001	0.001	0.001	0.001	0.001	0.001	0.000	0.001	0.001
V ³⁺	0.000	0.000	0.000	0.000	0.000	0.000	0.000	0.000	0.000	0.000	0.000	0.000	0.000	0.000	0.000	0.000	0.000
Mg ²⁺	0.000	0.000	0.000	0.000	0.000	0.000	0.000	0.000	0.000	0.000	0.000	0.000	0.000	0.000	0.000	0.000	0.000
Mn ²⁺	0.000	0.000	0.000	0.000	0.000	0.000	0.000	0.000	0.000	0.000	0.000	0.000	0.000	0.000	0.000	0.000	0.000
Fe ²⁺	0.001	0.000	0.001	0.000	0.000	0.001	0.001	0.001	0.000	0.000	0.000	0.000	0.000	0.001	0.000	0.000	0.000

NOTE: The following standards, X-ray lines and crystals were used for the EMP analyses: corundum, AlKa, TAP; diopside, MgKa, TAP; rutile, TiKa, PET; V element, VKa, PET; synthetic magnesiochromite, CrKa, LIF; synthetic rhodonite, MnKa, LIF; synthetic fayalite, FeKa, LIF. Compositions were recalculated on the basis of 3 O apfu.
c = core, m = middle, r = rim

Appendix A.1: Representative compositions of corundum from the Revelstoke Occurrence (con't)

pos. and min. assoc.							altered cor within an			cor within ms zone; altered at edges to ms and kfs					
	c	m	r cal	c	m	r	c	m	r	c	m	m	r	m	r
EPMA point	TD-G014-07A1-12-1	TD-G014-07A1-12-2	TD-G014-07A1-12-3	TD-G014-07A1-12-4	TD-G014-07A1-12-5	TD-G014-07A1-12-6	TD-G014-07-A2-5-1	TD-G014-07-A2-5-2	TD-G014-07-A2-5-3	TD-G014-07-A2-4	TD-G014-07-A2-5	TD-G014-07-A2-6	TD-G014-07-A2-7	TD-G014-07-A2-8	TD-G014-07-A2-9
TiO ₂ wt.%	0.14	0.12	0.06	0.17	0.02	0.03	0.15	0.11	0.20	0.02	0.25	0.03	0.21	0.16	0.22
Al ₂ O ₃	99.80	99.61	99.63	99.94	99.91	100.10	99.55	98.92	98.79	98.68	98.73	99.27	99.22	98.40	99.27
Cr ₂ O ₃	0.13	0.08	0.05	0.04	0.01	0.05	0.07	0.08	0.09	0.07	0.11	0.06	0.09	0.05	0.07
V ₂ O ₃	0.03	0.01	0.02	0.01	0.01	0.00	0.02	0.01	0.01	0.02	0.03	0.01	0.02	0.03	0.02
MgO	0.01	0.01	0.00	0.01	0.00	0.00	0.01	0.01	0.01	0.00	0.01	0.00	0.00	0.01	0.01
MnO	0.00	0.00	0.00	0.00	0.00	0.00	0.00	0.00	0.01	0.00	0.00	0.00	0.00	0.00	0.00
FeO	0.04	0.03	0.04	0.03	0.04	0.04	0.03	0.02	0.03	0.03	0.04	0.01	0.03	0.05	0.03
TOTAL	100.15	99.86	99.80	100.20	99.99	100.22	99.83	99.15	99.14	98.82	99.17	99.38	99.57	98.70	99.62
Ti ⁴⁺ apfu	0.002	0.002	0.001	0.002	0.000	0.000	0.002	0.001	0.003	0.000	0.003	0.000	0.003	0.002	0.003
Al ³⁺	1.995	1.996	1.998	1.996	1.999	1.998	1.996	1.997	1.995	1.998	1.993	1.998	1.995	1.995	1.995
Cr ³⁺	0.002	0.001	0.001	0.001	0.000	0.001	0.001	0.001	0.001	0.001	0.001	0.001	0.001	0.001	0.001
V ³⁺	0.000	0.000	0.000	0.000	0.000	0.000	0.000	0.000	0.000	0.000	0.000	0.000	0.000	0.000	0.000
Mg ²⁺	0.000	0.000	0.000	0.000	0.000	0.000	0.000	0.000	0.000	0.000	0.000	0.000	0.000	0.000	0.000
Mn ²⁺	0.000	0.000	0.000	0.000	0.000	0.000	0.000	0.000	0.000	0.000	0.000	0.000	0.000	0.000	0.000
Fe ²⁺	0.001	0.000	0.001	0.000	0.001	0.001	0.000	0.000	0.000	0.000	0.001	0.000	0.001	0.000	0.000

Appendix A.1: Representative compositions of corundum from the Revelstoke Occurrence (con't)

pos. and min. assoc.	pink cor grain with blue zones; also contains flincks										granular agg						
	blue					blue					r cal	c	r cal	c	m	r scp	c
EPMA point	TD-G014-07-B1-1	TD-G014-07-B1-2	TD-G014-07-B1-3	TD-G014-07-B1-4	TD-G014-07-B1-5	TD-G014-07-B1-6	TD-G014-07-B1-7	TD-G014-07-B1-8	TD-G014-07-B1-9	TD-G063b-09-19-1	TD-G063b-09-19-2	TD-G063b-09-19-3	TD-G063b-09-5-4	TD-G063b-09-5-5	TD-G063b-09-5-6	TD-G063b-09-23-7	TD-G063b-09-23-8
TiO ₂ wt.%	0.42	0.29	0.07	0.15	0.04	0.39	0.37	0.17	0.15	0.26	0.26	0.02	0.02	0.01	0.01	0.00	0.01
Al ₂ O ₃	99.11	99.31	99.39	99.24	99.53	98.55	98.58	98.99	98.76	99.56	99.86	99.87	99.87	99.50	99.61	99.69	99.74
Cr ₂ O ₃	0.04	0.07	0.08	0.12	0.04	0.09	0.11	0.11	0.05	0.12	0.10	0.15	0.10	0.11	0.09	0.05	0.05
V ₂ O ₃	0.02	0.02	0.01	0.02	0.01	0.03	0.03	0.02	0.02	0.05	0.03	0.01	0.00	0.00	0.00	0.01	0.00
MgO	0.02	0.01	0.00	0.01	0.00	0.01	0.02	0.01	0.01	0.01	0.02	0.00	0.00	0.00	0.00	0.00	0.01
MnO	0.00	0.00	0.00	0.00	0.00	0.00	0.00	0.01	0.00	0.00	0.00	0.00	0.00	0.00	0.00	0.00	0.00
FeO	0.05	0.04	0.03	0.01	0.03	0.06	0.06	0.05	0.03	0.05	0.05	0.04	0.04	0.03	0.04	0.03	0.03
TOTAL	99.66	99.74	99.58	99.55	99.65	99.13	99.17	99.36	99.02	100.05	100.32	100.09	100.03	99.65	99.75	99.78	99.84
Ti ⁴⁺ apfu	0.005	0.004	0.001	0.002	0.001	0.005	0.005	0.002	0.002	0.003	0.003	0.000	0.000	0.000	0.000	0.000	0.000
Al ³⁺	1.991	1.993	1.997	1.995	1.998	1.991	1.991	1.995	1.996	1.993	1.993	1.997	1.998	1.998	1.998	1.999	1.999
Cr ³⁺	0.001	0.001	0.001	0.002	0.001	0.001	0.001	0.001	0.001	0.002	0.001	0.002	0.001	0.001	0.001	0.001	0.001
V ³⁺	0.000	0.000	0.000	0.000	0.000	0.000	0.000	0.000	0.000	0.001	0.000	0.000	0.000	0.000	0.000	0.000	0.000
Mg ²⁺	0.001	0.000	0.000	0.000	0.000	0.000	0.001	0.000	0.000	0.000	0.001	0.000	0.000	0.000	0.000	0.000	0.000
Mn ²⁺	0.000	0.000	0.000	0.000	0.000	0.000	0.000	0.000	0.000	0.000	0.000	0.000	0.000	0.000	0.000	0.000	0.000
Fe ²⁺	0.001	0.001	0.000	0.000	0.000	0.001	0.001	0.001	0.000	0.001	0.001	0.001	0.000	0.001	0.000	0.000	0.000

Appendix A.1: Representative compositions of corundum from the Revelstoke Occurrence (con't)

pos. and min. assoc.	r ms	r	white + blue, but only white seems to have been probed										pink	pink	blue	blue	blue	blue	blue	m	m	blue	blue	pink		
			m	m	m	m	m	m	m	c	zc-1	zc-2	zc-3	zc-4	zc-5	zc-6	zc-7	zc-8	zc-9	zc-10	zc-11	zc-12	zc-13	zc-14	zc-15	zc-16
EPMA point TD-G063b-09-23-9																										
TiO ₂ wt.%			0.04	0.05	0.05	0.05	0.03	0.01	0.01	0.01	0.00													0.51	0.53	0.03
Al ₂ O ₃			99.89	98.79	98.52	98.45	98.58	98.67	98.42	97.80	98.59	98.77	98.82	99.45	99.37	98.13	98.45	98.17	97.59							
Cr ₂ O ₃			0.14	0.03	0.02	0.03	0.03	0.04	0.03	0.01	0.01	0.11	0.10	0.10	0.02	0.01	0.01	0.01	0.01	0.00	0.01	0.01	0.00	0.02	0.02	
V ₂ O ₃			0.00	0.00	0.01	0.01	0.01	0.02	0.02	0.01	0.01	0.01	0.01	0.01	0.02	0.03	0.01	0.01	0.01	0.01	0.01	0.01	0.01	0.01	0.01	
MgO			0.00	0.00	0.00	0.00	0.01	0.00	0.00	0.00	0.00	0.00	0.00	0.00	0.00	0.01	0.00	0.00	0.00	0.01	0.00	0.01	0.02	0.00	0.00	
MnO			0.00	0.00	0.01	0.00	0.01	0.00	0.00	0.00	0.00	0.00	0.00	0.00	0.00	0.00	0.00	0.00	0.00	0.00	0.00	0.00	0.00	0.00	0.00	
FeO			0.03	0.03	0.02	0.01	0.02	0.03	0.02	0.01	0.02	0.01	0.01	0.01	0.02	0.04	0.02	0.04	0.02	0.04	0.03	0.01	0.01	0.01	0.01	
TOTAL			100.10	98.90	98.63	98.55	98.69	98.77	98.50	97.84	98.63	98.93	98.97	99.66	99.62	98.37	99.03	98.76	97.66							
Ti ⁴⁺ apfu			0.001	0.001	0.001	0.001	0.000	0.000	0.000	0.000	0.000	0.000	0.000	0.000	0.002	0.002	0.003	0.007	0.007	0.000						
Al ³⁺			1.997	1.998	1.998	1.998	1.998	1.999	1.999	1.999	2.000	1.998	1.998	1.997	1.996	1.996	1.996	1.990	1.990	1.999						
Cr ³⁺			0.002	0.000	0.000	0.000	0.000	0.001	0.000	0.000	0.000	0.001	0.001	0.001	0.000	0.000	0.000	0.000	0.000	0.000						
V ³⁺			0.000	0.000	0.000	0.000	0.000	0.000	0.000	0.000	0.000	0.000	0.000	0.000	0.000	0.000	0.000	0.000	0.000	0.000						
Mg ²⁺			0.000	0.000	0.000	0.000	0.000	0.000	0.000	0.000	0.000	0.000	0.000	0.000	0.000	0.000	0.000	0.000	0.000	0.001	0.000					
Mn ²⁺			0.000	0.000	0.000	0.000	0.000	0.000	0.000	0.000	0.000	0.000	0.000	0.000	0.000	0.000	0.000	0.000	0.000	0.000						
Fe ²⁺			0.000	0.000	0.000	0.000	0.000	0.000	0.000	0.000	0.000	0.000	0.000	0.000	0.001	0.000	0.001	0.000	0.000	0.000						

Appendix A.1: Representative compositions of corundum from the Revelstoke Occurrence (con't)

pos. and min. assoc.	pink m	pink m	pink m	pink r	TD-G022-07C-17-1	TD-G022-07C-17-2	TD-G022-07C-17-3
EPMA point							
TiO ₂ wt.%	0.03	0.01	0.04	0.00	0.13	0.01	0.01
Al ₂ O ₃	98.64	97.69	98.77	98.53	99.51	99.94	99.77
Cr ₂ O ₃	0.03	0.07	0.08	0.07	0.08	0.03	0.04
V ₂ O ₃	0.02	0.01	0.01	0.02	0.06	0.03	0.02
MgO	0.00	0.00	0.00	0.00	0.00	0.00	0.00
MnO	0.00	0.00	0.00	0.01	0.00	0.00	0.00
FeO	0.03	0.02	0.02	0.01	0.04	0.02	0.03
TOTAL	98.75	97.80	98.92	98.64	99.82	100.03	99.87
Ti ⁴⁺ apfu	0.000	0.000	0.001	0.000	0.002	0.000	0.000
Al ³⁺	1.999	1.999	1.998	1.999	1.996	1.999	1.999
Cr ³⁺	0.000	0.001	0.001	0.001	0.001	0.000	0.001
V ³⁺	0.000	0.000	0.000	0.000	0.001	0.000	0.000
Mg ²⁺	0.000	0.000	0.000	0.000	0.000	0.000	0.000
Mn ²⁺	0.000	0.000	0.000	0.000	0.000	0.000	0.000
Fe ²⁺	0.000	0.000	0.000	0.000	0.001	0.000	0.000

Appendix A.2: Compositions of Calcite from the Revelstoke Occurrence

EPMA point	Cal in matrix with Phl			near Crn retro rxn			near Crn retro rxn			inclus in Kfs		sm grain		Cal inclus in Scp			
	c	m	r	r Ms	m	c	r Cal	m	c	c	r Kfs	r Cal	c	r Scp	c	r Scp	
	G11-02-08-01	G11-02-08-02	G11-02-08-03	G11-02c4	G11-02-01-5	G11-02-01-6	G11-02-01-7	G11-02-01-8	G11-02-01-9	G11-02-01-10	G11-02-02-11	G11-02-02-12	G11-02-02-13	G11-02-02-14	TD-G007-07-03-15	TD-G007-07-03-16	TD-G007-07-03-17
CO ₂ * wt.%	44.41	44.21	44.36	43.91	44.64	44.84	44.90	44.45	44.32	44.43	44.30	44.48	44.11	44.35	44.24	44.08	43.56
MgO	0.42	0.36	0.43	0.38	0.36	0.38	0.38	0.44	0.46	0.38	0.37	0.35	0.48	0.46	0.74	0.48	0.35
CaO	55.02	55.27	55.17	55.52	54.97	54.76	54.52	54.98	55.09	55.17	55.22	55.03	55.38	55.01	54.85	55.21	56.03
MnO	0.11	0.03	0.02	0.08	0.00	0.00	0.09	0.08	0.03	0.02	0.08	0.06	0.03	0.07	0.06	0.08	0.00
FeO	0.05	0.12	0.03	0.11	0.02	0.02	0.12	0.05	0.11	0.00	0.03	0.09	0.00	0.11	0.10	0.15	0.06
TOTAL	100.01	99.99	100.01	100.00	99.99	100.00	100.01	100.00	100.01	100.00	100.00	100.01	99.99	99.99	99.99	100.00	100.00
C ⁴⁺ apfu	1.005	1.003	1.004	0.999	1.008	1.011	1.012	1.006	1.004	1.005	1.004	1.006	1.001	1.004	1.002	1.001	0.994
Mg ²⁺	0.010	0.009	0.011	0.009	0.009	0.009	0.009	0.011	0.011	0.009	0.009	0.009	0.012	0.011	0.018	0.012	0.009
Ca ²⁺	0.977	0.984	0.980	0.991	0.974	0.969	0.964	0.976	0.979	0.980	0.982	0.977	0.986	0.978	0.975	0.984	1.003
Mn ²⁺	0.001	0.000	0.000	0.001	0.000	0.000	0.001	0.001	0.000	0.000	0.001	0.001	0.000	0.001	0.001	0.001	0.000
Fe ²⁺	0.001	0.002	0.000	0.002	0.000	0.000	0.002	0.001	0.001	0.000	0.000	0.001	0.000	0.001	0.001	0.002	0.001

NOTE: For the elements considered, the following standards, X-ray lines And crystals were used: dolomite, MgKa, TAP; Calcite, CaKa, PET; rhodochrosite, MnKa, LiF; siderite, FeKa, LiF.

Compositions were reCalculated on the basis of 3 O apfu. *C determined by stoichiometry

c = Crn, m = middle, r = rim

Appendix A.2: Compositions of Calcite from the Revelstoke Occurrence (con't)

EPMA point	inclusion in crn		near Crn, lrg grain												1 next to Phl, Pl, Ms agg			All surrounded by Cal on edge of Phl, Pl, Ms zone, except 6 next to Phl		
	r Crn	c	c	m	r Cal	c	r Ms alt	r An	c	r Scp	m	c	rim	middle	Crn	Crn	middle	rim		
CO ₂ * wt.%	43.57	43.70	43.83	43.42	42.74	43.01	43.59	43.60	43.32	43.28	43.51	42.72	43.61	43.47	43.45	43.79	44.13	43.10		
MgO	0.66	0.71	0.47	0.49	0.26	0.15	0.61	0.58	0.51	0.53	0.51	0.56	0.60	0.37	0.27	0.59	0.65	0.20		
CaO	55.65	55.44	55.55	56.02	56.90	56.69	55.72	55.69	56.03	55.94	55.80	56.47	55.54	56.02	56.19	55.33	55.03	56.49		
MnO	0.07	0.08	0.05	0.00	0.10	0.08	0.05	0.02	0.06	0.10	0.09	0.10	0.06	0.02	0.03	0.05	0.02	0.12		
FeO	0.05	0.06	0.09	0.07	0.00	0.08	0.03	0.12	0.08	0.14	0.09	0.15	0.20	0.12	0.05	0.25	0.17	0.09		
TOTAL	100.00	100.00	100.00	100.00	100.00	100.00	100.00	100.01	100.00	99.99	99.99	100.00	100.01	100	99.99	100.01	100	100		
C ⁴⁺ apfu	0.993	0.995	0.997	0.991	0.983	0.987	0.994	0.994	0.990	0.990	0.993	0.982	0.994	0.993	0.992	0.996	1.001	0.988		
Mg ²⁺	0.016	0.018	0.012	0.012	0.007	0.004	0.015	0.014	0.013	0.013	0.013	0.014	0.015	0.009	0.007	0.015	0.016	0.005		
Ca ²⁺	0.996	0.991	0.992	1.004	1.027	1.021	0.997	0.996	1.005	1.004	0.999	1.019	0.993	1.004	1.007	0.988	0.980	1.016		
Mn ²⁺	0.001	0.001	0.001	0.000	0.001	0.001	0.001	0.000	0.001	0.001	0.001	0.001	0.001	0.000	0.000	0.001	0.000	0.002		
Fe ²⁺	0.001	0.001	0.001	0.001	0.000	0.001	0.000	0.002	0.001	0.002	0.001	0.002	0.003	0.002	0.001	0.003	0.002	0.001		

Appendix A.2: Compositions of Calcite from the Revelstoke Occurrence (con't)

EPMA point	partly surround by Cal, partly surrounded by Phl			surrounded by Cal And small Phl grains, large Cal grain			surrounded by Cal, large			All surrounded by Cal, small grain			All surrounded by Cal, med grain			All surrounded by Cal		
	rim	middle	Crn	Crn	middle	rim	Crn	middle	rim	Crn	middle	rim	rim	middle	Crn	Crn	middle	rim
CO ₂ * wt.%	43.86	43.91	43.97	43.88	43.80	43.94	43.45	43.99	43.68	44.07	44.49	43.84	43.69	43.74	43.80	43.91	43.72	44.27
MgO	0.28	0.53	0.63	0.43	0.46	0.64	0.32	0.38	0.35	0.39	0.42	0.61	0.24	0.50	0.62	0.50	0.49	0.66
CaO	55.76	55.29	55.17	55.48	55.58	55.14	56.10	55.45	55.72	55.41	54.82	55.38	55.98	55.65	55.43	55.37	55.52	54.77
MnO	0.04	0.13	0.08	0.01	0.06	0.06	0.03	0.06	0.07	0.00	0.13	0.05	0.00	0.06	0.01	0.02	0.05	0.04
FeO	0.05	0.13	0.15	0.20	0.10	0.21	0.11	0.13	0.18	0.13	0.15	0.12	0.10	0.04	0.14	0.19	0.23	0.25
TOTAL	99.99	99.99	100	100	100	99.99	100.01	100.01	100	100	100.01	100	100.01	99.99	100	99.99	100.01	99.99
C ⁴⁺ apfu	0.998	0.998	0.999	0.998	0.997	0.998	0.992	1.000	0.996	1.001	1.006	0.997	0.996	0.996	0.996	0.998	0.996	1.003
Mg ²⁺	0.007	0.013	0.016	0.011	0.011	0.016	0.008	0.009	0.009	0.010	0.010	0.015	0.006	0.012	0.015	0.012	0.012	0.016
Ca ²⁺	0.996	0.987	0.984	0.990	0.993	0.983	1.005	0.989	0.997	0.987	0.973	0.988	1.001	0.994	0.990	0.988	0.992	0.974
Mn ²⁺	0.001	0.002	0.001	0.000	0.001	0.001	0.000	0.001	0.001	0.000	0.002	0.001	0.000	0.001	0.000	0.000	0.001	0.001
Fe ²⁺	0.001	0.002	0.002	0.003	0.001	0.003	0.002	0.002	0.003	0.002	0.002	0.001	0.001	0.002	0.003	0.003	0.003	0.003

Appendix A.2: Compositions of Calcite from the Revelstoke Occurrence (con't)

EPMA point	All surrounded by Cal, large grain			All surrounded by Cal, med grain			15 next to Cal (other side next to Phl)			inclusion within Pl			on edge of altered Crn					
	rim	middle	Crn	rim	middle	Crn	Crn	middle	rim	Crn	middle	rim	Crn	middle	rim	Crn	middle	rim
	TD-G014-07A2-13-7	TD-G014-07A2-13-8	TD-G014-07A2-13-9	TD-G014-07A2-13-10	TD-G014-07A2-13-11	TD-G014-07A2-13-12	TD-G014-07A2-14-13	TD-G014-07A2-14-14	TD-G014-07A2-14-15	TD-G014-07B1-1-1	TD-G014-07B1-1-2	TD-G014-07B1-1-3	TD-G014-07B1-1-4	TD-G014-07B1-1-5	TD-G014-07B1-1-6	TD-G014-07B1-4-7	TD-G014-07B1-4-8	TD-G014-07B1-4-9
CO ₂ * wt.%	43.92	43.42	43.88	43.52	44.31	43.50	44.07	43.77	44.24	43.50	43.28	43.63	43.88	43.77	44.09	44.11	43.94	43.91
MgO	0.53	0.43	0.42	0.44	0.65	0.67	0.51	0.52	0.70	0.38	0.40	0.34	0.70	0.70	0.74	0.70	0.74	0.14
CaO	55.32	55.97	55.44	55.88	54.82	55.57	55.23	55.52	54.87	56.02	56.19	55.93	55.20	55.30	54.97	54.97	55.12	55.87
MnO	0.05	0.04	0.04	0.00	0.05	0.08	0.02	0.02	0.00	0.01	0.06	0.00	0.07	0.06	0.02	0.05	0.02	0.05
FeO	0.19	0.14	0.21	0.17	0.17	0.18	0.17	0.16	0.19	0.08	0.08	0.10	0.15	0.17	0.19	0.17	0.18	0.03
TOTAL	100.01	100	99.99	100.01	100	100	100	99.99	100	99.99	100.01	100.00	100.00	100.00	100.01	100.00	100.00	100.00
C ⁴⁺ apfu	0.998	0.992	0.998	0.993	1.003	0.992	1.000	0.996	1.002	0.993	0.990	0.995	0.997	0.996	1.000	1.001	0.998	0.999
Mg ²⁺	0.013	0.011	0.010	0.011	0.016	0.017	0.013	0.013	0.017	0.009	0.010	0.008	0.017	0.017	0.018	0.017	0.018	0.003
Ca ²⁺	0.987	1.003	0.990	1.001	0.974	0.995	0.984	0.992	0.976	1.003	1.008	1.001	0.985	0.988	0.979	0.979	0.983	0.998
Mn ²⁺	0.001	0.001	0.001	0.000	0.001	0.001	0.000	0.000	0.000	0.001	0.000	0.001	0.001	0.001	0.000	0.001	0.000	0.001
Fe ²⁺	0.003	0.002	0.003	0.002	0.002	0.003	0.002	0.002	0.003	0.001	0.001	0.002	0.002	0.003	0.002	0.003	0.002	0.000

Appendix A.2: Compositions of Calcite from the Revelstoke Occurrence (con't)

EPMA point	surrounded by Cal, large grain			all surrounded by Cal, small grain			small grain, All surrounded by Cal, except one next to Phl			all surrounded by Cal			large grain, partly surrounded by Cal, partly surrounded by Phl			across Cal vein			
	Crn	middle	rim	Crn	middle	rim	Crn	middle	rim	Crn	middle	rim	Crn	middle	rim	Crn	middle	Crn	rim
	TD-G014-07B1-5-10	TD-G014-07B1-5-11	TD-G014-07B1-5-12	TD-G014-07B1-5-13	TD-G014-07B1-5-14	TD-G014-07B1-5-15	TD-G014-07B1-5-16	TD-G014-07B1-5-17	TD-G014-07B1-5-18	TD-G063b-09bc31	TD-G063b-09bc32	TD-G063b-09bc33	TD-G063b-09bc34	TD-G063b-09bc35	TD-G063b-09b-8-36	TD-G063b-09b-8-37	TD-G063b-09b-8-38	TD-G063b-09b-8-40	
CO ₂ * wt.%	44.23	44.41	44.43	44.13	44.40	44.27	43.95	43.79	43.64	43.24	43.75	43.78	43.83	43.65	43.06	43.43	42.98	43.31	
MgO	0.35	0.33	0.59	0.60	0.55	0.67	0.73	0.71	0.55	0.72	0.76	0.91	0.81	0.76	0.27	0.64	0.75	0.19	
CaO	55.31	55.14	54.80	55.12	54.85	54.84	55.05	55.27	55.65	55.73	55.20	55.01	55.06	55.38	56.59	55.72	56.16	56.33	
MnO	0.00	0.03	0.08	0.01	0.00	0.03	0.07	0.00	0.04	0.08	0.10	0.09	0.09	0.04	0.08	0.09	0.10	0.05	
FeO	0.12	0.08	0.11	0.13	0.20	0.20	0.20	0.23	0.12	0.22	0.20	0.21	0.21	0.17	0.00	0.13	0.02	0.12	
TOTAL	100.01	99.99	100.01	99.99	100.00	100.01	100.00	100.00	100.00	100.00	100.00	100.00	100.00	100.00	100.01	100.01	100.01	100.01	
C ⁴⁺ apfu	1.003	1.005	1.005	1.001	1.005	1.003	0.998	0.996	0.994	0.989	0.996	0.996	0.997	0.994	0.987	0.991	0.985	0.991	
Mg ²⁺	0.009	0.008	0.015	0.015	0.014	0.017	0.018	0.018	0.014	0.018	0.019	0.022	0.020	0.019	0.007	0.016	0.019	0.005	
Ca ²⁺	0.984	0.980	0.973	0.981	0.974	0.975	0.981	0.987	0.995	1.000	0.986	0.982	0.983	0.990	1.018	0.998	1.010	1.011	
Mn ²⁺	0.000	0.000	0.001	0.000	0.000	0.000	0.001	0.000	0.001	0.001	0.001	0.001	0.001	0.001	0.001	0.001	0.001	0.001	
Fe ²⁺	0.002	0.001	0.002	0.002	0.003	0.003	0.003	0.002	0.003	0.003	0.003	0.003	0.002	0.002	0.000	0.002	0.000	0.002	

Appendix A.2: Compositions of Calcite from the Revelstoke Occurrence (con't)

EPMA point	surrounded by scap And musc		surrounded by Pl, musc And scap		next to altered Crn grain And pyrite			Calcite in matrix near Phl segregation			large grain in Cal matrix			med grain in Cal matrix			
	Crn	Crn	Crn	rim	rim	middle	Crn	rim Phl	middle	rim Phl	c	r Cal	c	c	r		
	TD-G063b-09b-5-42	TD-G063b-09b-5-43	TD-G063b-09b-5-44	TD-G063b-09b-5-45	TD-G063b-09b-1-46	TD-G063b-09b-1-47	TD-G063b-09b-1-48	TD-G063b-09b10-49	TD-G063b-09b10-50	TD-G063b-09b10-51	TD-G063b-09bc52	TD-G063b-09bc53	TD-G020-07A1-19-1	TD-G020-07A1-19-2	TD-G020-07A1-21-3	TD-G020-07A1-21-4	TD-G020-07A1-21-5
CO ₂ * wt.%	43.11	43.51	43.52	43.52	43.47	43.22	43.33	43.76	43.80	44.45	44.60	44.40	42.89	43.18	43.57	43.81	43.9
MgO	0.04	0.00	0.07	0.06	0.34	0.65	0.62	0.55	0.71	0.31	0.29	0.26	0.46	0.41	0.39	0.47	0.45
CaO	56.78	56.30	56.18	56.30	56.16	55.84	55.67	55.38	55.20	53.33	53.41	53.56	56.59	56.29	56	55.61	55.49
MnO	0.05	0.09	0.11	0.08	0.01	0.11	0.09	0.09	0.14	0.56	0.53	0.63	0.04	0.01	0.01	0.01	0.05
FeO	0.02	0.10	0.12	0.04	0.02	0.19	0.29	0.22	0.15	1.36	1.18	1.15	0.02	0.1	0.03	0.1	0.11
TOTAL	100.00	100.00	100.01	99.99	100.00	100.01	100.00	100.00	100.00	100.00	100.01	100.00	100	99.99	100	100	100
C ⁴⁺ apfu	0.988	0.994	0.994	0.994	0.992	0.989	0.990	0.996	0.996	1.008	1.010	1.007	0.984	0.988	0.994	0.997	0.998
Mg ²⁺	0.001	0.000	0.002	0.001	0.009	0.016	0.015	0.014	0.018	0.008	0.007	0.006	0.012	0.01	0.01	0.012	0.011
Ca ²⁺	1.022	1.009	1.007	1.009	1.006	1.002	0.999	0.989	0.986	0.949	0.949	0.954	1.019	1.011	1.002	0.993	0.99
Mn ²⁺	0.001	0.001	0.002	0.001	0.000	0.002	0.001	0.001	0.002	0.008	0.007	0.009	0.001	0	0	0	0.001
Fe ²⁺	0.000	0.001	0.002	0.001	0.000	0.003	0.004	0.003	0.002	0.019	0.016	0.016	0	0.001	0	0.001	0.002

Appendix A.2: Compositions of Calcite from the Revelstoke Occurrence (con't)

EPMA point	med grain in Cal matrix		med grain in Cal matrix		sm grain in Cal matrix		lrg grain in Cal matrix										large grain		large grain	
	c	r Cal	r Cal	c	c	r Cal	c	r Cal	c	r Cal	r Cal	m	c		r	s	s	s	c	r
CO ₂ * wt.%	43.45	43.84	43.64	44.01	42.67	43.17	43.45	43.66	43.29	42.85	43.42	43.14	43.2	42.87	43.14	43.24	42.92	43		
MgO	0.4	0.32	0.44	0.37	0.44	0.39	0.43	0.38	0.4	0.42	0.41	0.47	0.42	0.45	0.44	0.53	0.42	0.46		
CaO	55.99	55.78	55.76	55.55	56.85	56.3	56.05	55.88	56.18	56.46	56.11	56.26	56.25	56.6	56.3	56.14	56.59	56.43		
MnO	0.01	0.02	0	0	0.02	0.07	0.01	0	0.05	0.11	0.04	0.03	0.02	0.01	0.07	0.06	0.03	0.02		
FeO	0.15	0.04	0.15	0.08	0.03	0.07	0.05	0.09	0.08	0.16	0.03	0.11	0.11	0.07	0.05	0.04	0.05	0.09		
TOTAL	100	100	99.99	100.01	100.01	100	99.99	100.01	100	100	100.01	100.01	100	100	100	100.01	100.01	100		
C ⁴⁺ apfu	0.992	0.998	0.995	1	0.981	0.988	0.992	0.995	0.99	0.984	0.992	0.988	0.989	0.984	0.988	0.989	0.985	0.986		
Mg ²⁺	0.01	0.008	0.011	0.009	0.011	0.01	0.011	0.009	0.01	0.011	0.01	0.012	0.01	0.011	0.011	0.013	0.011	0.012		
Ca ²⁺	1.003	0.996	0.997	0.99	1.026	1.012	1.004	0.999	1.008	1.018	1.006	1.011	1.01	1.02	1.012	1.008	1.019	1.015		
Mn ²⁺	0	0	0	0	0	0.001	0	0	0.001	0.002	0.001	0	0	0	0.001	0.001	0	0		
Fe ²⁺	0.002	0.001	0.002	0.001	0	0.001	0.001	0.001	0.002	0	0.002	0.002	0.001	0.001	0.001	0.001	0.001	0.001		

Appendix A.2: Compositions of Calcite from the Revelstoke Occurrence (con't)

EPMA point	sm grain c	sm grain c	sm grain c	med grain c	sm grain c	sm grain c	sm grain c	r	c		c	r		c	r	med grain in Cal matrix c	r	
	G020-7A1-24	G020-7A1-25	G020-7A1-26	G020-7A1-27	G020-7A1-28	G020-7A1-29	G020-7A1-30	G020-07B-34	G020-07B-35	G020-07B-36	G020-07B-37	G020-07B-38	G020-07B-39	G020-07B-40	G020-07B-41	G020-07B-42	G020-07B-43	G020-07B-44
CO ₂ * wt.%	43.23	43.39	43.45	42.7	43.92	42.77	44.26	42.54	42.96	43.26	43.16	42.89	42.89	42.77	43.17	43.34	42.83	42.96
MgO	0.04	0.48	0.58	0.48	0.69	0.22	1.1	0.65	0.68	0.66	0.62	0.62	0.78	0.56	0.48	0.50	0.44	0.49
CaO	56.7	56.08	55.87	56.69	55.14	56.9	53.17	56.71	56.31	55.96	56.08	56.33	56.10	56.53	56.19	56.08	56.67	56.43
MnO	0.02	0.03	0.01	0.04	0.07	0.05	0.05	0.04	0.00	0.00	0.00	0.05	0.05	0.04	0.00	0.04	0.00	0.01
FeO	0	0.03	0.1	0.1	0.19	0.07	1.41	0.06	0.05	0.13	0.14	0.11	0.17	0.10	0.16	0.03	0.06	0.10
TOTAL	99.99	100.01	100.01	100.01	100.01	100.01	99.99	100.00	100.00	100.01	100.00	100.00	99.99	100.00	100.00	99.99	100.00	99.99
C ⁴⁺ apfu	0.99	0.991	0.992	0.982	0.998	0.983	1.003	0.979	0.985	0.989	0.988	0.984	0.984	0.982	0.988	0.990	0.983	0.985
Mg ²⁺	0.001	0.012	0.014	0.012	0.017	0.006	0.027	0.016	0.017	0.016	0.015	0.016	0.020	0.014	0.012	0.012	0.011	0.012
Ca ²⁺	1.019	1.005	1.001	1.023	0.983	1.026	0.946	1.024	1.013	1.004	1.007	1.014	1.010	1.019	1.009	1.006	1.021	1.016
Mn ²⁺	0	0	0	0.001	0.001	0.001	0.001	0.001	0.000	0.000	0.000	0.001	0.001	0.001	0.000	0.001	0.000	0.000
Fe ²⁺	0	0	0.001	0.001	0.003	0.001	0.02	0.001	0.001	0.002	0.002	0.002	0.002	0.001	0.002	0.000	0.001	0.001

Appendix A.2: Compositions of Calcite from the Revelstoke Occurrence (con't)

EPMA point	large grain in Cal matrix				sm	sm	sm	sm	sm	sm	med	med	med	sm	large	large	med
	c	m	r	c	r	c	c	c	c	c	c	r	c	c	r	c	c
G020-07B-45	42.98	42.67	42.91	42.96	43.21	42.61	43.13	42.51	42.99	42.86	42.76	42.65	42.87	42.84	43.01	42.6	42.53
G020-07B-46																	42.77
G020-07B-47																	
G020-07B-48																	
G022-07C-1																	
G022-07C-2																	
G022-07C-3																	
G022-07C-4																	
G022-07C-5																	
G022-07C-6																	
G022-07C-7																	
G022-07C-8																	
G022-07C-9																	
G022-07C-10																	
G022-07C-11																	
G022-07C-12																	
G022-07C-13																	
G022-07C-14																	

Appendix A.2: Compositions of Calcite from the Revelstoke Occurrence (con't)

EPMA point	med	med	large	large	med	med	med grain next to	An	med grain next to	An	med grain next to An, ap, And kfs		med	sm grain	sm grain			
	r	c	c	r	r	c	r	c	r	c	r	r	c	c	r			
	G022-07C-15	G022-07C-16	G022-07C-17	G022-07C-18	G022-07C-19	G022-07C-20	G022-07C-5-21	G022-07C-5-22	G022-07C-5-23	G022-07C-5-24	G022-07C-3-25	G022-07C-3-26	G022-07C-3-27	G022-07C-3-28	G022-07C-29	G022-07C-30	G022-07C-31	G022-07C-32
CO ₂ * wt.%	43.09	42.99	42.89	42.75	42.88	43.33	43.02	42.25	42.52	42.42	42.2	42.47	42.9	42.15	42.27	43.13	42.27	43.33
MgO	0.72	0.68	0.88	0.87	0.74	0.86	0.73	0.83	0.76	0.74	0.68	0.64	0.69	0.67	0.46	0.59	0.55	0.67
CaO	56.12	56.18	56.17	56.36	56.32	55.7	56.06	56.87	56.68	56.6	56.94	56.7	56.41	56.99	57.06	56.2	57.04	55.87
MnO	0.04	0.03	0	0.02	0.01	0.03	0.04	0.01	0.03	0.04	0	0.05	0	0.07	0.08	0.04	0.03	0.02
FeO	0.03	0.12	0.07	0	0.04	0.07	0.15	0.04	0.01	0.19	0.17	0.14	0	0.13	0.13	0.04	0.11	0.11
TOTAL	100	100	100.01	100	99.99	99.99	100	100	100	99.99	99.99	100	100	100.01	100	100	100	100
C ⁴⁺ <i>apfu</i>	0.986	0.985	0.983	0.981	0.983	0.989	0.986	0.974	0.978	0.977	0.974	0.978	0.984	0.974	0.976	0.987	0.976	0.99
Mg ²⁺	0.018	0.017	0.022	0.022	0.019	0.021	0.018	0.021	0.019	0.019	0.017	0.016	0.017	0.017	0.012	0.015	0.014	0.017
Ca ²⁺	1.008	1.01	1.011	1.015	1.014	0.998	1.008	1.029	1.024	1.023	1.032	1.025	1.015	1.033	1.034	1.01	1.033	1.002
Mn ²⁺	0.001	0	0	0	0	0	0.001	0	0	0.001	0	0.001	0	0.001	0.001	0.001	0	0
Fe ²⁺	0	0.002	0.001	0	0.001	0.001	0.002	0.001	0	0.003	0.002	0.002	0	0.002	0.001	0.002	0.001	0.002

Appendix A.2: Compositions of Calcite from the Revelstoke Occurrence (con't)

EPMA point	3 is next to Cal, opposite side next to amph				All surrounded by Cal			All surrounded by Cal, large grain			All surrounded by Cal			All surrounded by Cal, small grain		
	Crn	middle	rim	Crn	middle	Crn	rim	middle	Crn	middle	rim	Crn	middle	rim	Crn	middle
G022-07C-33	TD-G013-07-2-01	TD-G013-07-2-02	TD-G013-07-2-03	TD-G013-07-3-04	TD-G013-07-3-05	TD-G013-07-3-06	TD-G013-07-4a-07	TD-G013-07-4a-08	TD-G013-07-4a-09	TD-G013-07-4a-10	TD-G013-07-4a-11	TD-G013-07-4a-12	TD-G013-07-4a-13	TD-G013-07-4a-14	TD-G013-07-4a-15	
CO ₂ * wt.%	42.91	43.46	44.04	43.76	43.57	43.82	43.41	42.83	43.67	43.49	43.26	42.98	43.44	42.90	43.37	43.37
MgO	0.39	0.67	0.63	0.67	0.74	0.66	0.74	0.88	0.84	0.79	0.84	0.83	0.84	0.82	0.82	0.80
CaO	56.62	55.82	55.28	55.56	55.66	55.45	55.79	56.18	55.46	55.66	55.80	56.13	55.62	56.13	55.75	55.77
MnO	0.02	0.00	0.05	0.00	0.00	0.04	0.01	0.01	0.00	0.03	0.04	0.03	0.00	0.05	0.01	0.00
FeO	0.06	0.05	0.01	0.01	0.03	0.03	0.06	0.11	0.03	0.03	0.05	0.03	0.10	0.11	0.05	0.06
TOTAL	100	100	100.01	100	100	100	100.01	100.01	100	100	99.99	100	100	100.01	100	100
C ⁴⁺ apfu	0.985	0.992	0.999	0.996	0.993	0.997	0.991	0.982	0.994	0.992	0.989	0.985	0.991	0.984	0.990	0.990
Mg ²⁺	0.01	0.017	0.016	0.017	0.018	0.016	0.018	0.022	0.021	0.020	0.021	0.021	0.021	0.021	0.020	0.020
Ca ²⁺	1.02	0.999	0.985	0.992	0.995	0.990	0.999	1.011	0.991	0.996	1.001	1.009	0.996	1.010	0.999	0.999
Mn ²⁺	0	0.000	0.001	0.000	0.000	0.001	0.000	0.000	0.000	0.001	0.000	0.000	0.001	0.000	0.000	0.000
Fe ²⁺	0.001	0.001	0.000	0.000	0.000	0.001	0.002	0.000	0.000	0.001	0.000	0.001	0.002	0.001	0.001	0.001

Appendix A.2: Compositions of Calcite from the Revelstoke Occurrence (con't)

EPMA point	sm grain, All surrounded by Cal, except 16 near px grain			All surrounded by Cal, very small grain			in contact w/ px, otherwise surrounded by Cal			surrounded by Cal, except 57 next to Px			surrounded by Cal			all surrounded by Cal, large grain		
	rim	middle	Crn	Crn	middle	rim	Crn	middle	rim	rim	Crn	Crn	rim	middle	Crn	rim	middle	Crn
CO ₂ * wt.%	43.21	43.31	43.43	42.91	43.87	43.34	44.51	43.93	44.35	44.48	44.31	44.82	44.44	44.10	44.43	44.63		
MgO	0.75	0.62	0.60	0.66	0.61	0.67	0.38	0.43	0.41	0.23	0.34	0.50	0.38	0.50	0.45	0.54		
CaO	56.00	55.96	55.87	56.36	55.45	55.90	52.97	53.28	53.10	53.46	53.77	52.88	53.56	53.20	52.82	52.62		
MnO	0.00	0.06	0.03	0.00	0.00	0.04	0.52	0.63	0.53	0.61	0.60	0.61	0.53	0.54	0.60	0.45		
FeO	0.04	0.05	0.08	0.08	0.06	0.05	1.62	1.74	1.61	1.22	0.99	1.19	1.09	1.67	1.71	1.77		
TOTAL	100	100	100.01	100.01	99.99	100	100.00	100.01	100.00	100.00	100.00	100.00	100.00	100.01	100.01	100.01	100.01	
C ⁴⁺ apfu	0.988	0.990	0.991	0.984	0.997	0.990	1.009	1.001	1.007	1.009	1.006	1.013	1.007	1.003	1.008	1.010		
Mg ²⁺	0.019	0.015	0.015	0.017	0.015	0.017	0.010	0.011	0.010	0.006	0.008	0.012	0.009	0.012	0.011	0.013		
Ca ²⁺	1.005	1.004	1.001	1.014	0.989	1.002	0.942	0.953	0.946	0.951	0.958	0.938	0.953	0.950	0.941	0.935		
Mn ²⁺	0.000	0.001	0.000	0.000	0.000	0.001	0.007	0.009	0.007	0.009	0.008	0.009	0.007	0.008	0.008	0.006		
Fe ²⁺	0.001	0.001	0.001	0.001	0.001	0.001	0.022	0.024	0.022	0.017	0.014	0.016	0.015	0.023	0.024	0.024		

Appendix A.3: Compositions of phlogopite from lithologies within marble at the Revelstoke Occurrence

pos. And min. assoc. EPMA point	r Cal G10-01-21-1	m G10-01-21-2	c G10-01-21-3	r Phl G10-01-21-4	c G10-01-21-10	c G10-01-21-11	c G10-01-20b-2	r Phl G10-01-20b-3	r G11-02-1	m G11-02-9-2	m G11-02-9-3	c G11-02-9-4	m G11-02-9-5	r Cal G11-02-9-9
SiO ₂ wt.%	38.4	37.36	36.65	37.37	36.68	36.84	36.86	36.17	37.05	37.38	37.45	36.67	37.14	37.39
TiO ₂	1.5	1.53	1.56	1.28	1.6	1.53	1.35	1.33	1.2	1.35	1.57	1.24	1.21	1.76
Al ₂ O ₃	23.67	22.85	23.37	23.53	22.48	22.94	23.83	23.14	23.16	23.3	23.21	23.6	23.46	22.53
Cr ₂ O ₃	0.1	0.05	0.13	0.04	0.05	0.09	0.22	0.08	0.05	0.14	0.04	0.09	0.13	0.03
V ₂ O ₃														
Fe ₂ O ₃	0	0	0	0	0	0	0	0	0	0	0	0	0	0
MgO	17.49	18.86	19	18.08	18.2	17.95	18.34	18.73	20.07	19.57	19.57	19.73	19.59	19.08
MnO	0.04	0.03	0.01	0.02	0.02	0	0.07	0	0.06	0.04	0.04	0.06	0	0.04
FeOt _{tot}	3.18	3.17	3.34	3.01	3.04	3.37	3.28	3.23	2.57	2.84	2.8	2.7	2.62	2.74
ZnO														
CaO	0.08	0.02	0.05	0.06	0.07	0.06	0.04	0.05	0.01	0.05	0.01	0.02	0.02	0.05
BaO	0.36	0.38	0.23	0.16	0.3	0.26	0.22	0.15	0.06	0.12	0.18	0.06	0.06	0.45
Na ₂ O	0.14	0.12	0.15	0.14	0.19	0.15	0.13	0.14	0.16	0.16	0.14	0.14	0.13	0.14
K ₂ O	10.52	10.86	10.33	10.29	10.37	10.1	9.58	10.59	10.64	10.87	10.89	10.86	11.01	10.63
F	0.24	0.27	0.23	0.22	0.22	0.23	0.23	0.22	0.29	0.31	0.3	0.28	0.29	0.36
CL	0.02	0	0.02	0.01	0.01	0.03	0	0.01	0.02	0	0	0.02	0	0
H ₂ O *	4.16	4.11	4.11	4.11	4.04	4.05	4.11	4.06	4.11	4.13	4.14	4.11	4.12	4.06
- (O=F,Cl)	-0.11	-0.11	-0.10	-0.09	-0.09	-0.10	-0.10	-0.09	-0.13	-0.13	-0.13	-0.12	-0.12	-0.15
TOTAL	99.79	99.50	99.08	98.23	97.18	97.50	98.16	97.81	99.32	100.13	100.21	99.46	99.66	99.11
Si ⁴⁺ apfu	2.693	2.643	2.599	2.659	2.650	2.649	2.622	2.601	2.612	2.620	2.623	2.588	2.614	2.650
Ti ⁴⁺	0.079	0.081	0.083	0.069	0.087	0.083	0.072	0.072	0.064	0.071	0.083	0.066	0.064	0.094
Al ³⁺	1.956	1.905	1.953	1.973	1.914	1.944	1.998	1.961	1.925	1.925	1.916	1.963	1.946	1.882
Cl ³⁺	0.006	0.003	0.007	0.002	0.003	0.005	0.012	0.005	0.003	0.008	0.002	0.005	0.007	0.002
V ³⁺	0.000	0.000	0.000	0.000	0.000	0.000	0.000	0.000	0.000	0.000	0.000	0.000	0.000	0.000
Fe ³⁺	0.000	0.000	0.000	0.000	0.000	0.000	0.000	0.000	0.000	0.000	0.000	0.000	0.000	0.000
Mg ²⁺	1.828	1.989	2.009	1.917	1.960	1.924	1.945	2.008	2.110	2.045	2.043	2.076	2.055	2.016
Mn ²⁺	0.002	0.002	0.001	0.001	0.001	0.000	0.004	0.000	0.004	0.002	0.002	0.004	0.000	0.002
Fe ²⁺	0.186	0.188	0.198	0.179	0.184	0.203	0.195	0.194	0.152	0.166	0.164	0.159	0.154	0.162
Zn ²⁺	0.000	0.000	0.000	0.000	0.000	0.000	0.000	0.000	0.000	0.000	0.000	0.000	0.000	0.000
Ca ²⁺	0.006	0.002	0.004	0.005	0.005	0.005	0.003	0.004	0.001	0.004	0.001	0.002	0.002	0.004
Ba ²⁺	0.010	0.011	0.006	0.004	0.008	0.007	0.006	0.004	0.002	0.003	0.005	0.002	0.002	0.012
Na ⁺	0.019	0.016	0.021	0.019	0.027	0.021	0.018	0.020	0.022	0.022	0.019	0.019	0.018	0.019
K ⁺	0.941	0.980	0.935	0.934	0.956	0.927	0.869	0.971	0.957	0.972	0.973	0.978	0.988	0.961
F	0.053	0.060	0.052	0.049	0.050	0.052	0.052	0.050	0.065	0.069	0.066	0.062	0.065	0.081
Cl ⁻	0.002	0.000	0.002	0.001	0.001	0.004	0.000	0.001	0.002	0.000	0.000	0.002	0.000	0.000
OH ⁻	1.944	1.940	1.946	1.949	1.949	1.944	1.948	1.949	1.933	1.931	1.934	1.935	1.935	1.919
vac. (M)	0.249	0.189	0.150	0.200	0.201	0.192	0.152	0.159	0.132	0.162	0.166	0.139	0.160	0.192
O ²⁻	10	10	10	10	10	10	10	10	10	10	10	10	10	10

*calculated from electroneutral formula assuming 12 anions and (OH+F+Cl)=2.

NOTE: Following standards, X-ray lines and crystals were used during EMP analysis: synthetic phlogopite, F Ka, MgKa, SiKa, TAP, KKa, PET; albite, NaKa, TAP; kyanite, AlKa, TAP; scapolite, CIKa, PET; diopside, CaKa, PET; rutile, TiKa, PET; synthetic magnesiochromite, CrKa, LiF; synthetic rhodonite, MnKa, LiF; synthetic fayalite, FeKa, LiF; barite, BaLa, PET.

Appendix A.3: Compositions of phlogopite from lithologies within marble at the Revelstoke Occurrence (con't)

pos. And min. assoc. EPMA point	m G11-02-9-10	c G11-02-9-11	r G11-02-01-14	c G11-02-01-15	r G11-02-08-16	m G11-02-08-17	c G11-02-08-18	G11-02-08-19	c G11-02-7c-24	r Kfs G11-02-7c-25	r Kfs G11-02-7c-26	c G11-02-7c-27	r Pl G11-02-07b-30
SiO ₂ wt.%	36.78	36.86	37.36	37.84	36.93	37.09	36.75	36.65	37.2	37.37	37.16	37.37	37.75
TiO ₂	1.54	1.43	1.53	1.55	1.45	1.73	1.36	1.13	1.25	1.24	1.28	1.08	1.88
Al ₂ O ₃	23.41	23.34	23.19	23.01	22.72	23.11	22.71	23.5	24.36	24.37	24.33	23.99	23.52
Cr ₂ O ₃	0.01	0.01	0.07	0.03	0	0.03	0.08	0.16	0.07	0.13	0.11	0.13	0.15
V ₂ O ₃								0.19	0.18	0.17	0.15	0.15	0.18
Fe ₂ O ₃	0	0	0	0	0	0	0	0	0	0	0	0	0
MgO	19.05	19.31	18.97	19.31	19.22	18.97	19.79	19.45	20.03	19.73	19.71	19.92	19.06
MnO	0.02	0.02	0.01	0	0.07	0.01	0	0.01	0.04	0	0.05	0.04	0.07
FeOt _{tot}	2.76	2.89	2.65	2.9	2.92	2.87	3.23	2.9	2.92	2.96	3.15	2.9	2.82
ZnO													
CaO	0.03	0	0.09	0.09	0.05	0	0.01	0.02	0	0	0	0	0.04
BaO	0.11	0.17	0.33	0.35	0.3	0.28	0.11	0.11	0.13	0.23	0.12	0.1	0.35
Na ₂ O	0.14	0.13	0.13	0.08	0.12	0.12	0.12	0.13	0.12	0.18	0.12	0.15	0.12
K ₂ O	10.82	10.83	10.94	10.85	10.69	10.86	10.54	10.83	11.15	10.94	11	10.88	11.17
F	0.22	0.26	0.3	0.31	0.28	0.26	0.28	0.24	0.55	0.53	0.5	0.66	0.38
CL	0	0	0.02	0.02	0.02	0	0.01	0.02	0.01	0.02	0	0.01	0.01
H ₂ O *	4.12	4.11	4.10	4.13	4.07	4.12	4.09	4.11	4.08	4.08	4.09	4.00	4.14
- (O+F, Cl)	-0.09	-0.11	-0.13	-0.14	-0.12	-0.11	-0.12	-0.11	-0.23	-0.23	-0.21	-0.28	-0.16
TOTAL	98.92	99.25	99.56	100.33	98.72	99.34	98.96	99.15	101.87	101.73	101.58	101.10	101.48
Si ⁴⁺ apfu	2.608	2.608	2.635	2.648	2.630	2.623	2.610	2.597	2.569	2.582	2.574	2.595	2.619
Ti ⁴⁺	0.082	0.076	0.081	0.082	0.078	0.092	0.073	0.060	0.065	0.064	0.067	0.056	0.098
Al ³⁺	1.957	1.946	1.928	1.898	1.907	1.927	1.901	1.962	1.983	1.985	1.986	1.964	1.923
Cl ³⁺	0.001	0.001	0.004	0.002	0.000	0.002	0.004	0.009	0.004	0.007	0.006	0.007	0.008
V ³⁺	0.000	0.000	0.000	0.000	0.000	0.000	0.000	0.000	0.011	0.010	0.009	0.008	0.010
Fe ³⁺	0.000	0.000	0.000	0.000	0.000	0.000	0.000	0.000	0.000	0.000	0.000	0.000	0.000
Mg ²⁺	2.014	2.037	1.995	2.015	2.040	2.000	2.095	2.054	2.062	2.032	2.035	2.062	1.971
Mn ²⁺	0.001	0.001	0.001	0.000	0.004	0.001	0.000	0.001	0.002	0.000	0.003	0.002	0.004
Fe ²⁺	0.164	0.171	0.156	0.170	0.174	0.170	0.192	0.172	0.169	0.171	0.182	0.168	0.164
Zn ²⁺	0.000	0.000	0.000	0.000	0.000	0.000	0.000	0.000	0.000	0.000	0.000	0.000	0.000
Ca ²⁺	0.002	0.000	0.007	0.007	0.004	0.000	0.001	0.002	0.000	0.000	0.000	0.000	0.003
Ba ²⁺	0.003	0.005	0.009	0.010	0.008	0.008	0.003	0.003	0.004	0.006	0.003	0.003	0.010
Na ⁺	0.019	0.018	0.018	0.011	0.017	0.016	0.017	0.018	0.016	0.024	0.016	0.020	0.016
K ⁺	0.979	0.978	0.985	0.969	0.971	0.980	0.955	0.979	0.982	0.964	0.972	0.964	0.989
F ⁻	0.049	0.058	0.067	0.069	0.063	0.058	0.063	0.054	0.120	0.116	0.110	0.145	0.083
Cl ⁻	0.000	0.000	0.002	0.002	0.002	0.000	0.001	0.002	0.001	0.002	0.000	0.001	0.001
OH ⁻	1.951	1.942	1.931	1.929	1.935	1.942	1.936	1.944	1.879	1.882	1.890	1.854	1.915
vac. (M)	0.173	0.160	0.200	0.186	0.167	0.186	0.125	0.145	0.135	0.148	0.138	0.136	0.203
O ²⁻	10	10	10	10	10	10	10	10	10	10	10	10	10

Appendix A.3: Compositions of phlogopite from lithologies within marble at the Revelstoke Occurrence (con't)

pos. And min. assoc. EPMA point	r Ms G11-02-07b-31	r G11-02-07a-35	c G11-02-07a-36	r G11-02-07a-37	r G11-02-07a-38	r Cal G11-02-11-42	c G11-02-11-43	c G11-02-11-44	r Cal G11-02-11-45	c G11-02-11-48	c TD-G014-07A2-01-57
SiO ₂ wt.%	37.64	37.19	37.1	37.69	37.58	36.96	37.12	38.45	37.54	37.78	35.52
TiO ₂	1.97	1.43	1.46	1.67	1.53	1.36	1.7	1.35	1.18	1.44	1.63
Al ₂ O ₃	23.66	24.25	24.09	23.43	23.6	23.69	23.32	23.71	23.7	23.18	23.18
Cr ₂ O ₃	0.04	0.04	0	0.06	0.16	0.05	0.05	0.06	0.01	0.12	0.19
V ₂ O ₃	0.2	0.19	0.12	0.15	0.17	0.2	0.17	0.12	0.12	0.12	0.27
Fe ₂ O ₃	0	0	0	0	0	0	0	0	0	0	0
MgO	19.59	20	20.06	19.59	20.01	19.79	19.28	19.74	20.67	19.7	17.99
MnO	0.08	0.04	0	0.04	0.03	0.08	0.04	0.1	0.02	0.05	0
FeOt _{tot}	2.94	2.98	2.95	2.74	2.9	2.96	2.95	2.81	2.86	3.01	5.02
ZnO											
CaO	0.03	0.04	0.02	0.03	0.02	0.01	0.03	0	0.02	0.03	0.1
BaO	0.28	0.11	0.02	0.33	0.17	0.17	0.16	0.3	0.29	0.35	0.14
Na ₂ O	0.16	0.15	0.12	0.13	0.15	0.17	0.13	0.15	0.13	0.13	0.16
K ₂ O	10.96	11.04	11.1	10.99	11.02	10.99	10.96	11.01	11.03	10.9	10.15
F	0.3	0.28	0.42	0.51	0.57	0.37	0.47	0.21	0.57	0.24	0.61
CL	0.01	0.02	0	0.01	0	0	0	0.01	0	0.02	0.02
H ₂ O *	4.20	4.20	4.13	4.07	4.07	4.12	4.05	4.26	4.08	4.19	3.87
- (O=F,Cl)	-0.13	-0.12	-0.18	-0.22	-0.24	-0.16	-0.20	-0.09	-0.24	-0.11	-0.26
TOTAL	101.93	101.84	101.41	101.22	101.74	100.76	100.23	102.19	101.98	101.15	98.59
Si ⁴⁺ apfu	2.598	2.568	2.571	2.617	2.598	2.582	2.605	2.640	2.590	2.627	2.557
Ti ⁴⁺	0.102	0.074	0.076	0.087	0.080	0.071	0.090	0.070	0.061	0.075	0.088
Al ³⁺	1.925	1.974	1.968	1.918	1.923	1.951	1.929	1.919	1.927	1.900	1.966
Cl ³⁺	0.002	0.002	0.000	0.003	0.009	0.003	0.003	0.003	0.001	0.007	0.011
V ³⁺	0.011	0.011	0.007	0.008	0.009	0.011	0.010	0.007	0.007	0.007	0.016
Fe ³⁺	0.000	0.000	0.000	0.000	0.000	0.000	0.000	0.000	0.000	0.000	0.000
Mg ²⁺	2.016	2.059	2.072	2.028	2.062	2.061	2.017	2.020	2.126	2.042	1.930
Mn ²⁺	0.005	0.002	0.000	0.002	0.002	0.005	0.002	0.006	0.001	0.003	0.000
Fe ²⁺	0.170	0.172	0.171	0.159	0.168	0.173	0.173	0.161	0.165	0.175	0.302
Zn ²⁺	0.000	0.000	0.000	0.000	0.000	0.000	0.000	0.000	0.000	0.000	0.000
Ca ²⁺	0.002	0.003	0.001	0.002	0.001	0.001	0.002	0.000	0.001	0.002	0.008
Ba ²⁺	0.008	0.003	0.001	0.009	0.005	0.005	0.004	0.008	0.008	0.010	0.004
Na ⁺	0.021	0.020	0.016	0.018	0.020	0.023	0.018	0.020	0.017	0.018	0.022
K ⁺	0.965	0.973	0.981	0.974	0.972	0.980	0.981	0.964	0.971	0.967	0.932
F ⁻	0.065	0.061	0.092	0.112	0.125	0.082	0.104	0.046	0.124	0.053	0.139
Cl ⁻	0.001	0.002	0.000	0.001	0.000	0.000	0.000	0.001	0.000	0.002	0.002
OH ⁻	1.933	1.937	1.908	1.887	1.875	1.918	1.896	1.953	1.876	1.945	1.859
vac. (M)	0.172	0.138	0.135	0.176	0.150	0.143	0.171	0.174	0.122	0.164	0.130
O ²⁻	10	10	10	10	10	10	10	10	10	10	10

Appendix A.3: Compositions of phlogopite from lithologies within marble at the Revelstoke Occurrence (con't)

pos. And min. assoc. EPMA point	r Kfs TD-G014-07A2-01-64	c TD-G014-07A2-01-65	c TD-G014-07A2-01-70	r Cal TD-G014-07A2-01-71	r An TD-G014-07B1-1-4	c TD-G014-07B1-1-5	r Cal TD-G014-07B1-1-6	c TD-G014-07B1-1-7	m TD-G014-07B1-1-8
SiO ₂ wt.%	35.79	35.46	36.47	35.93	37.6	36.7	36.96	36.98	36.87
TiO ₂	1.65	1.78	1.66	1.5	1.74	1.91	1.85	1.71	1.63
Al ₂ O ₃	23.51	23.35	23.65	23.73	22.45	22.65	22.49	23.46	23
Cr ₂ O ₃	0.11	0.06	0.16	0.13	0.11	0.04	0.12	0.15	0.07
V ₂ O ₃	0.22	0.25	0.2	0.21	0.26	0.19	0.16	0.24	0.22
Fe ₂ O ₃	0	0	0	0	0	0	0	0	0
MgO	17.47	16.96	17.85	17.99	18.01	17.58	17.84	17.93	17.77
MnO	0	0.03	0.06	0	0.05	0	0	0	0
FeOt _{tot}	5.37	5.57	5.08	4.73	4.95	5.04	5.03	4.84	4.83
ZnO									
CaO	0.14	0.1	0.12	0.23	0.02	0.05	0.02	0.04	0.07
BaO	0.32	0.18	0.33	0.26	0.33	0.32	0.37	0.22	0.22
Na ₂ O	0.18	0.18	0.2	0.19	0.18	0.12	0.13	0.24	0.13
K ₂ O	10.47	10.51	10.59	10.32	10.42	10.61	10.42	10.49	10.49
F	0.7	0.7	0.54	0.72	1.11	0.63	0.64	0.43	0.42
CL	0.01	0.01	0.01	0.01	0.01	0.02	0	0.03	0.02
H ₂ O *	3.85	3.82	3.99	3.86	3.72	3.90	3.91	4.05	4.01
- (O=F,Cl)	-0.30	-0.30	-0.23	-0.31	-0.47	-0.27	-0.27	-0.19	-0.18
TOTAL	99.49	98.66	100.68	99.50	100.49	99.49	99.67	100.62	99.57
Si ⁴⁺ apfu	2.562	2.562	2.575	2.560	2.652	2.620	2.631	2.603	2.621
Ti ⁴⁺	0.089	0.097	0.088	0.080	0.092	0.103	0.099	0.091	0.087
Al ³⁺	1.983	1.988	1.968	1.993	1.866	1.906	1.887	1.946	1.927
Cl ³⁺	0.006	0.003	0.009	0.007	0.006	0.002	0.007	0.008	0.004
V ³⁺	0.013	0.014	0.011	0.012	0.015	0.011	0.009	0.014	0.013
Fe ³⁺	0.000	0.000	0.000	0.000	0.000	0.000	0.000	0.000	0.000
Mg ²⁺	1.864	1.826	1.879	1.911	1.894	1.871	1.893	1.881	1.884
Mn ²⁺	0.000	0.002	0.004	0.000	0.003	0.000	0.000	0.000	0.000
Fe ²⁺	0.321	0.337	0.300	0.282	0.292	0.301	0.299	0.285	0.287
Zn ²⁺	0.000	0.000	0.000	0.000	0.000	0.000	0.000	0.000	0.000
Ca ²⁺	0.011	0.008	0.009	0.018	0.002	0.004	0.002	0.003	0.005
Ba ²⁺	0.009	0.005	0.009	0.007	0.009	0.009	0.010	0.006	0.006
Na ⁺	0.025	0.025	0.027	0.026	0.025	0.017	0.018	0.033	0.018
K ⁺	0.956	0.969	0.954	0.938	0.938	0.966	0.946	0.942	0.952
F ⁻	0.158	0.160	0.121	0.162	0.248	0.142	0.144	0.096	0.094
Cl ⁻	0.001	0.001	0.001	0.001	0.001	0.002	0.000	0.004	0.002
OH ⁻	1.840	1.839	1.878	1.837	1.751	1.855	1.856	1.901	1.903
vac. (M)	0.162	0.171	0.166	0.154	0.180	0.186	0.175	0.173	0.177
O ²⁻	10	10	10	10	10	10	10	10	10

Appendix A.3: Compositions of phlogopite from lithologies within marble at the Revelstoke Occurrence (con't)

pos. And min. assoc. EPMA point	r Cal TD-G014-07B1-1-9	r An TD-G014-07B1-1-10	c TD-G014-07B1-1-11	c TD-G014-07B1-3-28	r Cal TD-G014-07B1-3-29	c TD-G014-07B1-4-38	r An TD-G014-07B1-4-39	14A1-17-1	14A1-17-2	14A1-17-3	14A1-26-10
SiO ₂ wt.%	36.59	35.99	36.17	37.19	39.52	36.79	36.41	36.2266	37.3617	37.2372	36.5598
TiO ₂	1.46	1.6	1.86	1.52	0.82	1.8	1.92	1.5418	1.9072	1.8636	1.5895
Al ₂ O ₃	23.51	23.33	23.34	24.02	19.7	22.68	23.13	23.4996	23.0792	22.2697	23.945
Cr ₂ O ₃	0.05	0.28	0.23	0.21	0.08	0	0.01	0.0547	0	0.0295	0.0463
V ₂ O ₃	0.21	0.14	0.21	0.13	0.05	0.15	0.16	0.1721	0.1879	0.2486	0.0896
Fe ₂ O ₃	0	0	0	0	0	0	0	0	0	0	0
MgO	17.94	18.15	17.26	16.83	20.47	17.96	17.62	18.0761	18.0039	18.251	17.4937
MnO	0.01	0.02	0.02	0	0.04	0.01	0	0.0034	0.0238	0.017	0.0373
FeOt _{tot}	4.95	4.93	5.26	5.19	4.19	4.91	4.91	4.8286	4.9241	4.7143	4.9151
ZnO								0.0631	0	0.0253	0.0379
CaO	0.13	0.04	0.05	0.12	0.14	0.1	0.09	0	0.0012	0.0072	0.1429
BaO	0.28	0.25	0.22	0.17	0.15	0.26	0.46	0.2595	0.4113	0.3209	0.2842
Na ₂ O	0.17	0.13	0.14	0.15	0.15	0.14	0.14	0.1422	0.1587	0.1284	0.1218
K ₂ O	10.71	10.65	10.36	10.19	10.4	10.56	10.45	10.5402	10.6474	10.6677	10.5898
F	0.67	0.38	0.67	0.62	0.97	0.42	0.49	0.3654	0.8502	0.8181	0.5569
CL	0	0.01	0	0.04	0.05	0.01	0.01	0.0183	0.0207	0.0207	0.0191
H ₂ O *	3.92	4.03	3.88	3.94	3.79	4.01	3.97	3.84	3.42	3.41	3.67
- (O=F,Cl)	-0.28	-0.16	-0.28	-0.27	-0.42	-0.18	-0.21	-0.16	-0.36	-0.35	-0.24
TOTAL	100.32	99.77	99.39	100.05	100.10	99.62	99.56	99.48	100.63	99.68	99.86
Si ⁴⁺ apfu	2.590	2.564	2.584	2.626	2.781	2.619	2.596	2.578	2.623	2.639	2.588
Ti ⁴⁺	0.078	0.086	0.100	0.081	0.043	0.096	0.103	0.083	0.101	0.099	0.085
Al ³⁺	1.961	1.959	1.965	1.999	1.634	1.903	1.944	1.971	1.909	1.860	1.998
Cl ³⁺	0.003	0.016	0.013	0.012	0.004	0.000	0.001	0.003	0.000	0.002	0.003
V ³⁺	0.012	0.008	0.012	0.007	0.003	0.009	0.009	0.010	0.011	0.014	0.005
Fe ³⁺	0.000	0.000	0.000	0.000	0.000	0.000	0.000	0.000	0.000	0.000	0.000
Mg ²⁺	1.893	1.928	1.838	1.771	2.148	1.906	1.873	1.917	1.884	1.928	1.846
Mn ²⁺	0.001	0.001	0.001	0.000	0.002	0.001	0.000	0.000	0.001	0.001	0.002
Fe ²⁺	0.293	0.294	0.314	0.306	0.247	0.292	0.293	0.287	0.289	0.279	0.291
Zn ²⁺	0.000	0.000	0.000	0.000	0.000	0.000	0.000	0.003	0.000	0.001	0.002
Ca ²⁺	0.010	0.003	0.004	0.009	0.011	0.008	0.007	0.000	0.000	0.001	0.011
Ba ²⁺	0.008	0.007	0.006	0.005	0.004	0.007	0.013	0.007	0.011	0.009	0.008
Na ⁺	0.023	0.018	0.019	0.021	0.020	0.019	0.019	0.020	0.022	0.018	0.017
K ⁺	0.967	0.968	0.944	0.918	0.934	0.959	0.951	0.957	0.953	0.964	0.956
F	0.150	0.086	0.151	0.138	0.216	0.095	0.111	0.082	0.189	0.183	0.125
Cl ⁻	0.000	0.001	0.000	0.005	0.006	0.001	0.001	0.002	0.002	0.002	0.002
OH ⁻	1.850	1.913	1.849	1.857	1.778	1.904	1.888	1.916	1.809	1.814	1.873
vac. (M)	0.169	0.144	0.171	0.198	0.137	0.175	0.181	0.151	0.182	0.178	0.183
O ²⁻	10	10	10	10	10	10	10	10	10	10	10

Appendix A.3: Compositions of phlogopite from lithologies within marble at the Revelstoke Occurrence (con't)

pos. And min. assoc.	14A1-26-11	14A1-26-16	14A1-26-17	14A1-26-18	14A1-26-19	14A1-26-20	14A1-26-21	14A1-28-25	14A1-28-26	14A1-28-27	14A1-28-28	14A1-28-29	14A1-28-30	14A1-28-31	14A1-28-32
SiO ₂ wt.%	36.7757	36.3563	35.811	36.4399	36.0712	36.1432	35.8142	36.7551	36.4966	36.2832	35.9563	36.5601	38.3428	36.3876	36.1824
TiO ₂	1.7055	1.485	1.3922	1.5017	1.7258	1.7052	1.7062	1.1993	1.5256	1.4765	1.4472	1.6011	1.5759	1.4984	1.5797
Al ₂ O ₃	23.6625	24.3793	24.2577	24.2611	23.0603	23.3698	23.5771	23.9083	23.5638	23.741	23.8561	23.3334	22.3622	22.2766	22.1995
Cr ₂ O ₃	0.0084	0.1096	0.0295	0.0126	0	0.0462	0.0631	0.0757	0.0547	0.0462	0.0421	0	0.0379	0.1052	0.1136
V ₂ O ₃	0.0783	0.0435	0.0791	0.0513	0.1664	0.086	0.1185	0.1211	0.1551	0.1162	0.1504	0.0335	0.137	0.1612	0.0852
Fe ₂ O ₃	0	0	0	0	0	0	0	0	0	0	0	0	0	0	0
MgO	17.1737	17.3956	17.5728	17.9402	17.226	17.2104	17.3333	17.2964	17.4681	17.7893	17.7353	17.2377	17.3167	18.3477	18.205
MnO	0.0204	0.0136	0.017	0.0577	0	0.0475	0	0.0916	0.0339	0.0203	0.0509	0.078	0.0373	0.0034	0
FeOt _{tot}	4.8956	4.7717	4.8015	5.0144	4.9933	5.3167	5.0332	5.4401	5.4424	5.5706	5.3761	5.4778	5.2157	5.235	5.2625
ZnO	0	0.0295	0	0	0.0757	0.0841	0.1177	0.0421	0	0.0589	0.059	0.0084	0.0421	0	0
CaO	0.03	0.0301	0.0204	0.0625	0.1283	0.1139	0.1571	0	0.0409	0.0588	0.048	0.0672	0.1345	0.0852	0.1465
BaO	0.3479	0.2451	0.1937	0.1226	0.5213	0.4011	0.5162	0.1714	0.0784	0.3547	0.071	0.3596	0.2205	0.3304	0.2277
Na ₂ O	0.0969	0.1111	0.1567	0.1595	0.1432	0.1305	0.125	0.1011	0.1432	0.1658	0.1787	0.1568	0.146	0.1526	0.1353
K ₂ O	10.9328	10.7288	10.7861	10.7886	10.5185	10.5495	10.553	10.6292	10.7694	10.659	10.4698	10.799	10.6637	10.8153	10.6255
F	0.5749	0.6609	0.815	0.6949	0.5549	0.6577	0.8287	0.3475	0.3488	0.5182	0.7786	0.7604	0.6616	1.0004	0.5727
CL	0.0278	0.0119	0.0111	0.0008	0.0032	0	0.019	0.0262	0.0008	0.0119	0.0183	0.0087	0.0318	0.0143	0.0365
H ₂ O *	3.64	3.57	3.39	3.57	3.61	3.54	3.35	3.87	3.88	3.71	3.43	3.45	3.59	3.19	3.58
- (O=F,Cl)	-0.25	-0.28	-0.35	-0.29	-0.23	-0.28	-0.35	-0.15	-0.15	-0.22	-0.33	-0.32	-0.29	-0.42	-0.25
TOTAL	99.72	99.66	98.98	100.38	98.57	99.12	98.96	99.92	99.85	100.36	99.33	99.61	100.23	99.18	98.70
Si ⁴⁺ apfu	2.610	2.576	2.556	2.565	2.597	2.587	2.567	2.605	2.592	2.569	2.561	2.604	2.700	2.604	2.603
Ti ⁴⁺	0.091	0.079	0.075	0.080	0.093	0.092	0.092	0.064	0.082	0.079	0.078	0.086	0.083	0.081	0.085
Al ³⁺	1.979	2.036	2.041	2.013	1.956	1.972	1.992	1.997	1.972	1.981	2.002	1.959	1.856	1.879	1.882
Cl ³⁺	0.000	0.006	0.002	0.001	0.000	0.003	0.004	0.004	0.003	0.003	0.002	0.000	0.002	0.006	0.006
V ³⁺	0.004	0.002	0.005	0.003	0.010	0.005	0.007	0.007	0.009	0.007	0.009	0.002	0.008	0.009	0.005
Fe ³⁺	0.000	0.000	0.000	0.000	0.000	0.000	0.000	0.000	0.000	0.000	0.000	0.000	0.000	0.000	0.000
Mg ²⁺	1.817	1.837	1.870	1.883	1.849	1.837	1.852	1.827	1.849	1.878	1.883	1.830	1.818	1.957	1.952
Mn ²⁺	0.001	0.001	0.001	0.003	0.000	0.003	0.000	0.005	0.002	0.001	0.003	0.005	0.002	0.000	0.000
Fe ²⁺	0.291	0.283	0.287	0.295	0.301	0.318	0.302	0.322	0.323	0.330	0.320	0.326	0.307	0.313	0.317
Zn ²⁺	0.000	0.002	0.000	0.000	0.004	0.004	0.006	0.002	0.000	0.003	0.003	0.000	0.002	0.000	0.000
Ca ²⁺	0.002	0.002	0.002	0.005	0.010	0.009	0.012	0.000	0.003	0.004	0.004	0.005	0.010	0.007	0.011
Ba ²⁺	0.010	0.007	0.005	0.003	0.015	0.011	0.015	0.005	0.002	0.010	0.002	0.010	0.006	0.009	0.006
Na ⁺	0.013	0.015	0.022	0.022	0.020	0.018	0.017	0.014	0.020	0.023	0.025	0.022	0.020	0.021	0.019
K ⁺	0.990	0.970	0.982	0.969	0.966	0.963	0.965	0.961	0.976	0.963	0.951	0.981	0.958	0.987	0.975
F ⁻	0.129	0.148	0.184	0.155	0.126	0.149	0.188	0.078	0.078	0.116	0.175	0.171	0.147	0.226	0.130
Cl ⁻	0.003	0.001	0.001	0.000	0.000	0.000	0.002	0.003	0.000	0.001	0.002	0.001	0.004	0.002	0.004
OH ⁻	1.868	1.850	1.815	1.845	1.873	1.851	1.810	1.919	1.922	1.883	1.822	1.828	1.849	1.772	1.865
vac. (M)	0.206	0.180	0.164	0.157	0.195	0.184	0.184	0.167	0.168	0.153	0.142	0.188	0.224	0.151	0.150
O ²⁻	10	10	10	10	10	10	10	10	10	10	10	10	10	10	10

Appendix A.3: Compositions of phlogopite from lithologies within marble at the Revelstoke Occurrence (con't)

pos. And min. assoc.	14A1-28-33	14A1-28-34	14A1-28-35	14A1-28-36	14A1-28-37	14A1-28-38	14A1-28-39	14A1-28-40	14A1-28-41	14A1-28-42	14A1-28-43	14A1-28-44	14A1-28-45	14A1-28-47	14A1-28-48
SiO ₂ wt.%	36.2701	36.6534	36.2373	36.1166	36.3998	37.7722	36.4431	36.487	36.3932	36.3142	36.15	36.2004	35.9659	36.753	36.2189
TiO ₂	1.6256	1.6435	1.5525	1.4039	1.4765	1.8889	1.7339	1.4161	1.5697	1.5964	1.74	1.6791	1.5642	1.8434	1.8697
Al ₂ O ₃	23.5753	22.8551	22.7861	23.9293	23.2544	22.1357	22.9452	23.2935	23.4449	24.0196	23.1244	23.3163	23.2238	22.8712	23.289
Cr ₂ O ₃	0.0883	0.0462	0.0631	0.0673	0.122	0.0126	0.0084	0.0968	0.0715	0.0883	0.0757	0.0714	0.0757	0.1345	0.0378
V ₂ O ₃	0.1342	0.0975	0.1892	0.108	0.1162	0.1469	0.1283	0.0878	0.0985	0.1328	0.1048	0.1669	0.1273	0.1093	0.1162
Fe ₂ O ₃	0	0	0	0	0	0	0	0	0	0	0	0	0	0	0
MgO	17.5134	17.4364	17.664	18.1534	18.2936	17.4743	17.4527	18.091	17.2188	17.3234	17.2487	17.1692	17.5367	17.8034	17.2214
MnO	0.0237	0.0203	0	0.017	0.0712	0	0.0034	0.0238	0.0305	0.0034	0.0678	0.0678	0	0	0.0475
FeOt _{tot}	5.3091	5.5888	5.1916	5.2911	5.2701	5.3533	5.5587	5.2718	5.5732	5.6528	5.5014	5.6644	5.2639	5.4753	5.3924
ZnO	0.1178	0.164	0.0084	0.0884	0	0	0.0295	0.021	0	0	0.0463	0.0463	0.0547	0	0.1093
CaO	0	0.0264	0.0468	0.024	0.0432	0.0036	0.0228	0.0529	0.0384	0.2305	0.0468	0.0648	0.1405	0.0216	0
BaO	0.2227	0.3692	0.5162	0.1371	0.3011	0.3182	0.23	0.2351	0.1444	0.1346	0.1908	0.2079	0.1641	0.4182	0.2935
Na ₂ O	0.1539	0.1215	0.125	0.0957	0.1351	0.1093	0.1305	0.1153	0.1385	0.1474	0.0884	0.1004	0.0749	0.1225	0.1055
K ₂ O	10.7634	10.5893	10.4789	10.6642	10.6436	10.7859	10.6167	10.9294	10.7361	10.6399	10.8918	11.0962	10.8811	10.6823	10.9466
F	0.5554	0.6386	0.7766	0.6234	0.3821	0.4532	0.7268	0.2958	0.9165	0.3482	0.5219	0.6595	0.66	0.3476	0.5732
CL	0.0183	0.0143	0.0056	0.004	0.0143	0.027	0.0262	0.0103	0.004	0	0.0174	0.0166	0.0309	0.0127	0.0111
H ₂ O *	3.66	3.56	3.40	3.62	3.85	3.77	3.46	3.93	3.29	3.89	3.66	3.54	3.51	3.88	3.63
- (O=F,Cl)	-0.24	-0.27	-0.33	-0.26	-0.16	-0.20	-0.31	-0.13	-0.39	-0.15	-0.22	-0.28	-0.28	-0.15	-0.24
TOTAL	99.79	99.56	98.71	100.08	100.20	100.06	99.21	100.23	99.28	100.38	99.25	99.79	98.99	100.33	99.61
Si ⁴⁺ apfu	2.579	2.615	2.603	2.557	2.579	2.675	2.604	2.587	2.596	2.568	2.589	2.583	2.579	2.604	2.585
Ti ⁴⁺	0.087	0.088	0.084	0.075	0.079	0.101	0.093	0.076	0.084	0.085	0.094	0.090	0.084	0.098	0.100
Al ³⁺	1.976	1.921	1.929	1.996	1.942	1.847	1.933	1.946	1.971	2.002	1.952	1.961	1.963	1.910	1.959
Cl ³⁺	0.005	0.003	0.004	0.004	0.007	0.001	0.000	0.005	0.004	0.005	0.004	0.004	0.004	0.008	0.002
V ³⁺	0.008	0.006	0.011	0.006	0.007	0.008	0.007	0.005	0.006	0.008	0.006	0.010	0.007	0.006	0.007
Fe ³⁺	0.000	0.000	0.011	0.000	0.000	0.000	0.000	0.000	0.000	0.000	0.000	0.000	0.000	0.000	0.000
Mg ²⁺	1.857	1.854	1.892	1.916	1.932	1.845	1.859	1.912	1.831	1.826	1.842	1.826	1.875	1.881	1.832
Mn ²⁺	0.001	0.001	0.000	0.001	0.004	0.000	0.000	0.001	0.002	0.000	0.004	0.004	0.000	0.000	0.003
Fe ²⁺	0.316	0.333	0.312	0.313	0.312	0.317	0.332	0.313	0.332	0.334	0.330	0.338	0.316	0.324	0.322
Zn ²⁺	0.006	0.009	0.000	0.005	0.000	0.000	0.002	0.001	0.000	0.000	0.002	0.002	0.003	0.000	0.006
Ca ²⁺	0.000	0.002	0.004	0.002	0.003	0.000	0.002	0.004	0.003	0.017	0.004	0.005	0.011	0.002	0.000
Ba ²⁺	0.006	0.010	0.015	0.004	0.008	0.009	0.006	0.007	0.004	0.004	0.005	0.006	0.005	0.012	0.008
Na ⁺	0.021	0.017	0.017	0.013	0.019	0.015	0.018	0.016	0.019	0.020	0.012	0.014	0.010	0.017	0.015
K ⁺	0.976	0.964	0.960	0.963	0.962	0.974	0.968	0.989	0.977	0.960	0.995	1.010	0.995	0.966	0.997
F ⁻	0.125	0.144	0.176	0.140	0.086	0.101	0.164	0.066	0.207	0.078	0.118	0.149	0.150	0.078	0.129
Cl ⁻	0.002	0.002	0.001	0.000	0.002	0.003	0.003	0.001	0.000	0.000	0.002	0.002	0.004	0.002	0.001
OH ⁻	1.873	1.854	1.823	1.860	1.913	1.895	1.833	1.932	1.793	1.922	1.880	1.849	1.847	1.921	1.869
vac. (M)	0.172	0.179	0.166	0.133	0.138	0.207	0.170	0.155	0.175	0.172	0.179	0.185	0.172	0.169	0.189
O ²⁻	10	10	10	10	10	10	10	10	10	10	10	10	10	10	10

Appendix A.3: Compositions of phlogopite from lithologies within marble at the Revelstoke Occurrence (con't)

pos. And min. assoc.	14A1-28-49	14A1-28-53	14A1-28-54	14A1-28-55	1102-06-1	1102-06-2	1102-06-3	1102-06-4	1102-06-5	1102-06-6	1102-06-9	1102-06-10	1102-06-11	1102-06-12	1102-06-13
SiO ₂ wt.%	36.74	37.718	37.4951	37.3636	37.566	37.6133	36.8518	36.0931	37.3544	37.3291	36.5199	37.0895	36.9883	36.7633	36.5864
TiO ₂	1.9224	2.1825	2.1745	2.1025	1.6445	1.6136	1.2588	1.2846	1.6396	1.6522	1.4962	1.5261	1.2524	1.354	1.1973
Al ₂ O ₃	23.159	22.7373	22.3471	22.5368	23.0619	23.186	23.5329	24.0587	23.8519	23.2193	24.0216	23.5764	23.6238	24.249	24.1161
Cr ₂ O ₃	0.0042	0.08	0.0546	0.0631	0	0.0212	0	0.0212	0.0255	0	0.0127	0.0594	0.0382	0.0637	0
V ₂ O ₃	0.1431	0.1747	0.1507	0.1472	0.1212	0.1248	0.138	0.116	0.1616	0.0819	0.091	0.1037	0.118	0.1068	0.1381
Fe ₂ O ₃	0	0	0	0	0	0	0	0	0	0	0	0	0	0	0
MgO	17.5186	17.1839	16.8048	17.0197	19.5313	19.434	19.722	19.2034	18.9872	19.2279	19.6666	19.4717	19.5096	19.93	19.7341
MnO	0.0034	0	0	0.0203	0.0204	0.0715	0.0238	0	0.0989	0.0102	0.0068	0.017	0	0.058	0.0341
FeOt _{tot}	5.6338	5.2356	5.582	5.4449	2.8902	2.9488	2.9198	3.61	2.6722	2.5964	2.8656	2.6261	3.1152	2.8902	2.7827
ZnO	0.0126	0	0.0673	0.0294	0	0.0253	0.1013	0.0802	0	0	0.0634	0.1351	0.076	0.0085	0.0169
CaO	0	0	0.0539	0.0408	0.0277	0.0675	0.1388	0.0374	0.0278	0.0205	0.0097	0.0012	0.076	0.0229	0
BaO	0.2201	0.3719	0.3276	0.3522	0.5584	0.5705	0.3103	0.1844	0.1823	0.4433	0.1896	0.3545	0.133	0.0961	0.1257
Na ₂ O	0.1531	0.1028	0.1482	0.0767	0.1039	0.0951	0.1242	0.1492	0.1163	0.161	0.124	0.1304	0.0896	0.1672	0.1225
K ₂ O	10.6887	10.7539	10.6923	10.7609	10.7082	10.9493	11.211	10.7842	10.8191	10.9755	10.8667	10.7137	10.6612	10.7666	11.0332
F	0.6935	0.6109	0.54	0.6614	0.6492	0.7886	0.5097	0.3679	0.4083	0.4942	0.5632	0.5632	0.4399	0.4761	0.5986
CL	0	0	0.0341	0.019	0.0104	0.0127	0.0096	0.0319	0.0128	0	0	0.008	0.0072	0.004	0.0104
H ₂ O *	3.55	3.66	3.67	3.56	3.64	3.51	3.76	3.86	3.88	3.78	3.72	3.71	3.83	3.83	3.67
- (O=F,Cl)	-0.29	-0.26	-0.24	-0.28	-0.28	-0.33	-0.22	-0.16	-0.17	-0.21	-0.24	-0.24	-0.19	-0.20	-0.25
TOTAL	100.15	100.55	99.91	99.92	100.25	100.70	100.40	99.72	100.06	99.78	99.98	99.85	99.77	100.59	99.92
Si ⁴⁺ apfu	2.601	2.654	2.662	2.650	2.628	2.623	2.585	2.551	2.612	2.624	2.562	2.602	2.599	2.561	2.567
Ti ⁴⁺	0.102	0.116	0.116	0.112	0.087	0.085	0.066	0.068	0.086	0.087	0.079	0.081	0.066	0.071	0.063
Al ³⁺	1.932	1.886	1.870	1.884	1.901	1.906	1.945	2.004	1.966	1.924	1.986	1.949	1.956	1.991	1.994
Cl ³⁺	0.000	0.004	0.003	0.004	0.000	0.001	0.000	0.001	0.001	0.000	0.001	0.003	0.002	0.004	0.000
V ³⁺	0.008	0.010	0.009	0.008	0.007	0.007	0.008	0.007	0.009	0.005	0.005	0.006	0.007	0.006	0.008
Fe ³⁺	0.000	0.000	0.000	0.000	0.000	0.000	0.000	0.000	0.000	0.000	0.000	0.000	0.000	0.000	0.000
Mg ²⁺	1.849	1.803	1.779	1.800	2.037	2.021	2.062	2.023	1.979	2.015	2.057	2.037	2.043	2.070	2.064
Mn ²⁺	0.000	0.000	0.000	0.001	0.001	0.004	0.001	0.000	0.006	0.001	0.000	0.001	0.000	0.003	0.002
Fe ²⁺	0.334	0.308	0.331	0.323	0.169	0.172	0.171	0.213	0.156	0.153	0.168	0.154	0.183	0.168	0.163
Zn ²⁺	0.001	0.000	0.004	0.002	0.000	0.001	0.005	0.004	0.000	0.000	0.003	0.007	0.004	0.000	0.001
Ca ²⁺	0.000	0.000	0.004	0.003	0.002	0.005	0.010	0.003	0.002	0.002	0.001	0.000	0.006	0.002	0.000
Ba ²⁺	0.006	0.010	0.009	0.010	0.015	0.016	0.009	0.005	0.005	0.012	0.005	0.010	0.004	0.003	0.003
Na ⁺	0.021	0.014	0.020	0.011	0.014	0.013	0.017	0.020	0.016	0.022	0.017	0.018	0.012	0.023	0.017
K ⁺	0.965	0.965	0.968	0.974	0.956	0.974	1.003	0.972	0.965	0.984	0.973	0.959	0.955	0.957	0.988
F ⁻	0.155	0.136	0.121	0.148	0.144	0.174	0.113	0.082	0.090	0.110	0.125	0.125	0.098	0.105	0.133
Cl ⁻	0.000	0.000	0.004	0.002	0.001	0.002	0.001	0.004	0.002	0.000	0.000	0.001	0.001	0.000	0.001
OH ⁻	1.845	1.864	1.875	1.849	1.855	1.825	1.886	1.914	1.908	1.890	1.875	1.874	1.901	1.895	1.866
vac. (M)	0.174	0.220	0.230	0.217	0.171	0.181	0.162	0.133	0.184	0.192	0.141	0.167	0.144	0.126	0.138
O ²⁻	10	10	10	10	10	10	10	10	10	10	10	10	10	10	10

Appendix A.3: Compositions of phlogopite from lithologies within marble at the Revelstoke Occurrence (con't)

pos. And min. assoc.	1102-06-14	1102-06-15	1102-06-16	1102-06-17	1102-06-18	III-1	III-2	III-3	III-4	III-5	III-6	III-7	III-10	III-11	III-12	III-13	III-14	III-15	III-16	III-17	III-18	III-19
SiO ₂ , wt.%	36.8622	38.1143	36.8742	38.2357	37.019	40.312	40.06	37.95	36.957	37.9	37.71	36.78	38.326	38.26	39.416	39.154	39.498	38.15	37.25	37.21	37.18	37.49
TiO ₂	1.2375	1.7167	1.3279	1.6046	1.4104	0.8451	0.843	0.828	0.9354	0.885	0.861	0.63	1.1507	1.087	1.04	1.1266	1.1224	1.115	0.881	1.011	0.947	1.103
Al ₂ O ₃	23.774	23.1203	24.6414	22.5399	23.9995	18.343	17.34	19.78	21.471	20.24	20.7	22	19.429	19.36	19.43	18.87	18.756	20.05	21.09	20.69	20.93	20.44
Cr ₂ O ₃	0.034	0.0297	0.0679	0.0552	0.0255	0	0.051	0.03	0.0508	0	0.072	0	0.0381	0	0.1228	0.0594	0	0	0.004	0.038	0.047	0.11
V ₂ O ₃	0.0952	0.0942	0.0388	0.0884	0.1452	0.2357	0.154	0.155	0.2945	0.238	0.242	0.228	0.3172	0.259	0.2439	0.2724	0.2702	0.334	0.335	0.257	0.295	0.261
Fe ₂ O ₃	0	0	0	0	0	0	0	0	0	0	0	0	0	0	0	0	0	0	0	0	0	0
MgO	19.9118	18.828	19.2116	19.2938	19.3466	24.406	24.31	23.69	22.869	23.34	23.11	22.4	23.735	23.56	23.952	24.091	24.158	23.54	22.69	23.28	22.62	22.73
MnO	0.0273	0.0409	0.0034	0.0068	0.0545	0	0	0	0.0473	0.034	0	0	0	0	0	0.0169	0	0	0.024	0.041	0	
FeOt _{tot}	2.7902	2.6573	2.9629	2.5899	2.757	1.3443	1.28	1.508	1.3645	1.305	1.217	1.377	1.5282	1.623	1.7436	1.4186	1.464	1.364	1.44	1.476	1.331	1.475
ZnO	0.0929	0.1013	0.0507	0.0887	0.0549	0.0623	0	0.046	0.0166	0	0.087	0.083	0.0539	0.046	0.0788	0.1162	0.0955	0.046	0.05	0.095	0	0.079
CaO	0.0133	0	0	0.0338	0.0048	0.0049	0	0.057	0.0448	0.013	0.018	0.108	0	0.022	0.0085	0.0389	0	0.049	0.05	0.069	0.052	0.017
BaO	0.1626	0.298	0.2487	0.3768	0.357	0.3763	0.366	0.796	1.3722	0.933	1.053	1.376	0.7952	0.798	0.7462	0.5431	0.5407	1.158	1.279	1.294	1.26	1.443
Na ₂ O	0.1418	0.1063	0.1331	0.1269	0.1306	0.4571	0.4	0.499	0.6196	0.513	0.562	0.538	0.4742	0.484	0.5297	0.4782	0.456	0.512	0.638	0.518	0.572	0.484
K ₂ O	10.9517	10.7671	10.9749	10.6771	11.1716	9.9142	9.909	9.597	9.6135	9.579	9.601	9.504	9.8162	9.902	9.7262	9.9495	9.7345	9.56	9.485	9.724	9.667	9.507
F	0.6501	0.478	0.5624	0.8966	0.7032	2.2755	1.542	1.445	1.5993	1.085	1.297	0.911	1.3849	1.514	0.9878	1.2091	0.8927	0.786	0.732	0.766	0.768	1.16
CL	0.0167	0.0112	0.0128	0.0207	0.0159	0	0.008	0.005	0.0199	0.002	0.02	0.007	0.0176	0.022	0.0038	0.0238	0.0246	0.022	0.015	0.015	0	0.015
H ₂ O *	3.63	3.81	3.74	3.38	3.59	3.59	3.59	3.59	3.59	3.59	3.59	3.59	3.59	3.59	3.59	3.59	3.59	3.59	3.59	3.59	3.59	3.59
- (O=F,Cl)	-0.28	-0.20	-0.24	-0.38	-0.30	-0.96	-0.65	-0.61	-0.68	-0.46	-0.55	-0.39	-0.59	-0.64	-0.42	-0.51	-0.38	-0.34	-0.31	-0.33	-0.32	-0.49
TOTAL	100.11	99.97	100.61	99.63	100.48	101.20	99.20	99.36	100.18	99.20	99.58	99.15	100.07	99.88	101.20	100.42	100.23	99.93	99.21	99.72	98.97	99.41
Si ⁴⁺ apfu	2.581	2.665	2.570	2.679	2.587	2.787	2.817	2.677	2.601	2.670	2.654	2.602	2.687	2.692	2.720	2.726	2.744	2.670	2.630	2.621	2.633	2.652
Ti ⁴⁺	0.065	0.090	0.070	0.085	0.074	0.044	0.045	0.044	0.050	0.047	0.046	0.034	0.061	0.058	0.054	0.059	0.059	0.047	0.054	0.050	0.059	0.059
Al ³⁺	1.962	1.905	2.024	1.861	1.976	1.495	1.437	1.645	1.781	1.681	1.717	1.834	1.605	1.606	1.580	1.548	1.536	1.654	1.755	1.718	1.747	1.704
Cl ³⁺	0.002	0.002	0.004	0.003	0.001	0.000	0.003	0.002	0.003	0.000	0.004	0.000	0.002	0.000	0.007	0.003	0.000	0.000	0.000	0.002	0.003	0.006
V ³⁺	0.005	0.005	0.002	0.005	0.008	0.013	0.009	0.009	0.017	0.013	0.014	0.013	0.018	0.015	0.013	0.015	0.015	0.019	0.019	0.015	0.017	0.015
Fe ³⁺	0.000	0.000	0.000	0.000	0.000	0.000	0.000	0.000	0.000	0.000	0.000	0.000	0.000	0.000	0.000	0.000	0.000	0.000	0.000	0.000	0.000	
Mg ²⁺	2.079	1.963	1.996	2.015	2.015	2.516	2.548	2.491	2.399	2.452	2.424	2.362	2.481	2.472	2.464	2.500	2.502	2.456	2.388	2.444	2.388	2.397
Mn ²⁺	0.002	0.002	0.000	0.000	0.003	0.000	0.000	0.000	0.003	0.002	0.000	0.000	0.000	0.000	0.000	0.001	0.000	0.000	0.001	0.002	0.000	
Fe ²⁺	0.163	0.155	0.173	0.152	0.161	0.078	0.075	0.089	0.080	0.077	0.072	0.081	0.090	0.096	0.101	0.083	0.085	0.080	0.085	0.087	0.079	0.087
Zn ²⁺	0.005	0.005	0.003	0.005	0.003	0.003	0.000	0.002	0.001	0.000	0.005	0.004	0.003	0.002	0.004	0.006	0.005	0.002	0.003	0.005	0.000	0.004
Ca ²⁺	0.001	0.000	0.000	0.003	0.000	0.000	0.000	0.004	0.003	0.001	0.001	0.008	0.000	0.002	0.001	0.003	0.000	0.004	0.004	0.005	0.001	
Ba ²⁺	0.004	0.008	0.007	0.010	0.010	0.010	0.010	0.022	0.038	0.026	0.029	0.038	0.022	0.022	0.020	0.015	0.015	0.032	0.035	0.036	0.040	
Na ⁺	0.019	0.014	0.018	0.017	0.018	0.061	0.054	0.068	0.085	0.070	0.077	0.074	0.064	0.066	0.071	0.065	0.061	0.069	0.087	0.071	0.078	0.066
K ⁺	0.978	0.960	0.976	0.954	0.996	0.875	0.889	0.864	0.863	0.861	0.862	0.857	0.878	0.889	0.856	0.884	0.863	0.853	0.854	0.874	0.873	0.858
F	0.144	0.106	0.124	0.199	0.155	0.498	0.343	0.322	0.356	0.242	0.289	0.204	0.307	0.337	0.216	0.266	0.196	0.174	0.164	0.171	0.172	0.260
Cl ⁻	0.002	0.001	0.002	0.002	0.002	0.000	0.001	0.001	0.002	0.000	0.002	0.001	0.000	0.003	0.003	0.002	0.002	0.000	0.002	0.000	0.002	
OH ⁻	1.854	1.893	1.875	1.799	1.843	1.502	1.656	1.677	1.642	1.758	1.709	1.795	1.691	1.661	1.784	1.731	1.801	1.823	1.835	1.828	1.739	
vac. (M)	0.140	0.212	0.161	0.201	0.174	0.067	0.067	0.043	0.067	0.057	0.071	0.075	0.056	0.063	0.062	0.066	0.059	0.064	0.076	0.059	0.081	0.080
O ²⁻	10	10	10	10	10	10	10	10	10	10	10	10	10	10	10	10	10	10	10	10	10	10

Appendix A.3: Compositions of phlogopite from lithologies within marble at the Revelstoke Occurrence (con't)

pos. And min. assoc. EPMA point	III-20	III-21	IV-22	IV-23	IV-24	IV-25	IV-26	IV-27	IV-28	IV-29	IV-30	r Kfs TD-G063B-09-15-7	r Kfs TD-G063B-09-15-8	c TD-G063B-09-9	m TD-G063B-09-10	r Cal TD-G063B-09-11	c TD-G020-07B2-11-9
SiO ₂ wt.%	38.05	37.253	39.94	39.19	38.78	38.71	38.64	37.35	39.382	37.46	38.957	36.12	36.64	37.44	36.97	36.76	38.26
TiO ₂	1.131	0.9878	1.142	1.137	1.133	1.087	1.095	1.132	1.1355	1.012	1.1568	1.94	1.95	2.23	2.01	1.68	2.12
Al ₂ O ₃	19.43	21.201	17.75	18.45	18.93	18.73	19.21	20.54	18.75	20.27	19.002	22.14	22.31	20.42	21.91	22.84	18.51
Cr ₂ O ₃	0.076	0.0804	0	0.042	0.068	0.03	0.025	0.14	0.0424	0.123	0.144	0.07	0.09	0.05	0.11	0	0.17
V ₂ O ₃	0.358	0.2658	0.221	0.218	0.29	0.31	0.295	0.314	0.2779	0.348	0.2557	0.05	0.09	0.06	0.07	0.09	0.18
Fe ₂ O ₃	0	0	0	0	0	0	0	0	0	0	0	0	0	0	0	0	0
MgO	23.49	23.103	24.24	23.79	23.71	23.53	23.67	23.16	24.129	23.25	24.025	18.62	18.52	18.14	18.25	18.67	21.9
MnO	0	0.0439	0.058	0.017	0	0	0.017	0.034	0	0.01	0	0	0.04	0.04	0.05	0.04	0
FeOt _{tot}	1.416	1.497	1.43	1.479	1.511	1.304	1.4	1.356	1.5203	1.592	1.4543	4.44	4.45	4.99	4.88	4.74	3.18
ZnO	0.012	0.0538	0.087	0	0.12	0	0.021	0.037	0	0.021	0.0747						
CaO	0.001	0.0157	0.08	0.09	0.073	0.009	0.018	0.041	0.0194	0	0.0279	0.03	0.01	0.01	0	0.04	0.06
BaO	1.04	1.3648	0.55	0.403	0.842	0.867	0.744	1.504	0.5922	1.157	0.923	0.5	0.49	0.51	0.38	0.32	0.13
Na ₂ O	0.457	0.518	0.422	0.488	0.49	0.477	0.521	0.529	0.4515	0.492	0.4994	0.16	0.18	0.08	0.12	0.19	0.04
K ₂ O	9.668	9.4889	9.751	9.569	9.383	9.742	9.72	9.409	9.983	9.648	9.7684	10.47	10.42	10.6	10.56	10.34	10.59
F	0.938	0.9791	1.159	0.728	0.839	1.156	0.924	0.997	1.1262	1.098	0.6392	0.68	0.8	0.71	0.77	0.78	0.71
CL	0.005	0.0245	0.035	0.032	0.034	0.003	0.008	0.018	0.0606	0.022	0.0038	0.05	0.05	0.02	0.03	0.02	0.02
H ₂ O *	3.59	3.59	3.59	3.59	3.59	3.59	3.59	3.59	3.59	3.59	3.59	3.83	3.81	3.82	3.83	3.86	3.92
- (O=F,Cl)	-0.40	-0.42	-0.50	-0.31	-0.36	-0.49	-0.39	-0.42	-0.49	-0.47	-0.27	-0.30	-0.35	-0.30	-0.33	-0.30	-0.30
TOTAL	99.26	100.04	99.95	98.91	99.42	99.05	99.50	99.72	100.57	99.62	100.25	98.80	99.50	98.82	99.61	100.04	100.49
Si ⁴⁺ apfu	2.685	2.614	2.788	2.753	2.722	2.734	2.711	2.632	2.737	2.642	2.714	2.597	2.613	2.696	2.637	2.604	2.693
Ti ⁴⁺	0.060	0.052	0.060	0.060	0.058	0.058	0.060	0.059	0.054	0.061		0.105	0.105	0.121	0.108	0.090	0.112
Al ³⁺	1.616	1.753	1.460	1.528	1.566	1.559	1.589	1.705	1.536	1.685	1.560	1.876	1.875	1.733	1.842	1.907	1.536
Cl ³⁺	0.004	0.004	0.000	0.002	0.004	0.002	0.001	0.008	0.002	0.007	0.008	0.004	0.005	0.003	0.006	0.000	0.009
V ³⁺	0.020	0.015	0.012	0.012	0.016	0.018	0.017	0.018	0.015	0.020	0.014	0.003	0.005	0.003	0.004	0.005	0.067
Fe ³⁺	0.000	0.000	0.000	0.000	0.000	0.000	0.000	0.000	0.000	0.000	0.000	0.000	0.000	0.000	0.000	0.000	0.000
Mg ²⁺	2.470	2.417	2.522	2.491	2.481	2.477	2.476	2.433	2.499	2.445	2.495	1.996	1.969	1.947	1.940	1.971	2.298
Mn ²⁺	0.000	0.003	0.003	0.001	0.000	0.000	0.001	0.002	0.000	0.001	0.000	0.000	0.002	0.002	0.003	0.002	0.000
Fe ²⁺	0.084	0.088	0.083	0.087	0.089	0.077	0.082	0.080	0.088	0.094	0.085	0.267	0.265	0.300	0.291	0.281	0.187
Zn ²⁺	0.001	0.003	0.004	0.000	0.006	0.000	0.001	0.002	0.000	0.001	0.004	0.000	0.000	0.000	0.000	0.000	0.000
Ca ²⁺	0.000	0.001	0.006	0.007	0.005	0.001	0.001	0.003	0.001	0.000	0.002	0.002	0.001	0.000	0.003	0.005	
Ba ²⁺	0.029	0.038	0.015	0.011	0.023	0.024	0.020	0.042	0.016	0.032	0.025	0.014	0.014	0.014	0.011	0.009	0.004
Na ⁺	0.063	0.070	0.057	0.066	0.067	0.065	0.071	0.072	0.061	0.067	0.067	0.022	0.025	0.011	0.017	0.026	0.005
K ⁺	0.870	0.849	0.868	0.858	0.840	0.878	0.870	0.846	0.885	0.868	0.868	0.960	0.948	0.974	0.961	0.934	0.951
F	0.209	0.217	0.256	0.162	0.186	0.258	0.205	0.222	0.247	0.245	0.141	0.155	0.180	0.162	0.174	0.175	0.158
Cl ⁻	0.001	0.003	0.004	0.004	0.004	0.000	0.001	0.002	0.007	0.003	0.000	0.006	0.006	0.002	0.004	0.002	0.002
OH ⁻	1.790	1.780	1.740	1.834	1.810	1.741	1.794	1.776	1.745	1.752	1.859	1.839	1.814	1.836	1.823	1.823	1.840
vac. (M)	0.061	0.054	0.072	0.065	0.063	0.077	0.066	0.063	0.063	0.053	0.064	0.152	0.161	0.194	0.170	0.141	0.098
O ²⁻	10	10	10	10	10	10	10	10	10	10	10	10	10	10	10	10	10

Appendix A.3: Compositions of phlogopite from lithologies within marble at the Revelstoke Occurrence (con't)

pos. And min. assoc. EPMA point	m TD-G020-07B2-11-10	r Cal TD-G020-07B2-11-11	c TD-G020-07B2-12-12	m TD-G020-07B2-12-13	r Cal TD-G020-07B2-12-14
SiO ₂ wt.%	37.76	40.72	37.83	38.18	37.95
TiO ₂	1.89	1.74	2.17	2.22	2.02
Al ₂ O ₃	18.06	14.92	19.51	18.24	19.37
Cr ₂ O ₃	0.24	0.23	0.28	0.27	0.27
V ₂ O ₃	1.32	0.97	1.26	1.41	1.35
Fe ₂ O ₃	0	0	0	0	0
MgO	21.43	23.38	21.07	21.56	21.43
MnO	0.02	0	0	0.04	0.03
FeOt _{tot}	3.16	2.86	2.96	3.09	2.91
ZnO					
CaO	0.08	0.11	0.05	0.01	0.11
BaO	0.33	0.09	0.24	0.16	0.18
Na ₂ O	0.06	0.05	0.08	0.05	0.09
K ₂ O	10.37	10	10.69	10.44	10.52
F	0.76	1.19	0.5	0.57	0.64
CL	0.04	0.05	0.03	0.04	0.03
H ₂ O *	3.82	3.67	4.01	3.96	3.96
- (O=F,Cl)	-0.33	-0.51	-0.22	-0.25	-0.28
TOTAL	99.01	99.47	100.46	99.99	100.58
Si ⁴⁺ apfu	2.703	2.877	2.664	2.701	2.667
Ti ⁴⁺	0.102	0.092	0.115	0.118	0.107
Al ³⁺	1.524	1.242	1.619	1.521	1.604
Cl ³⁺	0.014	0.013	0.016	0.015	0.015
V ³⁺	0.076	0.055	0.071	0.080	0.076
Fe ³⁺	0.000	0.000	0.000	0.000	0.000
Mg ²⁺	2.287	2.462	2.212	2.274	2.245
Mn ²⁺	0.001	0.000	0.000	0.002	0.002
Fe ²⁺	0.189	0.169	0.174	0.183	0.171
Zn ²⁺	0.000	0.000	0.000	0.000	0.000
Ca ²⁺	0.006	0.008	0.004	0.001	0.008
Ba ²⁺	0.009	0.002	0.007	0.004	0.005
Na ⁺	0.008	0.007	0.011	0.007	0.012
K ⁺	0.947	0.901	0.960	0.942	0.943
F ⁻	0.172	0.266	0.111	0.128	0.142
Cl ⁻	0.005	0.006	0.004	0.005	0.004
OH ⁻	1.823	1.728	1.885	1.868	1.854
vac. (M)	0.105	0.089	0.128	0.107	0.113
O ²⁻	10	10	10	10	10

Appendix A.3: Compositions of phlogopite from lithologies within calc-gneiss at the Revelstoke Occurrence (con't)

pos. And min. assoc. EPMA point	edge of grt 53-1-1	edge of grt 53-1-2	leuc n to grt 53-1-4	leuc n to grt 53-1-5	incl w kyin grt 53-2-6	edge of grt 53-2-1	edge of grt 53-2-2	edge of grt 53-2-3	edge of grt 53-2-4	tourmaline 53-3-1	tourmaline 53-3-2	tourmaline 53-6-1	tourmaline 53-7-1	71-3-1	71-3-2	71-3-3
SiO ₂ wt.%	35.2759	34.6496	34.5449	34.5387	35.5582	34.8246	34.2328	34.7	34.4756	36.5454	36.2756	36.0692	37.1324	36.679	36.736	37.196
TiO ₂	4.037	3.9525	4.9175	4.6059	4.2438	3.5226	3.4681	3.4837	3.6533	4.0607	4.1079	3.3971	3.4747	4.306	4.1604	4.4646
Al ₂ O ₃	17.5003	17.8112	17.3677	17.6986	18.406	19.4885	19.7196	19.5788	19.3451	19.7928	19.0447	19.0747	20.4718	15.336	15.215	14.316
Cr ₂ O ₃	0.0912	0.1111	0.1626	0.0873	0.0599	0.0476	0.0159	0.0635	0.0357	0.1011	0	0.0893	0.2235	0.08	0.016	0.132
V ₂ O ₃	0	0	0	0.0536	0.0096	0	0	0.0527	0.0178	0.1627	0.1577	0.0954	0.1369	0.005	0	0.0365
Fe ₂ O ₃	0	0	0	0	0	0	0	0	0	0	0	0	0	0	0	0
MgO	9.2746	9.2688	8.8057	8.7905	9.4804	8.0221	7.9194	7.9947	8.1162	10.2047	10.8289	12.2876	11.1201	11.934	11.969	12.429
MnO	0.0819	0.0328	0.0752	0.059	0	0.118	0.0885	0.0197	0.0689	0.0795	0.0497	0	0.0398	0.0461	0.0494	0.1086
FeOt _{tot}	20.2091	20.198	20.4074	20.5809	18.5756	20.1534	20.5961	20.387	20.3815	14.9101	14.9627	13.8707	13.5742	18.687	18.68	18.509
ZnO	0.041	0.0451	0.1023	0.041	0.111	0	0.0862	0.0287	0	0	0	0.0207	0.0166	0.1399	0.0905	0.0453
CaO	0.0669	0.0808	0.0265	0.0161	0.022	0.0197	0	0.0486	0.0046	0.0782	0.014	0.0363	0.0562	0.0777	0.2086	0.2029
BaO	0.4237	0.4428	0.4536	0.4049	0.3108	0.1735	0.1594	0.1079	0.1431	0.2492	0.3132	0.0619	0.2049	0.2615	0.2826	0.2827
Na ₂ O	0.0516	0.0849	0.1417	0.1112	0.1136	0.0604	0.0971	0.0727	0.0788	0.1246	0.1348	0.1316	0.0942	0.0403	0.0837	0.0418
K ₂ O	9.195	8.7907	9.5283	9.29	9.9248	9.7602	9.3948	9.4454	9.8432	9.6573	9.7016	9.5369	9.7033	9.963	9.3304	9.727
F	0.9931	0.2724	0.4412	0.061	0.2928	0	0	0.2583	0.0915	0.0794	0.3629	0.4583	0.3505	0.0772	0.6272	0.263
CL	0.0138	0.0208	0	0.01	0.0054	0.0108	0	0.0108	0.0015	0.0047	0	0	0	0.0162	0.0116	0
H ₂ O *	3.43	3.77	3.70	3.89	3.84	3.94	3.92	3.80	3.89	4.01	3.84	3.78	3.92	3.97	3.67	3.88
- (O-F, Cl)	-0.42	-0.12	-0.19	-0.03	-0.12	0.00	0.00	-0.11	-0.04	-0.03	-0.15	-0.19	-0.15	-0.04	-0.27	-0.11
TOTAL	100.26	99.41	100.49	100.21	100.83	100.14	99.70	99.95	100.10	100.03	99.64	98.72	100.37	101.58	100.86	101.52
Si ⁴⁺ apfu	2.683	2.654	2.636	2.637	2.671	2.647	2.617	2.640	2.628	2.703	2.701	2.692	2.714	2.741	2.757	2.777
Ti ⁴⁺	0.231	0.228	0.282	0.265	0.240	0.201	0.199	0.199	0.209	0.226	0.230	0.191	0.191	0.242	0.235	0.251
Al ³⁺	1.568	1.608	1.562	1.593	1.629	1.746	1.777	1.755	1.738	1.725	1.671	1.678	1.763	1.351	1.346	1.260
Cl ³⁺	0.005	0.007	0.010	0.005	0.004	0.003	0.001	0.004	0.002	0.006	0.000	0.005	0.013	0.005	0.001	0.008
V ³⁺	0.000	0.000	0.000	0.003	0.001	0.000	0.000	0.003	0.001	0.010	0.009	0.006	0.008	0.000	0.000	0.002
Fe ³⁺	0.000	0.000	0.000	0.000	0.000	0.000	0.000	0.000	0.000	0.000	0.000	0.000	0.000	0.000	0.000	0.000
Mg ²⁺	1.051	1.059	1.002	1.001	1.061	0.909	0.903	0.907	0.922	1.125	1.202	1.367	1.212	1.330	1.339	1.383
Mn ²⁺	0.005	0.002	0.005	0.004	0.000	0.008	0.006	0.001	0.004	0.005	0.003	0.000	0.002	0.003	0.003	0.007
Fe ²⁺	1.285	1.294	1.302	1.314	1.167	1.281	1.317	1.297	1.299	0.922	0.932	0.866	0.830	1.168	1.172	1.156
Zn ²⁺	0.002	0.003	0.006	0.002	0.006	0.000	0.005	0.002	0.000	0.000	0.000	0.001	0.001	0.008	0.005	0.002
Ca ²⁺	0.005	0.007	0.002	0.001	0.002	0.002	0.000	0.004	0.000	0.006	0.001	0.003	0.004	0.006	0.017	0.016
Ba ²⁺	0.013	0.013	0.014	0.012	0.009	0.005	0.005	0.003	0.004	0.007	0.009	0.002	0.006	0.008	0.008	0.008
Na ⁺	0.008	0.013	0.021	0.016	0.017	0.009	0.014	0.011	0.012	0.018	0.019	0.019	0.013	0.006	0.012	0.006
K ⁺	0.892	0.859	0.928	0.905	0.951	0.946	0.916	0.917	0.957	0.911	0.921	0.908	0.905	0.950	0.893	0.927
F ⁻	0.239	0.066	0.106	0.015	0.070	0.000	0.000	0.062	0.022	0.019	0.085	0.108	0.081	0.018	0.149	0.062
Cl ⁻	0.002	0.003	0.000	0.001	0.001	0.001	0.000	0.001	0.000	0.001	0.000	0.000	0.002	0.001	0.000	0.000
OH ⁻	1.759	1.931	1.894	1.984	1.930	1.999	2.000	1.936	1.978	1.981	1.915	1.892	1.919	1.980	1.850	1.938
vac. (M)	0.171	0.148	0.200	0.179	0.228	0.206	0.180	0.193	0.196	0.278	0.252	0.196	0.267	0.161	0.148	0.156
O ²⁻	10	10	10	10	10	10	10	10	10	10	10	10	10	10	10	10

Appendix A.3: Compositions of phlogopite from lithologies within calc-gneiss at the Revelstoke Occurrence (con't)

pos. And min. assoc. EPMA point	next to grt																		incl 12-1			
	71-3-5	71-3-6	71-4b-1	72-1	72-2	72-3	72-4	72-5	72-6	72-8	72-9	72-10	72-11	72-12	72-13	72-14	72-16	72-17	72-18			
SiO ₂ wt.%	36.809	36.323	36.32	37.422	36.838	37.507	37.09	36.62	37.251	36.4669	36.4407	36.2698	36.8488	36.168	35.8	36.52	36.45	37.128	37.259	36.64	37.492	36.697
TiO ₂	2.9505	2.6592	3.869	4.6268	4.1576	3.9595	3.354	3.195	3.3847	2.1662	2.1065	2.0189	3.4066	3.6676	3.057	2.573	2.969	3.1401	3.1875	3.056	3.4731	2.7576
Al ₂ O ₃	14.728	14.611	14.295	14.208	13.923	14.139	14.021	14.28	14.252	14.6643	14.743	15.0714	14.964	15.437	14.66	14.66	14.55	14.308	14.634	14.41	14.553	19.206
Cr ₂ O ₃	0.0396	0.0435	0.1259	0.0998	0.0834	0.0716	0.0635	0.032	0.0952	0.0433	0.0906	0	0.1194	0.0914	0	0	0.115	0.0518	0.0838	0.072	0.0679	0.0441
V ₂ O ₃	0.0216	0.0562	0.0459	0	0	0	0	0.003	0	0	0	0	0.0115	0	0.023	0	0	0	0	0	0	0
Fe ₂ O ₃	0	0	0	0	0	0	0	0	0	0	0	0	0	0	0	0	0	0	0	0	0	0
MgO	11.705	11.554	9.3412	11.565	11.612	11.803	12.376	11.44	11.8	10.7139	10.9353	11.0673	11.295	11.065	12.04	12.07	12.27	12.397	12.413	12.08	11.984	11.352
MnO	0	0.0622	0.1273	0.0986	0.0721	0.1116	0.1279	0.161	0.1737	0.1894	0.2548	0.3265	0.1444	0.1967	0.122	0.128	0.118	0.2003	0.171	0.142	0.1152	0.0363
FeOt _{tot}	21.471	21.534	23.376	18.847	20.107	19.955	20.219	19.38	20.642	22.1915	22.2301	22.8414	19.3297	19.8	19.21	18.95	19.36	19.273	18.512	18.26	18.755	17.892
ZnO	0.0616	0.0329	0.0287	0	0.0287	0.0984	0.082	0.021	0.0205	0.1801	0.1474	0	0.078	0.0328	0.156	0	0.16	0.0575	0.115	0.156	0.037	0.0906
CaO	0.1135	0.118	0.1232	0.232	0.0605	0.0114	0.0629	0.601	0.1017	0.1733	0.0879	0.0262	0.1979	0.0137	0.803	0.106	0.172	0.0584	0.0757	0.054	0.1721	0
BaO	0.0493	0.1101	0.049	0.1599	0.1853	0.1479	0.1268	0.217	0.1853	0.1449	0.0678	0.028	0.2092	0.2394	0.092	0.141	0.111	0.167	0.2214	0.245	0.1037	0.3121
Na ₂ O	0.0866	0.0457	0.0761	0.0722	0.0592	0.0469	0.0257	0.041	0.0137	0.1398	0.1383	0.0892	0.1175	0.0998	0.042	0.061	0.069	0.0361	0.0628	0.064	0.045	0.1385
K ₂ O	9.5213	9.1563	9.3334	9.3246	9.1395	9.6932	9.55	9.136	9.6863	8.721	9.2744	8.9087	9.4186	9.5317	8.185	9.192	9.376	9.4779	9.5466	9.553	9.608	9.9053
F	0.4044	0.5803	0.1648	0.8695	0.9502	0.811	1.0545	1.249	0.883	0.8005	1.1079	0.8905	0.8893	1.0593	0.821	0.962	0.869	1.0437	1.0329	1.032	1.1325	0
CL	0.0062	0.0139	0.0061	0.027	0.0308	0.0154	0.0224	0.02	0.0223	0.037	0.0208	0.037	0.0208	0.0246	0.041	0.046	0.039	0.0154	0.0201	0.04	0.0255	0.0054
H ₂ O *	3.77	3.62	3.83	3.53	3.45	3.58	3.42	3.26	3.52	3.47	3.34	3.45	3.49	3.39	3.45	3.38	3.47	3.42	3.43	3.36	3.39	4.09
- (O=F, Cl)	-0.17	-0.25	-0.07	-0.37	-0.41	-0.34	-0.45	-0.53	-0.38	-0.35	-0.47	-0.38	-0.45	-0.36	-0.42	-0.37	-0.44	-0.44	-0.44	-0.48	0.00	
TOTAL	101.56	100.27	101.04	100.72	100.29	101.60	101.15	99.13	101.66	99.76	100.51	100.64	100.16	100.37	98.14	98.38	99.72	100.33	100.33	98.72	100.47	102.53
Si ⁴⁺ apfu	2.775	2.775	2.780	2.811	2.797	2.810	2.797	2.810	2.801	2.806	2.791	2.772	2.795	2.748	2.763	2.812	2.780	2.810	2.811	2.814	2.823	2.689
Ti ⁴⁺	0.167	0.153	0.223	0.261	0.237	0.223	0.190	0.184	0.191	0.125	0.121	0.116	0.194	0.210	0.177	0.149	0.170	0.179	0.181	0.177	0.197	0.152
Al ³⁺	1.309	1.316	1.289	1.258	1.246	1.249	1.249	1.292	1.263	1.330	1.331	1.358	1.338	1.382	1.333	1.330	1.308	1.276	1.301	1.304	1.291	1.659
Cl ³⁺	0.002	0.003	0.008	0.006	0.005	0.004	0.004	0.002	0.006	0.003	0.005	0.000	0.007	0.005	0.000	0.000	0.007	0.003	0.005	0.004	0.004	0.003
V ³⁺	0.001	0.003	0.003	0.000	0.000	0.000	0.000	0.000	0.000	0.000	0.000	0.000	0.001	0.000	0.001	0.000	0.000	0.000	0.000	0.000	0.000	
Fe ³⁺	0.000	0.000	0.000	0.000	0.000	0.000	0.000	0.000	0.000	0.000	0.000	0.000	0.000	0.000	0.000	0.000	0.000	0.000	0.000	0.000	0.000	
Mg ²⁺	1.315	1.316	1.066	1.295	1.314	1.318	1.391	1.309	1.323	1.229	1.249	1.261	1.277	1.253	1.386	1.386	1.396	1.399	1.396	1.382	1.345	1.240
Mn ²⁺	0.000	0.004	0.008	0.006	0.005	0.007	0.008	0.010	0.011	0.012	0.017	0.021	0.009	0.013	0.008	0.008	0.008	0.013	0.011	0.009	0.007	0.002
Fe ²⁺	1.354	1.376	1.496	1.184	1.277	1.251	1.275	1.244	1.298	1.428	1.424	1.460	1.226	1.258	1.240	1.220	1.235	1.220	1.168	1.173	1.181	1.097
Zn ²⁺	0.003	0.002	0.002	0.000	0.002	0.005	0.005	0.001	0.001	0.010	0.008	0.000	0.004	0.002	0.009	0.000	0.009	0.003	0.006	0.009	0.002	0.005
Ca ²⁺	0.009	0.010	0.010	0.019	0.005	0.001	0.005	0.049	0.008	0.014	0.007	0.002	0.016	0.001	0.066	0.009	0.014	0.005	0.006	0.004	0.014	0.000
Ba ²⁺	0.001	0.003	0.001	0.005	0.006	0.004	0.004	0.007	0.005	0.004	0.002	0.001	0.006	0.007	0.003	0.004	0.003	0.005	0.007	0.007	0.003	0.009
Na ⁺	0.013	0.007	0.011	0.011	0.009	0.007	0.004	0.006	0.002	0.021	0.021	0.013	0.017	0.015	0.006	0.009	0.010	0.005	0.009	0.010	0.007	0.020
K ⁺	0.916	0.893	0.911	0.893	0.885	0.927	0.919	0.894	0.929	0.856	0.906	0.869	0.911	0.924	0.806	0.903	0.912	0.915	0.919	0.936	0.923	0.926
F	0.096	0.140	0.040	0.207	0.228	0.192	0.252	0.303	0.210	0.195	0.268	0.215	0.213	0.255	0.200	0.234	0.210	0.250	0.246	0.251	0.270	0.000
Cl ⁻	0.001	0.002	0.001	0.003	0.004	0.002	0.003	0.003	0.003	0.005	0.003	0.005	0.003	0.005	0.006	0.006	0.005	0.002	0.003	0.005	0.003	0.001
OH ⁻	1.903	1.858	1.959	1.790	1.768	1.806	1.746	1.694	1.787	1.800	1.729	1.780	1.784	1.742	1.794	1.760	1.785	1.748	1.751	1.744	1.727	1.999
vac. (M)	0.076	0.054	0.127	0.179	0.119	0.137	0.087	0.149	0.107	0.066	0.062	0.011	0.153	0.131	0.092	0.095	0.096	0.101	0.128	0.138	0.151	0.159
O ²⁻	10	10	10	10	10	10	10	10	10	10	10	10	10	10	10	10	10	10	10	10	10	10

Appendix A.3: Compositions of phlogopite from lithologies within calc-gneiss at the Revelstoke Occurrence (con't)

pos. And min. assoc. EPMA point	inclu		edge		edge		n to Pl poik	n to Pl poik	incl in ky	
	12-2	12-3	12-4	12-5	12-6	12-7	12-8	12-9	12-10	
SiO ₂ wt.%	35.868	36.314	36.249	36.585	36.598		36.6769	36.2281	36.6999	37.155
TiO ₂	3.0896	2.8913	3.1229	3.1545	2.8808		2.8569	3.0109	2.8055	3.1861
Al ₂ O ₃	19.042	19.139	19.373	18.817	19.117		19.6239	19.3237	19.6646	18.762
Cr ₂ O ₃	0.008	0.0887	0.0161	0.0443	0.0081		0.0888	0.0323	0.0968	0.0806
V ₂ O ₃	0.004	0.0225	0.0212	0.0049	0		0.0034	0	0.0156	0.0395
Fe ₂ O ₃	0	0	0	0	0		0	0	0	0
MgO	11.443	12.086	11.816	11.925	11.924		11.9695	12.0093	11.6759	11.423
MnO	0.1252	0.0198	0.076	0.076	0.0529		0.0331	0.0629	0.0562	0.1156
FeOt _{tot}	17.57	15.64	15.726	16.064	16.054		15.5266	15.3267	15.8561	15.979
ZnO	0.0822	0.0989	0.0783	0.099	0.0784		0.0041	0.1362	0.0165	0
CaO	0	0.0323	0.053	0.0254	0.0046		0.0704	0.0254	0.0104	0.0357
BaO	0.3637	0.3082	0.2253	0.2514	0.223		0.2326	0.2328	0.2089	0.334
Na ₂ O	0.1339	0.1176	0.1073	0.1224	0.1382		0.1459	0.1115	0.1162	0.0671
K ₂ O	10.143	9.8685	10.215	9.8747	9.79		10.0414	9.8096	10.1398	9.8855
F	0.0646	0.8253	0.2942	0.4557	0.3738		0.1964	0.2454	0.5215	0.7319
CL	0.0008	0.0217	0.014	0.0008	0		0.0109	0	0	0.0023
H ₂ O *	4.02	3.62	3.91	3.83	3.87		3.98	3.92	3.82	3.69
- (O+F,Cl)	-0.03	-0.35	-0.13	-0.19	-0.16		-0.09	-0.10	-0.22	-0.31
TOTAL	101.93	100.74	101.17	101.14	100.96		101.38	100.37	101.48	101.18
Si ⁴⁺ apfu	2.653	2.686	2.674	2.698	2.700		2.689	2.683	2.693	2.735
Ti ⁴⁺	0.172	0.161	0.173	0.175	0.160		0.158	0.168	0.155	0.176
Al ³⁺	1.660	1.669	1.684	1.636	1.662		1.696	1.686	1.701	1.628
Cr ³⁺	0.000	0.005	0.001	0.003	0.000		0.005	0.002	0.006	0.005
V ³⁺	0.000	0.001	0.001	0.000	0.000		0.000	0.000	0.001	0.002
Fe ³⁺	0.000	0.000	0.000	0.000	0.000		0.000	0.000	0.000	0.000
Mg ²⁺	1.262	1.333	1.299	1.311	1.311		1.308	1.326	1.277	1.253
Mn ²⁺	0.008	0.001	0.005	0.005	0.003		0.002	0.004	0.003	0.007
Fe ²⁺	1.087	0.968	0.970	0.991	0.990		0.952	0.949	0.973	0.984
Zn ²⁺	0.004	0.005	0.004	0.005	0.004		0.000	0.007	0.001	0.000
Ca ²⁺	0.000	0.003	0.004	0.002	0.000		0.006	0.002	0.001	0.003
Ba ²⁺	0.011	0.009	0.007	0.007	0.006		0.007	0.007	0.006	0.010
Na ⁺	0.019	0.017	0.015	0.018	0.020		0.021	0.016	0.017	0.010
K ⁺	0.957	0.931	0.961	0.929	0.921		0.939	0.927	0.949	0.928
F ⁻	0.015	0.193	0.069	0.106	0.087		0.046	0.057	0.121	0.170
Cl ⁻	0.000	0.003	0.002	0.000	0.000		0.001	0.000	0.000	0.000
OH ⁻	1.985	1.804	1.930	1.894	1.913		1.953	1.943	1.879	1.829
vac. (M)	0.158	0.176	0.193	0.181	0.173		0.190	0.182	0.192	0.210
O ²⁻	10	10	10	10	10		10	10	10	10

Appendix A.4: Compositions of muscovite from lithologies within marble at the Revelstoke Occurrence

position EPMA point	r G10-01-19-1	m G10-01-19-2	c G10-01-19-3	r G10-01-08-1	m G10-01-08-2	c G10-01-08-3	G10-01-08-4	G10-01-08-5	r G10-01-mt-1	c G10-01-mt-2	r G10-01-mt-3	r G10-01-mt-4	m G10-01-mt-5
SiO ₂ wt.%	43.96	45.49	44.50	44.21	45.18	44.27	44.17	43.87	45.30	45.53	46.00	45.73	46.35
TiO ₂	1.66	0.83	1.57	0.74	1.27	0.82	0.45	0.51	1.09	0.99	0.93	0.80	0.60
Al ₂ O ₃	35.17	34.10	34.98	36.21	35.22	36.08	36.39	36.21	35.05	34.82	34.70	34.67	34.65
Cr ₂ O ₃	0.04	0.20	0.17	0.14	0.09	0.00	0.09	0.13	0.08	0.03	0.09	0.08	0.02
V ₂ O ₃													
MgO	0.86	1.13	0.86	0.60	0.73	0.55	0.38	0.42	0.79	0.93	1.01	0.95	1.00
CaO	0.05	0.01	0.02	0.04	0.05	0.10	0.05	0.14	0.02	0.02	0.00	0.00	0.01
MnO	0.00	0.00	0.01	0.05	0.01	0.07	0.00	0.04	0.00	0.03	0.02	0.01	0.00
FeO	0.16	0.14	0.19	0.24	0.15	0.16	0.13	0.11	0.06	0.08	0.16	0.12	0.07
BaO	1.47	1.04	1.13	1.52	1.16	1.15	1.70	1.59	1.19	1.19	1.20	1.08	0.98
Na ₂ O	0.25	0.22	0.23	0.35	0.22	0.28	0.27	0.32	0.23	0.21	0.23	0.23	0.26
K ₂ O	10.91	10.79	10.76	10.39	11.00	9.95	10.71	10.80	11.02	11.04	11.01	10.79	10.53
F	0.00	0.00	0.00	0.00	0.00	0.00	0.00	0.00	0.00	0.00	0.00	0.00	0.00
CL	0.03	0.00	0.00	0.01	0.00	0.00	0.00	0.00	0.00	0.01	0.01	0.01	0.00
H ₂ O *	4.40	4.42	4.43	4.42	4.46	4.41	4.41	4.40	4.45	4.45	4.47	4.44	4.46
O=F	0.00	0.00	0.00	0.00	0.00	0.00	0.00	0.00	0.00	0.00	0.00	0.00	0.00
O=CL	-0.01	0.00	0.00	0.00	0.00	0.00	0.00	0.00	0.00	0.00	0.00	0.00	0.00
TOTAL	98.95	98.37	98.85	98.92	99.54	97.84	98.75	98.54	99.28	99.33	99.83	98.91	98.93
Si ⁴⁺ apfu	2.987	3.088	3.014	2.994	3.038	3.011	3.000	2.990	3.052	3.066	3.081	3.084	3.113
Ti ⁴⁺	0.085	0.042	0.080	0.038	0.064	0.042	0.023	0.026	0.055	0.050	0.047	0.041	0.030
Al ³⁺	2.817	2.728	2.792	2.890	2.791	2.892	2.913	2.909	2.783	2.764	2.739	2.756	2.743
Cr ³⁺	0.002	0.011	0.009	0.007	0.005	0.000	0.005	0.007	0.004	0.002	0.005	0.004	0.001
V ³⁺	0.000	0.000	0.000	0.000	0.000	0.000	0.000	0.000	0.000	0.000	0.000	0.000	0.000
Mg ²⁺	0.087	0.114	0.087	0.061	0.073	0.056	0.038	0.043	0.079	0.093	0.101	0.096	0.100
Ca ²⁺	0.004	0.001	0.001	0.003	0.004	0.007	0.004	0.010	0.001	0.001	0.000	0.000	0.001
Mn ²⁺	0.000	0.000	0.001	0.003	0.001	0.004	0.000	0.002	0.000	0.002	0.001	0.001	0.000
Fe ²⁺	0.009	0.008	0.011	0.014	0.008	0.009	0.007	0.006	0.003	0.005	0.009	0.007	0.004
Ba ²⁺	0.039	0.028	0.030	0.040	0.031	0.031	0.045	0.042	0.031	0.031	0.031	0.029	0.026
Na ⁺	0.033	0.029	0.030	0.046	0.029	0.037	0.036	0.042	0.030	0.027	0.030	0.030	0.034
K ⁺	0.946	0.934	0.930	0.898	0.944	0.863	0.928	0.939	0.947	0.948	0.941	0.928	0.902
F	0.000	0.000	0.000	0.000	0.000	0.000	0.000	0.000	0.000	0.000	0.000	0.000	0.000
Cl ⁻	0.003	0.000	0.000	0.001	0.000	0.000	0.000	0.000	0.000	0.001	0.001	0.001	0.000
OH ⁻	1.993	2.000	2.000	1.998	2.000	2.000	2.000	2.000	2.000	1.998	1.998	1.998	2.000
O ²⁻	10.003	10.000	10.000	10.001	10.000	10.000	10.000	10.000	10.000	10.001	10.001	10.001	10.000

*calculated from electroneutral formula assuming 12 anions and (OH+F+Cl)=2.

NOTE: Following standards, X-ray lines and crystals were used during EMP analysis: synthetic phlogopite, F $\text{K}\alpha$, Mg $\text{K}\alpha$, Si $\text{K}\alpha$, TAP, K $\text{K}\alpha$, PET; albite, Na $\text{K}\alpha$, TAP; kyanite, Al $\text{K}\alpha$, TAP; scapolite, Cl $\text{K}\alpha$, PET; diopside, Ca $\text{K}\alpha$, PET; rutile, Ti $\text{K}\alpha$, PET; synthetic magnesiochromite, Cr $\text{K}\alpha$, LiF; synthetic rhodonite, Mn $\text{K}\alpha$, LiF; synthetic fayalite, Fe $\text{K}\alpha$, LiF; barite, Ba La , PET;

Appendix A.4: Compositions of muscovite from lithologies within marble at the Revelstoke Occurrence (con't)

position EPMA point	c G10-01-mt-6	r G10-01-mt-7	c G10-01-mt-8	r G10-01-mt-9	c G10-01-04-1	r G10-01-04-2	c G10-01-04-3	G10-01-02-1	G10-01-02-2	G10-01-02-3	G10-01-02-4	G10-01-02-5	G10-01-02-6
SiO ₂ wt.%	45.69	45.18	44.87	45.44	44.17	45.77	45.03	45.74	43.79	44.27	44.42	44.45	43.94
TiO ₂	0.60	1.06	1.20	1.10	1.68	0.91	0.79	1.10	1.73	1.86	1.11	1.61	1.33
Al ₂ O ₃	34.54	34.63	34.36	34.84	34.97	34.77	34.81	34.69	35.25	35.39	35.48	35.05	35.32
Cr ₂ O ₃	0.01	0.04	0.06	0.07	0.18	0.10	0.11	0.10	0.08	0.01	0.13	0.02	0.02
V ₂ O ₃													
MgO	0.91	0.94	0.96	0.93	0.74	1.02	0.95	0.92	0.84	0.75	0.49	0.72	0.80
CaO	0.02	0.03	0.01	0.01	0.03	0.00	0.02	0.01	0.01	0.00	0.07	0.01	0.00
MnO	0.00	0.00	0.00	0.02	0.03	0.00	0.04	0.03	0.00	0.00	0.00	0.00	0.06
FeO	0.00	0.14	0.12	0.06	0.20	0.00	0.09	0.15	0.22	0.19	0.15	0.13	0.16
BaO	1.04	1.35	1.21	1.26	0.73	1.10	1.15	1.23	0.76	0.72	1.22	0.76	1.43
Na ₂ O	0.26	0.21	0.23	0.16	0.30	0.23	0.21	0.25	0.27	0.29	0.31	0.27	0.21
K ₂ O	10.69	10.74	10.77	10.72	10.99	10.86	11.14	10.96	11.19	10.95	10.76	11.26	10.92
F	0.00	0.00	0.00	0.00	0.00	0.00	0.00	0.00	0.00	0.00	0.00	0.00	0.00
CL	0.00	0.00	0.00	0.00	0.01	0.02	0.00	0.01	0.01	0.00	0.00	0.01	0.00
H ₂ O *	4.42	4.43	4.40	4.45	4.41	4.45	4.42	4.46	4.40	4.44	4.41	4.42	4.40
O=F	0.00	0.00	0.00	0.00	0.00	0.00	0.00	0.00	0.00	0.00	0.00	0.00	0.00
O=CL	0.00	0.00	0.00	0.00	0.00	0.00	0.00	0.00	0.00	0.00	0.00	0.00	0.00
TOTAL	98.18	98.75	98.19	99.06	98.43	99.22	98.76	99.65	98.55	98.87	98.55	98.70	98.59
Si ⁴⁺ apfu	3.098	3.061	3.057	3.063	3.003	3.078	3.053	3.071	2.978	2.992	3.017	3.014	2.994
Ti ⁴⁺	0.031	0.054	0.062	0.056	0.086	0.046	0.040	0.056	0.089	0.095	0.057	0.082	0.068
Al ³⁺	2.760	2.765	2.759	2.768	2.802	2.756	2.782	2.745	2.826	2.819	2.840	2.801	2.836
Cr ³⁺	0.001	0.002	0.003	0.004	0.010	0.005	0.006	0.005	0.004	0.001	0.007	0.001	0.001
V ³⁺	0.000	0.000	0.000	0.000	0.000	0.000	0.000	0.000	0.000	0.000	0.000	0.000	0.000
Mg ²⁺	0.092	0.095	0.097	0.093	0.075	0.102	0.096	0.092	0.085	0.076	0.050	0.073	0.081
Ca ²⁺	0.001	0.002	0.001	0.001	0.002	0.000	0.001	0.001	0.001	0.000	0.005	0.001	0.000
Mn ²⁺	0.000	0.000	0.000	0.001	0.002	0.000	0.002	0.002	0.000	0.000	0.000	0.000	0.003
Fe ²⁺	0.000	0.008	0.007	0.003	0.011	0.000	0.005	0.008	0.013	0.011	0.009	0.007	0.009
Ba ²⁺	0.028	0.036	0.032	0.033	0.019	0.029	0.031	0.032	0.020	0.019	0.032	0.020	0.038
Na ⁺	0.034	0.028	0.030	0.021	0.040	0.030	0.028	0.033	0.036	0.038	0.041	0.035	0.028
K ⁺	0.925	0.928	0.936	0.922	0.953	0.932	0.964	0.939	0.971	0.944	0.932	0.974	0.949
F ⁻	0.000	0.000	0.000	0.000	0.000	0.000	0.000	0.000	0.000	0.000	0.000	0.000	0.000
Cl ⁻	0.000	0.000	0.000	0.000	0.001	0.002	0.000	0.001	0.001	0.000	0.000	0.001	0.000
OH ⁻	2.000	2.000	2.000	2.000	1.998	1.995	2.000	1.998	1.998	2.000	2.000	1.998	2.000
O ²⁻	10.000	10.000	10.000	10.000	10.001	10.002	10.000	10.001	10.001	10.000	10.001	10.001	10.000

Appendix A.4: Compositions of muscovite from lithologies within marble at the Revelstoke Occurrence (con't)

position EPMA point	G10-01-10-1	G10-01-10-2	G10-01-10-3	G10-01-10-4	G10-01-10-5	G10-01-17-1	G10-01-17-2	G10-01-17-3	r G10-01-21-5	c G10-01-21-6	c G10-01-21-7	m G10-01-21-8	r G10-01-21-9
SiO ₂ wt.%	44.02	44.20	45.12	44.70	45.35	44.68	46.13	44.77	45.35	43.62	44.34	44.12	44.64
TiO ₂	0.84	0.77	1.31	1.20	1.28	0.54	0.78	1.07	1.92	1.76	1.75	1.51	1.42
Al ₂ O ₃	36.54	36.15	34.89	35.06	35.60	33.96	34.36	34.21	33.95	34.74	35.20	35.29	35.35
Cr ₂ O ₃	0.09	0.00	0.11	0.10	0.10	0.03	0.03	0.11	0.09	0.09	0.03	0.02	0.08
V ₂ O ₃													
MgO	0.68	0.72	0.95	0.84	0.90	1.11	1.20	1.08	1.25	0.94	0.97	0.68	0.61
CaO	0.07	0.02	0.02	0.06	0.00	0.01	0.00	0.01	0.01	0.00	0.04	0.05	0.02
MnO	0.00	0.00	0.00	0.01	0.00	0.00	0.06	0.00	0.00	0.00	0.00	0.00	0.02
FeO	0.18	0.10	0.15	0.12	0.18	0.21	0.17	0.08	0.28	0.20	0.12	0.17	0.16
BaO	1.59	1.31	0.89	1.11	1.43	2.51	1.07	1.10	1.10	1.49	1.28	0.86	0.91
Na ₂ O	0.28	0.29	0.21	0.25	0.23	0.38	0.20	0.22	0.26	0.22	0.22	0.26	0.27
K ₂ O	10.35	10.98	11.10	10.96	10.99	10.18	10.61	10.74	10.67	10.99	11.02	10.82	10.98
F	0.00	0.00	0.00	0.00	0.00	0.00	0.00	0.00	0.00	0.00	0.00	0.00	0.00
CL	0.01	0.00	0.00	0.00	0.01	0.01	0.00	0.01	0.00	0.01	0.00	0.00	0.00
H ₂ O *	4.43	4.43	4.45	4.43	4.49	4.35	4.46	4.38	4.45	4.38	4.44	4.41	4.43
O=F	0.00	0.00	0.00	0.00	0.00	0.00	0.00	0.00	0.00	0.00	0.00	0.00	0.00
O=CL	0.00	0.00	0.00	0.00	0.00	0.00	0.00	0.00	0.00	0.00	0.00	0.00	0.00
TOTAL	99.08	98.97	99.20	98.84	100.56	97.97	99.07	97.78	99.33	98.37	99.40	98.25	98.81
Si ⁴⁺ apfu	2.976	2.993	3.041	3.028	3.024	3.073	3.102	3.060	3.055	2.986	2.994	3.001	3.020
Ti ⁴⁺	0.043	0.039	0.066	0.061	0.064	0.028	0.039	0.055	0.097	0.091	0.089	0.077	0.072
Al ³⁺	2.911	2.885	2.771	2.799	2.798	2.753	2.723	2.756	2.695	2.802	2.801	2.829	2.818
Cr ³⁺	0.005	0.000	0.006	0.005	0.005	0.002	0.002	0.006	0.005	0.002	0.001	0.004	0.000
V ³⁺	0.000	0.000	0.000	0.000	0.000	0.000	0.000	0.000	0.000	0.000	0.000	0.000	0.000
Mg ²⁺	0.069	0.073	0.095	0.085	0.089	0.114	0.120	0.110	0.126	0.096	0.098	0.069	0.062
Ca ²⁺	0.005	0.001	0.001	0.004	0.000	0.001	0.000	0.001	0.001	0.000	0.003	0.004	0.001
Mn ²⁺	0.000	0.000	0.000	0.001	0.000	0.000	0.003	0.000	0.000	0.000	0.000	0.000	0.001
Fe ²⁺	0.010	0.006	0.008	0.007	0.010	0.012	0.010	0.005	0.016	0.011	0.007	0.010	0.009
Ba ²⁺	0.042	0.035	0.024	0.029	0.037	0.068	0.028	0.029	0.029	0.040	0.034	0.023	0.024
Na ⁺	0.037	0.038	0.027	0.033	0.030	0.051	0.026	0.029	0.034	0.029	0.029	0.034	0.035
K ⁺	0.893	0.949	0.954	0.947	0.935	0.893	0.910	0.937	0.917	0.960	0.949	0.939	0.948
F ⁻	0.000	0.000	0.000	0.000	0.000	0.000	0.000	0.000	0.000	0.000	0.000	0.000	0.000
Cl ⁻	0.001	0.000	0.000	0.000	0.001	0.001	0.000	0.001	0.000	0.001	0.000	0.000	0.000
OH ⁻	1.998	2.000	2.000	2.000	1.998	1.998	2.000	1.998	2.000	1.998	2.000	2.000	2.000
O ²⁻	10.001	10.000	10.000	10.000	10.001	10.001	10.000	10.001	10.000	10.001	10.000	10.000	10.000

Appendix A.4: Compositions of muscovite from lithologies within marble at the Revelstoke Occurrence (con't)

position EPMA point	G11-02-6	G11-02-7	G11-02-8	G11-02-12	G11-02-13	G11-02-20	G11-02-21	G11-02-22	G11-02-23	G022-07C-12	G022-07C-13	G022-07C-30
SiO ₂ wt.%	45.30	44.60	45.04	44.90	44.85	44.88	45.55	45.07	44.07	47.47	47.27	46.36
TiO ₂	1.17	0.99	1.08	0.89	0.64	1.04	0.89	0.06	0.05	0.62	0.19	0.03
Al ₂ O ₃	35.84	36.21	36.06	36.45	36.85	34.53	34.24	35.39	35.62	34.17	33.63	37.27
Cr ₂ O ₃	0.00	0.05	0.00	0.03	0.04	0.06	0.04	0.00	0.05	0.00	0.00	0.04
V ₂ O ₃										0.04	0.01	0.01
MgO	0.58	0.56	0.63	0.55	0.60	1.20	1.25	0.73	0.92	1.45	2.18	0.64
CaO	0.29	0.16	0.12	0.03	0.08	0.05	0.88	0.03	8.41	0.28	0.38	2.18
MnO	0.02	0.02	0.00	0.00	0.03	0.00	0.04	0.02	0.04	0.02	0.00	0.01
FeO	0.18	0.14	0.09	0.08	0.19	0.15	0.21	0.21	0.55	0.11	0.20	0.19
BaO	1.35	0.95	1.05	0.96	1.20	1.32	1.05	0.73	0.17	0.84	0.98	1.62
Na ₂ O	0.36	0.30	0.21	0.23	0.24	0.19	0.20	0.26	0.44	0.25	0.20	0.48
K ₂ O	10.42	10.63	10.73	11.27	11.01	11.10	10.53	10.69	3.25	10.74	9.64	7.59
F	0.00	0.00	0.00	0.00	0.00	0.00	0.00	0.00	0.00	0.00	0.26	0.10
CL	0.00	0.01	0.00	0.01	0.00	0.01	0.01	0.02	0.05	0.03	0.01	0.02
H ₂ O *	4.49	4.45	4.47	4.47	4.49	4.42	4.45	4.39	4.46	4.52	4.23	4.47
O=F	0.00	0.00	0.00	0.00	0.00	0.00	0.00	0.00	0.00	0.00	-0.11	-0.04
O=CL	0.00	0.00	0.00	0.00	0.00	0.00	0.00	0.00	-0.01	-0.01	0.00	0.00
TOTAL	100.00	99.06	99.48	99.87	100.22	98.94	99.34	97.60	98.07	100.53	99.07	100.97
Si ⁴⁺ apfu	3.028	3.004	3.020	3.006	2.995	3.044	3.067	3.071	2.944	3.140	3.162	3.037
Ti ⁴⁺	0.059	0.050	0.054	0.045	0.032	0.053	0.045	0.003	0.003	0.031	0.010	0.001
Al ³⁺	2.823	2.874	2.850	2.876	2.900	2.760	2.718	2.842	2.805	2.664	2.652	2.877
Cr ³⁺	0.000	0.003	0.000	0.002	0.002	0.003	0.002	0.000	0.003	0.000	0.000	0.002
V ³⁺	0.000	0.000	0.000	0.000	0.000	0.000	0.000	0.000	0.000	0.002	0.001	0.001
Mg ²⁺	0.058	0.056	0.063	0.055	0.060	0.121	0.125	0.074	0.092	0.143	0.217	0.062
Ca ²⁺	0.021	0.012	0.009	0.002	0.006	0.004	0.063	0.002	0.602	0.020	0.027	0.153
Mn ²⁺	0.001	0.001	0.000	0.000	0.002	0.000	0.002	0.001	0.002	0.001	0.000	0.001
Fe ²⁺	0.010	0.008	0.005	0.004	0.011	0.009	0.012	0.012	0.031	0.006	0.011	0.010
Ba ²⁺	0.035	0.025	0.028	0.025	0.031	0.035	0.028	0.019	0.004	0.022	0.026	0.042
Na ⁺	0.047	0.039	0.027	0.030	0.031	0.025	0.026	0.034	0.057	0.032	0.026	0.061
K ⁺	0.888	0.913	0.918	0.963	0.938	0.960	0.905	0.929	0.277	0.906	0.823	0.634
F ⁻	0.000	0.000	0.000	0.000	0.000	0.000	0.000	0.000	0.000	0.000	0.055	0.021
Cl ⁻	0.000	0.001	0.000	0.001	0.000	0.001	0.001	0.002	0.006	0.003	0.001	0.002
OH ⁻	2.000	1.998	2.000	1.998	2.000	1.998	1.998	1.995	1.989	1.993	1.888	1.954
O ²⁻	10.000	10.001	10.000	10.001	10.000	10.001	10.001	10.002	10.006	10.003	10.056	10.023

Appendix A.4: Compositions of muscovite from lithologies within marble at the Revelstoke Occurrence (con't)

position EPMA point	G014-07B1-27	G014-07B1-29	G014-07B1-31	G014-07B1-32	G014-07B1-33	G014-07B1-34	G014-07B1-56	G014-07B1-36	G014-07B1-37	G014-07A2-56	G014-07A2-58
SiO ₂ wt.%	45.67	44.79	44.54	44.22	44.53	45.98	45.86	46.77	45.19	43.67	44.96
TiO ₂	0.27	0.45	1.18	1.11	1.85	1.18	1.24	0.85	1.29	1.68	0.04
Al ₂ O ₃	35.58	34.56	35.83	36.11	36.07	34.99	35.13	34.99	35.50	35.64	33.72
Cr ₂ O ₃	0.00	0.01	0.07	0.13	0.03	0.04	0.09	0.00	0.02	0.02	0.00
V ₂ O ₃	0.00	0.05	0.18	0.17	0.17	0.12	0.05	0.10	0.12	0.12	0.00
MgO	1.64	1.97	1.17	0.61	0.79	1.38	1.10	1.38	1.18	0.82	1.87
CaO	0.12	0.08	0.05	0.05	0.04	0.05	0.04	0.03	0.06	0.12	0.06
MnO	0.04	0.06	0.00	0.00	0.00	0.00	0.03	0.02	0.08	0.05	0.01
FeO	0.36	0.54	0.42	0.27	0.29	0.22	0.13	0.30	0.22	0.23	0.52
BaO	0.92	0.95	1.44	1.75	0.71	1.05	0.95	1.06	1.04	1.13	2.81
Na ₂ O	0.25	0.28	0.25	0.24	0.22	0.17	0.21	0.24	0.18	0.30	0.18
K ₂ O	10.94	10.67	10.40	10.51	10.48	10.88	10.71	10.96	10.49	10.50	10.15
F	0.00	0.04	0.10	0.01	0.16	0.09	0.05	0.03	0.12	0.30	0.12
CL	0.01	0.03	0.02	0.00	0.00	0.00	0.02	0.03	0.02	0.00	0.01
H ₂ O *	4.50	4.37	4.36	4.44	4.32	4.42	4.44	4.50	4.36	4.12	4.25
O=F	0.00	-0.02	-0.04	0.00	-0.07	-0.04	-0.02	-0.01	-0.05	-0.13	-0.05
O=CL	0.00	-0.01	0.00	0.00	0.00	0.00	0.00	-0.01	0.00	0.00	0.00
TOTAL	100.29	98.83	99.97	99.61	99.60	100.54	100.02	101.24	99.81	98.57	98.65
Si ⁴⁺ apfu	3.042	3.035	2.989	2.982	2.982	3.057	3.058	3.086	3.024	2.973	3.083
Ti ⁴⁺	0.014	0.023	0.060	0.056	0.093	0.059	0.062	0.042	0.065	0.086	0.002
Al ³⁺	2.793	2.760	2.834	2.870	2.847	2.742	2.760	2.721	2.800	2.859	2.725
Cr ³⁺	0.000	0.001	0.004	0.007	0.002	0.002	0.005	0.000	0.001	0.001	0.000
V ³⁺	0.000	0.003	0.010	0.009	0.009	0.006	0.003	0.005	0.006	0.007	0.000
Mg ²⁺	0.163	0.199	0.117	0.061	0.079	0.137	0.109	0.136	0.118	0.083	0.191
Ca ²⁺	0.009	0.006	0.004	0.004	0.003	0.004	0.003	0.002	0.004	0.009	0.004
Mn ²⁺	0.002	0.003	0.000	0.000	0.000	0.000	0.002	0.001	0.005	0.003	0.001
Fe ²⁺	0.020	0.031	0.024	0.015	0.016	0.012	0.007	0.017	0.012	0.013	0.030
Ba ²⁺	0.024	0.025	0.038	0.046	0.019	0.027	0.025	0.027	0.027	0.030	0.075
Na ⁺	0.032	0.037	0.033	0.031	0.029	0.022	0.027	0.031	0.023	0.040	0.024
K ⁺	0.930	0.922	0.890	0.904	0.895	0.923	0.911	0.923	0.895	0.912	0.888
F ⁻	0.000	0.009	0.021	0.002	0.034	0.019	0.011	0.006	0.025	0.065	0.026
Cl ⁻	0.001	0.003	0.002	0.000	0.000	0.000	0.002	0.003	0.002	0.000	0.001
OH ⁻	1.998	1.976	1.953	1.996	1.932	1.962	1.974	1.981	1.945	1.871	1.946
O ²⁻	10.001	10.012	10.023	10.002	10.034	10.019	10.013	10.010	10.028	10.065	10.027

Appendix A.4: Compositions of muscovite from lithologies within marble at the Revelstoke Occurrence (con't)

position EPMA point	G014-07A2-59	G014-07A2-60	G014-07A2-61	G014-07A2-62	G014-07A2-63	G014-07A2-66	G014-07A2-67	G014-07A2-68	G014-07A2-69	G063b-09-19	G063b-09-21	G063b-09-22	G063b-09-33
SiO ₂ wt.%	43.91	44.02	45.08	42.90	43.19	43.03	45.26	43.78	43.16	45.75	44.61	45.42	43.75
TiO ₂	1.47	1.47	0.96	1.42	1.80	1.84	0.97	1.35	1.33	0.26	0.14	0.09	0.58
Al ₂ O ₃	35.37	35.15	34.49	35.38	36.25	35.79	33.96	34.75	35.16	35.91	35.35	35.57	36.14
Cr ₂ O ₃	0.03	0.14	0.08	0.13	0.10	0.10	0.00	0.07	0.08	0.00	0.00	0.04	0.09
V ₂ O ₃	0.11	0.10	0.05	0.28	0.27	0.29	0.09	0.08	0.19	0.02	0.01	0.01	0.13
MgO	0.83	0.91	1.44	0.61	0.78	0.72	1.27	1.00	0.76	1.03	2.33	2.02	1.32
CaO	0.02	0.01	0.01	0.03	0.00	0.12	0.08	0.00	0.01	0.01	0.05	0.02	0.00
MnO	0.07	0.00	0.00	0.03	0.05	0.03	0.00	0.00	0.01	0.01	0.01	0.04	0.00
FeO	0.28	0.22	0.24	0.27	0.29	0.28	0.19	0.20	0.19	0.25	0.38	0.49	0.40
BaO	1.43	1.27	0.95	1.39	1.29	1.12	0.94	1.11	1.43	2.10	2.22	1.47	3.08
Na ₂ O	0.17	0.21	0.21	0.22	0.24	0.35	0.26	0.21	0.24	0.37	0.36	0.33	0.34
K ₂ O	10.33	10.93	11.13	10.74	10.34	10.55	10.56	10.91	10.61	10.33	10.31	10.67	10.12
F	0.02	0.00	0.19	0.00	0.00	0.14	0.10	0.05	0.04	0.00	0.19	0.12	0.16
CL	0.00	0.01	0.00	0.00	0.00	0.00	0.01	0.00	0.01	0.01	0.00	0.00	0.01
H ₂ O *	4.38	4.41	4.25	4.36	4.43	4.26	4.30	4.32	4.31	4.49	4.27	4.38	4.27
O=F	-0.01	0.00	-0.08	0.00	0.00	-0.06	-0.04	-0.02	-0.02	0.00	-0.08	-0.05	-0.07
O=CL	0.00	0.00	0.00	0.00	0.00	0.00	0.00	0.00	0.00	0.00	0.00	0.00	0.00
TOTAL	98.42	98.85	99.00	97.76	99.03	98.57	97.95	97.81	97.51	100.54	100.15	100.62	100.32
Si ⁴⁺ apfu	2.990	2.991	3.052	2.954	2.925	2.934	3.084	3.003	2.975	3.051	3.005	3.030	2.960
Ti ⁴⁺	0.075	0.075	0.049	0.074	0.092	0.094	0.050	0.070	0.069	0.013	0.007	0.005	0.030
Al ³⁺	2.838	2.815	2.752	2.871	2.894	2.876	2.727	2.809	2.856	2.823	2.807	2.796	2.882
Cr ³⁺	0.002	0.008	0.004	0.007	0.005	0.005	0.000	0.004	0.004	0.000	0.000	0.002	0.005
V ³⁺	0.006	0.005	0.003	0.015	0.015	0.016	0.005	0.004	0.010	0.001	0.001	0.001	0.007
Mg ²⁺	0.084	0.092	0.145	0.063	0.079	0.073	0.129	0.102	0.078	0.102	0.234	0.201	0.133
Ca ²⁺	0.001	0.001	0.001	0.002	0.000	0.009	0.006	0.000	0.001	0.001	0.004	0.001	0.000
Mn ²⁺	0.004	0.000	0.000	0.002	0.003	0.002	0.000	0.000	0.001	0.001	0.001	0.002	0.000
Fe ²⁺	0.016	0.013	0.014	0.016	0.016	0.016	0.011	0.011	0.011	0.014	0.021	0.027	0.023
Ba ²⁺	0.038	0.034	0.025	0.038	0.034	0.030	0.025	0.030	0.039	0.055	0.059	0.038	0.082
Na ⁺	0.022	0.028	0.028	0.029	0.032	0.046	0.034	0.028	0.032	0.048	0.047	0.043	0.045
K ⁺	0.897	0.947	0.961	0.943	0.893	0.918	0.918	0.955	0.933	0.879	0.886	0.908	0.874
F ⁻	0.004	0.000	0.041	0.000	0.000	0.030	0.022	0.011	0.009	0.000	0.040	0.025	0.034
Cl ⁻	0.000	0.001	0.000	0.000	0.000	0.001	0.000	0.001	0.001	0.000	0.000	0.000	0.001
OH ⁻	1.991	1.998	1.919	2.000	2.000	1.940	1.955	1.978	1.980	1.998	1.919	1.949	1.929
O ²⁻	10.004	10.001	10.041	10.000	10.000	10.030	10.023	10.011	10.010	10.001	10.040	10.025	10.035

Appendix A.4: Compositions of muscovite from lithologies within marble at the Revelstoke Occurrence (con't)

position EPMA point	G063b-09-34	G063b-09-35	G063b-09-36	G063b-09-37	G063b-09-38	G063b-09-39	G063b-09-40	G063b-09-41	G063b-09-42
SiO ₂ wt.%	44.11	43.63	43.26	43.74	44.13	43.62	43.52	43.50	44.46
TiO ₂	0.69	0.79	0.59	0.69	0.68	0.61	0.41	0.52	0.21
Al ₂ O ₃	36.23	35.42	34.67	35.86	35.23	34.70	35.88	35.14	36.01
Cr ₂ O ₃	0.12	0.23	0.14	0.19	0.21	0.04	0.02	0.06	0.00
V ₂ O ₃	0.15	0.08	0.09	0.03	0.02	0.01	0.01	0.05	0.00
MgO	1.07	1.52	2.93	1.68	2.14	2.90	2.30	2.90	1.98
CaO	0.02	0.00	0.00	0.00	0.07	0.00	0.01	0.02	0.07
MnO	0.00	0.00	0.02	0.03	0.04	0.00	0.01	0.01	0.00
FeO	0.32	0.37	0.58	0.48	0.41	0.46	0.63	0.59	0.40
BaO	2.91	3.10	2.84	3.23	2.94	2.84	2.60	2.72	2.97
Na ₂ O	0.30	0.35	0.35	0.28	0.33	0.37	0.32	0.27	0.39
K ₂ O	10.19	10.18	10.23	10.13	10.11	10.06	10.29	10.20	9.95
F	0.20	0.05	0.17	0.00	0.20	0.02	0.28	0.23	0.02
CL	0.00	0.00	0.00	0.01	0.00	0.00	0.00	0.02	0.00
H ₂ O *	4.26	4.37	4.24	4.44	4.26	4.40	4.17	4.20	4.45
O=F	-0.08	-0.02	-0.07	0.00	-0.08	-0.01	-0.12	-0.10	-0.01
O=CL	0.00	0.00	0.00	0.00	0.00	0.00	0.00	0.00	0.00
TOTAL	100.48	100.07	100.04	100.79	100.68	100.02	100.33	100.33	100.91
Si ⁴⁺ apfu	2.974	2.963	2.946	2.950	2.977	2.960	2.945	2.948	2.980
Ti ⁴⁺	0.035	0.040	0.030	0.035	0.035	0.031	0.021	0.027	0.011
Al ³⁺	2.879	2.835	2.782	2.850	2.801	2.775	2.862	2.806	2.845
Cr ³⁺	0.006	0.012	0.008	0.010	0.011	0.002	0.001	0.003	0.000
V ³⁺	0.008	0.004	0.005	0.002	0.001	0.001	0.001	0.003	0.000
Mg ²⁺	0.108	0.154	0.297	0.169	0.215	0.293	0.232	0.293	0.198
Ca ²⁺	0.001	0.000	0.000	0.000	0.005	0.000	0.001	0.001	0.005
Mn ²⁺	0.000	0.000	0.001	0.002	0.002	0.000	0.001	0.001	0.000
Fe ²⁺	0.018	0.021	0.033	0.027	0.023	0.026	0.036	0.033	0.022
Ba ²⁺	0.077	0.082	0.076	0.085	0.078	0.076	0.069	0.072	0.078
Na ⁺	0.039	0.046	0.046	0.037	0.043	0.049	0.042	0.035	0.051
K ⁺	0.877	0.882	0.889	0.872	0.870	0.871	0.888	0.882	0.851
F ⁻	0.043	0.011	0.037	0.000	0.043	0.004	0.060	0.049	0.004
Cl ⁻	0.000	0.000	0.000	0.001	0.000	0.000	0.002	0.000	
OH ⁻	1.915	1.979	1.927	1.998	1.915	1.991	1.880	1.897	1.992
O ²⁻	10.043	10.011	10.037	10.001	10.043	10.004	10.060	10.052	10.004

Appendix A.4: Compositions of margarite from lithologies within marble at the Revelstoke Occurrence (con't)

position EPMA point	Margarite		
	G063b-09-53	G063b-09-20	G022-07C-31
SiO ₂ wt.%	37.91	32.60	38.02
TiO ₂	1.96	0.06	0.48
Al ₂ O ₃	21.23	49.17	24.77
Cr ₂ O ₃	0.08	0.00	0.21
V ₂ O ₃	0.06	0.00	0.92
MgO	19.08	0.06	4.44
CaO	0.10	11.57	23.19
MnO	0.01	0.00	0.03
FeO	4.51	0.13	1.55
BaO	0.58	0.16	0.05
Na ₂ O	0.15	0.89	0.00
K ₂ O	10.28	0.79	0.00
F	0.86	0.00	0.35
CL	0.05	0.01	0.01
H ₂ O *	3.37	4.53	3.86
O=F	-0.36	0.00	-0.15
O=CL	-0.01	0.00	0.00
TOTAL	99.85	99.96	97.74
Si ⁴⁺ apfu	2.702	2.157	2.713
Ti ⁴⁺	0.105	0.003	0.026
Al ³⁺	1.783	3.835	2.083
Cr ³⁺	0.005	0.000	0.012
V ³⁺	0.003	0.000	0.053
Mg ²⁺	2.027	0.006	0.472
Ca ²⁺	0.008	0.820	1.773
Mn ²⁺	0.001	0.000	0.002
Fe ²⁺	0.269	0.007	0.092
Ba ²⁺	0.016	0.004	0.001
Na ⁺	0.021	0.114	0.000
K ⁺	0.935	0.067	0.000
F ⁻	0.194	0.000	0.079
Cl ⁻	0.006	0.001	0.001
OH-	1.600	1.998	1.840
O ²⁻	10.200	10.001	10.080

Appendix A.5: Compositions of plagioclase from lithologies within marble at the Revelstoke Occurrence

pos. and min. assoc.	c	c	r	r Ms	r	c	c	r Ms	r Kfs	r Kfs	r Kfs	c	c	r	r	r Ms	r Scp				
EPMA point	G10-01-55	G10-01-56	G10-01-57	G11-02-07a-2	G11-02-07a-3	G11-02-07a-4	G11-02-07b-5	G11-02-07b-9	G11-02-07b-10	G11-02-07b-13	G11-02-07b-14	G11-02-07c-18	G11-02-07c-19	G11-02-07c-22	G11-02-07c-23	G11-02-07c-24	G11-02-07c-25	G11-02-07c-29	G11-02-11-40	G11-02-11-41	TD-G007-07-5-4
SiO ₂ wt%	43.93	44.00	44.03	43.88	42.43	42.63	44.23	43.50	43.56	43.86	44.57	44.55	44.37	43.88	42.43	42.63	44.23	43.50	44.33	44.00	45.93
Al ₂ O ₃	36.17	35.79	36.40	36.15	36.11	36.21	35.78	36.07	36.14	36.06	35.98	35.85	35.88	36.15	36.11	36.21	35.78	36.07	35.93	36.14	34.47
MgO	0.00	0.00	0.01	0.00	0.00	0.00	0.00	0.00	0.00	0.00	0.00	0.01	0.00	0.00	0.00	0.00	0.00	0.00	0.00	0.02	0.00
CaO	19.58	19.51	19.76	19.37	19.38	19.58	19.18	19.21	19.59	19.31	19.16	19.16	19.28	19.37	19.38	19.58	19.18	19.21	19.23	19.50	18.13
MnO	0.00	0.00	0.03	0.00	0.00	0.00	0.00	0.01	0.00	0.00	0.01	0.02	0.00	0.00	0.00	0.00	0.00	0.01	0.01	0.00	0.00
FeO	0.04	0.00	0.00	0.12	0.06	0.05	0.03	0.04	0.00	0.00	0.01	0.01	0.00	0.12	0.06	0.05	0.03	0.04	0.01	0.00	0.01
BaO	0.06	0.00	0.02	0.01	0.00	0.00	0.00	0.00	0.02	0.01	0.03	0.04	0.03	0.01	0.00	0.00	0.00	0.00	0.00	0.00	0.02
Na ₂ O	0.52	0.62	0.47	0.58	0.55	0.46	0.62	0.44	0.40	0.62	0.66	0.61	0.67	0.58	0.55	0.46	0.62	0.44	0.59	0.50	1.31
K ₂ O	0.00	0.01	0.00	0.02	0.02	0.02	0.00	0.00	0.01	0.04	0.05	0.02	0.00	0.02	0.02	0.00	0.00	0.02	0.00	0.00	0.04
TOTAL	100.30	99.93	100.72	100.13	98.55	98.95	99.84	99.27	99.72	99.90	100.46	100.27	100.23	100.13	98.55	98.95	99.84	99.27	100.12	100.16	99.91
Si ⁴⁺ apfu	2.027	2.037	2.023	2.028	1.996	1.997	2.047	2.025	2.021	2.031	2.050	2.052	2.046	2.028	1.996	1.997	2.047	2.025	2.045	2.031	2.117
Al ³⁺	1.967	1.953	1.971	1.969	2.002	1.999	1.951	1.979	1.976	1.968	1.950	1.946	1.950	1.969	2.002	1.999	1.951	1.979	1.954	1.966	1.873
Mg ²⁺	0.000	0.000	0.001	0.000	0.000	0.000	0.000	0.000	0.000	0.000	0.000	0.001	0.000	0.000	0.000	0.000	0.000	0.000	0.001	0.000	0.000
Ca ²⁺	0.968	0.968	0.973	0.959	0.977	0.983	0.951	0.958	0.974	0.958	0.944	0.946	0.953	0.959	0.977	0.983	0.951	0.958	0.951	0.965	0.896
Mn ²⁺	0.000	0.000	0.001	0.000	0.000	0.000	0.000	0.000	0.000	0.000	0.000	0.001	0.000	0.000	0.000	0.000	0.000	0.000	0.000	0.000	0.000
Fe ²⁺	0.002	0.000	0.000	0.005	0.002	0.002	0.001	0.002	0.000	0.000	0.000	0.000	0.000	0.000	0.005	0.002	0.002	0.001	0.002	0.000	0.000
Ba ²⁺	0.001	0.000	0.000	0.000	0.000	0.000	0.000	0.000	0.000	0.000	0.001	0.001	0.001	0.000	0.000	0.000	0.000	0.000	0.000	0.000	0.000
Na	0.047	0.056	0.042	0.052	0.050	0.042	0.056	0.040	0.036	0.056	0.059	0.054	0.060	0.052	0.050	0.042	0.056	0.040	0.053	0.045	0.117
K ⁺	0.000	0.001	0.000	0.001	0.001	0.001	0.000	0.000	0.001	0.002	0.003	0.001	0.000	0.001	0.001	0.000	0.000	0.001	0.000	0.000	0.002
An mol%	0.95	0.94	0.96	0.95	0.95	0.96	0.94	0.96	0.96	0.94	0.94	0.95	0.94	0.95	0.95	0.96	0.94	0.96	0.95	0.96	0.883
Ab	0.05	0.05	0.04	0.05	0.05	0.04	0.06	0.04	0.04	0.06	0.05	0.06	0.05	0.05	0.05	0.04	0.06	0.04	0.05	0.04	0.115
Or	0.00	0.00	0.00	0.00	0.00	0.00	0.00	0.00	0.00	0.00	0.00	0.00	0.00	0.00	0.00	0.00	0.00	0.00	0.00	0.00	0.002

NOTE: The following standards, X-ray lines and crystals were used during EMP analysis: albite, Na K_A, TAP; anorthite, Al K_A, TAP;

diopside, Mg K_A, TAP; orthoclase, Si K_A, TAP; orthoclase, K K_A, PET; anorthite, Ca K_A, PET; synthetic fayalite, Fe K_A, LIF;

barite, Ba La PET. Compositions were recalculated on the basis of 8 O apfu

c = core, m = middle, r = rim

Appendix A.5: Compositions of plagioclase from lithologies within marble at the Revelstoke Occurrence (con't)

pos. and min. assoc.	c	r Cal	m Scp?	r alt	r alt	r Cal	r alt r Sc c Scp	r Scp	c	r mica	r Cal	r Kfs	r Cal	m	c	r Scp	r Cal	r Pl	c	r Kfs	
EPMA point	TD-G007-07-5-5	TD-G007-07-5-6	TD-G007-07-5-8	TD-G007-07-5-13	TD-G007-07-4-14	TD-G007-07-4-15	TD-G007-07-12-24	TD-G007-07-12-25	TD-G007-07-12-26	TD-G014-07A1-02-1	TD-G014-07A1-02-2	TD-G014-07A1-02-3	TD-G014-07A1-02-4	TD-G014-07A1-04-10	TD-G014-07A1-04-11	TD-G014-07A1-04-12	TD-G014-07A1-03-13	TD-G014-07A1-03-14	TD-G014-07A1-03-15	TD-G014-07A1-08-16	TD-G014-07A1-08-17
SiO ₂ wt%	44.16	44.33	45.82	44.70	44.12	44.03	44.72	46.32	45.83	44.28	44.57	43.84	44.17	43.73	44.11	43.77	44.23	44.17	43.77	43.79	43.88
Al ₂ O ₃	35.12	35.67	34.44	35.18	35.52	35.79	35.05	33.54	33.91	35.80	35.67	35.74	35.53	35.49	35.65	35.85	35.72	35.31	35.70	35.58	35.68
MgO	0.00	0.00	0.01	0.00	0.00	0.00	0.00	0.00	0.01	0.01	0.01	0.00	0.00	0.00	0.01	0.01	0.00	0.00	0.01	0.00	0.00
CaO	19.47	19.63	18.20	19.43	19.60	19.47	18.48	17.06	17.42	19.55	19.34	19.65	19.58	19.65	19.69	19.96	19.28	19.40	19.81	19.86	19.88
MnO	0.05	0.00	0.01	0.00	0.01	0.01	0.00	0.05	0.02	0.00	0.04	0.02	0.01	0.00	0.00	0.00	0.02	0.01	0.00	0.03	0.00
FeO	0.05	0.01	0.00	0.00	0.03	0.08	0.00	0.00	0.07	0.00	0.09	0.03	0.04	0.00	0.01	0.00	0.01	0.02	0.00	0.02	0.00
BaO	0.00	0.02	0.00	0.07	0.01	0.00	0.00	0.00	0.00	0.00	0.00	0.00	0.00	0.00	0.00	0.00	0.03	0.02	0.04	0.03	0.00
Na ₂ O	0.49	0.55	1.36	0.67	0.46	0.49	0.99	1.62	1.68	0.50	0.54	0.34	0.58	0.36	0.36	0.34	0.53	0.58	0.40	0.36	0.38
K ₂ O	0.00	0.00	0.01	0.01	0.01	0.02	0.01	0.03	0.01	0.01	0.02	0.02	0.03	0.00	0.02	0.01	0.03	0.02	0.00	0.02	0.00
TOTAL	99.34	100.21	99.85	100.06	99.76	99.89	99.25	98.62	98.95	100.15	100.28	99.64	99.94	99.23	99.85	99.94	99.86	99.53	99.72	99.70	99.82
Si ⁴⁺ apfu	2.056	2.046	2.114	2.066	2.046	2.039	2.078	2.156	2.132	2.044	2.054	2.036	2.045	2.039	2.043	2.028	2.047	2.053	2.033	2.035	2.035
Al ³⁺	1.927	1.941	1.873	1.916	1.941	1.953	1.919	1.840	1.859	1.948	1.937	1.956	1.939	1.950	1.946	1.958	1.948	1.934	1.954	1.948	1.950
Mg ²⁺	0.000	0.000	0.001	0.000	0.000	0.000	0.000	0.000	0.001	0.001	0.001	0.000	0.000	0.000	0.001	0.001	0.001	0.000	0.000	0.001	0.000
Ca ²⁺	0.971	0.971	0.900	0.962	0.974	0.966	0.920	0.851	0.868	0.967	0.955	0.978	0.972	0.982	0.977	0.991	0.956	0.966	0.986	0.989	0.988
Mn ²⁺	0.002	0.000	0.000	0.000	0.000	0.000	0.000	0.002	0.001	0.000	0.002	0.001	0.000	0.000	0.000	0.001	0.000	0.000	0.000	0.001	0.000
Fe ²⁺	0.002	0.000	0.000	0.000	0.001	0.003	0.000	0.000	0.003	0.000	0.003	0.001	0.002	0.000	0.000	0.000	0.000	0.001	0.000	0.001	0.000
Ba ²⁺	0.000	0.000	0.000	0.001	0.000	0.000	0.000	0.000	0.000	0.000	0.000	0.000	0.000	0.000	0.000	0.001	0.000	0.001	0.001	0.000	0.000
Na	0.044	0.049	0.122	0.060	0.041	0.044	0.089	0.146	0.152	0.045	0.048	0.031	0.052	0.033	0.032	0.031	0.048	0.052	0.036	0.032	0.034
K ⁺	0.000	0.000	0.001	0.001	0.001	0.001	0.002	0.001	0.001	0.001	0.001	0.002	0.000	0.001	0.001	0.002	0.001	0.000	0.001	0.000	0.000
An mol%	0.957	0.952	0.880	0.940	0.959	0.955	0.911	0.852	0.850	0.955	0.951	0.968	0.947	0.967	0.967	0.969	0.950	0.948	0.965	0.968	0.967
Ab	0.043	0.048	0.119	0.059	0.040	0.044	0.088	0.146	0.149	0.044	0.048	0.031	0.051	0.033	0.032	0.030	0.048	0.051	0.035	0.031	0.033
Or	0.000	0.000	0.001	0.001	0.001	0.001	0.002	0.001	0.001	0.001	0.001	0.002	0.000	0.001	0.001	0.002	0.001	0.000	0.001	0.000	0.000

Appendix A.5: Compositions of plagioclase from lithologies within marble at the Revelstoke Occurrence (con't)

pos. and min. assoc.	r mica	r Pl	r mica	r Pl mica	r mica	r	m	c	r	r	r Pl	c	c	r Pl	m	c	c	c	
EPMA point	TD-G014-07A1-01-30	TD-G014-07A1-01-31	TD-G014-07A1-01-32	TD-G014-07A1-01-33	TD-G014-07A1-01-34	TD-G014-07A2-01-53	TD-G014-07A2-01-54	TD-G014-07A2-01-55	TD-G014-07A2-05-72	TD-G014-07A2-05-73	TD-G014-07A2-05-74	TD-G014-07A2-05-75	TD-G014-07A2-05-76	TD-G014-07A2-09-78	TD-G014-07A2-09-79	TD-G014-07A2-09-80	TD-G014-07B1-01-1	TD-G014-07B1-01-2	
SiO ₂ wt%	44.12	44.15	43.93	44.04	44.15	45.19	44.60	44.73	44.88	44.92	44.77	44.53	45.03	45.02	44.47	44.90	44.52	44.78	44.99
Al ₂ O ₃	35.87	35.76	36.06	36.02	35.86	35.54	36.12	36.12	36.12	35.92	35.42	35.62	35.84	35.75	35.90	35.79	35.63	36.01	35.33
MgO	0.01	0.00	0.00	0.02	0.00	0.00	0.01	0.00	0.00	0.00	0.00	0.00	0.00	0.00	0.01	0.00	0.00	0.00	0.00
CaO	19.48	19.58	20.04	19.61	19.69	19.17	19.74	19.73	19.43	19.43	19.38	19.42	19.30	19.42	19.58	19.26	19.49	19.54	19.22
MnO	0.01	0.00	0.00	0.01	0.00	0.00	0.00	0.00	0.02	0.00	0.01	0.00	0.00	0.04	0.02	0.00	0.00	0.00	0.00
FeO	0.01	0.02	0.00	0.00	0.00	0.03	0.02	0.01	0.03	0.00	0.00	0.00	0.00	0.01	0.00	0.00	0.03	0.00	0.03
BaO	0.00	0.02	0.02	0.03	0.01	0.00	0.00	0.02	0.05	0.00	0.03	0.00	0.08	0.00	0.00	0.00	0.02	0.00	0.00
Na ₂ O	0.45	0.54	0.40	0.52	0.46	0.68	0.47	0.43	0.55	0.58	0.74	0.57	0.52	0.60	0.49	0.61	0.58	0.44	0.69
K ₂ O	0.02	0.02	0.02	0.02	0.01	0.01	0.01	0.01	0.01	0.01	0.01	0.01	0.01	0.02	0.00	0.00	0.01	0.00	0.00
TOTAL	99.97	100.09	100.47	100.27	100.18	100.62	100.96	101.06	101.09	100.86	100.36	100.15	100.78	100.86	100.47	100.56	100.28	100.77	100.26
Si ⁴⁺ apfu	2.040	2.041	2.026	2.033	2.039	2.072	2.043	2.046	2.051	2.057	2.062	2.054	2.063	2.062	2.046	2.061	2.053	2.052	2.072
Al ³⁺	1.955	1.948	1.960	1.959	1.952	1.921	1.950	1.947	1.946	1.938	1.923	1.937	1.935	1.930	1.947	1.936	1.936	1.945	1.917
Mg ²⁺	0.001	0.000	0.000	0.001	0.000	0.000	0.000	0.001	0.000	0.000	0.000	0.000	0.000	0.000	0.001	0.000	0.000	0.000	0.000
Ca ²⁺	0.965	0.970	0.990	0.970	0.974	0.942	0.969	0.967	0.952	0.953	0.957	0.960	0.947	0.953	0.965	0.947	0.963	0.959	0.948
Mn ²⁺	0.000	0.000	0.000	0.000	0.000	0.000	0.000	0.000	0.001	0.000	0.000	0.000	0.000	0.002	0.001	0.000	0.000	0.000	0.000
Fe ²⁺	0.000	0.001	0.000	0.000	0.000	0.001	0.001	0.000	0.001	0.000	0.000	0.000	0.000	0.000	0.000	0.001	0.000	0.001	0.001
Ba ²⁺	0.000	0.000	0.000	0.001	0.000	0.000	0.000	0.000	0.001	0.000	0.001	0.000	0.001	0.000	0.000	0.000	0.000	0.000	0.000
Na	0.040	0.048	0.036	0.047	0.041	0.060	0.042	0.038	0.049	0.051	0.066	0.051	0.046	0.053	0.044	0.054	0.052	0.039	0.062
K ⁺	0.001	0.001	0.001	0.001	0.001	0.001	0.001	0.001	0.001	0.001	0.001	0.001	0.001	0.001	0.000	0.001	0.000	0.000	0.000
An mol%	0.959	0.952	0.964	0.953	0.959	0.939	0.958	0.961	0.950	0.948	0.935	0.949	0.953	0.946	0.956	0.946	0.948	0.961	0.939
Ab	0.040	0.047	0.035	0.046	0.040	0.060	0.042	0.038	0.049	0.051	0.064	0.050	0.046	0.053	0.044	0.054	0.051	0.039	0.061
Or	0.001	0.001	0.001	0.001	0.001	0.001	0.001	0.001	0.001	0.001	0.001	0.001	0.001	0.001	0.000	0.001	0.000	0.000	0.000

Appendix A.5: Compositions of plagioclase from lithologies within marble at the Revelstoke Occurrence (con't)

pos. and min. assoc.	r Cal	r Ms + Cal	m	c	r Kfs	m	c	r Kfs	c	r Phl	c	r Crn	incl in Crn	r Ms	m	c	c	
EPMA point	TD-G014-07B1-01-3	TD-G014-07B1-12	TD-G014-07B1-13	TD-G014-07B1-14	TD-G014-07B1-03-20	TD-G014-07B1-03-21	TD-G014-07B1-22	TD-G014-07B1-03-25	TD-G014-07B1-03-26	TD-G014-07B1-04-40	TD-G014-07B1-04-41	TD-G014-07B1-04-42	TD-G014-07B1-04-43	TD-G014-07B1-04-44	TD-G014-07B1-04-45	TD-G014-07B1-04-46	TD-G014-07B1-04-47	TD-G063B-09-15-12
SiO ₂ wt%	44.22	44.90	44.60	46.07	44.87	44.56	44.36	44.26	44.55	44.85	44.87	44.36	44.82	44.51	44.80	44.73	44.61	43.77
Al ₂ O ₃	36.18	35.95	35.84	34.92	36.07	36.44	36.18	36.20	35.75	35.95	35.94	35.60	35.86	36.17	35.83	35.87	35.96	35.51
MgO	0.00	0.00	0.00	0.00	0.00	0.00	0.00	0.01	0.00	0.00	0.00	0.01	0.00	0.00	0.00	0.01	0.00	0.00
CaO	19.92	19.53	19.34	18.14	19.77	19.68	19.71	19.69	19.64	19.49	19.43	19.51	19.55	19.48	19.33	19.54	19.79	19.41
MnO	0.02	0.00	0.00	0.00	0.00	0.02	0.00	0.01	0.01	0.00	0.00	0.03	0.03	0.00	0.00	0.01	0.04	0.00
FeO	0.00	0.01	0.01	0.00	0.00	0.00	0.00	0.00	0.00	0.07	0.01	0.02	0.00	0.01	0.05	0.03	0.00	0.00
BaO	0.04	0.00	0.00	0.03	0.00	0.00	0.01	0.00	0.04	0.04	0.00	0.00	0.00	0.06	0.01	0.01	0.00	0.00
Na ₂ O	0.34	0.47	0.55	1.18	0.40	0.40	0.36	0.37	0.44	0.44	0.44	0.53	0.41	0.38	0.56	0.49	0.43	0.62
K ₂ O	0.01	0.04	0.02	0.03	0.03	0.01	0.01	0.02	0.01	0.02	0.01	0.01	0.01	0.02	0.01	0.00	0.00	0.00
TOTAL	100.73	100.90	100.36	100.37	101.14	101.11	100.63	100.56	100.44	100.86	100.70	100.07	100.68	100.56	100.65	100.70	100.84	99.31
Si ⁴⁺ apfu	2.032	2.055	2.053	2.112	2.050	2.037	2.038	2.035	2.051	2.054	2.057	2.050	2.056	2.044	2.057	2.053	2.046	2.039
Al ³⁺	1.959	1.939	1.944	1.887	1.942	1.963	1.959	1.961	1.939	1.941	1.941	1.939	1.939	1.957	1.938	1.940	1.944	1.950
Mg ²⁺	0.000	0.000	0.000	0.000	0.000	0.000	0.000	0.001	0.000	0.000	0.000	0.001	0.000	0.000	0.000	0.001	0.000	0.000
Ca ²⁺	0.981	0.958	0.954	0.891	0.968	0.964	0.970	0.970	0.969	0.957	0.954	0.966	0.961	0.958	0.951	0.961	0.972	0.969
Mn ²⁺	0.001	0.000	0.000	0.000	0.000	0.001	0.000	0.000	0.000	0.000	0.000	0.001	0.001	0.000	0.000	0.002	0.000	0.000
Fe ²⁺	0.000	0.000	0.000	0.000	0.000	0.000	0.000	0.000	0.000	0.003	0.000	0.001	0.000	0.000	0.002	0.001	0.000	0.000
Ba ²⁺	0.001	0.000	0.000	0.001	0.000	0.000	0.000	0.000	0.001	0.001	0.000	0.000	0.000	0.001	0.000	0.000	0.000	0.000
Na	0.030	0.042	0.049	0.105	0.035	0.035	0.032	0.033	0.039	0.039	0.039	0.047	0.036	0.034	0.050	0.044	0.038	0.056
K ⁺	0.001	0.002	0.001	0.002	0.002	0.001	0.001	0.001	0.001	0.001	0.001	0.001	0.001	0.001	0.001	0.000	0.000	0.000
An mol%	0.969	0.956	0.950	0.893	0.963	0.964	0.967	0.966	0.960	0.960	0.960	0.953	0.963	0.965	0.949	0.955	0.962	0.95
Ab	0.030	0.042	0.049	0.105	0.035	0.035	0.032	0.033	0.039	0.039	0.039	0.046	0.036	0.034	0.050	0.044	0.038	0.05
Or	0.001	0.002	0.001	0.002	0.002	0.001	0.001	0.001	0.001	0.001	0.001	0.001	0.001	0.001	0.001	0.000	0.000	0.00

Appendix A.5: Compositions of plagioclase from lithologies within marble at the Revelstoke Occurrence (con't)

pos. and min. assoc.	m	r Cal	r Kfs	c	r Ms alt wr	c	r	m	c	near Kfs	near cal	Pl w Ms alt sur by						
												Pl agg with Ap and Py	Ap	c	r			
EPMA point		TD-G063B-09-15-13	TD-G063B-09-15-14	TD-G063B-09-19-23	TD-G063B-09-19-24	TD-G063B-09-05-30	TD-G063B-09-31	TD-G063B-09-32	TD-G063B-09-51	TD-G063B-09-03-50	TD-G063B-09-03-52	TD-G022-07c-15-16	TD-G022-07c-15-17	TD-G022-07c-17-25	TD-G022-07c-17-26	TD-G022-07c-25-28	TD-G022-07c-25-29	
SiO ₂ wt%	44.17	44.23	45.24	44.64	44.15	44.41	43.96	43.70	43.49	44.25	45.20	44.94	45.59	43.84	44.05	44.04	43.88	43.70
Al ₂ O ₃	35.81	35.86	34.64	35.52	36.16	35.89	35.71	35.78	36.09	35.41	35.74	35.81	35.38	36.07	36.03	36.07	36.36	36.26
MgO	0.01	0.00	0.00	0.00	0.01	0.00	0.00	0.01	0.01	0.00	0.01	0.00	0.01	0.00	0.00	0.00	0.00	0.00
CaO	19.48	19.43	18.18	18.63	19.40	19.46	19.07	19.33	19.55	19.06	19.02	19.27	18.77	20.24	19.90	20.03	20.19	20.09
MnO	0.03	0.04	0.01	0.02	0.00	0.00	0.00	0.00	0.00	0.03	0.04	0.00	0.03	0.00	0.00	0.02	0.05	0.00
FeO	0.02	0.00	0.05	0.04	0.03	0.08	0.05	0.01	0.00	0.00	0.00	0.00	0.29	0.03	0.03	0.00	0.00	0.03
BaO	0.00	0.03	0.01	0.03	0.00	0.04	0.05	0.02	0.02	0.01	0.07	0.03	0.00	0.08	0.03	0.05	0.07	0.00
Na ₂ O	0.53	0.52	1.11	0.91	0.53	0.52	0.64	0.59	0.36	0.51	0.75	0.65	0.88	0.10	0.22	0.21	0.14	0.16
K ₂ O	0.01	0.00	0.03	0.04	0.00	0.02	0.01	0.02	0.00	0.08	0.02	0.03	0.05	0.02	0.03	0.01	0.03	0.01
TOTAL	100.06	100.11	99.27	99.83	100.28	100.42	99.49	99.46	99.52	99.35	100.85	100.73	101.00	100.38	100.29	100.43	100.72	100.25
Si ⁴⁺ apfu	2.041	2.043	2.100	2.064	2.035	2.045	2.043	2.033	2.022	2.057	2.069	2.060	2.084	2.024	2.032	2.030	2.019	2.018
Al ³⁺	1.951	1.952	1.895	1.936	1.964	1.948	1.956	1.962	1.977	1.940	1.928	1.935	1.906	1.962	1.959	1.960	1.971	1.974
Mg ²⁺	0.001	0.000	0.000	0.000	0.001	0.000	0.000	0.001	0.001	0.000	0.001	0.000	0.001	0.000	0.000	0.000	0.000	0.000
Ca ²⁺	0.965	0.961	0.904	0.923	0.958	0.960	0.949	0.963	0.974	0.949	0.933	0.947	0.919	1.001	0.984	0.989	0.995	0.994
Mn ²⁺	0.001	0.002	0.000	0.001	0.000	0.000	0.000	0.000	0.000	0.001	0.002	0.000	0.001	0.000	0.000	0.001	0.002	0.000
Fe ²⁺	0.001	0.000	0.002	0.002	0.001	0.003	0.002	0.000	0.000	0.000	0.000	0.000	0.011	0.001	0.001	0.000	0.000	0.001
Ba ²⁺	0.000	0.001	0.000	0.001	0.000	0.001	0.001	0.000	0.000	0.000	0.001	0.001	0.000	0.001	0.001	0.001	0.001	0.000
Na	0.047	0.047	0.100	0.082	0.047	0.046	0.058	0.053	0.032	0.046	0.067	0.058	0.078	0.009	0.020	0.019	0.012	0.014
K ⁺	0.001	0.000	0.002	0.002	0.000	0.001	0.001	0.001	0.000	0.005	0.001	0.002	0.003	0.001	0.002	0.001	0.002	0.001
An mol%	0.95	0.95	0.90	0.92	0.95	0.95	0.94	0.95	0.97	0.95	0.93	0.94	0.92	0.99	0.98	0.98	0.99	0.99
Ab	0.05	0.05	0.10	0.08	0.05	0.05	0.06	0.05	0.03	0.05	0.07	0.06	0.08	0.01	0.02	0.02	0.01	0.01
Or	0.00	0.00	0.00	0.00	0.00	0.00	0.00	0.00	0.00	0.01	0.00	0.00	0.00	0.00	0.00	0.00	0.00	0.00

Appendix A.5: Compositions of plagioclase from lithologies within marble at the Revelstoke Occurrence (con't)

pos. and min. assoc.	Irg grain near Kfs													
	c	r	c	m	r Cal	c	r Kfs	c	m	r Cal	r Cal	c	m	r Fe oxide
TD-G022-07B2-16-34														
TD-G022-07B2-16-35			TD-G020-07B2-03-15	TD-G020-07B2-03-16	TD-G020-07B2-03-17	TD-G020-07B2-01-21	TD-G020-07B2-01-22	TD-G020-07B2-04-26	TD-G020-07B2-04-27	TD-G020-07B2-04-28	TD-G020-07B2-04-30	TD-G020-07B2-18-35	TD-G020-07B2-18-36	TD-G020-07B2-18-37
SiO ₂ wt%	45.07	44.88	45.39	44.44	44.07	44.32	44.39	44.72	44.69	44.73	44.68	43.96	43.96	45.69
Al ₂ O ₃	35.31	35.83	35.55	35.85	36.11	35.59	35.60	35.53	35.50	35.60	35.79	35.85	35.78	35.19
MgO	0.00	0.00	0.02	0.00	0.00	0.01	0.00	0.00	0.00	0.01	0.01	0.00	0.00	0.01
CaO	19.34	19.43	18.92	19.88	19.87	19.60	19.66	19.44	19.46	19.61	19.60	19.89	19.77	19.19
MnO	0.00	0.01	0.00	0.02	0.01	0.00	0.03	0.00	0.00	0.00	0.01	0.00	0.00	0.00
FeO	0.07	0.00	0.00	0.00	0.07	0.00	0.03	0.08	0.00	0.01	0.03	0.00	0.02	0.20
BaO	0.00	0.02	0.00	0.02	0.00	0.01	0.05	0.01	0.01	0.00	0.00	0.00	0.04	0.00
Na ₂ O	0.59	0.51	0.75	0.42	0.27	0.42	0.44	0.45	0.46	0.45	0.48	0.27	0.21	0.67
K ₂ O	0.04	0.03	0.09	0.04	0.01	0.03	0.04	0.02	0.03	0.04	0.04	0.05	0.01	0.07
TOTAL	100.42	100.71	100.72	100.67	100.41	99.98	100.24	100.25	100.15	100.45	100.64	100.02	99.79	101.02
Si ⁴⁺ apfu	2.073	2.058	2.078	2.043	2.031	2.049	2.049	2.061	2.061	2.058	2.052	2.034	2.038	2.088
Al ³⁺	1.914	1.936	1.918	1.942	1.961	1.940	1.937	1.930	1.930	1.930	1.937	1.955	1.955	1.896
Mg ²⁺	0.000	0.000	0.001	0.000	0.000	0.001	0.000	0.000	0.000	0.001	0.001	0.000	0.000	0.001
Ca ²⁺	0.953	0.955	0.928	0.979	0.981	0.971	0.972	0.960	0.962	0.967	0.965	0.986	0.982	0.940
Mn ²⁺	0.000	0.000	0.000	0.001	0.000	0.000	0.001	0.000	0.000	0.000	0.000	0.000	0.000	0.000
Fe ²⁺	0.003	0.000	0.000	0.000	0.003	0.000	0.001	0.003	0.000	0.000	0.001	0.000	0.001	0.008
Ba ²⁺	0.000	0.000	0.000	0.000	0.000	0.000	0.001	0.000	0.000	0.000	0.000	0.000	0.001	0.000
Na	0.053	0.045	0.067	0.037	0.024	0.038	0.039	0.040	0.041	0.040	0.043	0.024	0.019	0.059
K ⁺	0.002	0.002	0.005	0.002	0.001	0.002	0.002	0.001	0.002	0.002	0.002	0.003	0.001	0.004
An mol%	0.95	0.95	0.93	0.96	0.98	0.96	0.96	0.96	0.96	0.96	0.96	0.97	0.98	0.94
Ab	0.05	0.04	0.07	0.04	0.02	0.04	0.04	0.04	0.04	0.04	0.04	0.02	0.02	0.06
Or	0.00	0.00	0.01	0.00	0.00	0.00	0.00	0.00	0.00	0.00	0.00	0.00	0.00	0.00

Appendix A.5: Compositions of K-feldspar from lithologies within marble at the Revelstoke Occurrence

			Kfs near cor alt to Ms		Kfs alt to Ms near An				r An		r An		Kfs w/n An Ms zone			r An		r An		r Kfs		r Kfs	
	r	c	r	c	c	c	c	c	r An	r An	r An	c	r An	r An	r An	r An	c	r Kfs	c	r Kfs	r Kfs	r Kfs	
SiO ₂ wt%	60.55	61.92	62.34	62.29	62.91	61.62	63.18	61.96	63.38	62.35	63.01	62.52	62.99	62.39	62.73	62.04	62.91	61.62					
Al ₂ O ₃	19.66	19.54	19.22	19.28	19.28	19.23	19.29	19.33	19.16	19.28	19.33	19.51	19.37	19.34	19.42	19.16	19.28	19.23					
MgO	0.00	0.00	0.02	0.00	0.01	0	0	0.01	0.00	0.00	0.01	0.00	0.00	0.00	0.00	0.00	0.00	0.00	0.01	0.00	0.01	0.00	
CaO	0.05	0.04	0.06	0.08	0.08	0.01	0.06	0.06	0.08	0.07	0.05	0.09	0.07	0.07	0.07	0.07	0.05	0.08	0.01	0.01	0.05	0.01	
MnO	0.00	0.02	0.00	0.02	0.01	0	0	0.01	0.02	0.00	0.00	0.01	0.00	0.02	0.00	0.00	0.00	0.01	0.00	0.00	0.01	0.00	
FeO	0.03	0.01	0.00	0.01	0	0.05	0.04	0.00	0.02	0.00	0.02	0.00	0.00	0.01	0.01	0.01	0.00	0.00	0.00	0.00	0.00	0.05	
BaO	4.46	3.26	2.78	2.93	2.59	2.72	2.22	2.74	2.34	2.38	2.50	2.48	2.51	2.50	2.38	2.65	2.59	2.72					
Na ₂ O	0.93	0.85	0.86	0.79	1.08	0.67	1.03	0.95	0.92	0.89	0.89	0.95	0.75	0.99	0.86	0.84	1.08	0.67					
K ₂ O	14.13	14.61	14.58	14.74	14.64	14.95	15.01	14.56	14.91	14.82	15.00	14.88	14.90	14.81	14.81	14.91	14.64	14.95					
TOTAL	99.81	100.25	99.86	100.14	100.6	99.25	100.83	99.62	100.83	99.79	100.81	100.44	100.59	100.13	100.28	99.65	100.60	99.25					
Si ⁴⁺ apfu	2.890	2.916	2.934	2.930	2.936	2.925	2.939	2.925	2.947	2.932	2.936	2.925	2.938	2.928	2.933	2.930	2.936	2.925					
Al ³⁺	1.106	1.085	1.066	1.069	1.06	1.076	1.057	1.075	1.050	1.069	1.062	1.076	1.065	1.070	1.070	1.067	1.060	1.076					
Mg ²⁺	0.000	0.000	0.001	0.000	0.001	0	0	0.001	0.000	0.000	0.001	0.000	0.000	0.000	0.000	0.000	0.000	0.001	0.000				
Ca ²⁺	0.003	0.002	0.003	0.004	0.004	0.001	0.003	0.003	0.004	0.004	0.002	0.005	0.003	0.004	0.004	0.003	0.004	0.001	0.000				
Mn ²⁺	0.000	0.001	0.000	0.001	0	0	0	0.000	0.001	0.000	0.000	0.000	0.000	0.001	0.000	0.000	0.000	0.000					
Fe ²⁺	0.001	0.000	0.000	0.000	0	0.002	0.002	0.000	0.001	0.000	0.001	0.000	0.000	0.000	0.000	0.000	0.000	0.000	0.002				
Ba ²⁺	0.083	0.060	0.051	0.054	0.047	0.051	0.04	0.051	0.043	0.044	0.046	0.045	0.046	0.046	0.044	0.049	0.047	0.051					
Na ⁺	0.086	0.078	0.078	0.072	0.098	0.062	0.093	0.087	0.083	0.081	0.080	0.086	0.068	0.090	0.078	0.077	0.098	0.062					
K ⁺	0.860	0.878	0.875	0.884	0.872	0.905	0.891	0.877	0.884	0.889	0.892	0.888	0.887	0.887	0.883	0.898	0.872	0.905					
An mol%	0.00	0.00	0.00	0.00	0.00	0.00	0.00	0.00	0.00	0.00	0.00	0.01	0.00	0.00	0.00	0.00	0.00	0.00	0.00				
Ab	0.09	0.08	0.08	0.08	0.10	0.06	0.09	0.09	0.09	0.08	0.08	0.09	0.07	0.09	0.08	0.08	0.08	0.10	0.06				
Or	0.91	0.92	0.92	0.92	0.90	0.93	0.90	0.91	0.91	0.92	0.91	0.93	0.90	0.92	0.92	0.90	0.92	0.90	0.93				

NOTE: The following standards, X-ray lines and crystals were used during EMP Analysis: albite, NaKa, TAP; Anorthite, AlKa, TAP; diopside, MgKa, TAP; orthoclase, SiKa, TAP; orthoclase, KKa, PET; Anorthite, CaKa, PET; synthetic fayalite, FeKa, LiF; barite, BaLa PET. Compositions were recalculated on the basis of 8 O apfu; c = core, m = middle, r = rim

Appendix A.5: Compositions of K-feldspar from lithologies within marble at the Revelstoke Occurrence (con't)

	pseudomor Ms by Kfs G11-02-07c-29	Kfs An Ms agg m c m			Kfs An Ms agg c r Ms			r Pl TD-G014-07A1-02-5			r mica TD-G014-07A1-02-6			r mica TD-G014-07A1-02-7			r Pl TD-G014-07A1-02-8			r Cal TD-G014-07A1-08-24			r Cal TD-G014-07A1-08-25			c TD-G014-07A1-08-26			m TD-G014-07A1-10-27			r Cal TD-G014-07A1-10-28			TD-G014-07A1-10-29							
SiO ₂ wt%	63.18	62.00	61.94	62.28	61.93	62.06	61.38	61.71	62.04	61.78	62.22	62.29	62.13	61.33	61.93	61.08	62.39																									
Al ₂ O ₃	19.29	19.30	19.11	19.23	19.35	19.37	19.27	19.28	19.34	19.34	19.16	19.24	19.08	19.35	19.16	19.25	19.14																									
MgO	0.00	0.01	0.01	0.00	0.00	0.00	0.00	0.00	0.00	0.00	0.01	0.00	0.01	0.00	0.00	0.00	0.00	0.00																								
CaO	0.06	0.15	0.08	0.06	0.07	0.08	0.06	0.06	0.08	0.05	0.06	0.06	0.06	0.06	0.02	0.06	0.05	0.05																								
MnO	0.00	0.03	0.02	0.00	0.00	0.04	0.00	0.02	0.03	0.00	0.00	0.00	0.00	0.00	0.00	0.00	0.00	0.00																								
FeO	0.04	0.01	0.00	0.03	0.03	0.00	0.07	0.00	0.00	0.00	0.00	0.00	0.00	0.00	0.00	0.03	0.00	0.03																								
BaO	2.22	2.73	2.39	2.31	2.60	2.65	3.62	4.15	3.49	3.23	3.58	3.47	3.11	4.10	3.16	5.03	3.16																									
Na ₂ O	1.03	0.80	0.94	0.89	0.86	0.97	0.85	0.87	0.76	0.78	0.83	0.71	0.69	0.77	0.71	0.68	0.75																									
K ₂ O	15.01	14.76	14.88	14.98	14.84	14.83	14.33	14.24	14.41	14.86	14.16	14.68	15.03	14.37	14.93	14.00	14.61																									
TOTAL	100.83	99.79	99.37	99.78	99.68	100.00	99.58	100.33	100.15	100.04	100.02	100.45	100.14	99.95	100.01	100.09	100.14																									
Si ⁴⁺ apfu	2.939	2.925	2.930	2.931	2.923	2.922	2.917	2.919	2.925	2.919	2.934	2.930	2.931	2.913	2.926	2.912	2.936																									
Al ³⁺	1.057	1.073	1.065	1.067	1.076	1.075	1.079	1.075	1.075	1.077	1.065	1.067	1.061	1.083	1.067	1.082	1.062																									
Mg ²⁺	0.000	0.001	0.001	0.000	0.000	0.000	0.000	0.000	0.000	0.000	0.000	0.000	0.001	0.000	0.001	0.000	0.000																									
Ca ²⁺	0.003	0.008	0.004	0.003	0.004	0.004	0.003	0.003	0.004	0.003	0.003	0.003	0.003	0.001	0.003	0.003	0.003																									
Mn ²⁺	0.000	0.001	0.001	0.000	0.000	0.002	0.000	0.001	0.001	0.000	0.000	0.000	0.000	0.000	0.000	0.000	0.000																									
Fe ²⁺	0.002	0.000	0.000	0.001	0.001	0.000	0.003	0.000	0.000	0.000	0.000	0.000	0.001	0.000	0.001	0.000	0.002																									
Ba ²⁺	0.040	0.050	0.044	0.043	0.048	0.049	0.067	0.077	0.064	0.060	0.066	0.064	0.057	0.076	0.059	0.094	0.058																									
Na ⁺	0.093	0.073	0.086	0.081	0.079	0.089	0.078	0.080	0.069	0.071	0.076	0.065	0.063	0.071	0.065	0.063	0.068																									
K ⁺	0.891	0.888	0.898	0.899	0.894	0.891	0.869	0.859	0.867	0.896	0.852	0.881	0.905	0.871	0.900	0.851	0.877																									
An mol%	0.00	0.01	0.00	0.00	0.00	0.00	0.00	0.00	0.00	0.00	0.00	0.00	0.00	0.00	0.00	0.00	0.00																									
Ab	0.09	0.08	0.09	0.08	0.08	0.09	0.08	0.08	0.07	0.07	0.08	0.07	0.06	0.08	0.07	0.07	0.07																									
Or	0.90	0.92	0.91	0.91	0.92	0.91	0.91	0.91	0.92	0.92	0.93	0.93	0.92	0.93	0.92	0.93	0.93																									

Appendix A.5: Compositions of K-feldspar from lithologies within marble at the Revelstoke Occurrence (con't)

	dark r TD-G014-07A2-1	light r TD-G014-07A2-3B-2	mid r TD-G014-07A2-3B-3	looks like Ms grain that was altered to Kfs c TD-G014-07A2-3B-4	light c TD-G014-07A2-01-48	dark c TD-G014-07A2-01-49	mid r TD-G014-07A2-01-50	light c TD-G014-07A2-01-51	light c TD-G014-07A2-01-52	light r Cal TD-G014-07B1-3-15	med c TD-G014-07B1-3-16	med r An TD-G014-07B1-3-17	med r An TD-G014-07B1-3-18	med r An TD-G014-07B1-3-19	med r Kfs TD-G014-07B1-3-24	med r TD-G063B-09-15-1	light m TD-G063B-09-15-2	
SiO ₂ wt%	62.78	61.73	61.36	62.65	58.62	62.83	61.10	59.76	59.01	60.85	63.51	63.23	61.21	62.63	63.51	60.42	59.74	58.83
Al ₂ O ₃	19.60	19.78	19.72	19.50	20.08	19.51	19.77	20.05	20.18	19.68	19.25	19.32	19.79	19.23	19.18	20.01	19.82	19.92
MgO	0.00	0.03	0.00	0.00	0.00	0.00	0.00	0.00	0.00	0.00	0.01	0.01	0.00	0.00	0.00	0.00	0.01	0.00
CaO	0.10	0.08	0.03	0.07	0.05	0.06	0.08	0.05	0.04	0.03	0.07	0.08	0.08	0.10	0.06	0.07	0.06	0.06
MnO	0.00	0.00	0.00	0.00	0.04	0.00	0.02	0.00	0.00	0.00	0.03	0.00	0.01	0.02	0.02	0.00	0.00	0.01
FeO	0.00	0.02	0.05	0.00	0.02	0.00	0.03	0.03	0.00	0.02	0.00	0.00	0.00	0.05	0.00	0.03	0.00	0.00
BaO	2.40	4.15	4.43	3.69	8.31	3.68	5.39	7.26	8.29	5.98	2.79	2.46	5.32	2.98	2.46	6.61	5.17	6.67
Na ₂ O	0.82	0.77	0.76	0.80	0.73	0.78	0.85	0.77	0.75	0.83	0.97	0.83	0.87	0.93	0.91	0.91	0.99	1.05
K ₂ O	14.97	14.17	14.28	14.54	12.70	14.38	13.71	13.12	12.81	13.19	14.78	15.07	13.59	14.46	14.62	13.04	13.36	12.94
TOTAL	100.67	100.73	100.63	101.25	100.55	101.24	100.95	101.04	101.08	100.58	101.41	101.00	100.87	100.40	100.76	101.09	99.15	99.48
Si ⁴⁺ apfu	2.927	2.905	2.901	2.925	2.844	2.929	2.893	2.863	2.846	2.896	2.943	2.939	2.896	2.935	2.951	2.875	2.877	2.855
Al ³⁺	1.077	1.097	1.099	1.073	1.148	1.072	1.103	1.132	1.147	1.104	1.051	1.058	1.103	1.062	1.050	1.122	1.125	1.139
Mg ²⁺	0.000	0.002	0.000	0.000	0.000	0.000	0.000	0.000	0.000	0.000	0.001	0.001	0.000	0.000	0.000	0.000	0.001	0.000
Ca ²⁺	0.005	0.004	0.002	0.004	0.003	0.003	0.004	0.003	0.002	0.002	0.003	0.004	0.004	0.005	0.003	0.004	0.003	0.003
Mn ²⁺	0.000	0.000	0.000	0.000	0.002	0.000	0.001	0.000	0.000	0.000	0.001	0.000	0.000	0.001	0.001	0.000	0.000	0.000
Fe ²⁺	0.000	0.001	0.002	0.000	0.001	0.000	0.001	0.001	0.000	0.001	0.000	0.000	0.000	0.002	0.000	0.001	0.000	0.000
Ba ²⁺	0.044	0.077	0.082	0.068	0.158	0.067	0.100	0.136	0.157	0.112	0.051	0.045	0.099	0.055	0.045	0.123	0.098	0.127
Na ⁺	0.074	0.070	0.070	0.072	0.069	0.071	0.078	0.072	0.070	0.077	0.087	0.075	0.080	0.084	0.082	0.084	0.092	0.099
K ⁺	0.890	0.851	0.861	0.866	0.786	0.855	0.828	0.802	0.788	0.801	0.874	0.894	0.820	0.864	0.867	0.792	0.821	0.801
An mol%	0.01	0.00	0.00	0.00	0.00	0.00	0.00	0.00	0.00	0.00	0.00	0.00	0.00	0.01	0.00	0.00	0.00	0.00
Ab	0.08	0.08	0.08	0.08	0.08	0.08	0.09	0.08	0.08	0.09	0.09	0.08	0.09	0.09	0.09	0.10	0.10	0.11
Or	0.92	0.92	0.92	0.92	0.92	0.92	0.91	0.91	0.91	0.91	0.91	0.92	0.91	0.91	0.91	0.90	0.90	0.89

Appendix A.5: Compositions of K-feldspar from lithologies within marble at the Revelstoke Occurrence (con't)

	light m	med m	light c	light c	Kfs in scp zone c	large isolated grain r Cal	intergrowth of Kfs An Ms r An	rimming Scp w Ms alt. sur by Cal Py Ap r Kfs	rimming scp sur by Cal r	inclusion Ms alt c								
	TD-G063B-09-15-3	TD-G063B-09-15-4	TD-G063B-09-15-5	TD-G063B-09-15-6	TD-G020-07B2-8-1	TD-G020-07B2-8-2	TD-G020-07B2-3-18	TD-G020-07B2-3-19	TD-G020-07B2-3-20	TD-G020-07B2-1-23	TD-G020-07B2-1-24	TD-G020-07B2-1-25	TD-G022-07C-14-1	TD-G022-07C-14-2	TD-G022-07C-14-3	TD-G022-07C-14-4	TD-G022-07C-14-5	TD-G022-07C-15-19
SiO ₂ wt%	59.15	59.49	58.30	59.18	63.63	63.71	63.37	63.88	63.89	63.72	63.62	63.65	64.72	64.55	64.46	64.58	64.94	64.61
Al ₂ O ₃	19.95	19.56	19.75	19.83	18.22	18.28	18.81	18.69	18.68	18.98	18.94	18.92	18.65	18.77	18.56	18.69	18.39	18.85
MgO	0.00	0.01	0.00	0.00	0.00	0.00	0.01	0.00	0.00	0.00	0.00	0.00	0.00	0.00	0.00	0.01	0.01	0.00
CaO	0.04	0.05	0.07	0.04	0.03	0.03	0.09	0.07	0.06	0.09	0.04	0.05	0.05	0.05	0.07	0.15	0.05	0.05
MnO	0.01	0.02	0.02	0.00	0.01	0.00	0.04	0.00	0.00	0.03	0.05	0.00	0.00	0.05	0.01	0.02	0.03	0.01
FeO	0.05	0.08	0.02	0.04	0.05	0.01	0.00	0.01	0.00	0.01	0.00	0.00	0.00	0.05	0.00	0.00	0.00	0.07
BaO	5.97	5.32	6.47	5.85	1.72	1.50	2.11	2.01	2.18	2.31	2.37	2.33	1.29	1.46	1.22	1.28	1.10	1.29
Na ₂ O	1.10	0.95	0.85	0.81	0.68	0.72	0.65	0.56	0.55	0.64	0.59	0.61	0.70	0.71	0.70	0.68	0.73	0.70
K ₂ O	13.19	13.58	13.25	13.53	15.23	15.39	15.18	15.29	15.33	15.03	15.24	15.20	15.45	15.33	15.40	15.62	15.51	15.65
TOTAL	99.46	99.06	98.73	99.28	99.57	99.64	100.26	100.51	100.69	100.81	100.85	100.76	100.91	100.94	100.50	100.93	100.76	101.27
Si ⁴⁺ apfu	2.860	2.878	2.854	2.866	2.984	2.983	2.960	2.972	2.971	2.960	2.959	2.960	2.983	2.977	2.983	2.979	2.994	2.973
Al ³⁺	1.137	1.115	1.139	1.132	1.007	1.009	1.035	1.025	1.024	1.039	1.038	1.037	1.013	1.020	1.012	1.016	0.999	1.022
Mg ²⁺	0.000	0.001	0.000	0.000	0.000	0.000	0.001	0.000	0.000	0.000	0.000	0.000	0.000	0.000	0.001	0.001	0.000	0.000
Ca ²⁺	0.002	0.003	0.004	0.002	0.002	0.002	0.005	0.003	0.003	0.004	0.002	0.002	0.002	0.003	0.007	0.002	0.002	0.004
Mn ²⁺	0.000	0.001	0.001	0.000	0.000	0.000	0.002	0.000	0.000	0.001	0.002	0.000	0.000	0.002	0.000	0.001	0.001	0.000
Fe ²⁺	0.002	0.003	0.001	0.002	0.002	0.000	0.000	0.000	0.000	0.000	0.000	0.000	0.002	0.000	0.000	0.000	0.000	0.003
Ba ²⁺	0.113	0.101	0.124	0.111	0.032	0.028	0.039	0.037	0.040	0.042	0.043	0.042	0.023	0.026	0.022	0.023	0.020	0.023
Na ⁺	0.103	0.089	0.081	0.076	0.062	0.065	0.059	0.051	0.050	0.058	0.053	0.055	0.063	0.063	0.063	0.061	0.065	0.062
K ⁺	0.813	0.838	0.827	0.836	0.911	0.919	0.905	0.907	0.909	0.891	0.904	0.902	0.909	0.909	0.919	0.912	0.919	0.919
An mol%	0.00	0.00	0.00	0.00	0.00	0.00	0.01	0.00	0.00	0.00	0.00	0.00	0.00	0.01	0.00	0.00	0.00	0.00
Ab	0.11	0.10	0.09	0.08	0.06	0.07	0.06	0.05	0.05	0.06	0.06	0.06	0.06	0.07	0.06	0.06	0.07	0.06
Or	0.89	0.90	0.91	0.91	0.93	0.93	0.93	0.94	0.94	0.93	0.94	0.94	0.93	0.93	0.94	0.93	0.93	0.93

Appendix A.5: Compositions of K-feldspar from lithologies within marble at the Revelstoke Occurrence (con't)

	in An, w eration r	next to Ap inclu c	Ms alteration around edge next to An m r			large grain sur by Cal near large An grain c m r		
	TD-G022-07C-15-20	TD-G022-07C-15-21	TD-G022-07C-15-22	TD-G022-07C-15-23	TD-G022-07C-15-24	TD-G022-07C-16-31	TD-G022-07C-16-32	TD-G022-07C-16-33
SiO ₂ wt%	64.51	68.12	64.51	64.40	64.38	63.67	63.58	64.32
Al ₂ O ₃	18.78	20.72	18.41	18.63	18.64	18.84	18.88	18.38
MgO	0.00	0.00	0.01	0.00	0.00	0.01	0.00	0.00
CaO	0.08	1.14	0.09	0.10	0.09	0.15	0.12	0.06
MnO	0.03	0.00	0.00	0.03	0.01	0.00	0.00	0.01
FeO	0.00	0.08	0.00	0.00	0.01	0.00	0.01	0.01
BaO	1.39	0.05	1.27	1.27	1.41	2.07	2.18	1.23
Na ₂ O	0.76	11.12	0.69	0.69	0.81	0.69	0.72	0.76
K ₂ O	15.31	0.06	15.57	15.28	15.56	15.27	15.13	15.46
TOTAL	100.86	101.29	100.55	100.40	100.91	100.70	100.62	100.23
Si ⁴⁺ apfu	2.977	2.946	2.987	2.982	2.976	2.961	2.959	2.987
Al ³⁺	1.021	1.056	1.005	1.017	1.015	1.032	1.036	1.006
Mg ²⁺	0.000	0.000	0.001	0.000	0.000	0.001	0.000	0.000
Ca ²⁺	0.004	0.053	0.004	0.005	0.004	0.007	0.006	0.003
Mn ²⁺	0.001	0.000	0.000	0.001	0.000	0.000	0.000	0.000
Fe ²⁺	0.000	0.003	0.000	0.000	0.000	0.000	0.000	0.000
Ba ²⁺	0.025	0.001	0.023	0.023	0.026	0.038	0.040	0.022
Na ⁺	0.068	0.932	0.062	0.062	0.073	0.062	0.065	0.068
K ⁺	0.901	0.003	0.920	0.903	0.917	0.906	0.898	0.916
An mol%	0.00	0.05	0.00	0.01	0.00	0.01	0.01	0.00
Ab	0.07	0.94	0.06	0.06	0.07	0.06	0.07	0.07
Or	0.93	0.00	0.93	0.93	0.92	0.93	0.93	0.93

Appendix A.6: Compositions of scapolite from lithologies within marble at the Revelstoke Occurrence

	TD-G020-07B2-8-3	TD-G020-07B2-8-4	TD-G020-07B2-8-5	TD-G020-07B2-10-6	TD-G020-07B2-10-7	TD-G020-07B2-10-8	TD-G022-07C-14-6	TD-G022-07C-14-7	TD-G022-07C-14-8	TD-G022-07C-14-9	TD-G022-07C-14-10	TD-G022-07C-14-11	TD-G007-07-16-1	TD-G007-07-16-2	TD-G007-07-16-3	TD-G007-07-05-9	TD-G007-07-05-10	TD-G007-07-05-11
SiO ₂ wt.%	46.00	46.49	47.83	45.55	46.96	46.12	46.19	46.03	45.90	46.44	46.58	46.22	46.19	45.00	45.97	46.85	45.91	46.65
Al ₂ O ₃	28.06	28.19	28.12	28.13	28.19	28.10	28.71	28.35	28.96	28.92	28.46	28.73	27.82	27.60	27.63	27.35	27.47	27.48
MgO	0.01	0.00	0.10	0.05	0.03	0.01	0.07	0.05	0.06	0.08	0.05	0.08	0.01	0.03	0.04	0.01	0.02	0.00
CaO	18.83	18.78	16.54	18.88	18.44	19.02	19.04	19.50	19.82	19.58	19.33	19.38	18.35	18.05	18.31	16.97	17.83	17.23
MnO	0.00	0.02	0.02	0.00	0.01	0.02	0.04	0.05	0.03	0.00	0.00	0.01	0.00	0.02	0.02	0.01	0.03	0.00
FeO	0.06	0.03	0.20	0.20	0.04	0.07	0.03	0.06	0.03	0.01	0.02	0.01	0.04	0.00	0.05	0.00	0.02	0.05
Na ₂ O	2.87	2.90	3.31	2.51	2.99	2.80	2.72	2.67	2.55	2.66	2.61	2.76	3.42	3.26	3.22	3.89	3.53	3.81
K ₂ O	0.31	0.29	0.50	0.32	0.41	0.29	0.33	0.31	0.28	0.32	0.36	0.34	0.39	0.32	0.40	0.40	0.36	0.37
SO ₃	0.00	0.01	0.02	0.01	0.02	0.00	0.05	0.01	0.05	0.05	0.01	0.00	0.12	0.01	0.05	0.00	0.00	0.01
Cl	0.38	0.30	0.47	0.27	0.35	0.30	0.23	0.20	0.22	0.22	0.21	0.24	0.33	0.30	0.31	0.80	0.50	0.86
CO ₂	1.78	1.84	1.78	1.83	1.82	1.83	1.87	1.88	1.88	1.89	1.89	1.88	1.78	1.78	1.79	1.57	1.70	1.54
O=Cl	-0.09	-0.07	-0.11	-0.06	-0.08	-0.07	-0.05	-0.05	-0.05	-0.05	-0.05	-0.05	-0.07	-0.07	-0.07	-0.18	-0.11	-0.19
TOTAL	98.22	98.78	98.78	97.69	99.18	98.49	99.23	99.07	99.73	100.12	99.48	99.59	98.37	96.30	97.72	97.67	97.26	97.80
Si ⁴⁺ apfu	6.981	6.999	7.088	6.945	7.028	6.985	6.926	6.953	6.882	6.921	6.976	6.926	7.018	6.965	7.024	7.109	7.037	7.083
Al ³⁺	5.019	5.001	4.912	5.055	4.972	5.015	5.074	5.047	5.118	5.079	5.024	5.074	4.982	5.035	4.976	4.891	4.963	4.917
Mg ²⁺	0.002	0.000	0.022	0.011	0.007	0.002	0.016	0.011	0.013	0.018	0.011	0.018	0.002	0.007	0.009	0.002	0.005	0.000
Ca ²⁺	3.062	3.029	2.626	3.084	2.957	3.086	3.059	3.156	3.184	3.126	3.102	3.112	2.987	2.993	2.998	2.759	2.928	2.803
Mn ²⁺	0.000	0.003	0.003	0.000	0.001	0.003	0.005	0.006	0.004	0.000	0.000	0.001	0.000	0.003	0.003	0.001	0.004	0.000
Fe ²⁺	0.008	0.004	0.025	0.026	0.005	0.009	0.004	0.008	0.004	0.001	0.003	0.001	0.005	0.000	0.006	0.000	0.003	0.006
Na ⁺	0.844	0.846	0.951	0.742	0.868	0.822	0.791	0.782	0.741	0.769	0.758	0.802	1.008	0.978	0.954	1.144	1.049	1.122
K ⁺	0.060	0.056	0.095	0.062	0.078	0.056	0.063	0.060	0.054	0.061	0.069	0.065	0.076	0.063	0.078	0.077	0.070	0.072
S ⁶⁺	0.000	0.001	0.002	0.001	0.002	0.000	0.006	0.001	0.006	0.006	0.001	0.000	0.014	0.001	0.006	0.000	0.000	0.001
Cl ⁻	0.098	0.077	0.118	0.070	0.089	0.077	0.058	0.051	0.056	0.056	0.053	0.061	0.085	0.079	0.080	0.206	0.130	0.221
C ⁴⁺	0.902	0.922	0.880	0.929	0.909	0.923	0.936	0.948	0.938	0.939	0.946	0.939	0.901	0.920	0.914	0.794	0.870	0.778
O ²⁻	24.063	24.029	23.811	24.035	24.010	24.070	24.025	24.109	24.094	24.071	24.048	24.059	24.143	24.050	24.107	24.031	24.083	24.062
CatSum	15.976	15.938	15.721	15.925	15.916	15.978	15.937	16.023	16.000	15.975	15.942	15.999	16.078	16.044	16.048	15.984	16.059	16.002
EqAn	0.673	0.667	0.637	0.685	0.657	0.672	0.691	0.682	0.706	0.693	0.675	0.691	0.661	0.678	0.659	0.630	0.654	0.639
XCI	0.098	0.077	0.118	0.070	0.089	0.077	0.058	0.051	0.056	0.056	0.053	0.061	0.085	0.079	0.080	0.206	0.130	0.221

*calculated from electroneutral formula assuming (Si+Al) = 12 apfu and (Cl+S+C)=1 apfu.

NOTE: Following standards, X-ray lines and crystals were used for EMP analysis: albite, NaKa , TAP; anorthite, AlKa , TAP; diopside, MgKa , TAP; orthoclase, SiKa , TAP; barite, SKa PET; scapolite, CIKa ,PET; orthoclase, KKa , PET; anorthite, CaKa , PET; synthetic fayalite, FeKa , LIF.

$$\text{EqAn} = (\text{Al}-3)/3$$

Appendix A.6: Compositions of scapolite from lithologies within marble at the Revelstoke Occurrence (con't)

	TD-G007-07-05-12	TD-G007-07-04-16	TD-G007-07-04-17	TD-G007-07-15-20	TD-G007-07-15-21	TD-G007-07-15-22	TD-G007-07-12-23	TD-G007-07-18	TD-G007-07-19	TD-G014-07A1-03-16	TD-G014-07A1-03-17	TD-G014-07A1-03-18	TD-G014-07A1-09-19	TD-G014-07A1-09-20	TD-G014-07A1-09-21	TD-G063B-09-05-25	TD-G063B-09-05-26	TD-G063B-09-05-28
SiO ₂ wt.%	45.82	44.98	43.87	44.21	44.27	44.24	45.58	44.42	45.91	45.89	45.45	45.95	46.69	44.01	45.34	47.47	47.05	47.00
Al ₂ O ₃	27.97	28.14	28.64	28.70	28.28	28.73	28.41	28.77	27.51	27.67	27.74	27.52	26.79	28.83	28.62	28.53	28.75	29.24
MgO	0.00	0.01	0.02	0.02	0.01	0.00	0.00	0.00	0.00	0.04	0.01	0.00	0.00	0.00	0.01	0.00	0.03	0.00
CaO	17.93	18.29	19.08	19.39	19.00	19.05	18.68	19.24	18.24	17.90	18.43	17.94	16.97	19.16	18.71	17.05	17.19	17.47
MnO	0.00	0.00	0.00	0.02	0.00	0.01	0.00	0.00	0.00	0.00	0.01	0.03	0.00	0.00	0.04	0.02	0.00	0.00
FeO	0.04	0.01	0.00	0.02	0.01	0.08	0.00	0.00	0.07	0.00	0.00	0.01	0.00	0.00	0.00	0.05	0.08	0.00
Na ₂ O	3.76	3.16	2.64	2.65	2.69	2.57	3.06	2.59	3.10	3.24	2.88	3.06	3.56	2.51	2.64	3.57	3.92	3.73
K ₂ O	0.26	0.48	0.42	0.46	0.42	0.56	0.39	0.40	0.44	0.70	0.57	0.61	0.71	0.59	0.88	0.97	1.04	0.77
SO ₃	0.08	0.00	0.07	0.08	0.04	0.07	0.03	0.01	0.06	0.00	0.02	0.07	0.04	0.00	0.02	0.03	0.01	0.00
Cl	0.67	0.39	0.35	0.33	0.33	0.37	0.53	0.29	0.30	0.44	0.38	0.37	0.53	0.40	0.54	1.01	1.05	1.02
CO ₂	1.61	1.75	1.75	1.76	1.76	1.75	1.70	1.81	1.79	1.74	1.75	1.75	1.68	1.75	1.70	1.51	1.49	1.52
O=Cl	-0.15	-0.09	-0.08	-0.07	-0.07	-0.08	-0.12	-0.07	-0.07	-0.10	-0.09	-0.08	-0.12	-0.09	-0.12	-0.23	-0.24	-0.23
TOTAL	97.99	97.13	96.76	97.57	96.74	97.34	98.26	97.46	97.35	97.52	97.16	97.23	96.85	97.16	98.37	99.98	100.37	100.52
Si ⁴⁺ apfu	6.979	6.907	6.782	6.798	6.846	6.797	6.918	6.805	7.033	7.015	6.979	7.035	7.159	6.772	6.881	7.024	6.976	6.924
Al ³⁺	5.021	5.093	5.218	5.202	5.154	5.203	5.082	5.195	4.967	4.985	5.021	4.965	4.841	5.228	5.119	4.976	5.024	5.076
Mg ²⁺	0.000	0.002	0.005	0.005	0.002	0.000	0.000	0.000	0.000	0.009	0.002	0.000	0.000	0.000	0.002	0.000	0.007	0.000
Ca ²⁺	2.926	3.009	3.160	3.195	3.148	3.136	3.038	3.158	2.994	2.932	3.032	2.943	2.788	3.159	3.042	2.703	2.731	2.757
Mn ²⁺	0.000	0.000	0.000	0.003	0.000	0.001	0.000	0.000	0.000	0.000	0.001	0.004	0.000	0.000	0.005	0.003	0.000	0.000
Fe ²⁺	0.005	0.001	0.000	0.003	0.001	0.010	0.000	0.000	0.009	0.000	0.000	0.001	0.000	0.000	0.000	0.006	0.010	0.000
Na ⁺	1.110	0.941	0.791	0.790	0.807	0.766	0.900	0.769	0.921	0.960	0.857	0.908	1.058	0.749	0.777	1.024	1.127	1.065
K ⁺	0.051	0.094	0.083	0.090	0.083	0.110	0.076	0.078	0.086	0.137	0.112	0.119	0.139	0.116	0.170	0.183	0.197	0.145
S ⁶⁺	0.009	0.000	0.008	0.009	0.005	0.008	0.003	0.001	0.007	0.000	0.002	0.008	0.005	0.000	0.002	0.003	0.001	0.000
Cl ⁻	0.173	0.101	0.092	0.086	0.086	0.096	0.136	0.075	0.078	0.114	0.099	0.096	0.138	0.104	0.139	0.253	0.264	0.255
C ⁴⁺	0.818	0.899	0.900	0.905	0.909	0.896	0.860	0.924	0.915	0.886	0.899	0.896	0.858	0.896	0.859	0.743	0.735	0.745
O ²⁻	24.124	24.035	24.071	24.124	24.081	24.065	24.067	24.027	24.089	24.054	24.069	24.059	24.053	24.029	24.042	23.968	24.034	23.951
CatSum	16.092	16.048	16.039	16.085	16.041	16.023	16.014	16.006	16.010	16.038	16.005	15.975	15.985	16.023	15.997	15.919	16.071	15.967
EqAn	0.674	0.698	0.739	0.734	0.718	0.734	0.694	0.732	0.656	0.662	0.674	0.655	0.614	0.743	0.706	0.659	0.675	0.692
XCI	0.173	0.101	0.092	0.086	0.086	0.096	0.136	0.075	0.078	0.114	0.099	0.096	0.138	0.104	0.139	0.253	0.264	0.255

Appendix A.6: Compositions of scapolite from lithologies within marble at the Revelstoke Occurrence (con't)

	TD-G063B-09-04-47	TD-G063B-09-04-48	TD-G063B-09-04-49	71-3-1	71-3-2	71-3-3	71-3-5	71-3-6	71-7-1	71-7-2	71-7-3	71-7-4	GR2-35	GR2-36	GR2-37	GR2-38	GR2-39	GR2-40
SiO ₂ wt.%	46.77	46.77	46.24	45.11	45.29	46.54	45.08	45.57	44.87	45.43	45.81	45.66	51.92	49.03	52.16	51.88	49.56	50.78
Al ₂ O ₃	28.55	28.33	28.75	29.69	29.35	28.72	29.03	29.11	28.74	29.00	29.08	28.91	25.56	26.86	25.32	25.66	27.20	26.31
MgO	0.00	0.00	0.01	0.05	0.02	0.03	0.01	0.02	0.05	0.03	0.00	0.03	0.03	0.00	0.01	0.00	0.02	0.00
CaO	16.89	16.62	16.98	20.59	20.48	18.86	20.39	20.52	20.05	20.24	19.98	20.17	12.07	14.90	11.62	12.49	14.96	13.88
MnO	0.02	0.00	0.01	0.02	0.00	0.03	0.00	0.00	0.03	0.04	0.00	0.03	0.05	0.02	0.02	0.00	0.00	0.00
FeO	0.04	0.06	0.08	0.18	0.16	0.32	0.25	0.33	0.31	0.32	0.12	0.22	0.37	0.05	0.11	0.02	0.12	0.00
Na ₂ O	3.61	3.55	3.49	2.19	2.35	2.25	2.23	2.30	2.41	2.07	2.33	2.49	6.80	5.49	7.13	6.72	5.24	5.82
K ₂ O	1.19	1.68	1.46	0.06	0.05	0.13	0.06	0.06	0.08	0.12	0.03	0.07	0.72	0.51	0.76	0.53	0.49	0.35
SO ₃	0.04	0.00	0.02	0.05	0.00	0.03	0.00	0.00	0.01	0.03	0.00	0.01	0.00	0.00	0.00	0.00	0.01	0.04
Cl	1.03	1.08	1.00	0.00	0.00	0.01	0.01	0.00	0.02	0.00	0.00	0.00	1.83	1.30	2.01	1.82	1.22	1.39
CO ₂	1.48	1.45	1.49	1.99	2.00	2.00	1.98	2.00	1.96	1.98	2.00	1.99	1.12	1.35	1.03	1.12	1.41	1.33
O=Cl	-0.23	-0.24	-0.23	0.00	0.00	0.00	0.00	0.00	0.00	0.00	0.00	0.00	-0.41	-0.29	-0.45	-0.41	-0.28	-0.31
TOTAL	99.38	99.30	99.30	99.93	99.70	98.91	99.03	99.91	98.52	99.26	99.35	99.58	100.06	99.22	99.73	99.84	99.96	99.59
Si ⁴⁺ apfu	6.979	7.002	6.925	6.758	6.804	6.947	6.822	6.846	6.838	6.848	6.864	6.872	7.594	7.291	7.633	7.582	7.286	7.450
Al ³⁺	5.021	4.998	5.075	5.242	5.196	5.053	5.178	5.154	5.162	5.152	5.136	5.128	4.406	4.709	4.367	4.418	4.714	4.550
Mg ²⁺	0.000	0.000	0.002	0.011	0.004	0.007	0.002	0.004	0.011	0.007	0.000	0.007	0.007	0.000	0.002	0.001	0.004	0.000
Ca ²⁺	2.700	2.666	2.725	3.305	3.296	3.016	3.306	3.303	3.274	3.269	3.208	3.253	1.891	2.375	1.822	1.955	2.357	2.182
Mn ²⁺	0.003	0.000	0.001	0.003	0.000	0.004	0.000	0.000	0.004	0.005	0.000	0.004	0.006	0.002	0.003	0.000	0.000	0.000
Fe ²⁺	0.005	0.008	0.010	0.023	0.020	0.040	0.032	0.041	0.040	0.040	0.015	0.028	0.045	0.006	0.013	0.003	0.014	0.000
Na ⁺	1.044	1.030	1.013	0.636	0.684	0.651	0.654	0.670	0.712	0.605	0.677	0.727	1.929	1.584	2.023	1.905	1.493	1.654
K ⁺	0.227	0.321	0.279	0.011	0.010	0.025	0.012	0.011	0.016	0.023	0.006	0.013	0.135	0.098	0.142	0.098	0.092	0.065
S ⁶⁺	0.004	0.000	0.002	0.006	0.000	0.003	0.000	0.000	0.001	0.003	0.000	0.001	0.000	0.000	0.000	0.001	0.004	
Cl ⁻	0.260	0.274	0.254	0.000	0.000	0.003	0.003	0.000	0.005	0.000	0.000	0.000	0.453	0.328	0.499	0.452	0.305	0.345
C ⁴⁺	0.735	0.726	0.744	0.994	1.000	0.994	0.997	1.000	0.994	0.997	1.000	0.999	0.547	0.672	0.501	0.548	0.694	0.651
O ²⁻	23.981	23.987	23.983	24.050	24.070	23.893	24.085	24.113	24.119	24.073	23.996	24.101	24.005	24.033	23.989	23.977	23.969	23.957
CatSum	15.979	16.025	16.031	15.989	16.015	15.743	16.006	16.030	16.056	15.949	15.906	16.031	16.013	16.064	16.006	15.961	15.961	15.902
EqAn	0.674	0.666	0.692	0.747	0.732	0.684	0.726	0.718	0.721	0.717	0.712	0.709	0.469	0.570	0.456	0.473	0.571	0.517
XCI	0.260	0.274	0.254	0.000	0.000	0.003	0.003	0.000	0.005	0.000	0.000	0.000	0.453	0.328	0.499	0.452	0.305	0.345

Appendix A.6: Compositions of scapolite from lithologies within marble at the Revelstoke Occurrence (con't)

	GR2-41	GR2-42	GR2-43	GR1-83	GR1-84	GR1-85	GR1-86
SiO ₂ wt.%	50.32	49.60	49.15	52.19	52.70	52.65	51.83
Al ₂ O ₃	26.50	26.79	26.98	25.43	25.09	25.40	25.28
MgO	0.00	0.11	0.00	0.00	0.01	0.00	0.01
CaO	14.38	15.15	14.94	11.65	11.75	12.43	12.32
MnO	0.02	0.05	0.00	0.01	0.01	0.01	0.03
FeO	0.00	0.18	0.02	0.12	0.08	0.06	0.33
Na ₂ O	5.72	4.83	5.43	7.87	6.99	6.49	6.81
K ₂ O	0.39	0.42	0.41	0.35	0.48	0.63	0.72
SO ₃	0.00	0.05	0.00	0.00	0.00	0.04	0.00
Cl	1.37	1.13	1.27	1.92	1.84	1.72	1.69
CO ₂	1.34	1.44	1.37	1.08	1.12	1.18	1.18
O=Cl	-0.31	-0.26	-0.29	-0.43	-0.42	-0.39	-0.38
TOTAL	99.74	99.51	99.29	100.19	99.65	100.22	99.81
Si ⁴⁺ apfu	7.404	7.333	7.286	7.622	7.687	7.650	7.620
Al ³⁺	4.596	4.667	4.714	4.378	4.313	4.350	4.380
Mg ²⁺	0.000	0.024	0.000	0.000	0.002	0.000	0.001
Ca ²⁺	2.267	2.399	2.373	1.823	1.836	1.935	1.941
Mn ²⁺	0.002	0.007	0.000	0.001	0.001	0.001	0.004
Fe ²⁺	0.000	0.023	0.002	0.015	0.009	0.008	0.041
Na ⁺	1.632	1.385	1.562	2.228	1.976	1.827	1.940
K ⁺	0.074	0.079	0.077	0.065	0.089	0.116	0.134
S ⁶⁺	0.000	0.006	0.000	0.000	0.000	0.004	0.000
Cl ⁻	0.342	0.284	0.320	0.476	0.456	0.424	0.422
C ⁴⁺	0.658	0.710	0.680	0.524	0.544	0.572	0.578
O ²⁻	23.995	24.016	23.997	24.035	23.951	23.969	24.045
CatSum	15.975	15.918	16.014	16.133	15.912	15.886	16.061
EqAn	0.532	0.556	0.571	0.459	0.438	0.450	0.460
XCI	0.342	0.284	0.320	0.476	0.456	0.424	0.422

Appendix A.7: Compositions of pyroxene from lithologies within marble at the Revelstoke Occurrence

	c G013-1	r G013-3	c G013-5	c G013-7	r G013-9	c G013-11	r G013-13	c G013-15	r G013-17	m G013-19	c G013-21	m G013-23	r G013-25	m G013-26
SiO ₂ wt.%	55.34	54.84	55.90	54.27	54.56	55.21	55.57	54.94	55.17	55.35	54.94	55.73	56.12	53.46
TiO ₂	0.00	0.04	0.00	0.02	0.03	0.05	0.07	0.02	0.02	0.03	0.07	0.04	0.01	0.08
Al ₂ O ₃	0.76	0.85	0.75	0.56	0.52	0.50	0.44	0.63	0.73	0.67	0.70	0.35	0.44	0.79
V ₂ O ₃	-	-	-	-	-	-	-	-	-	-	-	-	-	-
Cr ₂ O ₃	0.00	0.00	0.00	0.03	0.02	0.05	0.00	0.00	0.00	0.00	0.02	0.00	0.00	0.04
MgO	17.91	17.78	17.82	18.05	18.22	18.15	18.20	17.96	17.84	17.98	17.74	17.94	17.91	17.77
CaO	25.43	25.59	25.75	25.58	25.77	25.62	25.88	25.48	25.67	25.71	25.86	25.99	26.07	25.76
MnO	0.00	0.02	0.03	0.00	0.02	0.01	0.03	0.01	0.05	0.02	0.04	0.05	0.03	0.07
FeO	1.17	1.20	1.26	0.85	0.67	0.68	0.69	0.88	0.90	0.91	1.12	1.20	1.12	1.18
NiO	0.04	0.00	0.00	0.03	0.00	0.03	0.00	0.00	0.00	0.00	0.02	0.00	0.00	0.00
ZnO	-	-	-	-	-	-	-	-	-	-	-	-	-	-
Na ₂ O	0.18	0.21	0.19	0.16	0.14	0.13	0.08	0.18	0.20	0.20	0.16	0.10	0.11	0.15
TOTAL	100.83	100.52	101.70	99.54	99.95	100.44	100.96	100.10	100.59	100.87	100.66	101.39	101.82	99.30
Si ⁴⁺ apfu	1.986	1.978	1.990	1.976	1.977	1.987	1.990	1.986	1.985	1.986	1.979	1.992	1.995	1.959
Ti ⁴⁺	0.000	0.001	0.000	0.001	0.001	0.001	0.002	0.001	0.001	0.001	0.002	0.001	0.000	0.002
Al ³⁺	0.050	0.050	0.054	0.024	0.022	0.029	0.028	0.040	0.047	0.042	0.039	0.022	0.033	0.034
V ³⁺	-	-	-	-	-	-	-	-	-	-	-	-	-	-
Cr ³⁺	0.000	0.000	0.000	0.001	0.001	0.001	0.000	0.000	0.000	0.000	0.001	0.000	0.000	0.001
Mg ²⁺	0.958	0.956	0.946	0.980	0.984	0.974	0.971	0.968	0.957	0.962	0.953	0.956	0.949	0.971
Ca ²⁺	0.978	0.989	0.982	0.998	1.000	0.988	0.993	0.987	0.990	0.988	0.998	0.995	0.993	1.011
Mn ²⁺	0.000	0.001	0.001	0.000	0.001	0.000	0.001	0.000	0.002	0.001	0.001	0.001	0.001	0.002
Fe ²⁺	0.035	0.036	0.037	0.026	0.020	0.021	0.021	0.027	0.027	0.027	0.034	0.036	0.033	0.036
Ni ²⁺	0.001	0.000	0.000	0.001	0.000	0.001	0.000	0.000	0.000	0.000	0.001	0.000	0.000	0.000
Zn ²⁺	-	-	-	-	-	-	-	-	-	-	-	-	-	-
Na ⁺	0.013	0.014	0.013	0.012	0.010	0.009	0.006	0.013	0.014	0.014	0.011	0.007	0.008	0.011

Note: Following standards, X-ray lines and crystals were used for EMP analysis: albite, NaKa, TAP; kyanite,

AlKa, TAP; diopside, MgKa, TAP; diopside, SiKa, TAP; diopside, CaKa, PET; rutile, TiKa, PET;

synthetic magnesiochromite, CrKa, LIF; synthetic rhodonite, MnKa, LIF; synthetic fayalite, FeKa, LIF:

synthetic Ni₂SiO₄, NiKa, LIF. Formulae are normalized on 6 anions.

Appendix A.7: Compositions of pyroxene from SEDEX layers within marble at the Revelstoke Occurrence (con't)

	TD-G025-09-05-04	TD-G025-09-05-05	TD-G025-09-05-06	TD-G025-09-13-19	TD-G025-09-13-20	TD-G025-09-13-21	TD-G025-09-12-22	TD-G025-09-12-23
SiO ₂ wt.%	50.34	50.20	50.37	49.48	49.25	49.36	49.80	49.69
TiO ₂	0.00	0.00	0.00	0.00	0.01	0.01	0.03	0.02
Al ₂ O ₃	0.08	0.17	0.10	0.41	0.43	0.37	0.16	0.18
V ₂ O ₃	-	-	-	-	-	-	-	-
Cr ₂ O ₃	0.03	0.00	0.07	0.00	0.00	0.01	0.05	0.02
MgO	7.49	7.60	7.23	6.21	6.23	6.26	7.39	7.32
CaO	22.84	21.34	22.43	21.58	21.49	21.49	21.73	21.54
MnO	0.72	0.77	0.73	0.74	0.76	0.68	0.61	0.65
FeO	17.06	18.65	18.27	20.65	20.32	19.98	19.16	18.95
NiO	0.00	0.00	0.05	0.01	0.04	0.01	0.03	0.00
ZnO	-	-	-	-	-	-	-	-
Na ₂ O	0.14	0.17	0.15	0.29	0.18	0.20	0.12	0.15
TOTAL	98.70	98.90	99.40	99.37	98.71	98.37	99.08	98.52
Si ⁴⁺ apfu	1.994	1.991	1.990	1.976	1.977	1.984	1.979	1.984
Ti ⁴⁺	0.000	0.000	0.000	0.000	0.000	0.000	0.001	0.001
Al ³⁺	0.004	0.008	0.005	0.019	0.020	0.018	0.007	0.008
V ³⁺	-	-	-	-	-	-	-	-
Cr ³⁺	0.001	0.000	0.002	0.000	0.000	0.000	0.002	0.001
Mg ²⁺	0.442	0.449	0.426	0.370	0.373	0.375	0.438	0.436
Ca ²⁺	0.969	0.907	0.949	0.923	0.925	0.926	0.925	0.921
Mn ²⁺	0.024	0.026	0.024	0.025	0.026	0.023	0.021	0.022
Fe ²⁺	0.565	0.618	0.604	0.690	0.682	0.672	0.637	0.633
Ni ²⁺	0.000	0.000	0.002	0.000	0.001	0.000	0.001	0.000
Zn ²⁺	-	-	-	-	-	-	-	-
Na ⁺	0.011	0.013	0.011	0.022	0.014	0.016	0.009	0.012

Appendix A.7: Compositions of pyroxene from the host calc-gneiss at the Revelstoke Occurrence (con't)

	c 71-7-1	m 71-7-2	r 71-7-3	r 71-7-1b	r 71-7-2b	r 71-7-3b	r 71-3-3	m 71-3-4	c 71-3-5	c 71-4B-1	m 71-4B-2	m 71-4B-3	r 71-4B-4	r 71-4B-5	r 71-4B-6	c 71-4B-7	r 71-4B-8		r 71-4B-9	c 71-4B-10
SiO ₂ wt.%	51.91	51.89	51.92	51.09	51.17	51.67	51.85	52.06	51.88	51.67	51.54	50.91	50.98	51.09	50.52	50.85	50.67	50.83	50.94	
TiO ₂	0.08	0.11	0.08	0.09	0.08	0.06	0.03	0.11	0.06	0.10	0.19	0.08	0.04	0.08	0.06	0.04	0.05	0.04	0.08	
Al ₂ O ₃	1.39	1.40	1.37	1.15	0.78	0.77	0.64	1.24	0.58	1.66	1.81	0.97	0.64	0.99	0.88	0.97	1.19	0.87	0.62	
V ₂ O ₃	0.03	0.06	0.02	0.04	0.01	0.00	0.01	0.02	0.04	0.07	0.02	0.03	0.04	0.03	0.03	0.03	0.04	0.08	0.05	
Cr ₂ O ₃	0.00	0.05	0.00	0.01	0.01	0.04	0.00	0.01	0.04	0.05	0.01	0.05	0.03	0.00	0.02	0.00	0.02	0.29	0.02	
MgO	11.98	12.17	12.31	9.44	9.58	11.08	10.62	12.42	11.56	11.90	11.84	9.33	9.78	9.30	8.54	9.51	8.31	8.99	9.16	
CaO	23.11	23.58	23.44	22.87	23.36	23.36	22.75	23.57	24.10	23.48	23.45	22.94	23.20	23.11	22.62	23.07	22.69	22.98	22.97	
MnO	0.10	0.08	0.12	0.16	0.19	0.16	0.13	0.14	0.15	0.17	0.13	0.16	0.37	0.29	0.42	0.21	0.27	0.29	0.35	
FeO	11.09	9.97	10.42	14.29	15.05	12.54	13.35	10.59	11.62	10.94	10.72	15.06	14.99	15.10	16.74	14.94	16.41	15.48	15.48	
NiO	0.01	0.04	0.01	0.04	0.00	0.00	0.00	0.05	0.00	0.00	0.00	0.01	0.03	0.00	0.02	0.03	0.00	0.04	0.05	
ZnO	0.00	0.12	0.05	0.02	0.06	0.00	0.00	0.04	0.04	0.00	0.00	0.01	0.04	0.05	0.07	0.00	0.07	0.02	0.06	
Na ₂ O	0.14	0.21	0.25	0.20	0.12	0.16	0.15	0.19	0.12	0.24	0.19	0.16	0.13	0.12	0.18	0.15	0.11	0.19	0.12	
TOTAL	99.84	99.68	99.99	99.40	100.41	99.84	99.53	100.44	100.19	100.28	99.90	99.71	100.27	100.16	100.10	99.80	99.83	100.10	99.90	
Si ⁴⁺ apfu	1.961	1.957	1.951	1.972	1.959	1.966	1.986	1.950	1.961	1.942	1.944	1.963	1.953	1.963	1.955	1.957	1.966	1.959	1.967	
Ti ⁴⁺	0.002	0.003	0.002	0.003	0.002	0.002	0.001	0.003	0.002	0.003	0.005	0.002	0.001	0.002	0.002	0.001	0.001	0.001	0.002	
Al ³⁺	0.062	0.062	0.061	0.052	0.035	0.035	0.029	0.055	0.026	0.074	0.080	0.044	0.029	0.045	0.040	0.044	0.054	0.040	0.028	
V ³⁺	0.001	0.002	0.001	0.001	0.000	0.000	0.000	0.001	0.001	0.002	0.001	0.001	0.001	0.001	0.001	0.001	0.002	0.002		
Cr ³⁺	0.000	0.001	0.000	0.000	0.000	0.001	0.000	0.000	0.001	0.001	0.000	0.002	0.001	0.000	0.001	0.000	0.001	0.009	0.001	
Mg ²⁺	0.675	0.684	0.690	0.543	0.547	0.628	0.607	0.693	0.651	0.667	0.666	0.536	0.559	0.533	0.493	0.546	0.481	0.516	0.527	
Ca ²⁺	0.935	0.953	0.944	0.946	0.958	0.952	0.934	0.946	0.976	0.945	0.948	0.948	0.952	0.951	0.938	0.951	0.943	0.949	0.950	
Mn ²⁺	0.003	0.003	0.004	0.005	0.006	0.005	0.004	0.004	0.005	0.005	0.004	0.005	0.012	0.009	0.014	0.007	0.009	0.009	0.011	
Fe ²⁺	0.350	0.314	0.328	0.461	0.482	0.399	0.428	0.332	0.367	0.344	0.338	0.486	0.480	0.485	0.542	0.481	0.533	0.499	0.500	
Ni ²⁺	0.000	0.001	0.000	0.001	0.000	0.000	0.000	0.002	0.000	0.000	0.000	0.001	0.000	0.001	0.001	0.000	0.001	0.002	0.002	
Zn ²⁺	0.000	0.003	0.001	0.001	0.002	0.000	0.000	0.001	0.001	0.000	0.000	0.001	0.001	0.002	0.000	0.002	0.001	0.001	0.002	
Na ⁺	0.010	0.015	0.018	0.015	0.009	0.012	0.011	0.014	0.009	0.017	0.014	0.012	0.010	0.009	0.014	0.011	0.008	0.014	0.009	

Appendix A.7: Compositions of pyroxene from the host calc-gneiss at the Revelstoke Occurrence (con't)

	72-1	72-2	72-4	72-5	72-27-6	72-27-7	c	r	r	c	c	m	r	72-28-1	72-28-2
	72-1	72-2	72-4	72-5	72-27-6	72-27-7	72-28-8	72-28-9	72-28-10	72-28-11	72-29-12	72-29-13	72-29-14	72-28-1	72-28-2
SiO ₂ wt.%	51.71	52.17	51.03	51.26	51.97	51.86	50.63	51.83	51.28	51.36	51.11	51.29	51.26	50.60	51.87
TiO ₂	0.08	0.08	0.12	0.25	0.01	0.09	0.09	0.04	0.04	0.06	0.15	0.07	0.10	0.06	0.00
Al ₂ O ₃	1.31	1.43	1.11	1.44	0.48	0.73	0.96	0.72	0.54	0.67	0.94	1.02	0.81	1.32	0.65
V ₂ O ₃	0.04	0.04	0.01	0.04	0.02	0.02	0.03	0.00	0.02	0.02	0.01	0.01	0.01	0.01	0.01
Cr ₂ O ₃	0.00	0.04	0.00	0.00	0.00	0.00	0.01	0.04	0.00	0.00	0.00	0.03	0.03	0.00	0.01
MgO	12.70	12.73	10.31	10.60	10.93	11.06	10.64	10.68	11.08	11.02	10.05	10.15	10.51	11.43	10.80
CaO	23.55	23.57	23.16	23.11	23.51	23.10	23.20	23.08	23.43	23.24	23.14	22.98	23.04	21.27	23.17
MnO	0.12	0.11	0.25	0.24	0.27	0.25	0.23	0.25	0.24	0.25	0.29	0.29	0.23	0.28	0.29
FeO	9.18	9.30	13.13	12.67	13.00	12.53	12.63	12.96	12.33	12.57	13.30	13.29	13.46	13.44	12.44
NiO	0.01	0.00	0.02	0.01	0.00	0.00	0.00	0.00	0.01	0.01	0.00	0.00	0.00	0.00	0.00
ZnO	0.03	0.00	0.09	0.00	0.06	0.00	0.01	0.07	0.00	0.01	0.06	0.08	0.09	0.00	0.01
Na ₂ O	0.21	0.22	0.16	0.19	0.09	0.19	0.16	0.14	0.15	0.15	0.14	0.18	0.15	0.13	0.13
TOTAL	98.94	99.69	99.39	99.81	100.34	99.83	98.59	99.81	99.12	99.36	99.19	99.39	99.69	98.54	99.38
Si ⁴⁺ apfu	1.956	1.959	1.959	1.954	1.973	1.974	1.954	1.979	1.965	1.965	1.970	1.971	1.962	1.951	1.986
Ti ⁴⁺	0.002	0.002	0.003	0.007	0.000	0.003	0.003	0.001	0.001	0.002	0.004	0.002	0.003	0.002	0.000
Al ³⁺	0.058	0.063	0.050	0.065	0.021	0.033	0.044	0.032	0.024	0.030	0.043	0.046	0.037	0.060	0.029
V ³⁺	0.001	0.001	0.000	0.001	0.001	0.001	0.001	0.000	0.001	0.001	0.000	0.000	0.000	0.000	0.000
Cr ³⁺	0.000	0.001	0.000	0.000	0.000	0.000	0.000	0.001	0.000	0.000	0.000	0.001	0.001	0.000	0.000
Mg ²⁺	0.716	0.713	0.590	0.602	0.619	0.628	0.612	0.608	0.633	0.628	0.577	0.581	0.600	0.657	0.616
Ca ²⁺	0.955	0.948	0.953	0.944	0.956	0.942	0.959	0.944	0.962	0.952	0.955	0.946	0.945	0.878	0.950
Mn ²⁺	0.004	0.003	0.008	0.008	0.009	0.008	0.008	0.008	0.008	0.008	0.009	0.009	0.007	0.009	0.009
Fe ²⁺	0.290	0.292	0.421	0.404	0.413	0.399	0.408	0.414	0.395	0.402	0.429	0.427	0.431	0.433	0.398
Ni ²⁺	0.000	0.000	0.001	0.000	0.000	0.000	0.000	0.000	0.000	0.000	0.000	0.000	0.000	0.000	0.000
Zn ²⁺	0.001	0.000	0.003	0.000	0.002	0.000	0.000	0.002	0.000	0.000	0.002	0.003	0.000	0.000	0.000
Na ⁺	0.015	0.016	0.012	0.014	0.007	0.014	0.012	0.010	0.011	0.011	0.010	0.013	0.011	0.010	0.010

Appendix A.8: Compositions of garnet from the garnet-scapolite assemblage within marble at the Revelstoke Occurrence

	G2-50	G2-54	G2-55	G2-52	G2-53	G2-28	G2-29	G2-30	G2-31	G2-32	G2-56	G2-57	G2-58	G2-59	G2-60	G2-61	G2-64	G2-65	G1-87	G1-88	G1-89	G1-90
SiO ₂ wt.%	37.60	37.25	37.45	37.86	37.63	36.91	36.96	36.86	37.11	36.57	36.96	36.63	36.86	36.68	36.98	36.68	36.55	37.02	37.07	36.87	36.92	36.61
TiO ₂	0.10	0.11	0.09	0.03	0.02	0.00	0.00	0.00	0.00	0.00	0.00	0.00	0.00	0.00	0.00	0.00	0.00	0.00	0.00	0.00	0.00	0.00
Al ₂ O ₃	20.95	20.86	20.92	20.97	20.95	21.29	21.24	21.29	21.23	21.18	21.13	21.08	21.13	21.08	21.09	21.16	21.10	21.29	21.38	21.12	21.15	20.98
Cr ₂ O ₃	0.01	0.02	0.00	0.00	0.02	0.00	0.00	0.02	0.01	0.00	0.04	0.01	0.01	0.00	0.02	0.00	0.04	0.02	0.00	0.05	0.01	0.02
FeO	27.52	27.85	28.05	22.01	22.48	27.76	28.31	29.04	29.47	30.19	29.58	29.08	30.73	29.89	30.25	30.52	29.91	29.28	29.89	30.21	30.74	30.20
MnO	3.83	3.35	3.35	4.66	4.96	3.01	3.14	3.10	2.86	2.95	2.97	3.01	2.97	3.01	3.13	2.91	2.96	3.05	3.02	3.02	2.90	2.99
MgO	2.68	2.54	2.59	1.64	1.71	2.32	2.11	1.84	1.43	1.38	1.44	1.59	1.44	1.52	1.66	1.43	1.87	1.90	1.51	1.48	1.48	1.42
CaO	7.34	7.56	7.56	12.68	12.57	8.73	8.58	8.56	8.44	7.84	8.78	8.42	7.68	8.04	7.65	7.87	7.56	7.83	7.98	8.13	7.66	7.52
Na ₂ O	0.00	0.00	0.00	0.00	0.03	0.02	0.03	0.00	0.03	0.00	0.02	0.03	0.01	0.03	0.00	0.03	0.02	0.00	0.00	0.02	0.02	0.03
TOTAL	100.03	99.54	100.02	99.85	100.38	100.05	100.36	100.71	100.59	100.12	100.92	99.85	100.83	100.23	100.78	100.58	100.02	100.42	100.86	100.89	100.89	99.77
Si ⁴⁺ apfu	2.993	2.982	2.983	2.999	2.968	2.935	2.936	2.926	2.956	2.933	2.935	2.936	2.938	2.934	2.945	2.929	2.926	2.948	2.947	2.934	2.94	2.947
Ti ⁴⁺	0.006	0.007	0.005	0.002	0.001	0	0	0	0	0	0	0	0	0	0	0	0	0	0	0	0	0
Al ³⁺	1.966	1.968	1.964	1.958	1.947	1.995	1.988	1.992	1.993	2.002	1.978	1.991	1.985	1.987	1.979	1.992	1.991	1.998	2.003	1.981	1.985	1.991
Cr ³⁺	0.001	0.001	0	0	0.001	0	0	0.001	0.001	0	0.003	0.001	0.001	0	0.001	0	0.003	0.001	0	0.003	0.001	0.001
Fe ²⁺	1.832	1.864	1.869	1.458	1.483	1.846	1.88	1.928	1.963	2.025	1.964	1.949	2.048	2	2.014	2.038	2.003	1.95	1.987	2.01	2.047	2.033
Mn ²⁺	0.258	0.227	0.226	0.313	0.331	0.203	0.211	0.208	0.193	0.2	0.2	0.204	0.2	0.204	0.211	0.197	0.201	0.206	0.203	0.204	0.196	0.204
Mg ²⁺	0.318	0.303	0.308	0.194	0.201	0.275	0.25	0.218	0.17	0.165	0.17	0.19	0.171	0.181	0.197	0.17	0.223	0.226	0.179	0.176	0.176	0.17
Ca ²⁺	0.626	0.648	0.645	1.076	1.062	0.744	0.73	0.728	0.72	0.674	0.747	0.723	0.656	0.689	0.653	0.673	0.649	0.668	0.68	0.693	0.654	0.649
Na ⁺	0	0	0	0	0.005	0.003	0.005	0	0.005	0	0.003	0.005	0.002	0.005	0	0	0.005	0.003	0	0	0.003	0.005

Note: Following standards, X-ray lines and crystals were used for EMP analysis: albite, NaKa, TAP; kyanite,

AlKa, TAP; diopside, MgKa, TAP; diopside, SiKa, TAP; diopside, CaKa, PET; rutile, TiKa, PET;

synthetic magnesiochromite, CrKa, LiF; synthetic rhodonite, MnKa, LiF; synthetic fayalite, FeKa, LiF;

synthetic Ni₂SiO₄, NiKa, LiF. Formulae are normalized on 12 anions.

Appendix A.8: Compositions of garnet from the host calc-gneiss at the Revelstoke Occurrence (con't)

c 53-1-1	m 53-1-2	m 53-1-3	m 53-1-4	r 53-1-5	n to incl	rim	core	mid	n to incl	12-1	12-2	72-3-1	72-3-2	72-3-3	72-3-4	72-3-5	71-4b-1	71-4b-2	71-4b-3	71-4b-4	71-4b-5
37.35	37.33	37.2	37.25	37.36	37.04	37.46	37.47	37.09	37.39	37.36	37.32	37.01	37.35	37.01	37.2	37.32	37.68	37.93	38.24	38.04	37.73
-	-	-	-	-	-	-	-	-	-	-	-	-	-	-	-	-	-	-	-	-	-
21.66	21.65	21.49	21.51	21.65	21.57	21.59	21.5	21.75	21.65	21.79	21.85	21.62	21.76	21.66	21.69	21.65	21.33	21.83	22.05	22.12	21.36
0	0	0.03	0.05	0.02	0	0	0.01	0.04	0	0.05	0.02	0	0.01	0.03	0.03	0.02	0.06	0.01	0.05	0	0.04
2.65	2.52	2.57	2.71	3.11	2.84	2.91	2.39	2.49	2.66	4	3.93	2.98	3	2.89	3.11	3.34	1.3	3.48	3.75	3.75	1.43
6.93	7.48	7.1	7.08	6.93	6.85	6.99	7.51	6.9	7.01	6.37	6.2	6.84	6.86	6.82	6.84	7.13	14.25	11.23	11.39	11.67	13.81
0.52	0.55	0.4	0.36	0.41	1.02	0.35	0.44	0.49	0.31	0.31	0.34	0.53	0.49	0.55	0.37	0.42	1.74	1.09	1.15	1.02	1.38
31.21	31.03	30.75	31.09	30.66	30.49	30.41	30.85	31.31	31.49	30.29	31	30.9	31.02	30.56	30.91	30.18	23.87	24.76	23.93	24.36	24.5
0	0.04	0.02	0.05	0.01	0.02	0.03	0.03	0	0	0	0.04	0.04	0	0	0	0	0.03	0.04	0	0.02	-
100.32	100.6	99.56	100.1	100.15	99.83	99.74	100.2	100.07	100.51	100.17	100.66	99.92	100.53	99.52	100.15	100.06	100.23	100.36	100.6	100.96	100.27
2.964	2.954	2.974	2.960	2.960	2.950	2.981	2.978	2.954	2.962	2.946	2.933	2.942	2.951	2.955	2.949	2.954	2.970	2.958	2.967	2.942	2.972
-	-	-	-	-	-	-	-	-	-	-	-	-	-	-	-	-	-	-	-	-	-
2.026	2.019	2.024	2.015	2.022	2.025	2.025	2.014	2.041	2.021	2.025	2.024	2.026	2.026	2.038	2.026	2.020	1.981	2.007	2.016	2.016	1.983
0.000	0.000	0.002	0.003	0.001	0.000	0.000	0.001	0.003	0.000	0.003	0.001	0.000	0.001	0.002	0.002	0.001	0.004	0.001	0.003	0.000	0.002
0.314	0.297	0.306	0.321	0.367	0.337	0.345	0.283	0.296	0.314	0.470	0.460	0.353	0.353	0.344	0.368	0.394	0.153	0.405	0.434	0.432	0.168
0.589	0.634	0.608	0.603	0.588	0.585	0.596	0.640	0.589	0.595	0.538	0.522	0.583	0.581	0.583	0.581	0.605	1.203	0.938	0.947	0.967	1.166
0.035	0.037	0.027	0.024	0.028	0.069	0.024	0.030	0.033	0.021	0.021	0.023	0.036	0.033	0.037	0.025	0.028	0.116	0.072	0.076	0.067	0.092
2.072	2.053	2.056	2.066	2.032	2.031	2.024	2.050	2.085	2.086	1.997	2.037	2.054	2.050	2.040	2.049	1.998	1.573	1.615	1.552	1.576	1.614
0.000	0.006	0.003	0.008	0.002	0.003	0.005	0.005	0.000	0.000	0.000	0.006	0.006	0.000	0.000	0.000	0.000	0.005	0.006	0.000	0.005	0.003

Note: Following standards, X-ray lines and crystals were used for EMP analysis: albite, NaKa, TAP; kyanite,

AlKa, TAP; diopside, MgKa, TAP; diopside, SiKa, TAP; diopside, CaKa, PET; rutile, TiKa, PET;

synthetic magnesiochromite, CrKa, LIF; synthetic rhodonite, MnKa, LIF; synthetic fayalite, FeKa, LIF;

synthetic Ni2SiO4, NiKa, LIF. Formulae are normalized on 12 anions.

Appendix A.9: Representative compositions of amphibole from the marble, garnet-scapolite assemblage, and host calc-gneiss at the Revelstoke Occurrence

Sample	tremolite	grunerite / ferroanthophyllite				ferrohornblende		edenite		hastingsite		ferro-pargasite		potassic-ferropargasite		
	13-23	71-1	25-1	25-17	25-24	G2-25	GR2-27	g2-10	g2-11	g1-74	g2-17	g2-49	g1-66	g2-44		
	SiO ₂	56.23	51.25	52.13	50.50	50.14	47.70	47.69	41.70	37.84	39.34	39.42	38.18	38.03	35.05	
TiO ₂	0.15	0.06	0.00	0.00	0.00	0.48	0.47	0.36	0.36	0.10	0.11	0.18	0.77	0.23		
Al ₂ O ₃	2.69	4.03	0.33	0.32	0.42	5.28	5.22	9.37	11.80	9.90	14.03	14.30	14.61	17.47		
Fe ₂ O ₃ *	0.00	0.99	0.87	0.33	0.05	1.37	0.13	2.82	4.31	5.50	2.28	2.20	1.13	2.62		
V ₂ O ₃	0.00	0.04	0.00	0.00	0.00	0.02	0.00	0.01	0.01	0.03	0.03	0.00	0.01	0.03		
Cr ₂ O ₃	0.01	0.00	0.03	0.00	0.00	0.00	0.00	0.00	0.02	0.00	0.02	0.01	0.01	0.00		
MgO	22.84	13.57	10.64	9.25	8.25	10.01	9.61	6.79	4.48	4.96	6.62	5.56	5.88	3.22		
FeO*	1.74	14.91	20.86	33.60	34.95	18.95	20.15	20.45	21.79	21.18	18.63	19.69	20.09	21.22		
MnO	0.02	0.13	0.50	1.31	1.22	0.38	0.41	0.30	0.38	0.32	0.30	0.40	0.48	0.47		
CaO	13.42	11.86	11.30	1.31	1.36	11.83	11.45	11.60	11.40	11.39	11.72	11.54	11.48	11.15		
Na ₂ O	0.35	0.34	0.16	0.14	0.10	0.82	0.84	1.20	1.54	1.40	1.52	1.10	1.23	1.45		
K ₂ O	0.14	0.30	0.00	0.00	0.00	0.58	0.52	1.53	1.98	1.28	1.74	2.58	2.83	2.38		
F	0.17	0.29						0.08	0.18	0.16	0.15	0.36	0.16	0.00		
Cl		0.01				0.46	0.43	1.64	2.48	1.97	1.02	1.63	1.43	2.16		
H ₂ O*	2.11	1.91	1.98	1.91	1.89	1.86	1.85	1.45	1.14	1.28	1.59	1.30	1.46	1.30		
-(O=F,Cl)	-0.07	-0.12	0.00	0.00	0.00	-0.10	-0.10	-0.40	-0.63	-0.51	-0.29	-0.52	-0.39	-0.49		
Total	99.80	99.56	98.80	98.67	98.39	99.65	98.69	98.91	99.08	98.30	98.90	98.50	99.22	98.26		
^T Si	7.708	7.512	7.896	7.929	7.942	7.219	7.293	6.580	6.121	6.357	6.155	6.075	6.007	5.672		
^T Al	0.292	0.488	0.059	0.059	0.058	0.781	0.707	1.420	1.879	1.643	1.845	1.925	1.993	2.328		
^C Al	0.143	0.208	0.000	0.000	0.021	0.162	0.234	0.322	0.370	0.243	0.737	0.757	0.727	1.003		
Ti	0.015	0.007	0.000	0.000	0.000	0.055	0.054	0.043	0.044	0.013	0.013	0.021	0.092	0.029		
Fe ³⁺	0.000	0.109	0.099	0.039	0.006	0.156	0.015	0.335	0.524	0.669	0.268	0.263	0.135	0.319		
V	0.000	0.005	0.000	0.000	0.000	0.002	0.000	0.002	0.002	0.003	0.004	0.000	0.001	0.003		
Cr	0.001	0.000	0.004	0.000	0.000	0.000	0.000	0.000	0.002	0.000	0.003	0.001	0.002	0.000		
Mg	4.668	2.965	2.402	2.165	1.948	2.258	2.190	1.598	1.081	1.194	1.540	1.317	1.383	0.777		
^C Fe ²⁺	0.173	1.706	2.495	2.795	3.025	2.367	2.506	2.698	2.948	2.863	2.433	2.620	2.653	2.869		
^C Mn ²⁺	0.000	0.000	0.000	0.000	0.000	0.000	0.000	0.002	0.029	0.016	0.001	0.021	0.008	0.000		
^C Ca	0.000	0.000	0.000	0.000	0.000	0.000	0.000	0.000	0.000	0.000	0.000	0.000	0.000	0.000		
^B Fe ²⁺	0.027	0.121	0.147	1.617	1.605	0.033	0.071	0.000	0.000	0.000	0.000	0.000	0.000	0.002		
^B Mn ²⁺	0.002	0.016	0.064	0.174	0.164	0.048	0.053	0.038	0.024	0.027	0.039	0.033	0.057	0.064		
^B Ca	1.971	1.863	1.789	0.209	0.231	1.919	1.876	1.962	1.976	1.973	1.961	1.967	1.943	1.934		
^B Na	0.000	0.000	0.000	0.000	0.000	0.000	0.000	0.000	0.000	0.000	0.000	0.000	0.000	0.000		
^A Ca	0.000	0.000	0.045	0.011	0.000	0.000	0.000	0.000	0.000	0.000	0.000	0.000	0.000	0.000		
^A Na	0.093	0.097	0.047	0.043	0.031	0.239	0.248	0.367	0.484	0.439	0.459	0.339	0.376	0.455		
^A K	0.024	0.056	0.000	0.000	0.000	0.112	0.102	0.308	0.409	0.264	0.347	0.523	0.570	0.490		
^w F	0.074	0.134	0.000	0.000	0.000	0.000	0.000	0.040	0.092	0.080	0.075	0.181	0.082	0.000		
^w Cl	0.000	0.002	0.000	0.000	0.000	0.119	0.110	0.437	0.679	0.540	0.270	0.440	0.384	0.594		
^w OH	1.926	1.863	2.000	2.000	2.000	1.881	1.890	1.522	1.229	1.380	1.655	1.379	1.534	1.406		
O ₂ -	22.000	22.000	22.000	22.000	22.000	22.000	22.000	22.000	22.000	22.000	22.000	22.000	22.000	22.000		

Note: The following standards, X-ray lines and crystals were used: synthetic phlogopite, F_{Kα}, TAP; albite, Na_{Kα}, TAP; kyanite, Al_{Kα}, TAP;

diopside, Mg_{Kα}, TAP; diopside, Si_{Kα}, TAP; scapolite, Cl_{Kα}, PET; orthoclase, K_{Kα}, PET; diopside, Ca_{Kα}, PET; rutile, Ti_{Kα}, PET;

synthetic magnesiochromite, Cr_{Kα}, LIF; synthetic rhodonite, Mn_{Kα}, LIF; synthetic fayalite, Fe_{Kα}, LIF.

*calculated from electroneutral formula assuming 24 anions, (T+C+B)=15 and OH=(2-F-Cl). Cation site assignment after Leake et al. (2004):

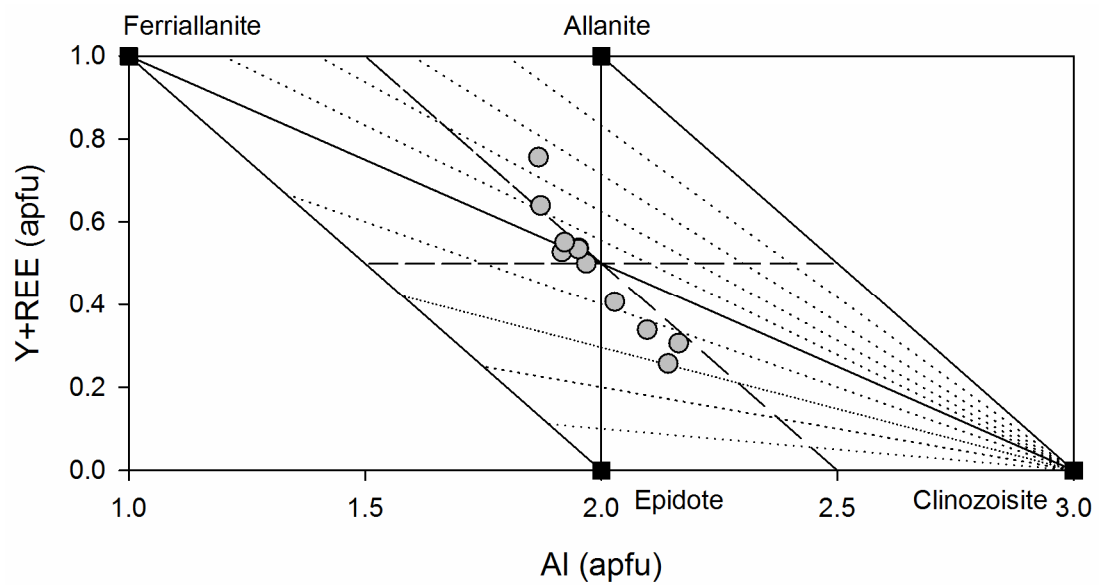
Nomenclature of amphiboles: additions and revisions to the International Mineralogical Association's amphibole nomenclature.

European Journal of Mineralogy 16, 191-196.

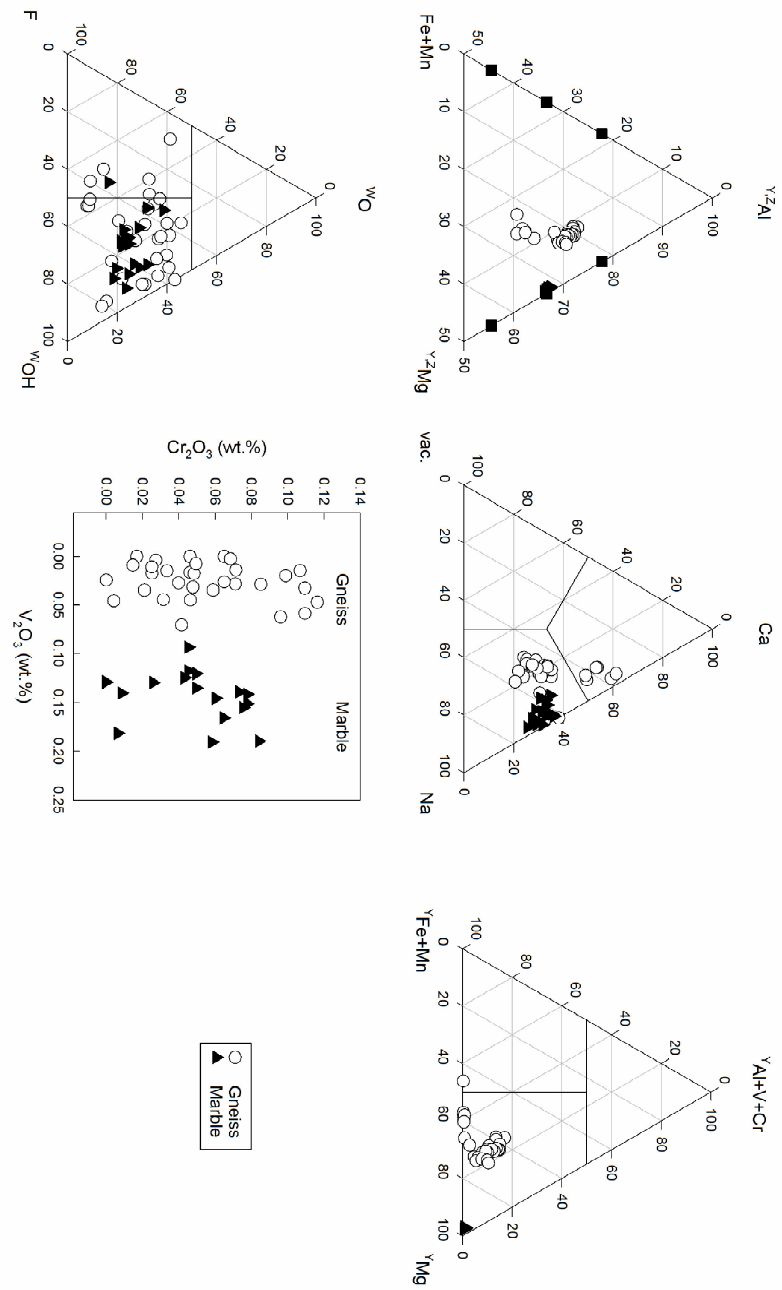
Appendix A.10: Representative compositional data for apatite and rutile from marble, and for Al,F-rich titanite in marble and calc-gneiss

Point #	apatite				rutile				Al,F-titanite		marble				calc-gneiss			
	20-6	20-1	22-6	20-6	marble (in Crn)				calc-gneiss (in Grt)				Point #	5-12-16	5-13-20	1-13-36	1-13-41	1-29-45
SO ₃ wt%	0.01	0.01	0.02	0.03	Nb ₂ O ₅ wt%	1.24	0.44	0.04	0.35	Nb ₂ O ₅ wt%	0.11	0.12	0.08	0.13	0.07	0.23		
P ₂ O ₅	41.06	40.86	41.01	41.13	Ta ₂ O ₅	0.05	0.00	0	0	Ta ₂ O ₅	0.02	0.02	0.20	0.02	0.06	0.25		
Al ₂ O ₃	0.01	0.01	0.01	0.01	SiO ₂	0.05	0.01	0.04	0.66	ZrO ₂	0.11	0.00	0.08	0.00	0.00	0.00		
MgO	0.03	0.01	0.01	0.02	TiO ₂	98.89	97.80	99.27	96.34	SnO ₂	0.04	0.05	0.03	0.02	0.01	0.00		
CaO	55.33	55.65	55.71	55.37	Al ₂ O ₃	0.00	0.00	0.00	0.00	TiO ₂	34.74	35.37	33.43	33.79	34.64	33.29		
MnO	0.00	0.05	0.01	0.02	V ₂ O ₃	0.64	0.09	0.00	0.00	SiO ₂	29.96	30.42	30.14	30.57	30.54	29.78		
FeO	0.02	0.01	0.02	0.03	Cr ₂ O ₃	0.18	0.09	0.09	0.22	V ₂ O ₃	0.21	0.12	0.28	0.17	0.25	0.16		
SrO	0.00	0.02	0.00	0.00	MgO	0.00	0.00	0.00	0.00	Cr ₂ O ₃	0.18	0.08	0.11	0.07	0.00	0.13		
F	2.32	2.93	2.50	1.90	CaO	0.38	0.07	0.03	0.00	Fe ₂ O ₃	0.30	0.26	0.74	0.74	0.62	0.90		
CL	0.99	0.92	1.19	0.86	MnO	0.06	0.00	0.02	0.04	Al ₂ O ₃	2.94	2.75	3.44	3.16	3.09	3.43		
H ₂ O *	0.40	0.13	0.27	0.64	FeO	0.12	0.04	0.33	0.47	MnO	0.04	0.07	0.05	0.09	0.03	0.03		
O=F	-0.98	-1.23	-1.05	-0.80	NiO	0.07	0.00	0.00	0.00	BaO	0.27	0.27	0.00	0.21	0.18	0.07		
O=CL	-0.22	-0.21	-0.27	-0.19	SnO	0.04	0.00	0.00	0.10	CaO	27.49	27.38	27.50	27.75	27.74	26.89		
TOTAL	98.97	99.16	99.43	99.01	TOTAL	101.72	98.54	99.82	98.18	Na ₂ O	0.01	0.01	0.01	0.00	0.01	0.02		
										F	0.61	0.66	1.23	1.33	1.19	1.14		
S ⁶⁺ apfu	0.001	0.001	0.001	0.002	Nb ⁵⁺ apfu	0.008	0.003	0.000	0.002	TOTAL	97.03	97.58	97.31	98.05	98.42	96.34		
P ⁵⁺	2.970	2.957	2.961	2.970	Ta ⁵⁺	0.000	0.000	0.000	0.000									
Al ³⁺	0.001	0.001	0.001	0.001	Si ⁴⁺	0.001	0.000	0.001	0.009	Ti ⁴⁺ apfu	1.001	1.011	1.006	1.014	1.009	1.006		
Mg ²⁺	0.004	0.001	0.001	0.003	Ti ⁴⁺	0.991	0.987	0.994	0.980	Mn ⁵⁺	0.002	0.002	0.001	0.002	0.001	0.004		
Ca ²⁺	5.066	5.097	5.090	5.061	Al ³⁺	0.000	0.000	0.000	0.000	Ta ⁵⁺	0.000	0.000	0.002	0.000	0.001	0.002		
Mn ²⁺	0.000	0.004	0.001	0.001	V ³⁺	0.007	0.001	0.000	0.000	Ti ⁴⁺	0.873	0.885	0.839	0.843	0.861	0.846		
Fe ²⁺	0.001	0.001	0.001	0.002	Cr ³⁺	0.002	0.001	0.001	0.002	Zr ⁴⁺	0.002	0.000	0.001	0.000	0.000	0.000		
Sr ²⁺	0.000	0.001	0.000	0.000	Mg ²⁺	0.000	0.000	0.000	0.000	Sn ⁴⁺	0.001	0.001	0.000	0.000	0.000	0.000		
F ⁻	0.627	0.792	0.674	0.513	Ca ²⁺	0.005	0.001	0.000	0.000	V ³⁺	0.006	0.003	0.007	0.005	0.007	0.004		
Cl ⁻	0.143	0.133	0.172	0.124	Mn ²⁺	0.001	0.000	0.000	0.000	Cr ³⁺	0.005	0.002	0.003	0.002	0.000	0.003		
OH ⁻	0.230	0.075	0.154	0.363	Fe ²⁺	0.001	0.000	0.004	0.005	Fe ³⁺	0.008	0.007	0.019	0.018	0.015	0.023		
					Ni ²⁺	0.001	0.000	0.000	0.000	Al ³⁺	0.116	0.108	0.135	0.124	0.120	0.136		
					Sn ²⁺	0.000	0.000	0.000	0.001	Ca ²⁺	0.984	0.975	0.984	0.986	0.982	0.973		
										Mn ²⁺	0.001	0.002	0.001	0.003	0.001	0.001		
										Ba ²⁺	0.004	0.004	0.000	0.003	0.002	0.001		
										Na ⁺	0.001	0.001	0.001	0.000	0.001	0.001		
										F ⁻	0.064	0.069	0.130	0.140	0.124	0.122		
										O ²⁻	4.913	4.925	4.869	4.865	4.881	4.882		

A.11 Classification of allanite



A.12 Classification of tourmaline



A.13 Whole-Rock Geochemistry of Lithologies from the Revelstoke Occurrence.

	Di-Gneiss		Bt-Gneiss		Marble			Mica-Feldspar Layers				
	G071 P	G070 P	G055 P	G058 P	G069A M	G014M U	G046 X	G014CS U	G023CS D	G023CS U	G063BCS M	G069BC S
P ₂ O ₅ (wt%)	0.11	0.16	0.06	0.03	0.01	<0.01	<0.01	0.17	0.05	0.08	0.03	0.04
SiO ₂	47.7	55.5	55.6	55.8	0.17	0.65	1.29	8.20	3.18	7.57	16.35	4.46
TiO ₂	0.64	0.71	0.78	0.77	<0.01	0.01	0.01	0.21	0.05	0.13	0.61	0.10
Al ₂ O ₃	15.3	17.15	18.8	18.8	0.03	0.32	0.32	6.43	2.21	6.65	11.60	2.08
Cr ₂ O ₃	0.01	0.01	0.01	0.01	<0.01	<0.01	<0.01	0.01	<0.01	<0.01	0.01	<0.01
Fe ₂ O ₃	5.29	6.74	5.47	7.16	0.54	0.21	1.99	0.66	0.21	0.41	2.18	1.33
MnO	0.06	0.09	0.07	0.07	0.03	0.03	0.13	0.03	0.04	0.03	0.05	0.17
MgO	3.31	3.42	2.77	2.92	0.34	0.57	9.48	1.31	1.41	2.32	7.66	4.40
CaO	17.25	8.32	7.17	3.97	55.6	54.3	41.5	44.40	51.80	44.70	29.90	45.80
SrO	0.08	0.06	0.03	0.05	0.03	0.07	0.08	0.07	0.08	0.08	0.05	0.07
BaO	0.07	0.14	0.41	0.08	0.06	0.01	0.01	0.12	0.02	0.06	0.21	0.09
Na ₂ O	1.02	0.38	0.57	1.32	0.05	0.05	0.06	0.12	0.07	0.12	0.22	0.14
K ₂ O	2.29	1.77	4.21	2.84	0.01	0.12	0.14	1.04	0.31	0.80	3.42	0.91
LOI (%)	3.09	0.89	1.2	1.7	43.4	43.9	43.6	35.4	40.4	34.7	24.7	39.2
Total (%)	96.2	95.3	97.2	95.5	100.5	100	98.6	98.2	99.8	97.7	97	98.8
C	1.37	0.25	0.32	0.36	12.25	12.1	12.15	9.82	11.15	9.81	6.78	11.55
S	0.27	0.33	0.36	0.31	<0.01	<0.01	<0.01	<0.01	<0.01	<0.01	0.26	<0.01
Rb (ppm)	120	125	179.5	150	0.2	2.6	6.5	39.7	15.7	31.7	143	42.3
Cs	4.77	6.49	4.85	5.63	0.02	0.07	0.44	0.72	0.6	1.3	5.25	1.85
Sr	755	519	292	397	287	584	654	581	641	632	414	564
Ba	678	1080	3430	710	9.7	59.4	76.6	1065	259	535	1705	831
V	142	110	87	91	7	11	10	66	28	58	91	32
Cr	90	90	120	100	<10	<10	<10	40	<10	30	70	10
Zr	121	183	127	114	<2	15	9	41	17	22	86	13
Hf	3.5	5.1	4.3	3.4	<0.2	0.4	0.3	1.2	0.5	0.8	2.7	0.4
Nb	16.9	36.1	22.4	18.3	<0.2	0.3	0.2	5.7	1.6	3.7	11.6	1.4
Ta	1.2	2.3	1.6	1.3	<0.1	<0.1	<0.1	0.4	0.1	0.2	0.9	0.1
Mo	<1	<1	<1	<1	<1	<1	<1	<1	<1	16	3	23
W	2	2	2	2	1	1	1	1	1	1	2	1
Co	13	10	13	12	<1	<1	<1	6	<1	<1	7	<1
Ni	30	26	33	40	<1	<1	<1	25	<1	3	23	4
Cu	27	30	31	34	<1	<1	<1	3	<1	1	18	<1
Zn	105	109	45	132	5	15	82	44	11	20	387	61
Ag	<0.5	<0.5	<0.5	<0.5	<0.5	<0.5	<0.5	<0.5	<0.5	<0.5	1.2	<0.5
Cd	<0.5	<0.5	<0.5	<0.5	<0.5	<0.5	<0.5	<0.5	<0.5	<0.5	0.9	<0.5
<0.00	<0.00	<0.00	<0.00	<0.00	<0.00	<0.00	<0.00	<0.00	<0.00	<0.00	<0.00	<0.00
Hg	5	5	0.009	0.007	0.012	0.008	0.013	0.012	0.013	0.009	0.012	0.012
Ga	24.2	26.9	28.2	28.3	<0.1	0.3	0.4	9.3	2.5	6.4	19.8	1.8
Tl	0.8	0.7	1.2	0.7	<0.5	<0.5	<0.5	<0.5	0.5	0.6	0.7	<0.5
Sn	2	3	3	3	<1	<1	<1	1	<1	<1	2	<1
Pb	19	12	21	19	6	19	28	12	7	6	758	19
As	<0.1	<0.1	<0.1	<0.1	<0.1	<0.1	<0.1	0.1	<0.1	<0.1	<0.1	<0.1
Sb	<0.05	<0.05	<0.05	<0.05	0.05	<0.05	<0.05	0.06	0.06	0.06	2.17	0.15
Bi	0.14	0.24	0.13	0.22	<0.01	0.11	<0.01	0.03	0.01	0.01	0.73	0.04
Se	0.5	0.5	0.6	0.4	0.2	0.2	0.3	0.3	0.2	0.2	0.9	0.2
Te	0.01	0.01	0.01	0.01	0.01	0.03	0.02	0.02	0.02	0.01	0.02	0.03
Y	24.1	28.6	27.3	24.7	<0.5	3.5	2.6	4.7	2	2.3	6.3	1.1
La	51.2	63.9	57.4	57.1	<0.5	3.1	1.6	5.8	3.9	4.2	33.2	1.2
Ce	89.9	114	102	100.5	<0.5	5.5	3.7	9.9	6.2	6.7	56.3	2
Pr	11.15	14.2	11.75	12.7	0.04	0.72	0.59	1.22	0.79	0.85	6.08	0.26
Nd	39.3	49.4	43.9	44.6	0.2	2.9	2.8	4.5	2.9	3.2	17.3	1.1
Sm	6.63	8.35	7.49	7.45	0.03	0.63	0.7	0.96	0.51	0.59	1.84	0.21
Eu	1.2	1.39	1.25	1.31	<0.03	0.32	0.52	0.31	0.08	0.09	0.19	0.04
Gd	5.96	7.47	6.71	6.61	<0.05	0.64	0.57	0.93	0.45	0.49	2.17	0.17
Tb	0.77	0.99	0.96	0.88	<0.01	0.08	0.08	0.13	0.06	0.07	0.22	0.03
Dy	4.21	5.37	4.93	4.68	<0.05	0.49	0.39	0.73	0.31	0.35	1.19	0.14
Ho	0.83	1.06	0.94	0.92	<0.01	0.1	0.07	0.15	0.06	0.07	0.26	0.03
Er	2.55	3.12	2.94	2.84	<0.03	0.29	0.18	0.46	0.2	0.23	0.88	0.12
Tm	0.36	0.43	0.42	0.4	<0.01	0.04	0.03	0.07	0.03	0.03	0.13	0.02
Yb	2.28	2.84	2.71	2.51	<0.03	0.24	0.17	0.49	0.18	0.22	0.99	0.14
Lu	0.36	0.42	0.43	0.38	<0.01	0.04	0.02	0.07	0.03	0.04	0.17	0.02
Th	15.55	18.45	17.35	17.8	<0.05	0.45	0.41	7.33	0.91	1.95	7.82	0.37
U	3.47	3.12	2.86	2.84	0.57	0.54	1.59	14.45	4.39	9.37	4.69	2.05
La _{CN} /Lu _{CN}	15.2	16.3	14.3	16.1		8.3	8.6	8.9	13.9	11.3	20.9	6.4
Eu / Eu* = (SmN+GdN)/2	0.57	0.53	0.53	0.56		1.53	2.44	0.99	0.50	0.50	0.29	0.63

A.14 Microthermometry Results of Fluid Inclusions within Corundum at the Revelstoke Occurrence

	(N=5)	max °C	min °C	avg °C	σ
homogenization temperature of CO ₂ bubble		23	15	18.2	2.9
melting temperature of CO ₂ -Ice		-73	-93.5	-82.1	9.0
melting temperature of CO ₂ -solid		-56.6	-58.2	-57.5	0.7
homogenization temperature of CO ₂ -vapour-liquid		27.2	24.7	25.7	1.0
% CO ₂		100	92	94.8	3.5
molar volume		65.3	61.5	63.0	1.5

Appendix B Compositional Data for the Kimmirut Sapphire Occurrence

Appendix B.1: Representative compositions of corundum from the Beluga Showing

	B6-1	6B-2	6B-3	6A-1	6A-2	6A-3	H-1	H-2	G-1	G-2	G-3	G-4	G-5	G-6	G-7	G-8	G-9	G-10
TiO ₂ wt.%	0.00	0.01	0.01	0.00	0.01	0.00	0.12	0.08	0.12	0.05	0.05	0.07	0.07	0.08	0.04	0.00	0.06	0.05
Al ₂ O ₃	100.39	100.91	100.53	100.76	100.25	100.68	99.96	100.05	95.56	99.78	99.36	98.04	99.08	97.55	99.75	97.90	99.41	99.07
V ₂ O ₃	0.00	0.00	0.00	0.01	0.00	0.00	0.00	0.00	0.00	0.00	0.00	0.00	0.00	0.00	0.00	0.00	0.00	0.00
Cr ₂ O ₃	0.01	0.00	0.01	0.00	0.01	0.00	0.00	0.00	0.00	0.00	0.00	0.00	0.00	0.00	0.00	0.00	0.00	0.00
Ga ₂ O ₃	-	-	-	-	-	-	0.01	0.01	0.01	0.01	0.01	0.00	0.01	0.02	0.02	0.01	0.02	0.01
MgO	0.00	0.00	0.00	0.00	0.00	0.00	0.00	0.00	0.00	0.00	0.00	0.00	0.00	0.00	0.00	0.00	0.00	0.00
MnO	0.00	0.00	0.00	0.00	0.00	0.00	0.00	0.00	0.00	0.00	0.00	0.00	0.00	0.00	0.00	0.00	0.00	0.01
FeO	0.04	0.04	0.05	0.04	0.04	0.04	0.12	0.12	0.07	0.08	0.13	0.04	0.02	0.06	0.07	0.02	0.06	0.07

NOTE: The following standards, X-ray lines and crystals were used for the EMP analyses: corundum, AlKa, TAP; diopside, MgKa, TAP; rutile, TiKa, PET; V element, VKa, PET; synthetic magnesiochromite, CrKa, LIF; synthetic rhodonite, MnKa, LIF; synthetic fayalite, FeKa, LIF.

Appendix B.1: Representative compositions of corundum from the Beluga Showing (con't)

	G-11	G-12	G-13	G-14	A-1	A-2	A-3	A-4	A-5	Max	Min	Avg	σ
TiO ₂ wt.%	0.11	0.05	0.30	0.21	0.16	0.14	0.04	0.12	0.13	0.30	0.00	0.08	0.07
Al ₂ O ₃	99.57	99.36	99.25	99.71	99.93	100.39	99.71	100.28	99.63	100.91	95.56	99.51	1.13
V ₂ O ₃	0.00	0.00	0.00	0.00	0.00	0.00	0.00	0.00	0.00	0.01	0.00	0.00	0.00
Cr ₂ O ₃	0.00	0.01	0.01	0.00	0.00	0.01	0.01	0.00	0.00	0.01	0.00	0.00	0.00
Ga ₂ O ₃	0.01	0.01	0.01	0.02	0.01	0.01	0.01	0.02	0.00	0.02	0.00	0.01	0.00
MgO	0.00	0.00	0.00	0.00	0.00	0.00	0.00	0.00	0.00	0.00	0.00	0.00	0.00
MnO	0.00	0.00	0.00	0.00	0.00	0.00	0.00	0.00	0.00	0.01	0.00	0.00	0.00
FeO	0.05	0.09	0.07	0.04	0.09	0.08	0.13	0.11	0.10	0.13	0.02	0.07	0.03

Appendix B.2: Compositions of Nepheline from the Bowhead Showing

	39-2-1	39-2-2	39-2-3	39-2-4	39-2-5	39-2-6	39-2-7	39-2-8	39-2-9	39-2-10	39-2-12	39-2-13	39-2-14	39-2-18	39-2-19	39-2-20
SiO ₂	43.03	44.19	43.28	43.58	43.09	43.54	43.42	43.81	43.57	43.63	43.05	43.76	43.58	44.28	43.61	43.66
Al ₂ O ₃	34.40	34.34	34.28	34.28	34.42	34.69	34.70	34.37	34.29	34.60	34.64	34.75	34.59	34.32	34.08	34.51
MgO	0.00	0.00	0.01	0.00	0.00	0.00	0.00	0.00	0.00	0.00	0.00	0.00	0.00	0.00	0.00	0.00
CaO	2.41	2.37	2.41	2.36	2.31	2.52	2.41	2.27	2.28	2.32	2.56	2.36	2.30	2.29	2.26	2.35
MnO	0.00	0.01	0.00	0.01	0.00	0.00	0.00	0.00	0.00	0.01	0.01	0.00	0.00	0.01	0.00	0.00
FeO	0.00	0.00	0.00	0.00	0.00	0.02	0.03	0.02	0.00	0.00	0.00	0.00	0.00	0.00	0.00	0.00
Na ₂ O	15.66	15.53	15.85	15.68	15.77	15.55	15.75	15.90	15.82	15.86	15.61	15.70	15.45	15.71	15.75	15.37
K ₂ O	3.84	3.93	3.93	3.87	3.79	4.08	3.89	3.73	3.91	3.90	4.06	3.92	3.97	3.77	3.79	3.89
TOTAL	99.34	100.37	99.76	99.78	99.38	100.40	100.20	100.10	99.87	100.32	99.93	100.49	99.89	100.38	99.49	99.78
Si ⁴⁺	4.121	4.179	4.131	4.151	4.123	4.127	4.122	4.157	4.149	4.136	4.105	4.138	4.143	4.184	4.164	4.152
Al ³⁺	3.882	3.827	3.856	3.848	3.882	3.875	3.882	3.844	3.848	3.866	3.892	3.873	3.876	3.822	3.835	3.868
Mg ²⁺	0.000	0.000	0.001	0.000	0.000	0.000	0.000	0.000	0.000	0.000	0.000	0.000	0.000	0.000	0.000	0.000
Ca ²⁺	0.247	0.240	0.246	0.241	0.237	0.256	0.245	0.231	0.233	0.236	0.262	0.239	0.234	0.232	0.231	0.239
Mn ²⁺	0.000	0.001	0.000	0.001	0.000	0.000	0.000	0.000	0.000	0.001	0.001	0.000	0.000	0.001	0.000	0.000
Fe ²⁺	0.000	0.000	0.000	0.000	0.000	0.002	0.002	0.002	0.000	0.000	0.000	0.000	0.000	0.000	0.000	0.000
Na ⁺	2.907	2.847	2.933	2.896	2.926	2.858	2.899	2.925	2.921	2.915	2.886	2.878	2.848	2.878	2.916	2.834
K ⁺	0.469	0.474	0.479	0.470	0.463	0.493	0.471	0.452	0.475	0.472	0.494	0.473	0.482	0.454	0.462	0.472

NOTE: The following standards, X-ray lines and crystals were used during EMP analysis: albite, NaKa, TAP; anorthite, AlKa, TAP; diopside, MgKa, TAP; orthoclase, SiKa, TAP; orthoclase, KKa, PET; anorthite, CaKa, PET; synthetic fayalite, FeKa, LIF; barite, BaLa PET. Compositions were recalculated on the basis of 16 O apfu

Appendix B.2: Compositions of Nepheline from the Bowhead Showing (con't)

	39-2-40	39-2-41	39-2-42	39-2-43	avg	stdev	min	max
SiO ₂	43.52	43.05	43.24	42.96	43.49	0.36	42.96	44.28
Al ₂ O ₃	34.58	34.51	34.46	34.21	34.45	0.18	34.08	34.75
MgO	0.00	0.00	0.00	0.00	0.00	0.00	0.00	0.01
CaO	2.40	2.33	2.51	2.43	2.37	0.08	2.26	2.56
MnO	0.00	0.00	0.01	0.02	0.00	0.01	0.00	0.02
FeO	0.00	0.00	0.01	0.00	0.00	0.01	0.00	0.03
Na ₂ O	15.60	15.82	15.61	15.72	15.69	0.14	15.37	15.90
K ₂ O	4.03	3.98	4.08	3.96	3.92	0.10	3.73	4.08
TOTAL	100.13	99.69	99.92	99.30	99.93	0.36	99.30	100.49
Si ⁴⁺	4.134	4.113	4.122	4.121	4.139	0.021	4.105	4.184
Al ³⁺	3.871	3.886	3.872	3.868	3.864	0.020	3.822	3.892
Mg ²⁺	0.000	0.000	0.000	0.000	0.000	0.000	0.000	0.001
Ca ²⁺	0.244	0.238	0.256	0.250	0.242	0.009	0.231	0.262
Mn ²⁺	0.000	0.000	0.001	0.002	0.000	0.001	0.000	0.002
Fe ²⁺	0.000	0.000	0.001	0.000	0.000	0.001	0.000	0.002
Na ⁺	2.873	2.930	2.885	2.924	2.894	0.030	2.834	2.933
K ⁺	0.488	0.485	0.496	0.485	0.475	0.012	0.452	0.496

Appendix B.3: Compositions of diopside from the Beluga Showing

	1-1	1-2	1-3	2-1	2-2	2-3	2-4	3-1	3-2	3-3	3-4	4-1	4-2	4-3
SiO ₂ wt.%	51.21	51.14	50.82	51.16	51.65	51.26	51.63	51.49	51.21	51.58	51.12	51.44	51.07	51.86
TiO ₂	1.27	1.42	1.30	1.34	1.33	1.32	1.31	1.34	1.29	1.21	1.27	1.30	1.28	1.10
Al ₂ O ₃	7.20	7.32	7.37	7.39	6.81	7.53	6.83	7.36	7.61	6.86	7.48	6.98	7.50	5.29
Cr ₂ O ₃	0.01	0.04	0.04	0.04	0.03	0.02	0.03	0.02	0.03	0.00	0.02	0.01	0.01	0.03
MgO	14.37	14.07	14.31	14.29	14.36	14.08	14.41	14.09	13.86	14.44	14.18	14.26	14.16	15.09
CaO	22.72	22.40	22.40	22.56	22.48	22.65	22.55	22.59	22.35	22.76	22.48	22.57	22.50	22.78
MnO	0.03	0.04	0.04	0.00	0.04	0.06	0.03	0.03	0.04	0.06	0.06	0.09	0.04	0.07
FeO	1.73	1.61	1.64	1.56	1.54	1.53	1.56	1.48	1.54	1.62	1.65	1.59	1.62	1.58
Na ₂ O	1.65	1.68	1.67	1.63	1.70	1.74	1.70	1.70	1.80	1.75	1.68	1.70	1.75	1.52
TOTAL	100.19	99.72	99.59	99.97	99.94	100.18	100.05	100.10	99.73	100.27	99.93	99.93	99.93	99.31
Si ⁴⁺ apfu	1.846	1.854	1.842	1.848	1.867	1.848	1.863	1.858	1.854	1.856	1.847	1.859	1.845	1.885
Ti ⁴⁺	0.034	0.039	0.035	0.036	0.036	0.036	0.036	0.036	0.035	0.033	0.035	0.035	0.035	0.030
Al ³⁺	0.306	0.313	0.315	0.315	0.290	0.320	0.291	0.313	0.325	0.291	0.319	0.297	0.319	0.227
Cr ³⁺	0.000	0.001	0.001	0.001	0.001	0.001	0.001	0.001	0.001	0.000	0.001	0.000	0.000	0.001
Fe ³⁺	0.047	0.044	0.045	0.042	0.042	0.041	0.042	0.040	0.042	0.044	0.045	0.043	0.044	0.043
Mg ²⁺	0.772	0.760	0.773	0.770	0.774	0.757	0.775	0.758	0.748	0.775	0.764	0.768	0.762	0.818
Ca ²⁺	0.878	0.870	0.870	0.873	0.870	0.875	0.872	0.874	0.867	0.878	0.870	0.874	0.871	0.887
Mn ²⁺	0.001	0.001	0.001	0.000	0.001	0.002	0.001	0.001	0.001	0.002	0.002	0.003	0.001	0.002
Na ⁺	0.115	0.118	0.117	0.114	0.119	0.122	0.119	0.119	0.126	0.122	0.118	0.119	0.123	0.107
Di = Ca+Mg	90.909	90.455	90.773	90.673	90.980	90.416	91.146	90.315	89.672	91.276	90.276	90.919	90.421	93.169
Jd = [6]Al	6.501	7.103	6.740	7.009	6.696	7.313	6.530	7.471	7.996	6.295	7.238	6.700	7.143	4.481
Ae = Fe3+	2.590	2.442	2.486	2.318	2.324	2.271	2.324	2.214	2.332	2.430	2.486	2.381	2.436	2.350

Note: Following standards, X-ray lines and crystals were used for EMP analysis: albite, NaKa, TAP; kyanite, AlKa, TAP; diopside, MgKa, TAP; diopside, SiKa, TAP; diopside, CaKa, PET; rutile, TiKa, PET; synthetic magnesiochromite, CrKa, LIF; synthetic rhodonite, MnKa, LIF; synthetic fayalite, FeKa, LIF; synthetic Ni₂SiO₄, NiKa, LIF. Formulae are normalized on 6 anions.

Appendix B.3: Compositions of diopside from the Beluga Showing (con't)

	4-4	4-5	4-6	4-7	max	min	avg	σ
SiO ₂ wt.%	50.68	50.83	51.05	51.12	51.86	50.68	51.24	0.31
TiO ₂	1.26	1.29	1.31	1.29	1.42	1.10	1.29	0.06
Al ₂ O ₃	7.78	7.75	7.67	7.78	7.78	5.29	7.25	0.57
Cr ₂ O ₃	0.00	0.05	0.05	0.00	0.05	0.00	0.02	0.02
MgO	14.15	13.95	14.07	14.09	15.09	13.86	14.24	0.26
CaO	22.37	22.18	22.56	22.47	22.78	22.18	22.52	0.15
MnO	0.08	0.03	0.04	0.02	0.09	0.00	0.04	0.02
FeO	1.54	1.63	1.53	1.62	1.73	1.48	1.59	0.06
Na ₂ O	1.70	1.67	1.68	1.73	1.80	1.52	1.69	0.06
TOTAL	99.55	99.38	99.96	100.12	100.27	99.31	99.88	0.27
Si ⁴⁺ apfu	1.837	1.848	1.845	1.843	1.89	1.84	1.85	0.01
Ti ⁴⁺	0.034	0.035	0.036	0.035	0.04	0.03	0.04	0.00
Al ³⁺	0.332	0.332	0.327	0.331	0.33	0.23	0.31	0.02
Cr ³⁺	0.000	0.001	0.001	0.000	0.00	0.00	0.00	0.00
Fe ³⁺	0.042	0.045	0.042	0.044	0.05	0.04	0.04	0.00
Mg ²⁺	0.764	0.756	0.758	0.757	0.82	0.75	0.77	0.01
Ca ²⁺	0.869	0.864	0.873	0.868	0.89	0.86	0.87	0.00
Mn ²⁺	0.002	0.001	0.001	0.001	0.00	0.00	0.00	0.00
Na ⁺	0.119	0.118	0.118	0.121	0.13	0.11	0.12	0.00
Di = Ca+Mg	90.221	89.503	90.160	89.878	93.17	89.50	90.62	0.78
Jd = [6]Al	7.459	8.011	7.518	7.688	8.01	4.48	6.99	0.78
Ae = Fe3+	2.320	2.486	2.322	2.434	2.59	2.21	2.39	0.09

Appendix B.3: Compositions of diopside from the Bowhead Showing (con't)

	39-2b-P16	39-2b-P17	39-2b-P18	39-2b-P19	39-2b-P20	39-2b-P21	39-2b-P22	39-2c-P23	39-2c-P24
SiO ₂ wt.%	51.63	52.09	52.85	51.86	51.87	51.38	51.63	52.29	52.35
TiO ₂	0.82	0.67	0.51	0.86	0.88	0.71	0.83	1.18	0.56
Al ₂ O ₃	6.68	6.60	3.55	6.36	6.23	6.40	5.90	5.38	4.74
Cr ₂ O ₃	0.02	0.02	0.00	0.00	0.00	0.00	0.00	0.01	0.00
MgO	14.54	14.82	16.09	14.65	15.04	14.84	14.85	14.97	15.27
CaO	22.82	23.03	24.20	23.01	23.47	22.82	23.50	23.12	23.58
MnO	0.00	0.00	0.04	0.03	0.04	0.00	0.02	0.06	0.10
FeO	1.28	1.11	1.14	1.24	1.25	1.20	1.15	1.25	1.18
Na ₂ O	1.72	1.53	1.17	1.68	1.54	1.65	1.53	1.65	1.55
TOTAL	99.51	99.87	99.55	99.69	100.32	99.00	99.41	99.90	99.32
Si ⁴⁺ apfu	1.868	1.878	1.913	1.874	1.862	1.866	1.871	1.888	1.897
Ti ⁴⁺	0.022	0.018	0.014	0.023	0.024	0.019	0.023	0.032	0.015
Al ³⁺	0.285	0.280	0.151	0.271	0.264	0.274	0.252	0.229	0.202
Cr ³⁺	0.001	0.001	0.000	0.000	0.000	0.000	0.000	0.000	0.000
Fe ³⁺	0.035	0.030	0.031	0.034	0.034	0.033	0.031	0.034	0.032
Mg ²⁺	0.784	0.796	0.868	0.789	0.805	0.803	0.802	0.806	0.825
Ca ²⁺	0.885	0.890	0.939	0.891	0.903	0.888	0.913	0.894	0.916
Mn ²⁺	0.000	0.000	0.001	0.001	0.001	0.000	0.001	0.002	0.003
Na ⁺	0.121	0.107	0.082	0.118	0.107	0.116	0.108	0.115	0.109
Di = Ca+Mg	90.954	90.841	95.710	91.503	92.625	91.653	92.904	93.458	93.753
Jd = [6]Al	7.139	7.543	2.648	6.645	5.531	6.558	5.417	4.673	4.523
Ae = Fe3+	1.907	1.616	1.642	1.852	1.844	1.789	1.679	1.869	1.723

Appendix B.3: Compositions of diopside from the Bowhead Showing (con't)

	max	min	avg	σ
SiO ₂ wt.%	52.85	51.38	51.99	0.43
TiO ₂	1.18	0.51	0.78	0.19
Al ₂ O ₃	6.68	3.55	5.76	0.98
Cr ₂ O ₃	0.02	0.00	0.01	0.01
MgO	16.09	14.54	15.01	0.43
CaO	24.20	22.82	23.28	0.42
MnO	0.10	0.00	0.03	0.03
FeO	1.28	1.11	1.20	0.06
Na ₂ O	1.72	1.17	1.56	0.15
TOTAL	100.32	99.00	99.62	0.36
Si ⁴⁺ apfu	1.91	1.86	1.88	0.02
Ti ⁴⁺	0.03	0.01	0.02	0.01
Al ³⁺	0.29	0.15	0.25	0.04
Cr ³⁺	0.00	0.00	0.00	0.00
Fe ³⁺	0.04	0.03	0.03	0.00
Mg ²⁺	0.87	0.78	0.81	0.02
Ca ²⁺	0.94	0.89	0.90	0.02
Mn ²⁺	0.00	0.00	0.00	0.00
Na ⁺	0.12	0.08	0.11	0.01
Di = Ca+Mg	95.71	90.84	92.60	1.48
Jd = [6]Al	7.54	2.65	5.63	1.45
Ae = Fe3+	1.91	1.62	1.77	0.10

Appendix B.4: Compositional data of phlogopite from the Beluga Showing

Beluga		1-1-1	1-1-2	1-1-3	1-1-4	1-1-5	1-1-6	1-1-7	1-1-8	1-1-9	1-1-10	1-1-11	1-1-12	1-1-13	1-1-14	1-1-15	1-1-16
SiO ₂ wt%	39.17	39.53	39.17	39.38	39.77	39.91	39.84	39.12	39.03	38.96	39.87	39.94	39.33	39.21	39.36	39.58	
TiO ₂	2.28	2.40	2.32	2.43	2.71	2.69	2.51	2.50	2.46	2.39	2.47	2.44	2.21	2.13	2.68	2.57	
Al ₂ O ₃	17.82	16.83	17.48	16.06	15.68	15.55	15.71	17.05	17.40	16.21	16.78	16.27	17.01	17.62	15.23	15.30	
Cr ₂ O ₃	0.04	0.00	0.00	0.00	0.06	0.06	0.02	0.05	0.00	0.07	0.11	0.02	0.00	0.04	0.04	0.04	
MgO	22.68	22.72	22.66	22.96	23.02	23.12	23.17	22.43	22.63	22.45	22.75	22.91	22.56	22.52	23.39	23.61	
CaO	0.01	0.02	0.00	0.02	0.07	0.04	0.04	0.00	0.02	0.03	0.02	0.01	0.01	0.01	0.00	0.00	
BaO	0.07	0.07	0.09	0.00	0.07	0.02	0.10	0.07	0.03	0.00	0.07	0.02	0.03	0.00	0.02	0.03	
MnO	0.07	0.01	0.02	0.00	0.07	0.04	0.00	0.01	0.00	0.03	0.03	0.00	0.02	0.03	0.00	0.02	
FeO	3.08	2.83	2.90	3.07	2.91	2.77	2.88	3.05	2.95	2.81	3.01	2.91	2.77	3.05	2.83	3.05	
Na ₂ O	0.28	0.26	0.22	0.19	0.22	0.23	0.23	0.22	0.25	0.29	0.37	0.31	0.27	0.27	0.28	0.24	
K ₂ O	10.68	10.63	10.64	10.52	10.71	10.89	10.42	10.42	10.49	10.30	10.65	10.59	10.54	10.89	10.81	10.37	
F	1.12	1.27	1.13	1.34	1.37	1.39	1.41	1.16	1.13	1.29	1.26	1.36	1.26	1.31	1.42	1.41	
CL	0.00	0.03	0.01	0.00	0.02	0.03	0.01	0.02	0.02	0.00	0.00	0.00	0.00	0.00	0.04	0.07	
H ₂ O *	3.75	3.64	3.71	3.58	3.58	3.57	3.56	3.67	3.70	3.56	3.68	3.61	3.63	3.64	3.52	3.53	
O=F	-0.47	-0.53	-0.48	-0.56	-0.58	-0.59	-0.59	-0.49	-0.48	-0.54	-0.53	-0.57	-0.53	-0.55	-0.60	-0.59	
O=CL	0.00	-0.01	0.00	0.00	0.00	-0.01	0.00	0.00	0.00	0.00	0.00	0.00	0.00	-0.01	-0.02		
Total	100.57	99.69	99.88	98.98	99.68	99.72	99.30	99.28	99.63	97.85	100.54	99.81	99.11	100.16	99.01	99.21	
Si ⁴⁺ apfu	2.746	2.792	2.762	2.803	2.816	2.824	2.825	2.775	2.758	2.801	2.795	2.816	2.791	2.761	2.809	2.814	
Ti ⁴⁺	0.120	0.127	0.123	0.130	0.144	0.143	0.134	0.133	0.131	0.129	0.130	0.129	0.118	0.113	0.144	0.137	
Al ³⁺	1.473	1.401	1.453	1.347	1.308	1.297	1.313	1.425	1.449	1.374	1.386	1.352	1.422	1.463	1.281	1.282	
Cr ³⁺	0.002	0.000	0.000	0.000	0.003	0.003	0.001	0.003	0.000	0.004	0.006	0.001	0.000	0.002	0.002	0.002	
Mg ²⁺	2.371	2.392	2.382	2.437	2.430	2.439	2.449	2.372	2.384	2.406	2.378	2.408	2.386	2.364	2.488	2.502	
Ca ²⁺	0.001	0.002	0.000	0.002	0.005	0.003	0.003	0.000	0.002	0.002	0.002	0.001	0.001	0.001	0.000	0.000	
Ba ²⁺	0.002	0.002	0.002	0.000	0.002	0.001	0.003	0.002	0.001	0.000	0.002	0.001	0.001	0.000	0.001	0.001	
Mn ²⁺	0.004	0.001	0.001	0.000	0.004	0.002	0.000	0.001	0.000	0.002	0.002	0.000	0.001	0.002	0.000	0.001	
Fe ²⁺	0.181	0.167	0.171	0.183	0.172	0.164	0.171	0.181	0.174	0.169	0.176	0.172	0.164	0.180	0.169	0.181	
Na ⁺	0.038	0.036	0.030	0.026	0.030	0.032	0.032	0.030	0.034	0.040	0.050	0.042	0.037	0.037	0.039	0.033	
K ⁺	0.955	0.958	0.957	0.955	0.967	0.983	0.942	0.943	0.946	0.945	0.952	0.953	0.954	0.978	0.984	0.940	
F ⁻	0.248	0.284	0.252	0.302	0.307	0.311	0.316	0.260	0.252	0.293	0.279	0.303	0.283	0.292	0.321	0.317	
Cl ⁻	0.000	0.004	0.001	0.000	0.002	0.004	0.001	0.002	0.002	0.000	0.000	0.000	0.000	0.000	0.005	0.008	
H ⁺	1.752	1.713	1.747	1.698	1.691	1.685	1.683	1.737	1.745	1.707	1.721	1.697	1.717	1.708	1.675		
O ²⁻	11.752	11.713	11.747	11.698	11.691	11.685	11.683	11.737	11.745	11.707	11.721	11.697	11.717	11.708	11.675		

*calculated from electroneutral formula assuming 12 anions and (OH+F+Cl)=2.

NOTE: Following standards, X-ray lines and crystals were used during EMP analysis: synthetic phlogopite, FK_A, MgK_A, SiK_A, TAP, KK_A, PET; albite, NaK_A, TAP; kyanite, AlK_A, TAP; scapolite, ClK_A, PET; diopside, CaK_A, PET; rutile, TiK_A, PET; synthetic magnesiochromite, CrK_A, LiF; synthetic rhodonite, MnK_A, LiF; synthetic fayalite, FeK_A, LiF; barite, BaLa, PET.

Appendix B.4: Compositional data of phlogopite from the Beluga Showing (con't)

	1-1-17	1-1-18	1-1-19	1-1-20	1-1-22	1-1-23	1-1-24	F-1	F-2	F-3	F-4	F-5	F-6	F-7	F-8	F-9
SiO ₂ wt%	40.45	40.27	40.73	40.85	40.58	39.46	40.08	40.43	39.76	39.96	39.83	39.87	39.92	40.07	39.98	39.85
TiO ₂	2.70	2.63	2.38	2.30	2.44	2.51	2.75	2.94	2.56	2.53	2.60	2.70	2.75	2.80	2.65	2.84
Al ₂ O ₃	15.03	15.06	13.71	13.46	13.64	14.95	14.89	14.77	15.26	15.34	15.29	14.74	15.18	14.85	14.14	14.69
Cr ₂ O ₃	0.00	0.06	0.07	0.04	0.00	0.06	0.03	0.00	0.07	0.05	0.05	0.05	0.07	0.02	0.01	0.00
MgO	23.44	23.61	24.10	24.34	24.51	23.73	23.63	23.75	23.39	23.28	23.57	23.87	23.49	23.52	24.02	23.59
CaO	0.05	0.03	0.06	0.07	0.05	0.01	0.00	0.00	0.03	0.01	0.01	0.00	0.01	0.00	0.00	0.00
BaO	0.04	0.01	0.00	0.17	0.08	0.04	0.06	0.03	0.00	0.02	0.05	0.02	0.00	0.05	0.00	0.09
MnO	0.09	0.01	0.03	0.06	0.07	0.00	0.06	0.00	0.00	0.04	0.04	0.00	0.02	0.00	0.06	0.14
FeO	3.01	2.84	2.77	2.63	2.79	3.08	2.97	3.16	3.02	3.00	2.78	2.61	2.96	2.99	2.96	3.08
Na ₂ O	0.22	0.21	0.26	0.20	0.22	0.25	0.22	0.25	0.30	0.28	0.30	0.31	0.37	0.34	0.18	0.34
K ₂ O	10.82	10.40	10.61	10.59	10.56	10.12	10.74	10.53	10.55	10.62	10.20	10.61	10.48	10.58	10.35	10.65
F	1.46	1.52	1.80	1.71	1.71	1.38	1.45	1.49	1.46	1.42	1.41	1.39	1.38	1.34	1.44	1.43
CL	0.00	0.09	0.07	0.00	0.03	0.00	0.03	0.01	0.01	0.00	0.01	0.04	0.07	0.02	0.03	0.08
H ₂ O *	3.57	3.50	3.35	3.40	3.40	3.54	3.54	3.55	3.53	3.56	3.55	3.55	3.57	3.59	3.51	3.53
O=F	-0.61	-0.64	-0.76	-0.72	-0.72	-0.58	-0.61	-0.63	-0.61	-0.60	-0.59	-0.59	-0.58	-0.56	-0.61	-0.60
O=CL	0.00	-0.02	-0.02	0.00	-0.01	0.00	-0.01	0.00	0.00	0.00	0.00	-0.01	-0.02	0.00	-0.01	-0.02
Total	100.26	99.58	99.16	99.10	99.36	98.55	99.84	100.28	99.32	99.51	99.10	99.16	99.67	99.60	98.72	99.69
Si ⁴⁺ apfu	2.848	2.846	2.896	2.906	2.882	2.821	2.835	2.843	2.824	2.832	2.827	2.834	2.825	2.838	2.854	2.829
Ti ⁴⁺	0.143	0.140	0.127	0.123	0.130	0.135	0.146	0.156	0.137	0.135	0.139	0.144	0.146	0.149	0.142	0.152
Al ³⁺	1.247	1.254	1.149	1.128	1.142	1.260	1.241	1.224	1.277	1.281	1.279	1.235	1.266	1.240	1.190	1.229
Cr ³⁺	0.000	0.003	0.004	0.002	0.000	0.003	0.002	0.000	0.004	0.003	0.003	0.003	0.004	0.001	0.001	0.000
Mg ²⁺	2.460	2.487	2.554	2.581	2.595	2.529	2.492	2.490	2.477	2.459	2.494	2.529	2.478	2.484	2.557	2.496
Ca ²⁺	0.004	0.002	0.005	0.005	0.004	0.001	0.000	0.000	0.002	0.001	0.001	0.000	0.001	0.000	0.000	0.000
Ba ²⁺	0.001	0.000	0.000	0.005	0.002	0.001	0.002	0.001	0.000	0.001	0.001	0.001	0.000	0.001	0.000	0.003
Mn ²⁺	0.005	0.001	0.002	0.004	0.004	0.000	0.004	0.000	0.000	0.002	0.002	0.000	0.001	0.000	0.004	0.008
Fe ²⁺	0.177	0.168	0.165	0.156	0.166	0.184	0.176	0.186	0.179	0.178	0.165	0.155	0.175	0.177	0.177	0.183
Na ⁺	0.030	0.029	0.036	0.028	0.030	0.035	0.030	0.034	0.041	0.038	0.041	0.043	0.051	0.047	0.025	0.047
K ⁺	0.972	0.938	0.962	0.961	0.957	0.923	0.969	0.945	0.956	0.960	0.924	0.962	0.946	0.956	0.943	0.964
F ⁻	0.325	0.340	0.405	0.385	0.384	0.312	0.324	0.331	0.328	0.318	0.317	0.312	0.309	0.300	0.325	0.321
Cl ⁻	0.000	0.011	0.008	0.000	0.004	0.000	0.004	0.001	0.001	0.000	0.001	0.005	0.008	0.002	0.004	0.010
H ⁺	1.675	1.649	1.587	1.615	1.612	1.688	1.672	1.667	1.671	1.682	1.682	1.683	1.683	1.697	1.671	1.669
O ²⁻	11.675	11.649	11.587	11.615	11.612	11.688	11.672	11.667	11.671	11.682	11.682	11.683	11.697	11.671	11.669	

Appendix B.4: Compositional data of phlogopite from the Beluga Showing (con't)

	F-10	F-11	F-12	F-13	F-14	F-15	F-16	F-17	F-18	max	min	avg	σ
SiO ₂ wt%	38.72	39.76	39.69	39.91	40.49	40.00	39.84	39.93	39.70	40.85	38.72	39.79	0.48
TiO ₂	2.08	2.22	2.24	2.58	2.83	2.63	2.85	2.53	2.51	2.94	2.08	2.53	0.20
Al ₂ O ₃	16.74	16.20	15.58	15.59	14.89	14.62	14.73	15.84	15.62	17.82	13.46	15.58	1.07
Cr ₂ O ₃	0.00	0.02	0.00	0.00	0.03	0.01	0.10	0.00	0.00	0.11	0.00	0.03	0.03
MgO	23.00	23.20	23.03	23.30	24.25	23.87	23.83	23.09	23.10	24.51	22.43	23.32	0.53
CaO	0.00	0.01	0.00	0.00	0.00	0.00	0.01	0.04	0.00	0.07	0.00	0.02	0.02
BaO	0.00	0.00	0.07	0.03	0.07	0.04	0.04	0.02	0.11	0.17	0.00	0.04	0.04
MnO	0.09	0.05	0.00	0.04	0.02	0.04	0.01	0.06	0.06	0.14	0.00	0.03	0.03
FeO	2.78	2.91	2.75	2.90	3.10	3.03	2.91	3.02	2.86	3.16	2.61	2.92	0.13
Na ₂ O	0.32	0.20	0.36	0.26	0.38	0.26	0.32	0.38	0.34	0.38	0.18	0.27	0.06
K ₂ O	10.58	10.47	10.55	10.52	10.65	10.69	10.66	10.34	10.49	10.89	10.12	10.56	0.16
F	1.25	1.41	1.59	1.40	1.27	1.41	1.39	1.40	1.52	1.80	1.12	1.39	0.14
CL	0.05	0.00	0.00	0.02	0.05	0.04	0.00	0.04	0.02	0.09	0.00	0.02	0.02
H ₂ O *	3.59	3.57	3.44	3.57	3.68	3.55	3.57	3.57	3.49	3.75	3.35	3.57	0.08
O=F	-0.53	-0.59	-0.67	-0.59	-0.53	-0.59	-0.59	-0.59	-0.64	-0.47	-0.76	-0.59	0.06
O=CL	-0.01	0.00	0.00	0.00	-0.01	-0.01	0.00	-0.01	0.00	0.00	-0.02	-0.01	0.01
Total	98.66	99.43	98.64	99.52	101.16	99.58	99.68	99.66	99.18	101.16	97.85	99.48	0.59
Si ⁴⁺ apfu	2.767	2.813	2.834	2.824	2.827	2.838	2.823	2.821	2.822	2.91	2.75	2.82	0.03
Ti ⁴⁺	0.112	0.118	0.120	0.137	0.149	0.140	0.152	0.134	0.134	0.16	0.11	0.13	0.01
Al ³⁺	1.410	1.351	1.311	1.300	1.225	1.222	1.230	1.319	1.309	1.47	1.13	1.30	0.09
Cr ³⁺	0.000	0.001	0.000	0.000	0.002	0.001	0.006	0.000	0.000	0.01	0.00	0.00	0.00
Mg ²⁺	2.451	2.447	2.452	2.458	2.524	2.524	2.517	2.432	2.448	2.60	2.36	2.46	0.06
Ca ²⁺	0.000	0.001	0.000	0.000	0.000	0.000	0.001	0.003	0.000	0.01	0.00	0.00	0.00
Ba ²⁺	0.000	0.000	0.002	0.001	0.002	0.001	0.001	0.001	0.003	0.01	0.00	0.00	0.00
Mn ²⁺	0.005	0.003	0.000	0.002	0.001	0.002	0.001	0.004	0.004	0.01	0.00	0.00	0.00
Fe ²⁺	0.166	0.172	0.164	0.172	0.181	0.180	0.172	0.178	0.170	0.19	0.16	0.17	0.01
Na ⁺	0.044	0.027	0.050	0.036	0.051	0.036	0.044	0.052	0.047	0.05	0.03	0.04	0.01
K ⁺	0.965	0.945	0.961	0.950	0.949	0.967	0.964	0.932	0.951	0.98	0.92	0.95	0.01
F ⁻	0.283	0.316	0.359	0.313	0.280	0.316	0.312	0.313	0.342	0.41	0.25	0.31	0.03
Cl ⁻	0.006	0.000	0.000	0.002	0.006	0.005	0.000	0.005	0.002	0.01	0.00	0.00	0.00
H ⁺	1.711	1.684	1.641	1.684	1.714	1.679	1.688	1.682	1.656	1.75	1.59	1.69	0.03
O ²⁻	11.711	11.684	11.641	11.684	11.714	11.679	11.688	11.682	11.656	11.75	11.59	11.69	0.03

Appendix B.4: Compositional data of phlogopite from the Bowhead Showing (con't)

Bowhead		M31	M38	M39	M35	M30	M34	M40	M32	M33	M36	M37	M41	M26	M27	M25	M26
SiO ₂ wt%		41.14	40.61	41.19	41.17	40.99	40.83	41.21	41.01	41.08	40.61	40.49	41.07	41.22	40.79	41.21	41.22
TiO ₂		2.02	1.69	1.79	1.91	2.00	1.96	1.81	2.01	2.02	1.77	1.74	1.76	1.77	1.76	1.81	1.77
Al ₂ O ₃		14.39	15.84	14.82	14.62	14.91	14.50	15.22	14.52	14.48	15.00	15.49	15.11	15.09	15.34	15.20	15.09
Cr ₂ O ₃		0.02	0.00	0.07	0.01	0.06	0.01	0.00	0.00	0.00	0.00	0.04	0.03	0.00	0.00	0.01	0.00
MgO		25.44	24.71	25.21	25.52	25.23	25.41	25.26	25.35	25.08	25.03	24.78	25.14	25.26	24.73	24.98	25.26
CaO		0.00	0.01	0.00	0.01	0.02	0.01	0.00	0.02	0.01	0.02	0.00	0.01	0.01	0.00	0.00	0.01
BaO		0.03	0.10	0.10	0.13	0.02	0.08	0.03	0.00	0.00	0.03	0.01	0.08	0.03	0.16	0.02	0.03
MnO		0.05	0.01	0.00	0.03	0.03	0.01	0.03	0.00	0.00	0.01	0.03	0.02	0.06	0.00	0.00	0.06
FeO		2.20	2.27	2.18	2.08	2.28	2.10	1.96	2.10	2.11	2.20	2.07	2.28	1.96	2.18	2.21	1.96
Na ₂ O		0.34	0.33	0.30	0.38	0.30	0.27	0.29	0.35	0.30	0.29	0.31	0.29	0.28	0.30	0.29	0.28
K ₂ O		10.56	10.55	10.63	10.43	10.55	10.78	10.68	10.68	10.73	10.56	10.51	10.56	10.65	10.69	10.73	10.65
F		2.05	1.86	1.98	2.08	1.89	1.96	1.90	2.00	2.04	1.94	1.83	1.99	2.09	1.86	1.92	2.09
CL		0.01	0.00	0.07	0.04	0.00	0.00	0.00	0.03	0.00	0.05	0.01	0.01	0.04	0.05	0.00	0.04
H ₂ O *		3.32	3.41	3.35	3.31	3.41	3.35	3.42	3.34	3.31	3.34	3.40	3.36	3.31	3.39	3.40	3.31
O=F		-0.86	-0.78	-0.83	-0.88	-0.80	-0.83	-0.80	-0.84	-0.86	-0.82	-0.77	-0.84	-0.88	-0.78	-0.81	-0.88
O=CL		0.00	0.00	-0.02	-0.01	0.00	0.00	0.00	-0.01	0.00	-0.01	0.00	0.00	-0.01	-0.01	0.00	-0.01
Total		100.71	100.61	100.84	100.83	100.90	100.45	101.01	100.56	100.31	100.02	99.94	100.87	100.88	100.46	100.97	100.88
Si ⁴⁺ apfu		2.870	2.834	2.870	2.867	2.854	2.859	2.860	2.865	2.876	2.852	2.842	2.859	2.866	2.854	2.865	2.866
Ti ⁴⁺		0.106	0.089	0.094	0.100	0.105	0.103	0.095	0.106	0.106	0.094	0.092	0.092	0.093	0.093	0.095	0.093
Al ³⁺		1.183	1.303	1.217	1.200	1.223	1.197	1.245	1.196	1.195	1.242	1.281	1.240	1.236	1.265	1.245	1.236
Cr ³⁺		0.001	0.000	0.004	0.001	0.003	0.001	0.000	0.000	0.000	0.000	0.002	0.002	0.000	0.000	0.001	0.000
Mg ²⁺		2.646	2.571	2.619	2.649	2.618	2.653	2.614	2.640	2.618	2.621	2.593	2.609	2.618	2.580	2.589	2.618
Ca ²⁺		0.000	0.001	0.000	0.001	0.001	0.001	0.000	0.001	0.001	0.002	0.000	0.001	0.001	0.000	0.000	0.001
Ba ²⁺		0.001	0.003	0.003	0.004	0.001	0.002	0.001	0.000	0.000	0.001	0.000	0.002	0.001	0.004	0.001	0.001
Mn ²⁺		0.003	0.001	0.000	0.002	0.002	0.001	0.002	0.000	0.000	0.001	0.002	0.001	0.004	0.000	0.000	0.004
Fe ²⁺		0.128	0.132	0.127	0.121	0.133	0.123	0.114	0.123	0.124	0.129	0.121	0.133	0.114	0.128	0.128	0.114
Na ⁺		0.046	0.045	0.041	0.051	0.040	0.037	0.039	0.047	0.041	0.039	0.042	0.039	0.038	0.041	0.039	0.038
K ⁺		0.940	0.939	0.945	0.927	0.937	0.963	0.946	0.952	0.958	0.946	0.941	0.938	0.945	0.954	0.952	0.945
F ⁻		0.452	0.411	0.436	0.458	0.416	0.434	0.417	0.442	0.452	0.431	0.406	0.438	0.460	0.412	0.422	0.460
Cl ⁻		0.001	0.000	0.008	0.005	0.000	0.000	0.000	0.004	0.000	0.006	0.001	0.001	0.005	0.006	0.000	0.005
H ⁺		1.546	1.589	1.555	1.537	1.584	1.566	1.583	1.554	1.548	1.563	1.593	1.561	1.536	1.582	1.578	1.536
O ²⁻		11.546	11.589	11.555	11.537	11.584	11.566	11.583	11.554	11.548	11.563	11.593	11.561	11.536	11.582	11.578	11.536

Appendix B.4: Compositional data of phlogopite from the Bowhead Showing (con't)

	M27	M25	max	min	avg	σ
SiO ₂ wt%	40.79	41.21	41.22	40.49	40.99	0.24
TiO ₂	1.76	1.81	2.02	1.69	1.84	0.11
Al ₂ O ₃	15.34	15.20	15.84	14.39	15.01	0.38
Cr ₂ O ₃	0.00	0.01	0.07	0.00	0.01	0.02
MgO	24.73	24.98	25.52	24.71	25.12	0.25
CaO	0.00	0.00	0.02	0.00	0.01	0.01
BaO	0.16	0.02	0.16	0.00	0.06	0.05
MnO	0.00	0.00	0.06	0.00	0.02	0.02
FeO	2.18	2.21	2.28	1.96	2.14	0.10
Na ₂ O	0.30	0.29	0.38	0.27	0.31	0.03
K ₂ O	10.69	10.73	10.78	10.43	10.63	0.09
F	1.86	1.92	2.09	1.83	1.96	0.08
CL	0.05	0.00	0.07	0.00	0.02	0.02
H ₂ O *	3.39	3.40	3.42	3.31	3.36	0.04
O=F	-0.78	-0.81	-0.77	-0.88	-0.83	0.04
O=CL	-0.01	0.00	0.00	-0.02	-0.01	0.01
Total	100.46	100.97	101.01	99.94	100.65	0.31
Si ⁴⁺ apfu	2.854	2.865	2.88	2.83	2.86	0.01
Ti ⁴⁺	0.093	0.095	0.11	0.09	0.10	0.01
Al ³⁺	1.265	1.245	1.30	1.18	1.23	0.03
Cr ³⁺	0.000	0.001	0.00	0.00	0.00	0.00
Mg ²⁺	2.580	2.589	2.65	2.57	2.61	0.02
Ca ²⁺	0.000	0.000	0.00	0.00	0.00	0.00
Ba ²⁺	0.004	0.001	0.00	0.00	0.00	0.00
Mn ²⁺	0.000	0.000	0.00	0.00	0.00	0.00
Fe ²⁺	0.128	0.128	0.13	0.11	0.12	0.01
Na ⁺	0.041	0.039	0.05	0.04	0.04	0.00
K ⁺	0.954	0.952	0.96	0.93	0.95	0.01
F ⁻	0.412	0.422	0.46	0.41	0.43	0.02
Cl ⁻	0.006	0.000	0.01	0.00	0.00	0.00
H ⁺	1.582	1.578	1.59	1.54	1.57	0.02
O ²⁻	11.582	11.578	11.59	11.54	11.57	0.02

Appendix B.5: Compositional data of muscovite from the Beluga and Bowhead Showings

	Beluga													Bowhead				
	D-1	C-1	C-2	C-3	C-4	C-6	C-7	C-9	C-10	C-11	C-12	C-14	max	min	avg	σ	M28	M29
SiO ₂ wt%	44.17	45.26	44.84	45.85	45.46	44.89	44.60	44.87	45.05	45.19	44.68	44.68	45.85	44.17	44.96	0.42	44.83	45.18
TiO ₂	0.05	0.07	0.18	0.02	0.04	0.00	0.00	0.03	0.05	0.00	0.00	0.02	0.18	0.00	0.04	0.05	0.03	0.04
Al ₂ O ₃	37.01	37.46	36.92	37.86	37.70	37.25	37.32	37.32	37.64	37.65	37.20	37.30	37.86	36.92	37.39	0.27	38.33	38.61
Cr ₂ O ₃	0.03	0.02	0.00	0.00	0.04	0.00	0.00	0.00	0.00	0.00	0.00	0.07	0.07	0.00	0.01	0.02	0.00	0.00
MgO	0.03	0.02	0.03	0.00	0.00	0.03	0.00	0.01	0.00	0.00	0.03	0.04	0.04	0.00	0.02	0.01	0.12	0.03
CaO	0.05	0.01	0.00	0.00	0.03	0.00	0.01	0.00	0.00	0.00	0.03	0.01	0.05	0.00	0.01	0.02	0.12	0.17
BaO	0.00	0.05	0.02	0.04	0.00	0.03	0.00	0.00	0.00	0.00	0.02	0.00	0.05	0.00	0.01	0.02	0.17	0.01
MnO	0.01	0.02	0.00	0.00	0.00	0.00	0.07	0.00	0.05	0.04	0.00	0.00	0.07	0.00	0.02	0.02	0.00	0.00
FeO	0.10	0.05	0.06	0.00	0.04	0.07	0.03	0.04	0.01	0.01	0.08	0.01	0.10	0.00	0.04	0.03	0.02	0.04
Na ₂ O	0.74	0.78	0.77	1.01	1.05	0.80	0.65	0.66	0.71	0.88	0.70	0.92	1.05	0.65	0.81	0.13	1.61	1.91
K ₂ O	10.68	10.84	10.79	10.39	10.28	10.83	10.80	10.84	10.71	10.57	10.91	10.50	10.91	10.28	10.68	0.19	9.30	8.63
F	0.00	0.00	0.00	0.00	0.00	0.00	0.00	0.00	0.00	0.00	0.00	0.00	0.00	0.00	0.00	0.00	0.00	0.00
CL	0.00	0.02	0.08	0.03	0.02	0.00	0.06	0.00	0.00	0.02	0.03	0.00	0.08	0.00	0.02	0.02	0.00	0.07
H ₂ O *	4.40	4.48	4.42	4.52	4.50	4.45	4.42	4.45	4.48	4.48	4.43	4.45	4.52	4.40	4.46	0.03	4.51	4.52
O=F	0.00	0.00	0.00	0.00	0.00	0.00	0.00	0.00	0.00	0.00	0.00	0.00	0.00	0.00	0.00	0.00	0.00	0.00
O=CL	0.00	0.00	-0.02	-0.01	0.00	0.00	-0.01	0.00	0.00	0.00	-0.01	0.00	0.00	-0.02	0.00	0.01	0.00	-0.02
Total	97.27	99.08	98.09	99.72	99.16	98.35	97.95	98.22	98.70	98.84	98.11	98.00	99.72	97.27	98.46	0.64	99.04	99.19
Si ⁴⁺ apfu	3.007	3.024	3.027	3.033	3.025	3.021	3.014	3.021	3.016	3.020	3.017	3.014	3.033	3.007	3.020	0.007	2.982	2.989
Ti ⁴⁺	0.003	0.004	0.009	0.001	0.002	0.000	0.000	0.002	0.003	0.000	0.000	0.001	0.009	0.000	0.002	0.002	0.002	0.002
Al ³⁺	2.969	2.949	2.937	2.952	2.956	2.955	2.972	2.962	2.970	2.966	2.960	2.965	2.972	2.937	2.959	0.010	3.005	3.010
Cr ³⁺	0.002	0.001	0.000	0.000	0.002	0.000	0.000	0.000	0.000	0.000	0.000	0.004	0.004	0.000	0.001	0.001	0.000	0.000
Mg ²⁺	0.003	0.002	0.003	0.000	0.000	0.003	0.000	0.001	0.000	0.000	0.003	0.004	0.004	0.000	0.002	0.001	0.012	0.003
Ca ²⁺	0.004	0.001	0.000	0.000	0.002	0.000	0.001	0.000	0.000	0.000	0.002	0.001	0.004	0.000	0.001	0.001	0.009	0.012
Ba ²⁺	0.000	0.001	0.001	0.001	0.000	0.001	0.000	0.000	0.000	0.000	0.001	0.000	0.001	0.000	0.000	0.000	0.004	0.000
Mn ²⁺	0.001	0.001	0.000	0.000	0.000	0.000	0.004	0.000	0.003	0.002	0.000	0.000	0.004	0.000	0.001	0.001	0.000	0.000
Fe ²⁺	0.006	0.003	0.003	0.000	0.002	0.004	0.002	0.002	0.001	0.001	0.005	0.001	0.006	0.000	0.003	0.002	0.001	0.002
Na ⁺	0.098	0.101	0.101	0.130	0.135	0.104	0.085	0.086	0.092	0.114	0.092	0.120	0.135	0.085	0.105	0.016	0.208	0.245
K ⁺	0.927	0.924	0.929	0.877	0.873	0.930	0.931	0.931	0.915	0.901	0.940	0.904	0.940	0.873	0.915	0.021	0.789	0.728
F ⁻	0.000	0.000	0.000	0.000	0.000	0.000	0.000	0.000	0.000	0.000	0.000	0.000	0.000	0.000	0.000	0.000	0.000	0.000
Cl ⁻	0.000	0.002	0.009	0.003	0.002	0.000	0.007	0.000	0.000	0.002	0.003	0.000	0.009	0.000	0.002	0.003	0.000	0.008
H ⁺	2.000	1.998	1.991	1.997	1.998	2.000	1.993	2.000	2.000	1.998	1.997	2.000	2.000	1.991	1.998	0.003	2.000	1.992
O ²⁻	12	12	12	12	12	12	12	12	12	12	12	12	12	12	12	12	12	12

*calculated from electroneutral formula assuming 12 anions and (OH+F+Cl)=2.

NOTE: The following standards, X-ray lines and crystals were used during EMP analysis: synthetic phlogopite, FK_A, MgK_A, SiK_A, TAP, KK_A, PET; albite, NaK_A, TAP; kyanite, AlK_A, TAP; scapolite, ClK_A, PET; diopside, CaK_A, PET; rutile, TiK_A, PET; synthetic magnesiochromite, CrK_A, LiF; synthetic rhodonite, MnK_A, LiF; synthetic fayalite, FeK_A, LiF; barite, BaLa, PET.

Appendix B.6: Compositional data of plagioclase from the Beluga Showing
Symplectite

	1-1-1	1-1-2	1-1-3	1-1-4	1-1-5	1-1-6	1-1-7	1-1-8	1-1-9	1-1-16	1-1-17	1-1-18	1-1-19	1-1-20	1-1-21	1-1-22	10-3
SiO ₂ wt.%	61.61	60.68	60.76	60.33	61.22	60.33	61.24	60.91	61.47	61.84	62.19	61.69	62.11	63.75	64.50	63.81	67.18
Al ₂ O ₃	24.61	24.36	24.62	23.96	24.86	24.65	24.37	24.29	24.14	23.36	23.25	23.35	23.37	21.98	22.12	21.73	21.94
MgO	0.00	0.00	0.00	1.56	0.00	0.00	0.00	0.00	0.01	0.00	0.00	0.00	0.01	0.00	0.00	0.02	0.00
CaO	5.47	5.44	5.44	4.89	5.51	5.09	5.42	5.12	5.07	4.07	4.21	4.09	3.97	2.67	2.50	2.68	2.20
MnO	0.00	0.00	0.04	0.01	0.02	0.05	0.00	0.05	0.00	0.00	0.00	0.00	0.01	0.00	0.00	0.01	0.05
FeO	0.08	0.04	0.00	0.06	0.02	0.05	0.05	0.00	0.00	0.00	0.03	0.00	0.04	0.04	0.06	0.06	0.00
Na ₂ O	8.47	8.48	8.43	8.30	8.40	8.42	8.46	8.51	8.60	9.15	9.24	9.13	9.45	9.97	10.24	10.09	10.57
K ₂ O	0.11	0.15	0.11	0.09	0.07	0.27	0.11	0.17	0.16	0.20	0.23	0.22	0.41	0.16	0.17	0.22	0.03
TOTAL	100.35	99.15	99.40	99.20	100.10	98.86	99.65	99.05	99.45	98.62	99.15	98.48	99.37	98.57	99.59	98.62	101.97
Si ⁴⁺ apfu	2.724	2.718	2.713	2.700	2.713	2.710	2.727	2.728	2.740	2.774	2.778	2.772	2.772	2.849	2.853	2.853	2.892
Al ³⁺	1.282	1.286	1.296	1.264	1.298	1.305	1.279	1.282	1.268	1.235	1.224	1.237	1.229	1.158	1.153	1.145	1.113
Mg ²⁺	0.000	0.000	0.000	0.104	0.000	0.000	0.000	0.000	0.001	0.000	0.000	0.000	0.001	0.000	0.000	0.001	0.000
Ca ²⁺	0.259	0.261	0.260	0.234	0.262	0.245	0.259	0.246	0.242	0.196	0.201	0.197	0.190	0.128	0.118	0.128	0.101
Mn ²⁺	0.000	0.000	0.002	0.000	0.001	0.002	0.000	0.002	0.000	0.000	0.000	0.000	0.000	0.000	0.000	0.000	0.002
Fe ²⁺	0.003	0.001	0.000	0.002	0.001	0.002	0.002	0.000	0.000	0.000	0.001	0.000	0.001	0.001	0.002	0.002	0.000
Na ⁺	0.726	0.736	0.730	0.720	0.722	0.733	0.730	0.739	0.743	0.796	0.800	0.795	0.818	0.864	0.878	0.875	0.882
K ⁺	0.006	0.009	0.006	0.005	0.004	0.015	0.006	0.010	0.009	0.011	0.013	0.013	0.023	0.009	0.010	0.013	0.002
Or	0.01	0.01	0.01	0.01	0.00	0.02	0.01	0.01	0.01	0.01	0.01	0.01	0.02	0.01	0.01	0.01	0.00
Ab	0.73	0.73	0.73	0.75	0.73	0.74	0.73	0.74	0.75	0.79	0.79	0.79	0.79	0.86	0.87	0.86	0.90
An	0.26	0.26	0.26	0.24	0.27	0.25	0.26	0.25	0.24	0.20	0.20	0.20	0.18	0.13	0.12	0.13	0.10

NOTE: The following standards, X-ray lines and crystals were used during EMP analysis: albite, NaKa, TAP; anorthite, AlKa, TAP; diopside, MgKa, TAP; orthoclase, SiKa, TAP; orthoclase, KKa, PET; anorthite, CaKa, PET; synthetic fayalite, FeKa, LIF; barite, BaLa PET. Compositions were recalculated on the basis of 8 O apfu

Appendix B.6: Compositional data of plagioclase from the Beluga Showing (con't)

Symplectite

	10-4	10-5	10-6	3-7	3-10	3-11	3-12	3-13	3-14	3-15	3-19	19-3	19-4	19-5	11-6	11-7	B-1
SiO ₂ wt.%	65.86	66.43	65.62	64.43	64.58	64.96	65.16	65.08	64.92	64.77	59.83	65.23	62.34	62.64	61.79	61.82	65.02
Al ₂ O ₃	22.42	21.97	22.36	22.95	22.93	23.05	22.78	22.74	23.06	22.78	24.71	22.43	24.50	23.69	25.03	24.73	22.36
MgO	0.00	0.00	0.02	0.00	0.00	0.00	0.01	0.00	0.00	0.00	3.93	0.00	0.01	0.01	0.00	0.01	0.00
CaO	2.89	2.39	2.85	3.93	3.98	3.74	3.62	3.55	3.62	3.51	0.36	2.89	5.14	4.77	6.01	5.86	3.13
MnO	0.00	0.00	0.04	0.00	0.01	0.00	0.05	0.00	0.03	0.00	0.04	0.01	0.00	0.00	0.01	0.00	0.00
FeO	0.03	0.00	0.02	0.08	0.00	0.01	0.03	0.01	0.02	0.00	1.18	0.00	0.06	0.01	0.03	0.00	0.00
Na ₂ O	10.02	10.57	10.05	9.33	9.15	9.52	9.42	9.56	9.62	9.70	7.38	10.14	8.63	9.04	8.26	8.46	9.47
K ₂ O	0.00	0.00	0.04	0.04	0.11	0.05	0.20	0.19	0.09	0.12	2.75	0.04	0.05	0.13	0.13	0.12	0.11
TOTAL	101.22	101.36	101.00	100.76	100.76	101.33	101.27	101.13	101.36	100.88	100.18	100.74	100.73	100.29	101.26	101.00	100.09
Si ⁴⁺ apfu	2.861	2.880	2.858	2.820	2.825	2.825	2.836	2.836	2.824	2.831	2.666	2.850	2.741	2.766	2.710	2.718	2.855
Al ³⁺	1.148	1.123	1.148	1.184	1.182	1.181	1.168	1.168	1.182	1.173	1.298	1.155	1.269	1.233	1.294	1.282	1.157
Mg ²⁺	0.000	0.000	0.001	0.000	0.000	0.000	0.001	0.000	0.000	0.000	0.261	0.000	0.001	0.001	0.000	0.001	0.000
Ca ²⁺	0.134	0.111	0.133	0.184	0.187	0.174	0.169	0.166	0.169	0.164	0.017	0.135	0.242	0.226	0.282	0.276	0.147
Mn ²⁺	0.000	0.000	0.001	0.000	0.000	0.000	0.002	0.000	0.001	0.000	0.002	0.000	0.000	0.000	0.000	0.000	0.000
Fe ²⁺	0.001	0.000	0.001	0.003	0.000	0.000	0.001	0.000	0.001	0.000	0.044	0.000	0.002	0.000	0.001	0.000	0.000
Na ⁺	0.844	0.889	0.849	0.792	0.776	0.803	0.795	0.808	0.811	0.822	0.638	0.859	0.736	0.774	0.702	0.721	0.806
K ⁺	0.000	0.000	0.002	0.002	0.006	0.003	0.011	0.011	0.005	0.007	0.156	0.002	0.003	0.007	0.007	0.007	0.006
Or	0.00	0.00	0.00	0.00	0.01	0.00	0.01	0.01	0.01	0.01	0.19	0.00	0.00	0.01	0.01	0.01	0.01
Ab	0.86	0.89	0.86	0.81	0.80	0.82	0.82	0.82	0.82	0.83	0.79	0.86	0.75	0.77	0.71	0.72	0.84
An	0.14	0.11	0.14	0.19	0.19	0.18	0.17	0.17	0.17	0.17	0.02	0.14	0.25	0.22	0.28	0.27	0.15

Appendix B.6: Compositional data of plagioclase from the Beluga Showing (con't)

Symplectite

	B-7	B-8	B-10	D-3	D-12	F-2	F-3	F-4	max	min	avg	σ
SiO ₂ wt.%	63.79	63.40	65.10	63.42	65.31	63.71	63.60	63.02	67.18	59.83	63.27	1.87
Al ₂ O ₃	22.86	23.48	21.89	23.16	22.34	22.85	22.43	23.04	25.03	21.73	23.27	0.96
MgO	0.00	0.00	0.01	0.01	0.00	0.00	0.00	0.00	3.93	0.00	0.13	0.64
CaO	3.51	4.31	2.79	4.04	2.92	3.90	3.68	4.01	6.01	0.36	3.93	1.17
MnO									0.05	0.00	0.01	0.02
FeO	0.01	0.02	0.00	0.00	0.00	0.04	0.01	0.04	1.18	0.00	0.05	0.18
Na ₂ O	9.39	9.11	10.20	9.35	9.79	9.44	9.42	8.86	10.57	7.38	9.23	0.71
K ₂ O	0.08	0.07	0.04	0.07	0.04	0.15	0.20	0.17	2.75	0.00	0.19	0.41
TOTAL	99.64	100.39	100.03	100.05	100.40	100.09	99.34	99.14	101.97	98.48	100.10	0.92
Si ⁴⁺ apfu	2.821	2.790	2.864	2.799	2.859	2.812	2.826	2.804	2.89	2.67	2.79	0.06
Al ³⁺	1.191	1.218	1.135	1.205	1.153	1.188	1.174	1.208	1.31	1.11	1.21	0.06
Mg ²⁺	0.000	0.000	0.001	0.001	0.000	0.000	0.000	0.000	0.26	0.00	0.01	0.04
Ca ²⁺	0.166	0.203	0.132	0.191	0.137	0.184	0.175	0.191	0.28	0.02	0.19	0.06
Mn ²⁺									0.00	0.00	0.00	0.00
Fe ²⁺	0.000	0.001	0.000	0.000	0.000	0.001	0.000	0.001	0.04	0.00	0.00	0.01
Na ⁺	0.805	0.777	0.870	0.800	0.831	0.808	0.811	0.764	0.89	0.64	0.79	0.06
K ⁺	0.005	0.004	0.002	0.004	0.002	0.008	0.011	0.010	0.16	0.00	0.01	0.02
Or	0.01	0.00	0.00	0.00	0.00	0.01	0.01	0.01	0.19	0.00	0.01	0.03
Ab	0.82	0.79	0.87	0.80	0.86	0.81	0.81	0.79	0.90	0.71	0.80	0.05
An	0.17	0.21	0.13	0.19	0.14	0.18	0.18	0.20	0.28	0.02	0.19	0.06

Appendix B.6: Compositional data of plagioclase from the Beluga Showing (con't)

Ms+Cal+Ab+Crn zone

	1-1-11	1-1-12	1-1-13	1-1-14	1-1-15	3-16	3-20	19-1	19-2	max	min	avg	σ
SiO ₂ wt.%	67.55	67.58	68.94	67.80	68.66	62.43	56.81	69.74	67.31	69.74	56.81	66.31	3.89
Al ₂ O ₃	20.17	20.09	19.81	19.83	20.06	21.94	22.70	19.98	20.92	22.70	19.81	20.61	0.98
MgO	0.00	0.00	0.00	0.00	0.00	0.63	0.02	0.01	0.01	0.63	0.00	0.07	0.20
CaO	0.29	0.35	0.01	0.17	0.20	1.02	0.31	0.10	1.23	1.23	0.01	0.41	0.40
MnO	0.01	0.00	0.00	0.00	0.00	0.02	0.00	0.00	0.00	0.02	0.00	0.00	0.01
FeO	0.00	0.00	0.00	0.00	0.00	0.13	0.05	0.00	0.04	0.13	0.00	0.02	0.04
Na ₂ O	11.45	11.50	11.66	11.77	11.61	11.18	12.63	11.77	10.92	12.63	10.92	11.61	0.45
K ₂ O	0.00	0.03	0.02	0.03	0.02	0.52	0.21	0.09	0.04	0.52	0.00	0.11	0.16
TOTAL	99.47	99.55	100.44	99.60	100.55	97.87	92.73	101.69	100.47	101.69	92.73	99.15	2.48
Si ⁴⁺ apfu	2.966	2.967	2.994	2.976	2.981	2.822	2.729	2.993	2.933	2.99	2.73	2.93	0.09
Al ³⁺	1.044	1.040	1.014	1.026	1.026	1.169	1.285	1.011	1.074	1.29	1.01	1.08	0.09
Mg ²⁺	0.000	0.000	0.000	0.000	0.000	0.042	0.001	0.001	0.001	0.04	0.00	0.01	0.01
Ca ²⁺	0.014	0.016	0.000	0.008	0.009	0.049	0.016	0.005	0.057	0.06	0.00	0.02	0.02
Mn ²⁺	0.000	0.000	0.000	0.000	0.000	0.001	0.000	0.000	0.000	0.00	0.00	0.00	0.00
Fe ²⁺	0.000	0.000	0.000	0.000	0.000	0.005	0.002	0.000	0.001	0.01	0.00	0.00	0.00
Na ⁺	0.975	0.979	0.982	1.002	0.977	0.980	1.176	0.979	0.923	1.18	0.92	1.00	0.07
K ⁺	0.000	0.002	0.001	0.002	0.001	0.030	0.013	0.005	0.002	0.03	0.00	0.01	0.01
Or	0.00	0.00	0.00	0.00	0.00	0.03	0.01	0.01	0.00	0.03	0.00	0.01	0.01
Ab	0.99	0.98	1.00	0.99	0.99	0.93	0.98	0.99	0.94	1.00	0.93	0.98	0.02
An	0.01	0.02	0.00	0.01	0.01	0.05	0.01	0.01	0.06	0.06	0.00	0.02	0.02

Appendix B.6: Compositional data of plagioclase from the Bowhead Showing (con't)
Symplectite

	39-2-32	39-2-33	39-2-34	39-2-35	39-2-36	39-2-37	39-2-38	39-2-39	max	min	avg	σ
SiO ₂ wt.%	62.41	62.90	62.47	62.36	61.71	63.39	63.60	62.37	63.60	61.71	62.65	0.58
Al ₂ O ₃	23.86	23.70	23.44	23.94	23.98	23.40	23.32	24.28	24.28	23.32	23.74	0.31
MgO	0.00	0.00	0.00	0.00	0.00	0.00	0.01	0.00	0.01	0.00	0.00	0.00
CaO	5.31	4.75	4.90	5.02	5.35	4.56	4.40	5.42	5.42	4.40	4.96	0.36
MnO	0.04	0.01	0.02	0.00	0.00	0.00	0.00	0.00	0.04	0.00	0.01	0.01
FeO	0.00	0.06	0.08	0.02	0.04	0.00	0.00	0.03	0.08	0.00	0.03	0.03
Na ₂ O	8.71	8.99	8.84	8.76	8.55	9.08	9.02	8.61	9.08	8.55	8.82	0.18
K ₂ O	0.08	0.06	0.11	0.09	0.08	0.06	0.03	0.06	0.11	0.03	0.07	0.02
TOTAL	100.41	100.47	99.86	100.19	99.71	100.49	100.38	100.77	100.77	99.71	100.29	0.33
Si ⁴⁺ apfu	2.755	2.771	2.771	2.756	2.744	2.788	2.797	2.743	2.80	2.74	2.77	0.02
Al ³⁺	1.241	1.230	1.225	1.247	1.257	1.213	1.209	1.259	1.26	1.21	1.24	0.02
Mg ²⁺	0.000	0.000	0.000	0.000	0.000	0.000	0.001	0.000	0.00	0.00	0.00	0.00
Ca ²⁺	0.251	0.224	0.233	0.238	0.255	0.215	0.207	0.255	0.26	0.21	0.23	0.02
Mn ²⁺	0.001	0.000	0.001	0.000	0.000	0.000	0.000	0.000	0.00	0.00	0.00	0.00
Fe ²⁺	0.000	0.002	0.003	0.001	0.001	0.000	0.000	0.001	0.00	0.00	0.00	0.00
Na ⁺	0.745	0.768	0.760	0.751	0.737	0.774	0.769	0.734	0.77	0.73	0.75	0.01
K ⁺	0.005	0.003	0.006	0.005	0.005	0.003	0.002	0.003	0.01	0.00	0.00	0.00
Or	0.00	0.00	0.01	0.01	0.01	0.00	0.00	0.00	0.01	0.00	0.00	0.00
Ab	0.74	0.77	0.76	0.76	0.74	0.78	0.79	0.74	0.79	0.74	0.76	0.02
An	0.25	0.23	0.23	0.24	0.26	0.22	0.21	0.26	0.26	0.21	0.24	0.02

Appendix B.6: Compositional data of plagioclase from the Bowhead Showing (con't)
 Mica-Plg nodule

	39-2-26	39-2-27	39-2-28	39-2-29	39-2-31	max	min	avg	σ
SiO ₂ wt.%	69.28	68.57	67.48	67.58	67.90	69.28	67.48	68.16	0.68
Al ₂ O ₃	19.73	19.56	20.18	20.23	20.12	20.23	19.56	19.96	0.27
MgO	0.00	0.01	0.00	0.00	0.00	0.01	0.00	0.00	0.00
CaO	0.34	0.28	0.48	0.35	0.47	0.48	0.28	0.38	0.08
MnO	0.01	0.01	0.00	0.04	0.03	0.04	0.00	0.02	0.01
FeO	0.00	0.04	0.03	0.00	0.00	0.04	0.00	0.01	0.02
Na ₂ O	11.41	11.49	10.81	11.47	11.49	11.49	10.81	11.33	0.26
K ₂ O	0.04	0.00	0.15	0.28	0.02	0.28	0.00	0.10	0.10
TOTAL	100.81	99.96	99.13	99.95	100.03	100.81	99.13	99.98	0.53
Si ⁴⁺ apfu	2.998	2.994	2.970	2.960	2.968	3.00	2.96	2.98	0.02
Al ³⁺	1.006	1.007	1.047	1.044	1.036	1.05	1.01	1.03	0.02
Mg ²⁺	0.000	0.001	0.000	0.000	0.000	0.00	0.00	0.00	0.00
Ca ²⁺	0.016	0.013	0.023	0.016	0.022	0.02	0.01	0.02	0.00
Mn ²⁺	0.000	0.000	0.000	0.001	0.001	0.00	0.00	0.00	0.00
Fe ²⁺	0.000	0.001	0.001	0.000	0.000	0.00	0.00	0.00	0.00
Na ⁺	0.957	0.973	0.923	0.974	0.974	0.97	0.92	0.96	0.02
K ⁺	0.002	0.000	0.008	0.016	0.001	0.02	0.00	0.01	0.01
Or	0.00	0.00	0.01	0.02	0.00	0.02	0.00	0.01	0.01
Ab	0.98	0.99	0.97	0.97	0.98	0.99	0.97	0.98	0.01
An	0.02	0.01	0.02	0.02	0.02	0.02	0.01	0.02	0.00

Appendix B.7: Compositional data for scapolite from the Beluga Showing

	10-1	10-2	10-3	10-4	10-6	3-7	3-8	3-9	3-10	3-11	3-12	3-13	3-14	3-15	3-16
SiO ₂ wt%	50.10	50.19	50.67	50.44	50.20	53.87	51.93	54.26	49.84	49.97	50.12	50.02	50.19	52.95	51.23
Al ₂ O ₃	25.83	25.66	25.68	25.43	25.81	23.94	24.56	23.73	25.70	25.55	25.63	25.39	25.22	24.34	24.96
MgO	0.00	0.02	0.03	0.00	0.01	0.02	0.00	0.00	0.00	0.00	0.01	0.22	0.01	0.00	0.01
CaO	13.53	13.36	13.46	13.34	13.74	9.99	11.59	9.75	13.68	13.59	13.47	13.21	12.90	10.88	12.24
MnO	0.01	0.01	0.00	0.06	0.00	0.01	0.01	0.02	0.00	0.01	0.02	0.03	0.00	0.01	0.00
FeO	0.01	0.00	0.03	0.02	0.00	0.00	0.06	0.05	0.01	0.01	0.03	0.01	0.00	0.01	0.00
Na ₂ O	5.69	5.93	5.91	6.00	5.93	8.13	7.14	8.41	5.85	5.91	5.78	5.66	6.38	7.42	6.62
K ₂ O	0.54	0.56	0.47	0.54	0.41	0.76	0.75	0.66	0.59	0.53	0.59	0.61	0.55	0.65	0.63
SO ₃	0.21	0.17	0.09	0.20	0.18	0.12	0.17	0.03	0.08	0.13	0.16	0.06	0.02	0.14	0.13
CL	2.86	2.86	3.00	2.99	2.91	5.11	4.12	4.90	3.00	2.86	3.03	2.87	3.27	4.45	3.71
CO ₂ *	1.25	1.27	1.17	1.09	1.21	0.00	0.00	0.00	1.12	1.27	1.05	1.28	0.81	0.00	0.25
O=CL	-0.65	-0.65	-0.68	-0.67	-0.66	-1.15	-0.93	-1.11	-0.68	-0.65	-0.68	-0.65	-0.74	-1.00	-0.84
TOTAL	99.39	99.38	99.83	99.43	99.74	100.80	99.40	100.70	99.20	99.18	99.21	98.72	98.61	99.85	98.94
Si ⁴⁺ apfu	7.464	7.488	7.513	7.527	7.472	7.875	7.705	7.919	7.464	7.488	7.487	7.508	7.537	7.783	7.623
Al ³⁺	4.536	4.512	4.487	4.473	4.528	4.125	4.295	4.081	4.536	4.512	4.513	4.492	4.463	4.217	4.377
Mg ²⁺	0.000	0.004	0.007	0.000	0.002	0.004	0.000	0.000	0.000	0.000	0.002	0.049	0.002	0.000	0.002
Ca ²⁺	2.160	2.136	2.138	2.133	2.191	1.565	1.843	1.525	2.195	2.182	2.156	2.125	2.076	1.714	1.951
Mn ²⁺	0.001	0.001	0.000	0.008	0.000	0.001	0.001	0.002	0.000	0.001	0.003	0.004	0.000	0.001	0.000
Fe ²⁺	0.001	0.000	0.004	0.002	0.000	0.000	0.007	0.006	0.001	0.001	0.004	0.001	0.000	0.001	0.000
Na ⁺	1.644	1.715	1.699	1.736	1.711	2.304	2.054	2.380	1.699	1.717	1.674	1.647	1.857	2.115	1.910
K ⁺	0.103	0.107	0.089	0.103	0.078	0.142	0.142	0.123	0.113	0.101	0.112	0.117	0.105	0.122	0.120
S ⁶⁺	0.023	0.019	0.010	0.022	0.020	0.013	0.019	0.003	0.009	0.015	0.018	0.007	0.002	0.015	0.015
CL ⁻	0.722	0.723	0.754	0.756	0.734	1.266	1.036	1.212	0.761	0.726	0.767	0.730	0.832	1.109	0.936
C ⁴⁺	0.254	0.258	0.236	0.221	0.246	0.000	0.000	0.000	0.230	0.259	0.215	0.263	0.166	0.000	0.050
O ²⁻	24.986	25.008	24.924	24.958	25.009	24.138	24.341	24.148	24.939	25.036	24.902	24.997	24.749	24.218	24.455
EqAn	0.512	0.504	0.496	0.491	0.509	0.375	0.432	0.360	0.512	0.504	0.504	0.497	0.488	0.406	0.459
XCl	0.723	0.723	0.754	0.757	0.734	0.990	0.982	0.998	0.761	0.726	0.767	0.730	0.832	0.987	0.935

*calculated from electroneutral formula assuming (Si+Al) = 12 apfu and (Cl+S+C)=1 apfu.

NOTE: Following standards, X-ray lines and crystals were used for EMP analysis: albite, NaKa , TAP; anorthite, AlKa , TAP; diopside, MgKa, TAP; orthoclase, SiKa, TAP; barite, SKa PET; scapolite, ClKa ,PET; orthoclase, KKa, PET; anorthite, CaKa, PET; synthetic fayalite, FeKa, LIF.

Appendix B.7: Compositional data for scapolite from the Beluga Showing (con't)

	3-17	3-18	3-19	19-1	19-2	19-3	19-4	19-5	19-6	19-7	19-8	19-9	19-10	19-11	19-12
SiO ₂ wt%	49.98	49.64	50.27	50.22	50.29	49.81	49.73	49.81	49.24	49.87	50.31	50.12	50.70	49.18	48.75
Al ₂ O ₃	26.09	26.12	25.87	26.13	25.95	26.01	25.96	25.56	25.52	25.62	25.79	25.57	26.12	26.30	26.23
MgO	0.01	0.02	0.01	0.00	0.01	0.00	0.02	0.00	0.04	0.01	0.04	0.02	0.04	0.05	0.02
CaO	13.95	14.13	13.32	13.95	14.06	13.93	13.59	13.76	13.21	13.25	13.45	13.22	13.41	14.43	15.02
MnO	0.00	0.02	0.05	0.02	0.02	0.00	0.00	0.00	0.00	0.00	0.00	0.00	0.00	0.00	0.00
FeO	0.02	0.00	0.00	0.11	0.02	0.00	0.02	0.00	0.04	0.04	0.09	0.05	0.03	0.06	0.00
Na ₂ O	5.91	5.66	5.74	5.93	5.86	5.94	5.94	5.84	6.23	6.04	6.35	6.28	6.30	5.26	5.47
K ₂ O	0.42	0.49	0.54	0.50	0.53	0.57	0.54	0.56	0.27	0.68	0.66	0.63	0.63	0.51	0.44
SO ₃	0.12	0.01	0.11	0.18	0.11	0.14	0.11	0.15	0.15	0.20	0.11	0.12	0.11	0.05	0.15
CL	2.88	2.93	3.18	3.03	2.93	3.02	3.06	2.95	3.12	3.18	3.25	3.38	3.48	2.53	2.46
CO ₂ *	1.29	1.27	0.92	1.08	1.24	1.09	1.04	1.13	0.89	0.83	0.83	0.64	0.59	1.73	1.73
O=CL	-0.65	-0.66	-0.72	-0.68	-0.66	-0.68	-0.69	-0.67	-0.70	-0.72	-0.73	-0.76	-0.79	-0.57	-0.56
TOTAL	100.02	99.63	99.29	100.47	100.36	99.82	99.32	99.10	98.00	99.00	100.15	99.26	100.63	99.52	99.71
Si ⁴⁺ apfu	7.429	7.407	7.470	7.439	7.462	7.428	7.429	7.478	7.450	7.474	7.481	7.494	7.467	7.361	7.343
Al ³⁺	4.571	4.593	4.530	4.561	4.538	4.572	4.571	4.522	4.550	4.526	4.519	4.506	4.533	4.639	4.657
Mg ²⁺	0.002	0.004	0.002	0.000	0.002	0.000	0.004	0.000	0.009	0.002	0.009	0.004	0.009	0.011	0.004
Ca ²⁺	2.222	2.259	2.121	2.214	2.235	2.226	2.175	2.213	2.141	2.128	2.143	2.118	2.116	2.314	2.424
Mn ²⁺	0.000	0.003	0.006	0.003	0.003	0.000	0.000	0.000	0.000	0.000	0.000	0.000	0.000	0.000	0.000
Fe ²⁺	0.002	0.000	0.000	0.014	0.002	0.000	0.002	0.000	0.005	0.005	0.011	0.006	0.004	0.008	0.000
Na ⁺	1.703	1.637	1.654	1.703	1.686	1.718	1.721	1.700	1.827	1.755	1.831	1.821	1.799	1.526	1.598
K ⁺	0.080	0.093	0.102	0.094	0.100	0.108	0.103	0.107	0.052	0.130	0.125	0.120	0.118	0.097	0.085
S ⁶⁺	0.013	0.001	0.012	0.020	0.012	0.016	0.012	0.017	0.017	0.022	0.012	0.013	0.012	0.006	0.017
CL ⁻	0.726	0.741	0.801	0.761	0.737	0.763	0.775	0.751	0.800	0.808	0.819	0.856	0.869	0.642	0.628
C ⁴⁺	0.261	0.258	0.187	0.219	0.251	0.221	0.213	0.233	0.183	0.170	0.169	0.130	0.119	0.353	0.355
O ²⁻	25.032	24.983	24.752	24.967	25.037	24.961	24.884	24.996	24.837	24.818	24.846	24.718	24.661	25.226	25.388
EqAn	0.524	0.531	0.510	0.520	0.513	0.524	0.524	0.507	0.517	0.509	0.506	0.502	0.511	0.546	0.552
XCl	0.726	0.741	0.801	0.761	0.737	0.763	0.775	0.750	0.800	0.808	0.819	0.857	0.869	0.641	0.628

Appendix B.7: Compositional data for scapolite from the Beluga Showing (con't)

	19-13	11-14	11-15	11-16	11-17	11-18	11-19	11-20	11-21	11-22	11-23	11-24	11-25	11-26	11-27
SiO ₂ wt%	48.98	46.43	47.37	47.44	47.00	47.81	46.97	45.80	49.39	49.19	48.27	47.98	45.62	48.04	47.34
Al ₂ O ₃	26.44	28.17	27.48	27.42	27.61	27.37	27.54	28.24	26.01	26.04	26.89	27.36	28.21	27.18	27.70
MgO	0.06	0.02	0.01	0.00	0.02	0.01	0.00	0.12	1.62	0.00	0.01	0.00	0.00	0.00	0.65
CaO	14.17	18.10	16.34	16.10	17.12	16.54	16.87	16.56	10.77	14.78	15.86	16.59	17.40	16.03	13.69
MnO	0.03	0.00	0.03	0.00	0.00	0.02	0.01	0.07	0.00	0.00	0.04	0.00	0.01	0.01	0.00
FeO	0.00	0.04	0.10	0.00	0.00	0.00	0.00	0.00	0.07	0.02	0.03	0.00	0.02	0.00	0.12
Na ₂ O	5.38	3.92	4.39	4.68	4.24	4.61	4.38	3.98	5.85	5.60	5.05	4.62	3.70	5.00	4.43
K ₂ O	0.46	0.17	0.20	0.21	0.26	0.28	0.23	0.56	0.12	0.36	0.36	0.30	0.21	0.27	1.23
SO ₃	0.17	0.17	0.07	0.08	0.16	0.03	0.17	0.07	0.07	0.18	0.08	0.05	0.07	0.10	0.12
CL	2.45	1.11	1.30	1.56	1.33	1.82	1.53	1.28	0.59	2.53	1.93	1.72	1.04	1.82	1.77
CO ₂ *	1.76	3.39	3.22	2.89	3.12	2.61	2.86	3.20	4.11	1.64	2.44	2.73	3.48	2.57	2.62
O=CL	-0.55	-0.25	-0.29	-0.35	-0.30	-0.41	-0.35	-0.29	-0.13	-0.57	-0.44	-0.39	-0.23	-0.41	-0.40
TOTAL	99.34	101.27	100.21	100.03	100.56	100.69	100.21	99.59	98.47	99.77	100.53	100.97	99.53	100.61	99.27
Si ⁴⁺ apfu	7.334	6.997	7.127	7.138	7.091	7.166	7.096	6.950	7.404	7.390	7.244	7.177	6.941	7.199	7.102
Al ³⁺	4.666	5.003	4.873	4.862	4.909	4.834	4.904	5.050	4.596	4.610	4.756	4.823	5.059	4.801	4.898
Mg ²⁺	0.013	0.004	0.002	0.000	0.004	0.002	0.000	0.027	0.362	0.000	0.002	0.000	0.000	0.000	0.145
Ca ²⁺	2.273	2.922	2.634	2.595	2.767	2.656	2.731	2.692	1.730	2.379	2.550	2.659	2.837	2.574	2.201
Mn ²⁺	0.004	0.000	0.004	0.000	0.000	0.003	0.001	0.009	0.000	0.000	0.005	0.000	0.001	0.001	0.000
Fe ²⁺	0.000	0.005	0.013	0.000	0.000	0.000	0.000	0.000	0.009	0.003	0.004	0.000	0.003	0.000	0.015
Na ⁺	1.562	1.145	1.281	1.365	1.240	1.340	1.283	1.171	1.700	1.631	1.469	1.340	1.092	1.453	1.289
K ⁺	0.088	0.033	0.038	0.040	0.050	0.054	0.044	0.108	0.023	0.069	0.069	0.057	0.041	0.052	0.235
S ⁶⁺	0.019	0.019	0.008	0.009	0.018	0.003	0.019	0.008	0.008	0.020	0.009	0.006	0.008	0.011	0.014
CL ⁻	0.622	0.283	0.331	0.398	0.340	0.462	0.392	0.329	0.150	0.644	0.491	0.436	0.268	0.462	0.450
C ⁴⁺	0.359	0.697	0.661	0.593	0.642	0.534	0.589	0.663	0.842	0.336	0.500	0.558	0.724	0.527	0.536
O ²⁻	25.247	26.330	26.055	25.882	26.130	25.788	25.984	26.028	26.298	25.336	25.734	25.861	26.215	25.783	25.563
EqAn	0.555	0.668	0.624	0.621	0.636	0.611	0.635	0.683	0.532	0.537	0.585	0.608	0.686	0.600	0.633
XCl	0.622	0.283	0.331	0.398	0.340	0.462	0.392	0.329	0.150	0.644	0.491	0.436	0.268	0.462	0.450

Appendix B.7: Compositional data for scapolite from the Beluga Showing (con't)

	11-28	11-29	11-30	BA1-2	BA1-3	BA1-4	BA1-5	BA1-6	BA1-8	BA1-9	1-1-1	1-1-2	1-1-4	1-1-5	1-1-6
SiO ₂ wt%	49.23	49.07	49.69	48.50	48.47	47.41	46.26	46.52	46.24	45.64	49.68	49.90	49.79	49.49	49.11
Al ₂ O ₃	26.55	26.45	26.10	26.03	26.55	27.04	27.84	27.93	27.91	28.04	25.47	25.52	25.68	25.84	26.13
MgO	0.03	0.01	0.00	0.02	0.03	0.01	0.02	0.00	0.00	0.04	0.00	0.00	0.00	0.00	0.01
CaO	15.37	15.07	14.06	14.54	15.42	16.38	17.33	17.32	17.12	16.90	12.97	13.03	12.97	13.51	14.13
MnO	0.00	0.00	0.02	0.00	0.00	0.02	0.01	0.02	0.00	0.00	0.01	0.00	0.01	0.02	0.06
FeO	0.03	0.08	0.00	0.03	0.01	0.00	0.00	0.01	0.00	0.00	0.13	0.10	0.00	0.05	0.00
Na ₂ O	5.24	5.44	6.04	5.63	5.10	4.69	4.01	4.06	4.00	4.07	6.18	6.12	6.27	6.05	5.92
K ₂ O	0.35	0.38	0.31	0.39	0.31	0.32	0.25	0.28	0.24	0.24	0.47	0.49	0.29	0.23	0.38
SO ₃	0.16	0.16	0.11	0.10	0.10	0.03	0.07	0.04	0.12	0.11	0.22	0.08	0.13	0.19	0.14
CL	2.13	2.33	2.66	2.41	2.13	1.72	1.27	1.19	1.23	1.19	3.70	3.65	3.64	3.23	3.21
CO ₂ *	2.18	1.92	1.55	1.79	2.17	2.69	3.21	3.35	3.24	3.27	0.15	0.31	0.30	0.77	0.82
O=CL	-0.48	-0.53	-0.60	-0.54	-0.48	-0.39	-0.29	-0.27	-0.28	-0.27	-0.83	-0.82	-0.82	-0.73	-0.72
TOTAL	100.79	100.38	99.94	98.89	99.81	99.92	99.98	100.45	99.82	99.23	98.15	98.37	98.26	98.65	99.18
Si ⁴⁺ apfu	7.337	7.338	7.412	7.351	7.292	7.176	7.021	7.027	7.012	6.960	7.480	7.487	7.463	7.429	7.375
Al ³⁺	4.663	4.662	4.588	4.649	4.708	4.824	4.979	4.973	4.988	5.040	4.520	4.513	4.537	4.571	4.625
Mg ²⁺	0.007	0.002	0.000	0.005	0.007	0.002	0.005	0.000	0.000	0.009	0.000	0.000	0.000	0.000	0.002
Ca ²⁺	2.454	2.415	2.247	2.361	2.486	2.657	2.818	2.803	2.782	2.761	2.092	2.095	2.083	2.173	2.274
Mn ²⁺	0.000	0.000	0.003	0.000	0.000	0.003	0.001	0.003	0.000	0.000	0.001	0.000	0.001	0.003	0.008
Fe ²⁺	0.004	0.010	0.000	0.004	0.001	0.000	0.000	0.001	0.000	0.000	0.016	0.013	0.000	0.006	0.000
Na ⁺	1.514	1.577	1.747	1.654	1.488	1.376	1.180	1.189	1.176	1.203	1.804	1.780	1.822	1.761	1.724
K ⁺	0.067	0.072	0.059	0.075	0.059	0.062	0.048	0.054	0.046	0.047	0.090	0.094	0.055	0.044	0.073
S ⁶⁺	0.018	0.018	0.012	0.011	0.011	0.003	0.008	0.005	0.014	0.013	0.025	0.009	0.015	0.021	0.016
CL ⁻	0.538	0.591	0.672	0.619	0.543	0.441	0.327	0.305	0.316	0.308	0.944	0.928	0.925	0.822	0.817
C ⁴⁺	0.444	0.392	0.315	0.370	0.446	0.555	0.665	0.691	0.670	0.680	0.031	0.063	0.061	0.157	0.167
O ²⁻	25.596	25.463	25.190	25.373	25.567	25.869	26.140	26.185	26.122	26.119	24.462	24.477	24.458	24.766	24.843
EqAn	0.554	0.554	0.529	0.550	0.569	0.608	0.660	0.658	0.663	0.680	0.507	0.504	0.512	0.524	0.542
XCl	0.538	0.590	0.673	0.619	0.543	0.441	0.327	0.305	0.316	0.308	0.944	0.928	0.924	0.822	0.817

Appendix B.7: Compositional data for scapolite from the Beluga Showing (con't)

	1-1-7	1-1-8	1-1-9	1-1-10	1-1-11	1-1-12	1-1-13	max	min	avg	σ
SiO ₂ wt%	48.75	48.17	47.61	47.31	47.58	47.15	46.84	54.26	45.62	49.04	1.78
Al ₂ O ₃	26.66	26.34	26.73	27.00	26.63	26.85	27.09	28.24	23.73	26.30	1.00
MgO	0.41	0.30	0.00	0.00	0.00	0.00	0.00	1.62	0.00	0.06	0.22
CaO	13.02	14.15	15.41	14.95	14.55	15.08	15.13	18.10	9.75	14.34	1.77
MnO	0.02	0.00	0.00	0.01	0.03	0.02	0.00	0.07	0.00	0.01	0.02
FeO	0.01	0.00	0.04	0.03	0.03	0.00	0.00	0.13	0.00	0.02	0.03
Na ₂ O	5.74	5.26	4.84	5.02	4.95	4.97	4.97	8.41	3.70	5.52	0.93
K ₂ O	0.34	0.44	0.34	0.42	0.58	0.41	0.39	1.23	0.12	0.45	0.18
SO ₃	0.06	0.11	0.03	0.11	0.21	0.05	0.09	0.22	0.01	0.12	0.05
CL	2.88	2.92	2.03	2.33	2.24	2.29	2.30	5.11	0.59	2.59	0.92
CO ₂ *	1.29	1.15	2.29	1.88	1.92	1.94	1.90	4.11	0.00	1.65	1.02
O=CL	-0.65	-0.66	-0.46	-0.53	-0.51	-0.52	-0.52	-0.13	-1.15	-0.59	0.21
TOTAL	98.53	98.18	98.86	98.53	98.22	98.24	98.19	101.27	98.00	99.53	0.81
Si ⁴⁺ apfu	7.297	7.297	7.222	7.174	7.231	7.181	7.136	7.92	6.94	7.35	0.21
Al ³⁺	4.703	4.703	4.778	4.826	4.769	4.819	4.864	5.06	4.08	4.65	0.21
Mg ²⁺	0.091	0.068	0.000	0.000	0.000	0.000	0.000	0.36	0.00	0.01	0.05
Ca ²⁺	2.088	2.297	2.504	2.429	2.369	2.461	2.470	2.92	1.53	2.31	0.30
Mn ²⁺	0.003	0.000	0.000	0.001	0.004	0.003	0.000	0.01	0.00	0.00	0.00
Fe ²⁺	0.001	0.000	0.005	0.004	0.004	0.000	0.000	0.02	0.00	0.00	0.00
Na ⁺	1.666	1.545	1.423	1.476	1.458	1.468	1.468	2.38	1.09	1.60	0.26
K ⁺	0.065	0.085	0.066	0.081	0.112	0.080	0.076	0.24	0.02	0.09	0.03
S ⁶⁺	0.007	0.013	0.003	0.013	0.024	0.006	0.010	0.03	0.00	0.01	0.01
CL ⁻	0.731	0.750	0.522	0.599	0.577	0.591	0.594	1.27	0.15	0.66	0.23
C ⁴⁺	0.263	0.238	0.475	0.389	0.399	0.403	0.396	0.84	0.00	0.34	0.21
O ²⁻	24.878	24.966	25.564	25.316	25.359	25.355	25.335	26.33	24.14	25.23	0.57
EqAn	0.568	0.568	0.593	0.609	0.590	0.606	0.621	0.69	0.36	0.55	0.07
XCl	0.730	0.749	0.522	0.598	0.577	0.591	0.594	1.00	0.15	0.65	0.21

Appendix B.7: Compositional data for scapolite from the Bowhead Showing (con't)

	39-2 2b-S1	39-2 2b-S2	39-2 2b-S3	39-2 2b-S4	39-2 2b-S5	39-2 2b-S6	39-2 2b-S7	39-2 2b-S8	39-2 2b-S9	39-2 2d-S10	39-2 2d-S11
SiO ₂ wt%	46.73	48.35	46.94	46.41	48.31	48.15	45.44	45.48	48.53	48.90	49.38
Al ₂ O ₃	27.19	26.32	26.62	26.75	25.79	25.50	27.58	27.57	26.10	26.09	25.61
MgO	0.01	0.01	0.00	0.00	0.02	0.01	0.00	0.00	0.00	0.00	0.00
CaO	16.36	14.95	15.80	16.12	14.61	14.47	17.38	17.36	14.64	14.87	13.80
MnO	0.00	0.00	0.02	0.00	0.00	0.05	0.01	0.03	0.03	0.00	0.00
FeO	0.00	0.01	0.00	0.01	0.00	0.02	0.08	0.00	0.03	0.03	0.02
Na ₂ O	4.56	5.39	4.87	4.54	5.61	5.71	4.16	4.10	5.49	5.46	6.06
K ₂ O	0.17	0.39	0.23	0.29	0.33	0.33	0.24	0.26	0.33	0.35	0.42
SO ₃	0.00	0.30	0.00	0.12	0.13	0.12	0.06	0.14	0.00	0.18	0.15
CL	1.87	2.55	2.16	2.08	2.93	3.06	1.66	1.70	2.94	3.02	3.03
CO ₂ *	2.49	1.51	2.10	2.11	1.10	0.91	2.66	2.57	1.19	1.01	1.01
O=CL	-0.42	-0.58	-0.49	-0.47	-0.66	-0.69	-0.37	-0.38	-0.66	-0.68	-0.68
TOTAL	98.96	99.21	98.25	97.96	98.16	97.64	98.90	98.83	98.62	99.23	98.80
Si ⁴⁺ apfu	7.119	7.310	7.193	7.146	7.366	7.388	6.996	6.999	7.345	7.367	7.448
Al ³⁺	4.881	4.690	4.807	4.854	4.634	4.612	5.004	5.001	4.655	4.633	4.552
Mg ²⁺	0.002	0.002	0.000	0.000	0.005	0.002	0.000	0.000	0.000	0.000	0.000
Ca ²⁺	2.670	2.422	2.594	2.659	2.387	2.379	2.867	2.863	2.374	2.400	2.230
Mn ²⁺	0.000	0.000	0.003	0.000	0.000	0.006	0.001	0.004	0.004	0.000	0.000
Fe ²⁺	0.000	0.001	0.000	0.001	0.000	0.003	0.010	0.000	0.004	0.004	0.003
Na ⁺	1.347	1.580	1.447	1.355	1.658	1.699	1.242	1.223	1.611	1.595	1.772
K ⁺	0.033	0.075	0.045	0.057	0.064	0.065	0.047	0.051	0.064	0.067	0.081
S ⁶⁺	0.000	0.034	0.000	0.014	0.015	0.014	0.007	0.016	0.000	0.020	0.017
CL ⁻	0.483	0.653	0.561	0.543	0.757	0.796	0.433	0.443	0.754	0.771	0.774
C ⁴⁺	0.517	0.313	0.439	0.443	0.228	0.190	0.560	0.540	0.246	0.209	0.209
O ²⁻	25.715	25.309	25.537	25.597	25.058	24.991	25.945	25.911	25.006	25.012	24.964
EqAn	0.63	0.56	0.60	0.62	0.54	0.54	0.67	0.67	0.55	0.54	0.52
XCl	0.48	0.65	0.56	0.54	0.76	0.80	0.43	0.44	0.75	0.77	0.77

Appendix B.7: Compositional data for scapolite from the Bowhead Showing (con't)

	39-2 2d-S12	39-2 2d-S13	39-2 2d-S14	39-2 2d-S15	max	min	avg	σ
SiO ₂ wt%	49.34	48.83	49.54	48.99	49.54	45.44	47.95	1.35
Al ₂ O ₃	25.77	25.44	25.31	25.47	27.58	25.31	26.21	0.75
MgO	0.00	0.00	0.00	0.00	0.02	0.00	0.00	0.01
CaO	14.19	13.94	14.02	13.98	17.38	13.80	15.10	1.17
MnO	0.02	0.00	0.00	0.00	0.05	0.00	0.01	0.02
FeO	0.05	0.06	0.00	0.00	0.08	0.00	0.02	0.02
Na ₂ O	5.99	5.86	5.87	5.97	6.06	4.10	5.31	0.66
K ₂ O	0.40	0.40	0.39	0.43	0.43	0.17	0.33	0.08
SO ₃	0.16	0.04	0.20	0.14	0.30	0.00	0.12	0.08
CL	3.23	3.13	3.24	3.17	3.24	1.66	2.65	0.57
CO ₂ *	0.77	0.90	0.71	0.81	2.66	0.71	1.46	0.70
O=CL	-0.73	-0.71	-0.73	-0.72	-0.37	-0.73	-0.60	0.13
TOTAL	99.19	97.90	98.55	98.25	99.23	97.64	98.56	0.49
Si ⁴⁺ apfu	7.428	7.435	7.490	7.441	7.49	7.00	7.30	0.16
Al ³⁺	4.572	4.565	4.510	4.559	5.00	4.51	4.70	0.16
Mg ²⁺	0.000	0.000	0.000	0.000	0.01	0.00	0.00	0.00
Ca ²⁺	2.289	2.274	2.271	2.275	2.87	2.23	2.46	0.21
Mn ²⁺	0.003	0.000	0.000	0.000	0.01	0.00	0.00	0.00
Fe ²⁺	0.006	0.008	0.000	0.000	0.01	0.00	0.00	0.00
Na ⁺	1.748	1.730	1.721	1.758	1.77	1.22	1.57	0.19
K ⁺	0.077	0.078	0.075	0.083	0.08	0.03	0.06	0.01
S ⁶⁺	0.018	0.005	0.023	0.016	0.03	0.00	0.01	0.01
CL ⁻	0.824	0.808	0.830	0.816	0.83	0.43	0.68	0.14
C ⁴⁺	0.158	0.188	0.147	0.168	0.56	0.15	0.30	0.15
O ²⁻	24.882	24.888	24.861	24.892	25.95	24.86	25.24	0.38
EqAn	0.52	0.52	0.50	0.52	0.67	0.50	0.57	0.05
XCl	0.82	0.81	0.83	0.82	0.83	0.43	0.68	0.14

Appendix B.8: Representative compositional data for accessory minerals from the Beluga showing.

tourmaline					
	5-1	5-2	5-3	5-4	5-5
SiO ₂ wt.%	35.88	35.62	35.46	35.42	35.50
TiO ₂	0.50	0.48	0.29	0.06	0.07
B ₂ O ₃ *	10.91	10.93	10.92	10.90	10.92
Al ₂ O ₃	37.19	37.62	37.86	38.31	38.46
Cr ₂ O ₃	0.01	0.01	0.00	0.00	0.03
FeO	1.00	1.08	1.03	1.37	1.24
MnO	0.00	0.00	0.00	0.02	0.04
MgO	8.86	8.80	8.76	8.24	8.22
CaO	0.39	0.58	0.58	0.48	0.48
Na ₂ O	2.91	2.81	2.79	2.94	2.90
K ₂ O	0.05	0.05	0.04	0.03	0.06
F	0.22	0.41	0.30	0.28	0.27
H ₂ O *	3.11	3.05	3.12	3.07	3.06
-O=(F+Cl)	-0.09	-0.17	-0.13	-0.12	-0.12
Total	100.95	101.26	101.04	101.02	101.15
Si ⁴⁺ apfu	5.717	5.663	5.645	5.647	5.650
Ti ⁴⁺	0.060	0.057	0.035	0.007	0.009
B ³⁺	3.000	3.000	3.000	3.000	3.000
Al ³⁺	6.983	7.050	7.104	7.200	7.216
V ³⁺	0.000	0.000	0.000	0.000	0.000
Cr ³⁺	0.001	0.002	0.000	0.000	0.004
Fe ²⁺	0.133	0.144	0.138	0.183	0.164
Mn ²⁺	0.000	0.000	0.000	0.003	0.005
Mg ²⁺	2.105	2.085	2.078	1.960	1.952
Ca ²⁺	0.066	0.098	0.098	0.083	0.082
Na ⁺	0.899	0.867	0.863	0.909	0.895
K ⁺	0.009	0.010	0.009	0.007	0.013
F ⁻	0.112	0.206	0.151	0.140	0.138
OH ⁻	3.309	3.230	3.315	3.270	3.252
O ²⁻	27.580	27.564	27.533	27.589	27.611

Tourmaline

*B₂O₃ was fixed at the nominal value of 3.25 wt.% and H₂O was calculated by stoichiometry

The formula was calculated using 15 (Si, Ti, B, Al, V, Cr, Fe, Mn, Mg)

NOTE: The following standards, X-ray lines and crystals were used during EMP analysis:

synthetic fluorophlogopite, FK α , TAP; albite, NaK α , TAP; kyanite, AlK α , TAP;

diopside, MgK α , TAP; diopside, SiK α , TAP; scapolite, Cl K α , PET; orthoclase, KK α , PET; diopside, CaK α , PET;

rutile, TiK α , PET; synthetic magnesiochromite, CrK α , LIF; synthetic rhodonite, MnK α , LIF;

synthetic fayalite, FeK α , LIF; gahnite, ZnK α , LIF.

Appendix B.8: Representative compositional data for accessory minerals from the Beluga showing.

sanbornite		titanite		metamict monazite	
		01-01		86-04-1	
SiO ₂ wt.%	42.76	UO ₃	0.00	P ₂ O ₅	12.51
TiO ₂	0.27	Nb ₂ O ₅	0.04	SiO ₂	1.31
Al ₂ O ₃	0.58	Ta ₂ O ₅	0.00	TiO ₂	0.02
CaO	0.05	P ₂ O ₅	0.04	Al ₂ O ₃	5.79
MgO	0.01	SiO ₂	30.47	CaO	0.77
MnO	0	TiO ₂	37.20	MgO	0.07
FeO	0.06	Al ₂ O ₃	1.77	MnO	0.00
SrO	0	V ₂ O ₃	0.10	FeO	0.00
BaO	54.98	Cr ₂ O ₃	0.03	Na ₂ O	0.01
Na ₂ O	0.16	FeO	0.07	K ₂ O	0.05
F	0.03	MnO	0.03	Y ₂ O ₃	0.41
CL	0.02	MgO	0.00	La ₂ O ₃	14.42
O=F	-0.01	CaO	28.26	Ce ₂ O ₃	26.62
O=CL	0	Na ₂ O	0.00	Pr ₂ O ₃	2.84
Total	98.9	ZrO ₂	0.57	Nd ₂ O ₃	9.71
		SnO ₂	0.00	Sm ₂ O ₃	0.95
Si ⁴⁺ apfu	3.91	Pr ₂ O ₃	0.00	Gd ₂ O ₃	2.31
Ti ⁴⁺	0.019	ThO ₂	0.07	ThO ₂	7.71
Al ³⁺	0.063	Sc ₂ O ₃	0.00	Total	85.50
Ca ²⁺	0.005	Y ₂ O ₃	0.00		
Mg ²⁺	0.001	La ₂ O ₃	0.00		
Mn ²⁺	0	Ce ₂ O ₃	0.03		
Fe ²⁺	0.005	Nd ₂ O ₃	0.01		
Sr ²⁺	0	Sm ₂ O ₃	0.04		
Ba ²⁺	1.97	Gd ₂ O ₃	0.09		
Na ⁺	0.028	F	0.46		
F ⁻	0.009	Total	99.26		
Cl ⁻	0.003				
O ²⁻	9.94				

Sanbornite

Calculated on the basis of 6 cations.

NOTE: Following standards, X-ray lines and crystals were used during EMP analysis:

synthetic phlogopite, FKa, MgKa, SiKa, TAP, KKa, PET; albite, NaKa, TAP; kyanite, AlKa, TAP;
scapolite, CIKa, PET; diopside, CaKa, PET; rutile, TiKa, PET; synthetic magnesiochromite, CrKa, LIF;
synthetic rhodonite, MnKa, LIF; synthetic fayalite, FeKa, LIF; barite, BaLa, PET.

Appendix B.8: Representative compositional data for accessory minerals from the Beluga showing.

	U-Th Oxides and silicates			metamict				
	thorianite	metamict	metamict					
	36953	37318	37683	38414	38779	39144	39510	38049
UO ₃	12.88	1.42	23.76	10.37	0.00	0.00	0.00	0.12
ThO ₂	77.11	55.52	13.35	8.01	0.13	0.02	0.07	0.24
SiO ₂	0.19	18.58	17.80	28.89	36.11	38.87	42.05	40.91
Al ₂ O ₃	0.03	0.64	6.00	11.70	14.62	15.24	14.09	14.79
PbO	7.44	0.00	5.86	2.02	0.12	0.10	0.08	0.21
K ₂ O	0.00	0.00	0.20	0.28	0.27	1.04	0.72	0.43
Total	97.65	76.16	66.97	61.27	51.25	55.26	57.03	56.70

Appendix B.9 Whole rock major element analysis of calc-silicates from the Beluga Showing

Sample	BA-1	BA-2	BA-3	BA-4	BA-5
P ₂ O ₅	0.03	0.02	0.02	0.02	0.02
SiO ₂	45.19	45.86	46.07	45.37	46.54
TiO ₂	0.92	1.07	1.03	0.93	0.95
Al ₂ O ₃	15.26	11.47	13.3	15.32	14.92
Cr ₂ O ₃	0.01	0.01	0.01	0.01	0.01
Fe ₂ O ₃	1.47	1.83	1.53	1.43	1.47
FeO	1.16	1.42	1.16	1.16	1.09
MnO	0.02	0.03	0.03	0.02	0.02
MgO	9.28	11.46	10.53	9.59	9.87
CaO	15.82	18.86	17.62	16.07	16.92
SrO	0.02	<0.01	0.01	0.03	0.02
BaO	0.02	0.01	0.02	0.02	0.02
Na ₂ O	2.96	2.43	2.68	2.94	2.55
K ₂ O	2.45	1.55	1.86	2.37	1.88
LOI	5.58	4.56	4.37	5.1	3.95
Total	99.02	99.17	99.07	99.22	99.13
H ₂ O-	0.04	0.01	0.06	0.04	0.02
H ₂ O+	0.89	0.66	0.66	1.12	1.22
C	1.15	0.95	0.93	1.05	0.66
CO ₂	4.2	3.5	3.4	3.8	2.4

Appendix B.9 Whole rock trace element analysis of calc-silicates from the Beluga Showing

Sample	BA-1	BA-2	BA-3	BA-4	BA-5	Sample	BA-1	BA-2	BA-3	BA-4	BA-5
Rb	80.2	47.1	56	71.2	55.9	Li	17.6	14.2	13.9	14.5	16.2
Cs	3.5	1.9	2.5	3.2	2.1	Be	1.84	2.01	1.93	1.78	1.84
Sr	305	131.5	230	368	423	B	60	60	90	100	80
Ba	64.9	38.5	49.7	51	69.5	F	1580	1050	1240	1390	1030
Sc	11.8	13.8	12.3	9.9	11.2	Cl	570	230	690	800	460
V	218	263	236	221	247	Cl	490	270	620	810	510
Cr	110	130	100	100	100						
Zr	196	248	212	198.5	220						
Hf	6	8	7	7	7						
Nb	4	3	4	3	3						
Ta	0.5	0.5	0.5	<0.5	0.5						
Mo	<2	<2	<2	<2	<2						
W	1	1	1	2	3						
Co	2.4	3.2	2.3	2.5	2.3						
Ni	5	6	5	5	6						
Cu	5	7	6	5	<5						
Zn	32	35	31	29	34						
Ag	<1	<1	<1	<1	<1						
Ga	27	27	26	27	28						
Tl	<0.5	<0.5	<0.5	<0.5	<0.5						
Sn	3	3	3	3	3						
Pb	<5	<5	<5	<5	<5						
Re	0.002	0.003	<0.002	0.003	<0.002						
Se	3	9	4	4	3						
Te	<0.05	0.27	0.07	0.06	<0.05						
Y	3.5	3.9	3.7	3.3	3.5						
La	2.7	2.7	2.7	2.9	2.6						
Ce	6.4	6.4	6.2	5.5	5.7						
Pr	0.8	0.9	0.9	0.9	0.8						
Nd	3.9	4.3	4.3	3.5	3.7						
Sm	1.2	1.4	1.3	1.1	1.2						
Eu	0.2	0.2	0.2	0.2	0.3						
Gd	0.9	1	1	0.9	0.9						
Tb	0.1	0.2	0.2	0.1	0.1						
Dy	0.8	0.9	0.8	0.7	0.8						
Ho	0.1	0.2	0.2	0.1	0.2						
Er	0.4	0.5	0.4	0.4	0.4						
Tm	<0.1	0.1	0.1	<0.1	<0.1						
Yb	0.4	0.5	0.4	0.4	0.4						
Lu	0.1	0.1	0.1	<0.1	0.1						
Th	1	1	1	1	1						
U	1.7	1.8	2.1	1.7	1.7						